UNIVERSITÉ DE STRASBOURG

ÉCOLE DOCTORALE 414

Institut de Biologie Moléculaire des Plantes

THÈSE

présentée par :

Adrien TROLET

soutenue le : **14 septembre 2018**

pour obtenir le grade de : **Docteur de l'université de Strasbourg**

Discipline/ Spécialité : Science de la vie et de la santé, aspects moléculaire et cellulaire de la biologie

Cell cycle-dependent regulation and function of ARGONAUTE 1 in plants

THÈSE dirigée par :
M. Pascal Genschik Docteur, Université de Strasbourg

RAPPORTEURS :
M. Crisanto Guttierez Professeur, Université de Madrid
Mme. Cécile Raynaud Docteur, Université Paris-Saclay

AUTRES MEMBRES DU JURY :
Mme. Laurence Marechal-Drouard Docteur, Université de Strasbourg
M. Arp Schnittger Professeur, Université de Hambourg

Acknowledgments

First, I want to thank Pascal Genschik for hosting me in the lab and supervising my work during these four years of thesis, as well as Marie -Claire Criqui, who helped me a lot at the bench, especially with BY-2 cells and synchronization experiments.

I want to thank also Blake C. Meyers and Patricia Baldrich for our great and fruitful collaboration on the bioinformatic analysis.

I also thank Cécile Raynaud, Laurence Maréchal-Drouard, Cristanto Gutierrez and Arp Schnittger for accepting to evaluate my thesis.

I want also to thank all IBMP colleagues and especially people from the IBMP platforms:

-Sandrine and Malek for the sequencing and their help on the qRT-PCR.

-Nicolas and Laurence for their help and advices on gel filtration experiments.

-Jérôme from the microscopy platform for his help on the confocal and ImageJ software.

-All the gardeners, Richard, Michel, Fabrice and Sebastien, who took care of my plants.

Many thanks to all the member of the 612 lab , and to those who leaved, for sharing advices, the nice scientific discussions, and also the less serious ones!

Finally, I want to thank my friends, Chloe, Cédric, Marieke, Marion, Marco, Pierre, Thibaut, Maxime, Franck, Lucie and Hélène, for all the nice moments we had in and out of the lab, and my family for their unshakeable support.

List of figures and tables

List of abbreviations

A-D		E-M	
AFB	AUXIN-RELATED F-BOX PROTEIN	E2	Ubiquitin conjugating enzyme
AGO	ARGONAUTE	E2F	ADENOVIRUS EARLY GENE 2 BINDING FACTOR
AMP	Adenosine monophosphate	E3	Ubiquitin Ligase
APC/C	Anaphase-promoting comple/cyclosome	EDC	*N*-(3-dimethylaminopropyl)-*N*′-ethylcarbodiimide hydrochloride
ARF	AUXIN-RESPONSE FACTOR	EDTA	Ethylene diaminetetraacetic acid
Arg	Arginine	eGFP	ENHANCED GFP
ATP	Adenosine triphosphate	eIF	EUKARYOTIC INITATION FACTOR
AUX/IAA	AUXIN/INDOLE ACETIC ACID REPRESSOR	EMS	Ethylmethane sulfonate
bp	Base pair	FBW2	F-BOX WITH WD40 2
BY-2	*N.tabacum* cultivar Bright yellow-2	FOXM1	FORKHEAD BOX M1
CAK	CDK-activating kinase	G1	Gap1 phase
CB	Coomassie blue	G2	Gap2 phase
CCS52	CELL CYCLE SWITCH PROTEIN 52	Gb	Giga base
CDC2	CELL DIVISION CONTROL	GEO	Gene expression omnibus
CDH1	CDC20 HOMOLOGUE 1	GFP	GREEN FLUORESCENT PROTEIN
CDK	CYCLIN-DEPENDENT KINASE	GLD-2	GOLDEN-2
cDNA	Complementary DNA	Glu	Glutamic acid
CDT1/2	CDC10 DEPENDENT TRANSCRIPT 1/2	GO	Gene ontology
CIP	CDK INIBITORY PROTEIN	GRF	GROWTH-REGULATING FACTOR
CKI	CDK-inhibitor	GW	Glycine-tryptophane repeat
CYC	CYCLIN	H2B	Histone H2B
DAPI	4′,6-diamidino-2-phenylindole	HEN1	HUA ENHANCER1
DAS	days after stratification	HESO1	SUPPRESSOR OF HEN1
D-box	Destruction box	hetsiRNA	Heterochromatic siRNA
DCL1-4	DICER-LIKE PROTEIN 1-4	HTR2	HISTONE-THREE RELATED 2
DCP1	DECAPPING PROTEIN 1	HYL1	HYPONASTIC LEAVES 1
DDX3/6	DEAD-BOX HELICASE 3/6	Inc	Incorporation
DE	Differentially expressed	INK4	INHIBITOR OF CDK4
DEL1-3	DP-E2F-LIKE 1-3	IP	Immunoprecipitation
DMSO	Dimehylsulfoxide	kDa	Kilo Dalton
DNA	Deoxyribonucleic acid	KIP	KINASE INHIBITORY PROTEIN
DP	DIMERIZATION PARTNER	KRP	KIP-RELATED PROTEIN
DRB	DOUBLE-STRANDED RNA BINDING PROTEIN	lncRNA	Long non-coding RNA
DREAM	DP, RB-LIKE, E2F AND MUVB	M	Mitosis
dsRNA	Double-stranded RNA	M.W.	Molecular weigth
DTT	Dithiothreitol	MCC	MITOTIC CHECKPOINT COMPLEX
DUF	DOMAIN OF UNKNOWN FUNCTION	MCM	MINICHROMOSOME MAINTENANCE
DUO1	DUO POLLEN 1	MI	Mitotic index
		MID	MIDDLE domain
		miRISC	miRNA-associated RISC
		miRNA	micro RNA
		mRNA	Messenger RNA
		MYB	MYELOBLASTOSIS

N-R		S-X	
NAC1	NAC DOMAIN-CONTAINING PROTEIN 1	S	DNA synthesis phase
NCBI	National center of biotechnology information	SAC	SPINDLE ATTACHMENT COMPLEX
NES	Nuclear export signal	SAM	Shoot apcal meristem
NLS	Nuclear localisation signal	SCF	SKP1 CULLIN1 F-box complex
nt	Nucleotide	SCN	Stem cell niche
ORC	ORIGIN RECOGNITION COMPLEX SUBUNIT	SDN1	SMALL RNA DEGRADING ENZYME 1
PAGE	Polyacrylamide gel electrophoresis	SDS	Sodium dodecyl-sulfate
PARE	Paralell analysis of RNA ends	SE	SERRATE
PAZ	PIWI/ARGONAUTE/ZWILLE domain	SGS3	SUPRESSOR OF GENE SILENCING 3
P-bodies	Processing-bodies	SHR	SHORTROOT
PCNA	PROLIFERATIVE CELL NUCLEAR ANTIGEN	SIM	SIAMESE
PEG	Polyethylene glycol	siRNA	Small interfering RNA
PIWI	P-ELEMENT INDUCED WIMPY TESTIS domain	SKP1/2	S-PHASE KINASE-ASSOCIATED PROTEIN 1/2
PLT	PLETHORA	SMR	SIAMESE-RELATED
PNK	POLY-NUCLEOTIDE KINASE	SPL	SQUAMOSA PROMOTER-BINDING-LIKE PROTEIN
PTGS	Post-transcriptional gene silencing	SQN	SQUINT
QC	Quiescent center	sRNA	Small RNA
qRT-PCR	Quantitative real-time PCR	tasiRNA	Trans-acting RNA
RACE	Rapid amplication of cDNA ends	TCP	TEOSINTE BRANCHED 1, CYCLOIDEA, AND PCNA-BINDING FACTOR
RAM	Root apical meristem	T-DNA	Transfer DNA
rasiRNA	Repeat-associated RNA	TF	Transcription factor
RB/RBR	RETINOBLASTOMA/RETINOBALSTOMA-RELATED	TGS	Transcriptional gene silencing
RBL1/2	RB-LIKE 1/2	Thr	Threonine
RBX1	RING-BOX 1	TIR1	TRANSPORT INHIBITOR RESPONSE 1
RdDM	RNA-dependent DNA methylation	TRBP	TAR RNA-BINDING PROTEIN
Rep	Replicate	tRF	tRNA-derived fragment
RING	REALLY INTERESTING NEW GENE	tRNA	Transfer RNA
RIP	RNA immunoprecipitation	TuYV	Turnip yellows virus
RISC	RNA-INDUCED SILENCING COMPLEX	Tyr	Tyrosine
RNA	Ribonucleic adic	U2B"	U2 SMALL NUCLEAR RIBONUCLEOPROTEIN B
RNA POLII/IV	RNA polymerase II/IV	Ubi	Ubiquitin
RNAi	RNA silencing	UPS	Ubiquitin proteasome system
RNA-seq	RNA sequencing	UTR	Unstranslated region
RNP	Ribonucleoprotein	Val	Valine
rpm	Rotation per minute	XRN1-4	EXORIBONUCLEASE 1-4
RPM	Reads per million		
RPS5	RIBOSOMAL PROTEIN S5		

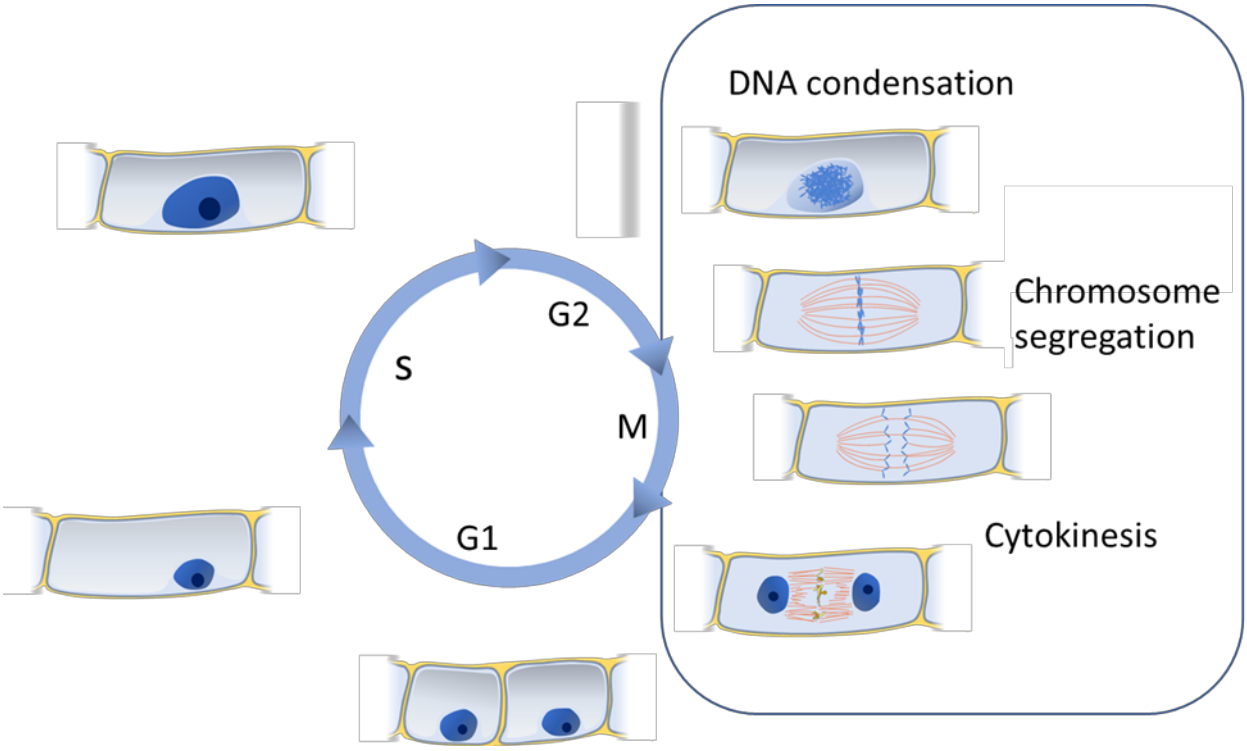

Figure 1 : The plant cell division cycle.

The Gap1 phase (G1) prepares entry of the cell in S phase during which the DNA is replicated. S phase is then followed by the Gap2 (G2) phase in which the cell is repairing DNA replication errors before the Mitosis (M). In mitosis, the nuclear envelop breaks down and the two genomic copies are separated. In late mitosis the two nuclear envelop reform and the cellular compartment is split by cytokinesis.

Introduction

A. The cell cycle in eukaryotes

1. General principles of cell cycle

The cell cycle is a biological process in which a mother cell gives rise to two genetically identical daughter cells. During this process, the cellular components, including the genome, are first duplicated and then equally distributed in the two newly formed cells. The cell cycle is fundamental, as it is involved in vegetative reproduction of unicellular organisms, but also in organ growth and sexual reproduction of more complex eukaryotes.

Cell cycle research started during the 19th century. In 1855, The German Rudolf Virchow was the first to claim that "a cell arises from another cell". Subsequently, different researchers described in detail the cytological aspect of cell division (Nurse et al., 1998). However, our mechanistic understanding of cell cycle regulation was only exploding in the 80s, with the development of molecular biology. The work of Paul Nurse and others (Leland Hartwell and Tim Hunt) on core cell cycle genes in yeast and human was awarded by a Nobel prize in Medicine and Physiology in 2001.

The cell cycle consists of the progression through four successive phases in a unidirectional way (Figure 1). The genome is first duplicated during the DNA synthesis phase (S). The two copies of the genome are then separated during mitosis (M), reaching the opposite sides of the cell before cytokinesis. In between these two main events, there are two latency phases called gap 1 and 2 (G1 and G2) where cells are checking the proper completion of the previous phase and preparing all the components that are required for the transition to the next phase. The M-phase of the cell cycle can itself also be subdivided into four steps: the prophase, metaphase, anaphase and telophase (Figure 2). During the prophase, the DNA is condensed into highly coiled chromosomes, the nuclear envelop breaks down and the mitotic spindle starts to form in the cytoplasm. In metaphase, the chromosomes reach the virtual plane of division (or metaphase plane) and attach to the mitotic spindle though specific regions on the chromatids, called kinetochores. Once paired to the microtubule fibers of the mitotic spindle, sister chromatids are separated and migrate in opposite directions during the

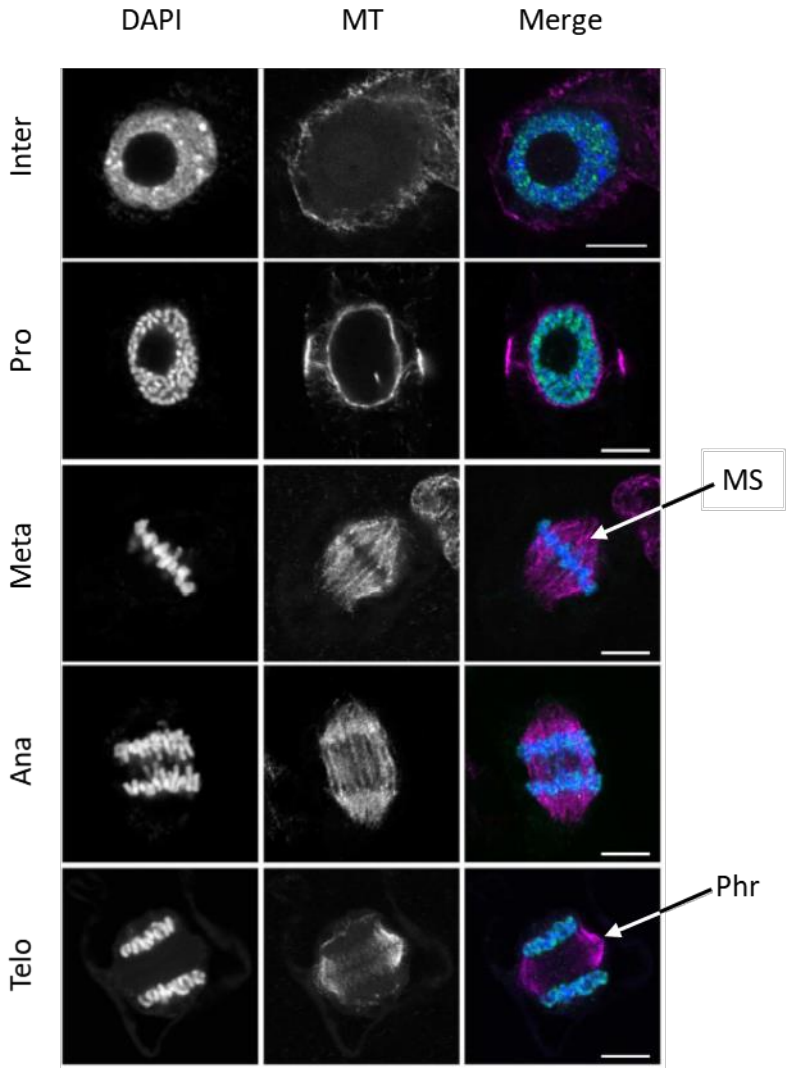

Figure 2 : Confocal imaging of mitosis in tobacco BY-2 cell suspension (adapted from Kurita et al., 2017).

DNA staining is realized using DAPI and microtubules were immunolabelled with anti-α-tubulin. During prophase DNA is condensed and MTs start to invade the nuclear compartment. In metaphase, the nuclear envelope has already disappeared, chromosomes reach the equatorial plan and the mitotic spindle attaches kinetochores. During anaphase, sister chromatids are separated and reach the opposite sides of the cell. The last step is the telophase, where the nuclear envelop reforms, DNA decondenses and the phragmoplast assembles the new cell plate. DAPI: 4',6-diamidino-2-phenylindole, MT: microtubules, MS: mitotic spindle, Phr: phragmoplast, Inter: interphase, Pro: prophase, Meta: metaphase, Ana: anaphase, Telo: telophase, scale bar: 50µm.

anaphase. Finally, the telophase consists of the reformation of the nuclear envelope and nuclear organelles, and the decondensation of the chromatin. The telophase occurs at the same time as scission of the cellular compartment, or cytokinesis. In animal cells, cytokinesis involves a contractile ring of actin filaments. In contrast, plant cells are coated with a cell wall conferring rigidity and preventing division in a similar matter. Instead, cytokinesis in plants requires active transport of material to the equatorial plate. This is achieved by a structure composed of microtubules, the phragmoplast, that is in charge of guiding the cell wall components through Golgian vesicular trafficking towards the division plane (Figure 1).

The sequential control of interconnected processes that constitute the cell cycle is critical for all organisms. In animals, the misregulation of cell division leads to abnormal cell proliferation and may cause tumorigenesis. Plants differ from animals by the fact that their organ development mainly occurs post-embryonically. Moreover, plants are sessile organisms. By consequence, they must adapt their developmental rate to face the resource availability, the environmental conditions and attack by pathogens. The cell cycle needs to be tightly regulated during the whole lifespan of the plant and this is accomplished by a set of essential "core cell cycle" genes. The following part of this thesis aims to give an overview of the cell cycle regulatory pathways in eukaryotes, with a particular emphasis on plants.

2. Cell cycle regulation

The evidence for molecular regulation of cell proliferation was provided in frog oocytes (Masui and Markert, 1971). Injection of progesterone-treated oocyte extracts was shown to stimulate mitosis and meiosis, suggesting the existence of a cytosolic "maturation/mitosis-promoting factor" (MPF). This MPF was then further discovered in *Schizosaccharomyces pombe* and characterized as a protein dimer containing the kinase CDC2 (CELL CYCLE CONTROL 2) and its cyclin partner (Gautier et al., 1988, 1990), two crucial players in the cell cycle further described below.

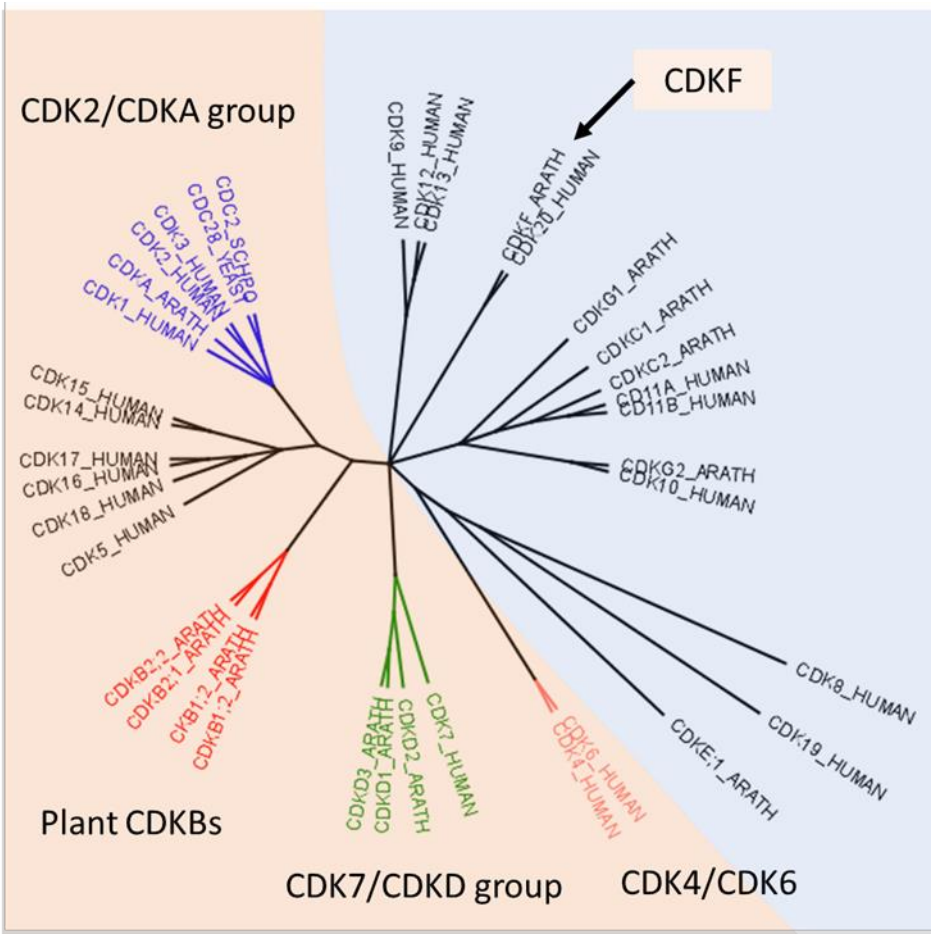

Figure 3 : Phylogenic comparison of yeast, human and plant CDKs based on protein sequences.

The orange group refers to CDKs involved in cell cycle regulation and the light blue group to transcription-related CDKs. The CDK2/CDKA subgroup (indicated in blue) includes CDKs with the canonical PSTAIRE motif in the cyclin-binding domain. Plants have gained a specific class of CDK, CDKBs with a PPTALRE and PS/PTTLRE motif (CDKB1 and CDKB2, respectively). The CDK4/CDK6 subgroup has no clear homologs in plants. The CDK7/CDKD subgroup corresponds to CDK-activating kinases (CAKs). Interestingly, the plant CAK CDKF is not related to this subgroup. YEAST: *Saccharomyces cerevisiae*, SCHPO: *Schizosaccharomyces pombe*, *ARATH: Arabidopsis thaliana.* Alignment was performed using MUSCLE multiple sequence alignment algorithm. The tree was build using Geneious program (Neighbour-joining method).

a. CDKs drive progression through the cell cycle

Cyclin-dependent kinases (CDKs) are serine-threonine kinases that require association with activating subunits called cyclins (CYCs) for their enzymatic activity (Malumbres, 2014). CDKs are found in all eukaryotes, including *Saccharomyces cerevisiae* (CDC28, PHO85, KIN28, SRB10, BUR1, CTK1), *Schizosaccharomyces pombe* (CDC2), Human (CDK1-20) and plants (CDKA-G). CDKs are classified in two groups: they are either involved in cell cycle regulation or transcriptional regulation (Malumbres, 2014; Joubès et al., 2000). Although the steady state level of cell cycle-related CDKs remains overall constant in proliferative tissues, their activity needs to be modulated during progression through the different cell cycle phases. This modulation is brought by interaction with cyclins that are, unlike CDKs, expressed and degraded at specific time periods during the cell cycle. Thus, different CDK/CYC complexes are formed during the cell cycle, which possess affinity for a wide variety of substrates, orchestrating the sequential activation of molecular processes such as transcription of cell cycle genes, DNA replication, DNA repair, chromatin packaging, cytoskeleton rearrangement and mitotic spindle assembly (Chi et al., 2008; Holt et al., 2010; Anders et al., 2011).

b. Diversity and functions of eukaryotic CDK/Cyclins complexes

The eukaryotic CDKs

Among the twenty human CDKs, only CDK1, 2, 3, 4 and 6 are promoting cell cycle transitions (Malumbres, 2014). These CDKs are classified in two subfamilies: the CDK1-2-3 and CDK4-6 groups (Figure 3). CDK1 is able to bind to all cyclins in the absence of other CDKs and is sufficient to drive a minimal cell cycle activity at early stages of embryogenesis (Santamaría et al., 2007). In addition, *cdk1-/-* knockdown or genetic substitution of *CDK1* by *CDK2* leads to embryo lethality, indicating that CDK1 is essential for cell division (Santamaría et al., 2007; Satyanarayana et al., 2008). Interestingly, *cdk2, 3, 4* and *6* mutations show genetic interactions. Mice *cdk2-/-*, *cdk4-/-* and *cdk6-/-* single mutants develop normally (Berthet et al., 2003; Ye, 2001; Tsutsui et al., 1999; Malumbres et al., 2004) and exhibit only phenotypes in highly specialized cell types. However, *cdk2-/-; cdk4-/-* and *cdk4-/-; cdk6-/-*

double mutants are embryonic lethal, suggesting at least a partial redundancy of CDK functions (Berthet et al., 2006; Malumbres et al., 2004).

Plant CDKs are divided in eight classes: CDKA to G (Figure 3). The *Arabidopsis thaliana* genome encodes a unique CDKA (CDKA1;1), four CDKBs (CDKB1;1-2 and CDKB2;1-2) , two CDKC (CDKC;1-2), three CDKD (CDKD;1-3), three CDKE (CDKE;1-3), one CDKF (CDKF;1) and two CDKG (CDKG;1-2) (Gutierrez, 2009; Van Leene et al., 2010). A-type CDKs share a conserved PSTAIRE cyclin-binding also found in yeast CDC2/CDC28 and in human CDK1,2 and 3 kinases (De Veylder et al., 2003, 2007). CDKBs are plant-specific CDKs that possess PPTALRE and PS/PTTLRE motifs (for CDKB1s and CDKB2s, respectively) (De Veylder et al., 2003, 2007). CDKA is absolutely required for the plant cell cycle. Indeed, loss of Arabidopsis CDKA affects pollen development and induces embryonic lethality (Iwakawa et al., 2006; Nowack et al., 2006). In addition, CKDA;1 but not CDKB is able to complement both *S. cerevisiae cdc28-/-* and *S. pombe cdc2-/-* mutants, indicating that CDKA;1 shares common functions with its yeast homologs (Ferreira et al., 1991; Porceddua et al., 1999). In contrast to CDKA, lack of CDKB1;1 function does not affect the overall cell cycle progression and mutants manage to develop normally. However, *cdkb1;1* mutant shows a fewer number of cells that are larger in size, which correlates with an increased ploidy level compared to control plants (Boudolf et al., 2016). This mutant is also impaired in stomatal division (Boudolf et al., 2016). Moreover, Arabidopsis *cdkb2;1* mutant plants show alteration of the shoot apical meristem organization (Andersen et al., 2008). This suggests that, although B-type CDKs functions are still unclear, they are involved in plant-specific processes. To a lesser extent, CDKDs and CDKF;1 are also playing a role in the cell cycle by activating others CDKs (Shimotohno, 2004; Umeda et al., 2005). This function will be discussed later in a dedicated chapter.

Cyclins

The term “cyclin” refers to the instability of these proteins. The discovery of the first cyclins was done in sea urchins eggs, where researchers highlighted the degradation of this protein during cell division (Evans et al., 1983). Cyclins are characterized by the presence of two common domains: the cyclin box that is necessary for CDK activation and that determines the substrate specificity, and the destruction box (D-box), required for their

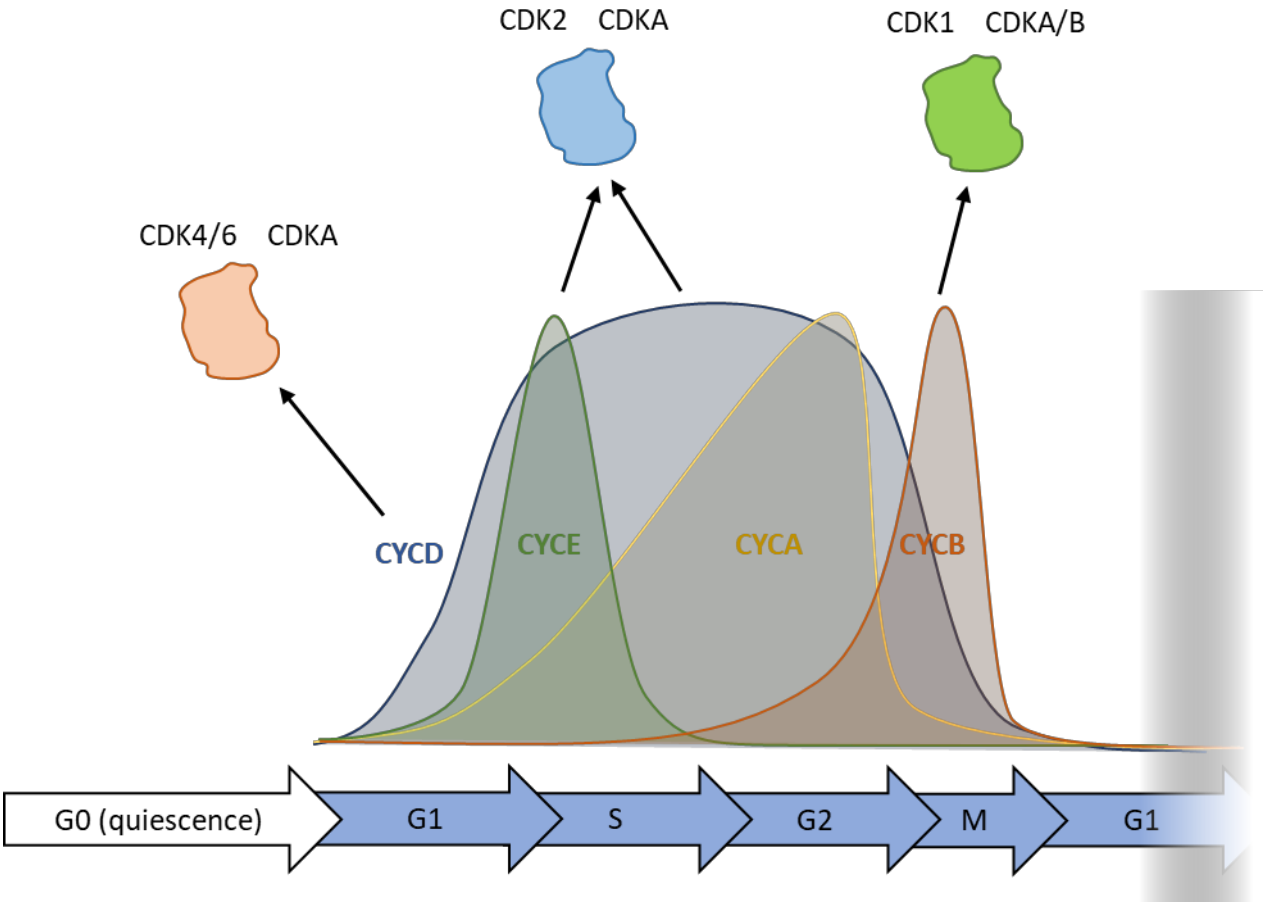

Figure 4 : Accumulation of cyclins and CDK activation through the mammalian cell cycle.

The steady state level of cyclins changes during cell cycle. Cyclins D is expressed upon mitogenic stimuli and remains constant during cell cycle. Cyclin E is expressed at G1/S transition. Cyclin A accumulates in S phase and G2, whereas Cyclin B in G2/M. The sharp decline observed for cyclins depends on their rapid destruction by the 26S proteasome. Cyclin concentration modulates CDK activity to coordinate specific cell cycle events, such as transcriptional burst, chromatin compaction and mitotic spindle dynamics.

proteolysis (Glotzer et al., 1991; Horton and Templeton, 1997). Eukaryotic cyclins are classified in two groups: the mitotic cyclins, that include A and B-type cyclins, and interphase cyclins, comprising the C, D and E-type cyclins. Different cyclins show specific accumulation patterns during cell cycle, that are related to their functions (Figure 4). CYCDs accumulate in early G1 and CYCEs during G1-S transition. Mitotic cyclins start to accumulate during G2 and reach a peak in mitosis. However, CYCA are degraded in prophase while CYCB are degraded later to exit mitosis(reviewed in Genschik et al., 2014).

In plants, a large family of cyclins is present, including more than 50 cyclins distributed in nine classes. Arabidopsis counts 10 CYCA (CYCA1;1-2 , CYCA2;1-4 and CYCA3;1-4), 11 CYCB (CYCB1;1-5, CYCB2;1-5 and CYCB3;1) and 10 CYCD (CYCD1;1, CYCD2, CYCD3;1-3, CYCD4;1, CYCD4;2, CYCD5;1, CYCD6;1 and CYCD7;1) (Nieuwland et al., 2007). As their human homologs, some of these plant cyclins have been well characterized. However other classes of plant cyclins have also been identified, including CYCC, CYCH, CYCL, CYCP , CYCT and SDS (SOLO DANCERS) (Nieuwland et al., 2007; Van Leene et al., 2011), but for most of them, their functions still need to be further investigated.

c. Regulation of CDK activity

CDK activation by cyclins

The ATP-binding pocket of CDKs is localized in a cleft in between the N-terminal and the C-terminal lobes. In absence of cyclins, a helix-loop called activation-loop or “T-loop” interferes with this domain (De Bondt et al., 1993; Morgan, 1997) (Figure 5). This results in the inability to bind to the substrates and in the mispositioning of the ATP molecule, preventing the transfer of the phosphate group. Upon CDK/CYC interaction, the T-loop is translocated and CDK activity is promoted. Cyclins not only activate CDKs, but also provide additional motifs required for relocalization of CDKs in the nucleus (Brown et al., 1999; Pines and Hunter, 1991) or for substrate recognition, thereby determining the CDK specificity.

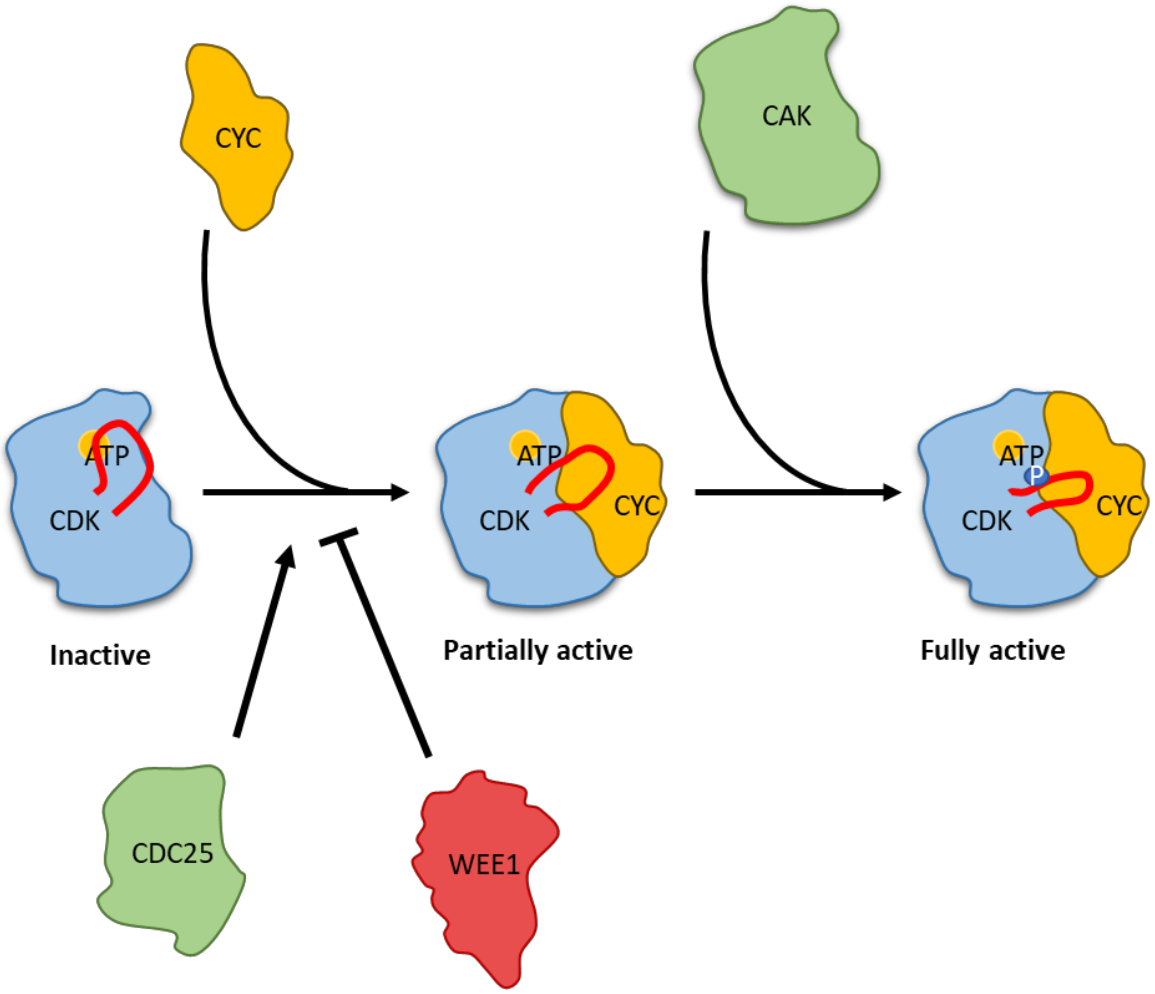

Figure 5 : Modulation of CDK activity.

When a CDK is not associated with cyclins, the T-loop (in red) interferes with the ATP-binding pocket, resulting in the inability to transfer a phosphate group. In addition, it also prevents interaction with the substrate. When bound to a cyclin, the T-loop is translocated. Cyclins also provide additional motifs that are required to bind specific substrates. Phosphorylation of the Thr160/Thr161 residues within the T-loop by CDK-activating kinases (CAKs) also participates to enhance CDK activity. Note that the WEE1 kinase and the CDC25 phosphatase play antagonistic roles on CDK activity by respectively adding and removing inhibitory phosphorylation marks on Thr14/Tyr15 residues.

Post-translational modifications of CDKs

While binding with cyclins is sufficient to activate CDKs, they require phosphorylation to be fully functional. Phosphorylation of the Thr160 residue of the human CDK2 or Thr161 of yeast CDC2, that is inside the T-loop, has been shown to enhance affinity of some CDK/CYC pairs (Ducommun et al., 1991; Desai et al., 1995; Russo et al., 1996) (Figure 5). Enzymes that catalyze this phosphorylation are named CDK-activating kinases (CAKs). CAKs have been identified as CDK/CYC-related dimers: MOP1/MCS2 and CDK7/CYC-H, respectively in fission yeast and human (Fesquet et al., 1993; Fisher and Morgan, 1994; Damagnez et al., 1995). In *Arabidopsis thaliana*, four CAKs have been identified: CDKF;1^{CAK1At}, CDKD;3^{CAK2At}, CDKD;1^{CAK3At} et CDKD;2^{CAK4At} (Shimotohno, 2004; Umeda et al., 2005). While CDKDs are related to the human CDK7, CDKF function is not dependent of CYC-H binding and is specific to plants.

Besides activation, CDKs can be post-translationally inhibited. Phosphorylation of Thr14/Tyr15 residues of the human CDK1 by the kinases WEE1 and MYT1 inhibits both ATP fixation and substrate binding to CDK, thus preventing entry into mitosis (Berry and Gould, 1996; Booher et al., 1997) (Figure 5). Arabidopsis WEE1, as well as the human WEE1/MYT1 kinases have been described to control the G2/M checkpoint and induce cell cycle arrest upon DNA damage sensing (De Schutter et al., 2007) (Figure 5). Dephosphorylation of these residues is required for the entry in mitosis. This process is performed by CDC25A, B and C phosphatases in human (Strausfeld et al., 1991; Morgan, 1997). Interestingly, plants seem to lack CDC25 function and it is still unclear and debated how WEE1 inhibition is released in mitosis (Boudolf et al., 2006).

CDK/Cyclins inhibitors (CKIs)

Besides phosphorylation, inhibition of CDK activity is also mediated by CDK-binding proteins that are the CDK inhibitors (CKIs). In human, two distinct families of CKIs exist: the KIP/CIP (KINASE INHIBITORY PROTEIN / CDK INHIBITORY PROTREIN) proteins and INK4 (INHIBITOR OF CDK4/6) (Besson et al., 2008). CKIs that belong to the INK4 (p16^{INK4a}, p15 ^{INK4b}, p18 ^{INK4c}, p19 ^{INK4d}) family bind only to CDK4 and 6 and prevent binding to D-type cyclins (Serrano et al., 1993; Hirai et al., 1995) (Figure 6). CKIs from the KIP/CIP

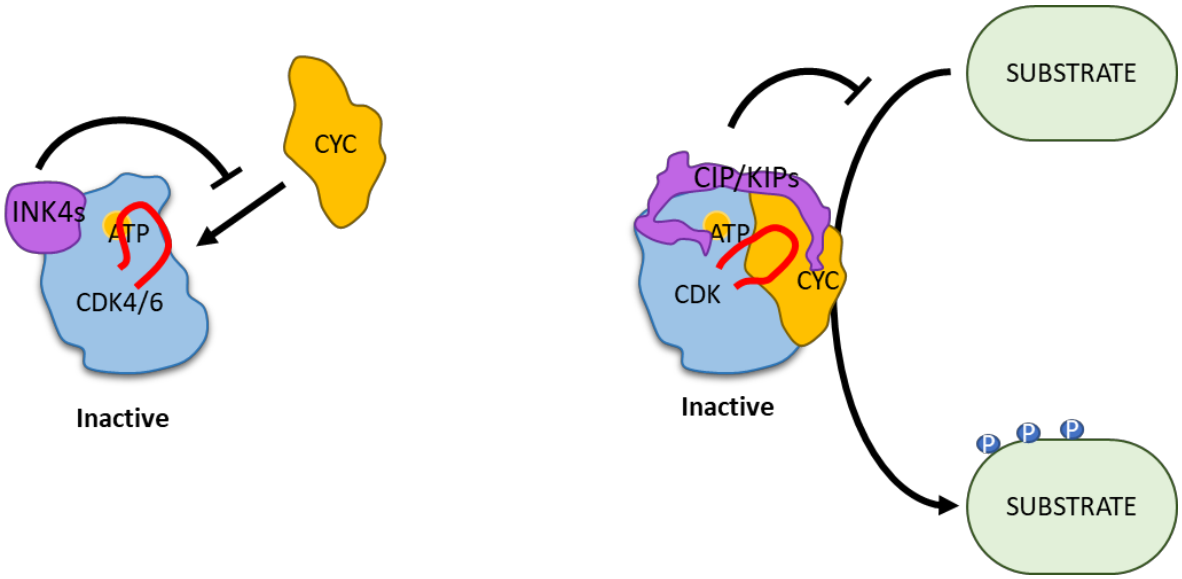

Figure 6 : Mode of action of CDK inhibitors.

Mammalian INK4 proteins are specifically binding CDK4 and CDK6 and interfere with cyclin association. In contrast, CIP/KIPs are able to bind to any CDK or CDK/cyclin complexes and inhibit substrate recognition.

family ($p21^{CIP1}$, $p27^{KIP1}$, $p57^{KIP2}$) inhibit the activity of cyclin -D, A, E and B-dependent kinases by binding to CDK/CYC complexes (Besson et al., 2008) (Figure 6). While the modes of action CKIs are similar, their function is specific to certain biological contexts (Cánepa et al., 2007). As such, INK4 proteins are involved in cellular senescence, apoptosis and DNA repair (Cánepa et al., 2007). p21 is expressed in response to DNA damage and induces cell cycle arrest during gap phases. p27 is involved in cell cycle exit in normal conditions. In addition to p27, p57 is also an essential gene during mouse embryogenesis, as it is required for proper cell differentiation (Tateishi et al., 2012).

In Arabidopsis, 21 CKIs are present, divided into two groups. The KRP/ ICK (KIP-related protein/ inhibitor of CDC2 kinase) family is composed of seven members that are orthologs of the human KIP/CIPs (Kumar and Larkin, 2017), and that show a high level of functional redundancy. The other family, the SIM/SMR (SIAMESE/SIAMESE-RELATED) counts 14 members (SIM and SMR1-13) (Kumar and Larkin, 2017). They are specific to plants and share no homology with any other eukaryotic CKIs. Like in animals, plant CKIs play distinct functions on plant growth and development mainly because of differences in their expression patternsF (Kumar et al., 2015). KRPs have been shown to stimulate endoreduplication by blocking mitosis (Verkest et al., 2005), and even promote cell cycle arrest and cell death at high expression level (Schnittger et al., 2003) . Interestingly, several members of the SIM/SMRs family were found to be transcriptionally induced in response to stress, leading to the hypothesis that SMRs may be involved in integrating environmental signals with cell cycle control (Peres et al., 2007; Yi et al., 2014; Kumar and Larkin, 2017). For instance, oxidative stress, or hydroxyurea, induces reactive oxygen species (ROS) production and *SMR4*, *SMR5*, and *SMR7* transcript levels, and *smr5* and *smr7* mutants are more tolerant to hydroxyurea treatments (Yi et al., 2014). More recently it was shown that under moderate drought, both the *SMR1* transcript and SMR1 protein accumulate and that *smr1* mutants show less growth inhibition of young leaves under drought (Dubois et al., 2018).

d. Selective degradation of cell cycle components

To orchestrate cell cycle progression, cells not only require the synthesis of cell cycle specific regulators but also need their quick and selective degradation with a specific timing.

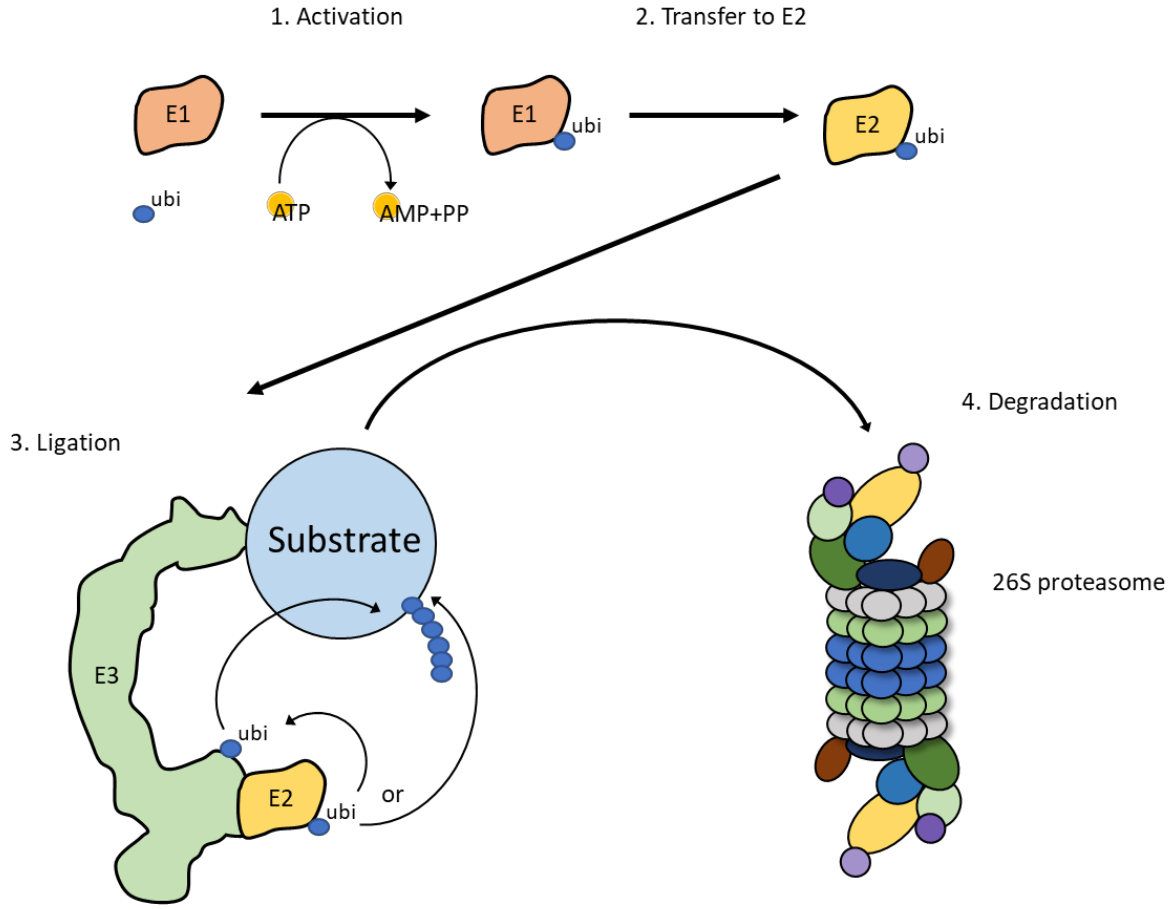

Figure 7 : Principles of the ubiquitin proteasome system (UPS).

(1) Ubiquitin is first activated by a ubiquitin activating (E1) enzyme by a process that is ATP-dependent. (2) The E1 transfers the ubiquitin peptide to the ubiquitin conjugating enzyme (E2). (3) Then, the E2 associates with the ubiquitin ligating (E3) enzyme. Either the E2 directly transfers ubiquitin to the substrate, or ubiquitin is first transferred to the E3 that is subsequently in charge of substrate ubiquitination. Ubiquitin is attached to the ε-amine of lysine residues of target proteins. The polyubiquitination of the substrate often triggers its degradation by the 26S proteasome. Prior to substrate degradation the ubiquitin chain is depolymerized and ubiquitin can further be reused by an E1. Ubi: ubiquitin, ATP: Adenosine triphosphate, AMP: Adenosine monophosphate, PP: Pyrophosphate.

This process involves the ubiquitin proteasome system (UPS) (Mocciaro and Rape, 2012; Genschik et al., 2014) that is based on enzymes called E3 ubiquitin protein ligases (E3s). E3 ligases act as monomer or protein complexes to catalyze covalent attachment and/or polymerization of a small 76-amino acids peptide called ubiquitin on Lysine residues. Ubiquitination is a post-translational modification that, depending on the topology of the ubiquitin chain, is involved in either DNA repair, chromatin remodeling, signaling, cellular trafficking or 26S proteasome-dependent degradation (Ciechanover et al., 2000; Kwon and Ciechanover, 2017). The mechanism of ubiquitin transfer to a substrate requires three different steps (Figure 7) (Ciechanover et al., 2000; Vierstra, 2009; Callis, 2014). Ubiquitin is first adenylated on the C-terminal position by the "activating enzyme" E1 and transferred on a E1 cysteine residue. It is subsequently transferred to a cysteine residue of a "conjugating" E2 enzyme. Depending on the type E3, ubiquitin-coupled E2 can either bind to the E3 and directly be conjugated the substrate or can first be transferred to a cysteine residue on the E3, that will further be in charge of substrate ubiquitination, resulting in its degradation by the 26S proteasome. Cell cycle-specific proteolysis involves four classes of E3: the SCF (SKP1/Cullin1/F-box) E3s, the APC/C (Anaphase promoting complex/cyclosome) complex, the monomeric RING-proteins and CRL4-CDT2 (Mocciaro and Rape, 2012; Genschik et al., 2014) (Figure 8).

SCF complexes

SCF complexes are assembled around the CUL1 (CULLIN 1) scaffolding protein (Petroski and Deshaies, 2005). The CUL1 is forming a bridge to bring together the catalytic module composed of RBX1 (RING-BOX 1) and the E2, and the substrate recognition module, including both SKP1 (called ASK1-2 in Arabidopsis, for ARABIDOPSIS SKP1 HOMOLOGUE 1/2) and an F-box protein. F-box proteins are adaptor proteins that provide the specificity for the substrate (Kipreos and Pagano, 2000; Lechner et al., 2006; Reitsma et al., 2017). In animals, the SCF^{SKP2} (S- PHASE KINASE ASSOCIATED PROTEIN 2) is playing a role from the G1/S transition to the exit from the S phase (Figure 9). It triggers ubiquitination of CKIs such as $p21^{CIP1}$ and $p27^{KIP1}$ (Nakayama, 2000; Starostina and Kipreos, 2012), thus promoting re-entry into the cell cycle, but also ubiquitination of S phase-specific components like cyclin E, E2Fs transcription factors and CDT1 (Nakayama, 2000; Marti et al., 1999; Li et al., 2003), leading to the transcriptional repression of S-phase genes and

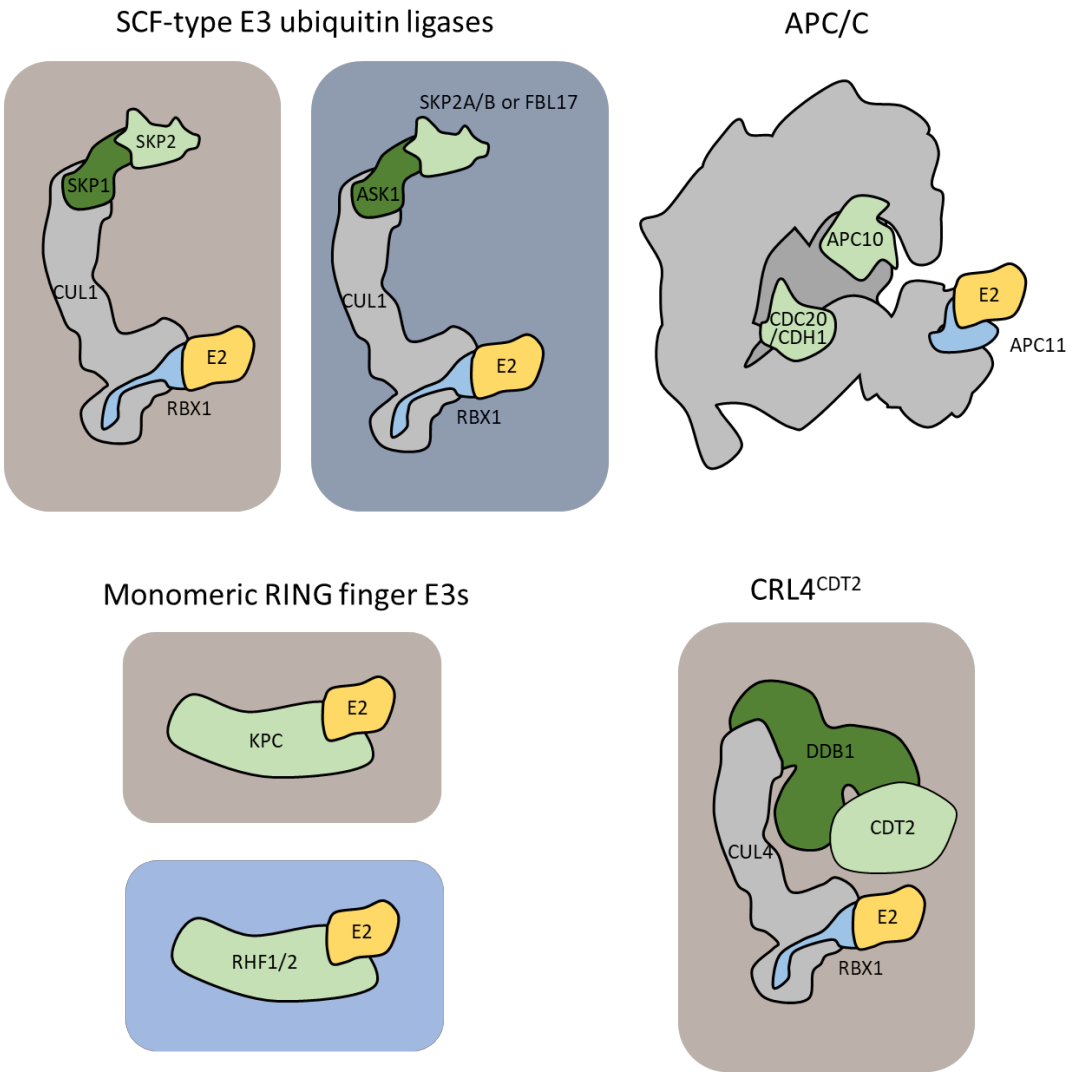

Figure 8 : Different classes of ubiquitin E3 ligases involved in cell cycle regulation.

Grey corresponds to the scaffolding proteins (and most of the subunits for the APC/C). Proteins in light green are required for substrate recognition. The E2 conjugating enzymes are represented in yellow. Dark green and blue proteins bridge respectively the substrate recognition modules and the E2s to the scaffold. Orange in background refers to animal specific E3s, whereas the blue refers to plant E3s. SCF and CRL4 are both cullin-based E3s and contain the RING-finger protein RBX1 that interacts with the E2. They possess a different substrate recognition module: SKP1 or ASK1 (in plants)/Fbox proteins for the SCF and DDB1/DCAF proteins for the CRL4 complex. The APC/C is the largest E3, which is composed of core subunits (APC1-15) and several coactivators (CDC20 and CDH1/CCS52). APC10 and coactivator proteins are required for substrate recognition, while APC11 binds to the E2 enzyme. The last class represents monomeric RING finger E3 ubiquitin ligases that bind directly to their substrates and to the E2s though their RING domain.

replication shutdown. Homozygous *skp2* mice are smaller but still viable (Nakayama, 2000). However, cells show a lower growth rate, higher level of polyploidy and increased apoptosis, suggesting that, even though SKP2 is not crucial for cell cycle progression, it is involved in controlling chromosome duplication. Two homologs of SKP2, SKP2a and SKP2b, have been identified in Arabidopsis (del Pozo et al., 2002). While SKP2a has been shown to mediate degradation of E2Fc/DPb, SKP2b was proposed to target KRPs to the proteasome (Ren et al., 2008). Double knockout mutants of SKP2a and SKP2b do not alter plant growth and development, suggesting the existence of other E3s that control the entry and the proper completion of the S phase. Another Arabidopsis F-box protein, FBL17, has also been identified as a master regulator of cell cycle during male gametogenesis, and more recently, of cell proliferation and endoreduplication (Kim et al., 2008; Gusti et al., 2009; Noir et al., 2015). *fbl17* mutants show a significantly reduced growth rate together with defects in chromosome separation. At the molecular level, the KRP2 protein level increased in *fbl17* mutants, affecting the activity of CDKA;1 (Noir et al., 2015).

Anaphase-promoting complex/Cyclosome

The Anaphase Promoting Complex/Cyclosome (APC/C) is a large E3 ubiquitin ligase complex including at least 12 subunits and necessary coactivators that are CDC20 (CELL CYCLE CONTROL 20) and CDH1 (CDC20 HOMOLOG 1) in human or CCS52 in plants (Peters, 2006; Genschik et al., 2014). Among these proteins, $DOC1^{APC10}$ is also in charge of binding the substrate, APC11 binds to the E2 conjugating enzyme and APC2, that shares homology with the CULLINs, is docking both $DOC1^{APC10}$ and APC11. CDC20 and CDH1 together with $DOC1^{APC10}$ are required for the specificity of the substrate (Chang and Barford, 2014). The role of the APC/C is crucial for mitosis and its activity is highly regulated during cell cycle progression (Figure 10). During S phase and G2, the APC/C is inactivated by EMI1 (EARLY MITOTIC INHIBITOR 1) to allow accumulation of CYCLIN A and B, thus promoting DNA replication and progression through G2. At the onset of mitosis EMI1 degradation is mediated by another E3: $SCF^{\beta\text{-}TrCP}$ (Margottin-Goguet et al., 2003), triggering the destruction of CYCLIN A by the APC/C^{CDC20}.However, the main feature of APC/C^{CDC20} is the polyubiquitination of the SECURIN in metaphase. Once the SECURIN is degraded, the SEPARASE is released and then cleaves the COHESIN rings that maintain the sister

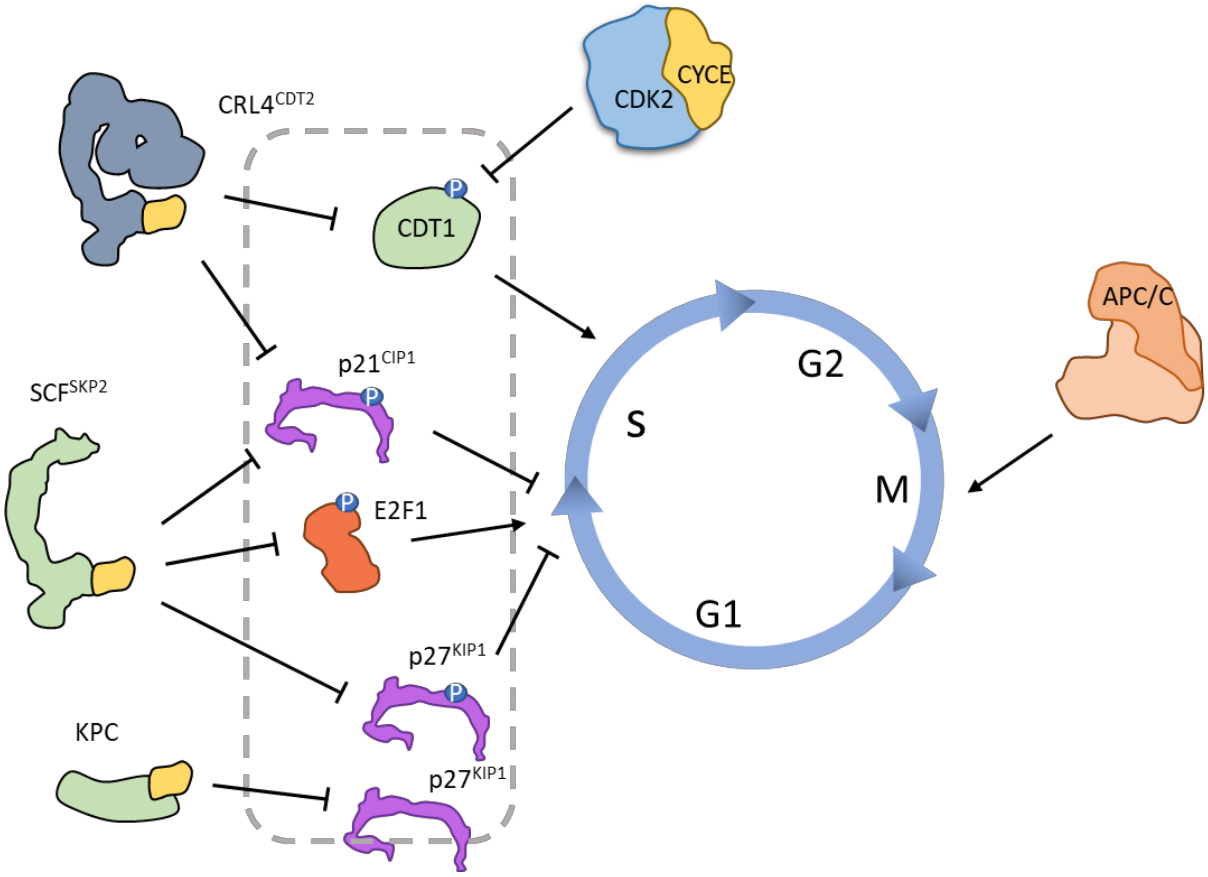

Figure 9 : Progression through cell cycle is controlled by different E3 ubiquitin ligases.

The G1/S transition requires the degradation of CDK inhibitors. Mammalian KPC and SCF^{SKP2} E3s ubiquitinylate $p21^{CIP1}$ and $p27^{KIP1}$ allowing cell cycle re-entry. In S phase, E2F1 level is tightly controlled by the SCF^{SKP2} to finely modulate S phase gene expression. In addition, $CRL4^{CDT2}$ targets p21 and CDT1 to prevent DNA overreplication during S phase. Note that SCF^{SKP2} and $CRL4^{CDT2}$ target specifically proteins that are phosphorylated by CDK2/CYCE complex. Lastly, the APC/C activity is mostly required to orchestrate Mitosis.

chromatids together (Zur and Brandeis, 2001). This mechanism is also controlled negatively by three SAC (Spindle Assembly Checkpoint) proteins, MAD2 (MITOTIC ARREST-DEFICIENT 2), BUB3 (BUDDING UNINHIBITED BY BENZYMIDAZOL 3), and BUBR1(BUB1-RELATED) that form the MCC (Mitotic Checkpoint Complex) and sequester CDC20 in order to check the proper attachment of the sister chromatids before enabling chromatids segregation (London and Biggins, 2014; Komaki and Schnittger, 2017). During telophase, APC/C^{CDH1} mediates CYCLIN B degradation and allow exit from mitosis. During mitosis, AURORA-A kinase phosphorylates the GEMININ to protect it from being recognized by the APC/C. GEMININ binds to CDT1 (CDC10-DEPENDENT TRANSCRIPT 1), thus preventing the assembly of the replication complex (Tsunematsu et al., 2015). During G1, AURORA-A is ubiquitinated by APC^{CDH1} and degraded, allowing the subsequent degradation of the non-phosphorylated form of the GEMININ by the 26S proteasome.

Monomeric RING E3 ligases

In human, a monomeric RING E3 called KPC1 (KIP1 ubiquitination-promoting complex 1) promotes the degradation of $p27^{KIP1}$ during G1 (Figure 9) (Liu et al., 2008; Morgan, 1997; Kamura et al., 2004). In contrast to SCF^{SKP2} activity, KPC1-mediated $p27^{KIP1}$ ubiquitination does not depend on its phosphorylation by CDK2. In addition, KCP1 has also a role in limiting tumour development (Kravtsova-Ivantsiv et al., 2015). NF-κB1 is a transcriptional regulator that is involved in several cellular processes including cell proliferation. However, the NF-κB1precursor (p105) needs to be processed by the 26S proteasome to form an active p50 dimer. Hence, it was shown that accumulation of KPC1 triggers p105 polyubiquitination and its subsequent processing (Kravtsova-Ivantsiv et al., 2015).

A possible plant ortholog of KPC1, called RKP (RELATED TO KPC1) has been identified in Arabidopsis(Liu et al., 2008). Loss of RKP leads to accumulation of KRP1, but does not affect plant growth (Ren et al., 2008). Notably, two additional RING E3 ligases, RHF1a and RHF2a (RING-H2 GROUP F1A/2A), that are required for plant gametogenesis, have also been identified (Liu et al., 2008). Indeed, *rhf1a rhf2a* double mutant shows an increased level of KRP6 protein that correlates with cell division defect in both male and female gametophyte.

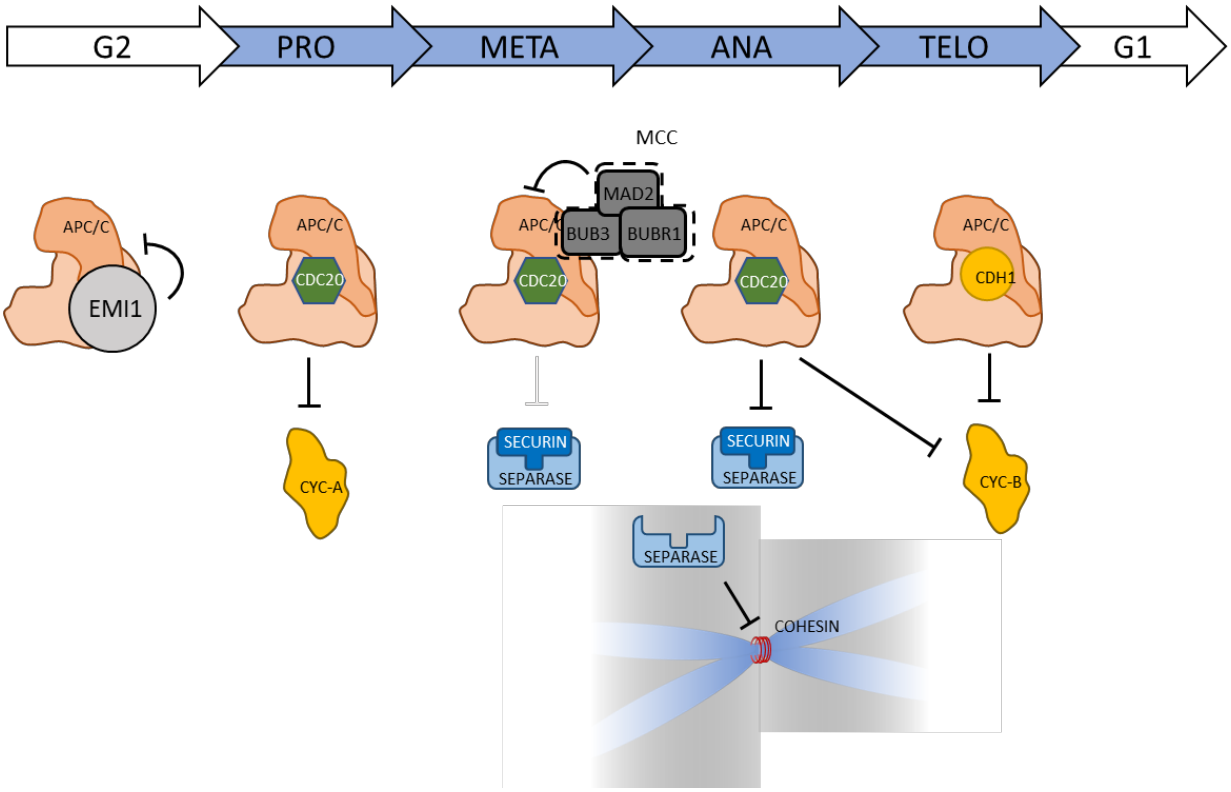

Figure 10 : APC/C activity during Mitosis.

In S and G2, APC/C activity is inhibited by EMI1 that binds to it through its dBox motif. The APC/C becomes then activated from prophase to telophase by binding coactivators CDC20 and CDH1 (or CDC20 and CCS52 in plants). In metaphase, the APC/C activity is temporally blocked by the MCC (mitotic checkpoint complex) composed of MAD2, BUB3 and BUBR1. When the mitotic spindle attachment to kinetochores is complete and all chromosomes are aligned on the equatorial plate, APC/C activity is released and can trigger SECURIN degradation. Consequently, SEPARASE is activated and degrades the COHESIN ring, thus initiating chromatids segregation. In telophase, APC/C also polyubiquitinylates B-type cyclins allowing exit from mitosis.

The mammalian $CRL4^{CDT2}$ complex

Cullin–RING ligase 4 (CRL4) are structurally and functionally related to the SCF. CRL4 ubiquitin ligases are composed of a CULLIN 4 scaffold that binds the E2 and a substrate recognition module including an adaptor protein called DDB1 (DNA DAMAGE-BINDING PROTEIN 1) and a DCAF protein (DDB1-CULLIN4 ASSOCIATED FACTOR) (Havens and Walter, 2011; Jackson and Xiong, 2009). One of these complexes, $CRL4^{CDT2}$, contains the DCAF CDT2 (CDC10-DEPENDENT TRANSCRIPT 2) and is involved in the control DNA replication and DNA repair. CDT1 protein is required for the recruitment of the MCM2-7 (MINICHROMOSOME MAINTENANCE 2-7) helicase at origin of replication (Nishitani et al., 2004). This process occurs during G1 and CDT1 is immediately destroyed in S phase to prevent any reinitiation and overreplication (Figure 9) (Nishitani et al., 2004). Chromatin-associated CDT1 degradation was shown to be dependent of CRL4-type E3, and particularly $CRL4^{CDT2}$ (Higa et al., 2006; Jin et al., 2006; Ralph et al., 2006; Sansam et al., 2006) . In addition, $CRL4^{CDT2}$-dependent degradation of CDT1 has also been observed in response to DNA damage (Higa et al., 2006; Ralph et al., 2006).

e. Transcriptional regulation of cell cycle genes

During cell cycle progression, cells are going through several waves of intensive gene transcription, especially during G1/S and G2/M transitions. This transcriptional regulatory process is driven by the activity of CDK/CYC complexes.

Control of G1/S transition

In animals and plants, the G1/S transition is mainly governed by the RB/E2F pathway. E2Fs (ADENOVIRUS EARLY GENE 2 BINDING FACTOR) proteins are transcription factors that promote the transcription of genes required in S phase, especially core cell cycle genes (CDC6, CDC25, CYCE,…) and components for replication (ORCs, CDT1, MCM3, PCNA, POLα, …) (Stevens and La Thangue, 2003; Gutierrez, 2009). In non-proliferating cells, E2Fs are bound to the transcriptional inhibitor called RETIBLASTOMA (RB) (Dick

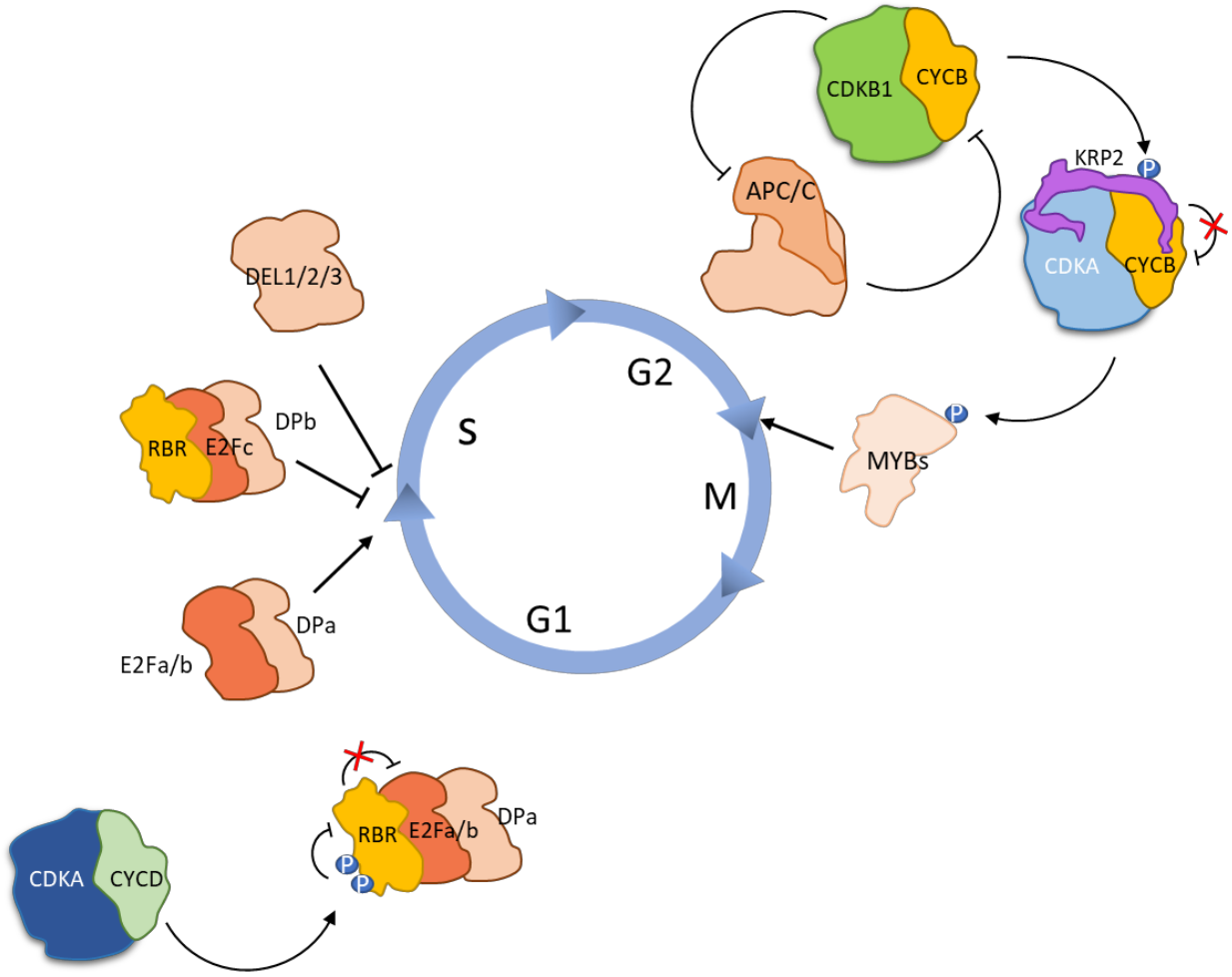

Figure 11 : Transcriptional control of G1/S and G2/M transitions in plants.

CDK/Cyclin complexes are negatively controlled by CDK inhibitors (not represented). Once the CDKA/cyclin D complexes are active at G1/S, they phosphorylate RBR, thus releasing E2Fs transactivating activity. E2Fs and their coactivators DPs transcriptionally control genes that are required for entry in S phase and DNA replication. Note that E2Fc and DEL proteins are transcriptional inhibitors. The G2/M transition requires the accumulation of B-type cyclins. CDKB/CYCB complex both represses APC/C and the CDK inhibitors such as KRP2, allowing the CDKA/CYCB to further activate M phase specific MYBs transcription factors.

and Rubin, 2013). Upon mitogenic stimuli, RB is phosphorylated by CYCD-E/CDK2 complexes leading to the activation of transcription by E2Fs. In human, the E2F family comprises six E2Fs (E2F1-6) and two more distant DP members (DIMERIZATION PARTNER, DP1 and DP2), whereas the pocket protein family is composed of 3 members: RB, p107^{RBL1} and p130^{RBL2} (RETINOBLASTOMA LIKE 1-2). E2Fs can be classified in three subgroups, E2F1-3, E2F4-5 and E2F6. They all possess the common E2F-binding site that targets the consensus promoter sequence (TTTSSCGS) and the DP dimerization binding sequence. However, the E2F4-5 subgroup lacks the CYCA-binding site and the nuclear localization signal (NLS) present in the E2F1-3 subgroup but acquired a nuclear export signal (NES) instead. E2F6 is even more distant, as it also lacks the transactivation domain and therefore acts as a transcriptional repressor most likely by titrating E2F-promoter sequences (reviewed in Stevens and La Thangue, 2003). The transcriptional inhibition by RB proteins works through different mechanisms. Binding to E2F is sufficient to hide the transactivating domain and repress the recruitment of the transcriptional machinery. In addition, RB can also bind chromatin-remodelling proteins, such as histone deacetylases (HDACs) and the Polycomb complex (Luo et al., 1998; Dahiya et al., 2001). Note that in mammals, the retinoblastoma-E2F pathway is also regulated by the ubiquitin-proteasome system (Sengupta and Henry, 2015).

The E2F pathway is also highly conserved in worms, flies and plants (Shen, 2002; Van Den Heuvel and Dyson, 2008; Berckmans and De Veylder, 2009). The Arabidopsis genome encodes three E2Fs (E2Fa, b and c), two DPs (DPa and DPb) and one RB-related protein (RBR1) (Figure 11). In parallel, three other non-canonical E2F proteins are also present. Conversely to E2F and DP, E2Fd^{DEL1}, E2Fe^{DEL2} and E2Ff^{DEL3} (DP AND E2F LIKE) do not need to form a E2F/DP dimer to bind to DNA. Plant E2Fs are not only regulated through the binding with RBR1 but are also subjected to transcriptional and post-translational regulatory mechanisms (Ramirez-parra et al., 2008). For instance, E2Fa, E2Fb, E2Fc and E2Ff^{DEL3}are strongly enriched in proliferating cells and E2fb and c show a cell cycle regulated expression pattern, peaking in S phase (Menges et al., 2005). Moreover, E2Fs and DPs can be phosphorylated by CDK/CYC complexes. Although the role of E2F/DP phosphorylation is not fully understood, phosphorylated forms of E2Fc and DPb are targeted to 26S proteasomal degradation by the SCF^{SKP2A} (del Pozo et al., 2002).

Control of G2/M transition

In human, transcriptional activation of G2/M-related genes requires two transcription factors that are B-MYB (B-MYELOBLASTOSIS) and FOXM1 (FORKHEAD BOX M1). B-MYB belongs to the MYB family, that is composed of 3 members: A-MYB, B-MYB, C-MYB (or MYBL2, MYBL1 and MYB, respectively) (Musa et al., 2017). While A-MYB and C-MYB are expressed in specific cell types, B-MYB is highly enriched in proliferative cells (Ness, 2003). The essential nature of B-MYB transactivation activity is illustrated by the early embryonic lethality of B-MYB knockout mutation in mice (Tanaka et al., 1999). In parallel, the *foxm1 -/-* mutation shows also an embryonic lethal phenotype in mice, delays G2 phase and strongly impairs chromosome segregation and cytokinesis in cultured cells (Kalin et al., 2011; Laoukili et al., 2005). Both B-MYB and FOXM1 interact with specific binding sites present in the promoter region of G2/M expressed genes. Among B-MYB/FOXM1-responsive genes, one can find components of the core cell cycle machinery (CYCA/Bs, CDK1/2, CDC25B, PLK1) and genes involved in mitotic spindle assembly and cytokinesis (Musa et al., 2017; Costa, 2005). The timing of B-MYB and FOXM1 activity is however different, which can be partly explained by their activation through CDK/CYC complexes. B-MYB and FOXM1 are activated by phosphorylation in G1/S and G2/M by CDK2/CYCA and CDK1/CYCB complexes, subsequently promoting the recruitment of a $p300^{CBP}$ coactivator (Schubert et al., 2004; Major et al., 2004).

Plants also possess MYB-related proteins. Arabidopsis genome encodes more than hundred MYB proteins. Among them, MYB3R1,2,3,4,5 are involved in the regulation of G2/M genes by activating or repressing their expression (Haga et al., 2007, 2011). Like human MYBs, MYB3Rs bind to a MYB-specific activation (MSA) cis-element that is sufficient to drive or inhibit gene expression (Ito, 1998). Consistent with their function in the regulation of mitotic-related genes, loss of both MYB3R1 and 4 induces defects during cytokinesis but do not lead to embryonic lethality, suggesting that other factors might be involved in this process (Haga et al., 2007, 2011). Studies on a synchronized BY-2 tobacco cell suspension revealed that transcription of *NtMYBs* genes occur during G2/M (Figure 11) (Ito et al., 2001). In addition, phosphorylation by CDKA/CYCA and B complexes has been shown to activate *NtMYBs* transactivation capability (Araki et al., 2004).

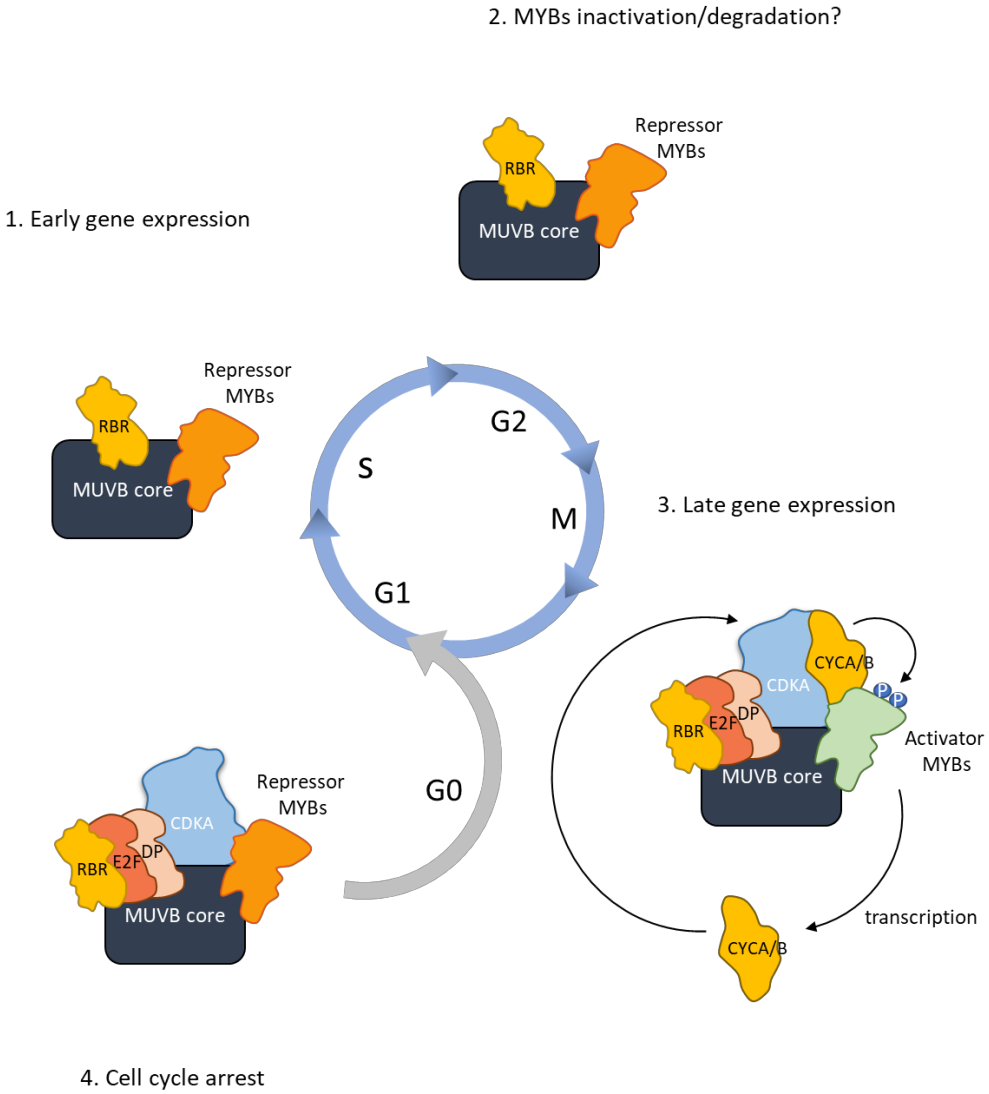

Figure 12 : Plant MUVB complex oscillates between transcriptional activation and repression.

In proliferative cells, MUVB complex is regulating both early and late gene expression. **(1)** During G1, S and G2, the MUVB core associates with RBR and repressor MYBs, to repress expression of M phase related genes. This process is acting synchronously with the activation of S phase gene by the E2F/DP pathway. **(2)** In late G2, repressor MYBs are repressed, presumably by proteasomal degradation. **(3)** At the start of mitosis, MUVB binds with activator MYBs to activate expression of M phase genes. CDKA is also a part of the complex and contributes to enhance MYBs transactivation activity by phosphorylation. In parallel, it also binds to the E2F/DP/RBR module to repress expression of S phase gene. **(4)** In quiescent cells, MUVB complex integrates both RBR/E2F/DP module and repressor MYBs to repress both S and M phase gene expression.

The DREAM and MMB complexes

More recent studies highlighted the existence of a larger MUVB-containing complex that control cell cycle transitions by activating and repressing transcription of cell cycle-specific genes (Fischer and Müller, 2017). The human core MUVB complex (MULTI VULVA-B) is composed of five proteins that are LIN9, LIN37, LIN52, LIN54 and $p55^{RBBP4}$ (RETINOBLASTOMA-BINDING PROTEIN 4). LIN9 was proposed to bring all the components of the MUVB complex together. LIN52 and LIN54 bind p107/p130 and CHR DNA motif (cell cycle gene homology region), respectively. p55 interacts with histones H3 and H4 by a WD40 motif and possibly participates in gene repression by interacting with chromatin remodelling complexes. Positive or negative control of gene expression is depending on additional proteins that are bound to MUVB. For instance, E2F1-3/DP/p107 or p130/MUVB, also called DREAM (DP, RB-like, E2Fs and MUVB), repress G1/S genes expression while B-MYB/FOXM1/MUVB or MUVB-MMB (MYB-MUVB) activates the expression of G2/M genes.

In Arabidopsis, components of the DREAM-like complex have also been identified (Magyar et al., 2016). The plant MUVB-like core complex includes the LIN54 ortholog TCX5 (TSO1-LIKE CxC 5) and the LIN9 orthologs ALY2/3 (ALWAYS EARLY 2 and 3) (Magyar et al., 2016; Fischer and Müller, 2017). RBR1, CDKA, E2Fs, DPs and MYB3Rs proteins can also be part of the DREAM. The plant DREAM complex functions are less documented than its mammalian counterpart. However, recent studies showed that, it can activate or repress expression of G2/M gene in a phase-specific fashion (Figure 12) (Kobayashi et al., 2015a, 2015b).

f. Cell cycle regulation by non-coding RNAs

As we discussed it in the previous part, cell cycle gene expression is timely controlled by specific transcription factors. However, transcription is not sufficient to explain the rapid turnover of the transcripts from one phase to the other. Recent researches revealed that other transcriptional and post-transcriptional pathways involving non-coding RNAs are playing a role in silencing these genes.

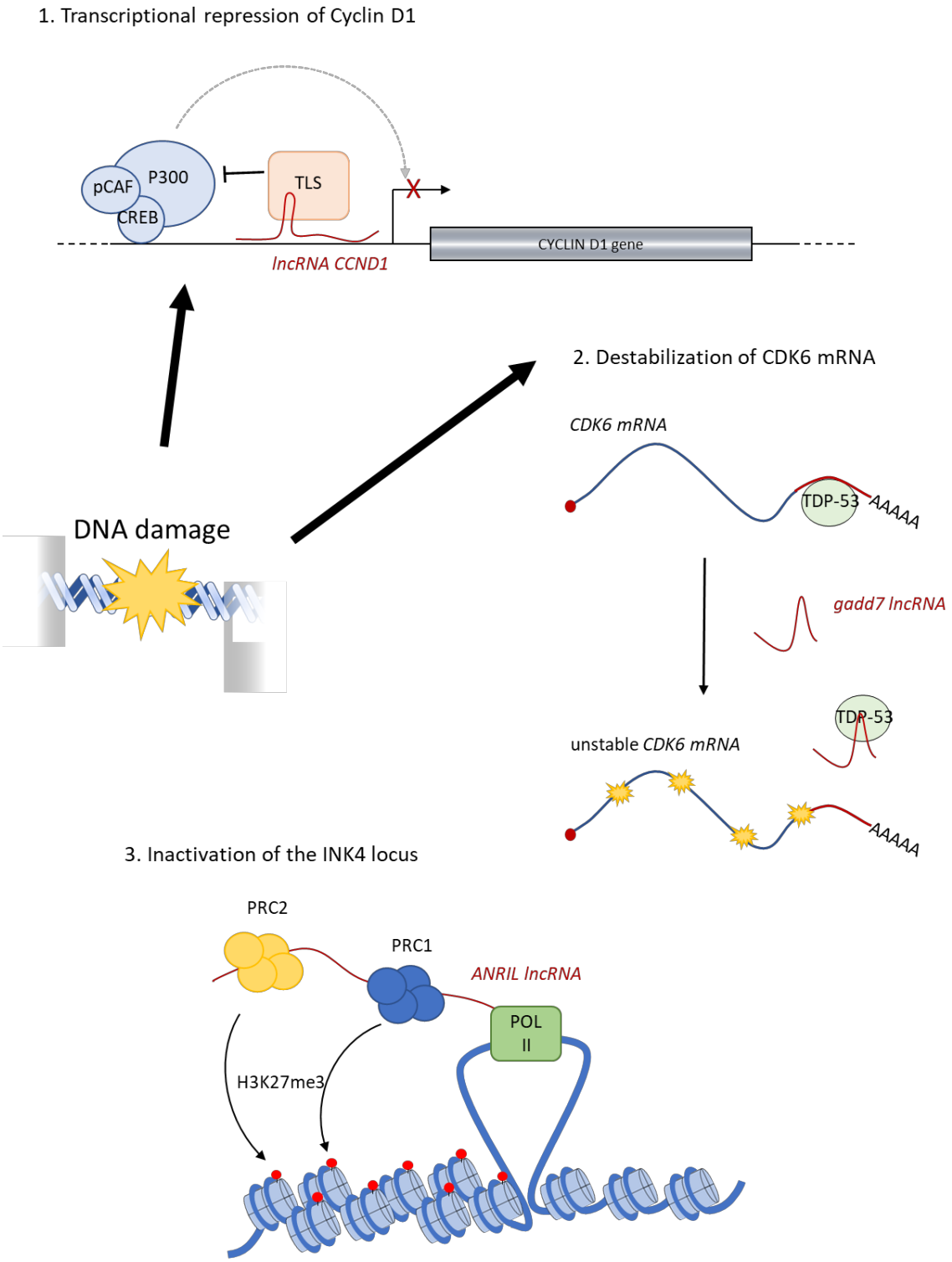

Figure 13 : Long non-coding RNAs trigger cell cycle arrest upon DNA damage and control CKI expression.

Upon genotoxic stresses, several long non-coding RNAs (lncRNAs) are expressed to inhibit cell proliferation. **(1)** lncRNA *CCND1* binds to the promoter region of cyclin D1 gene and recruits TLS. TLS further inhibits histone acetyltransferase activity of p300, leading to the transcriptional silencing of CYCD1. **(2)** Under normal condition TDP-53 binds o the 3' UTR of the *CDK6* mRNA to enhance its stability. Upon DNA damage, the *gadd7* lncRNA is expressed and titrates TDP-53, resulting in the degradation of unprotected *CDK6* transcripts. **(3)** INK4 locus code for 4 genes: the CKIs INK4^{a} and INK4^{b}, the ARF tumor suppressor and *ANRIL* lncRNA. *ANRIL* is transcribed by the RNA POLII and locally recruits the polycomb complexes PCR1 and PCR2 to perform chromatin silencing.

Long non-coding RNAs (LncRNAs)

LncRNAs are 200 or more nucleotides (nt)-long RNAs that are not translated into proteins. This class of RNA has been described to regulate a wide spectrum of biological processes, such as genomic imprinting, cell differentiation and cell cycle, and therefore contributes to cancer initiation when misregulated or mutated (Kitagawa et al., 2013; Wapinski and Chang, 2011; Li et al., 2016). LncRNAs are able to control gene expression by several mechanisms, including epigenetic silencing, transcription, translational inhibition, splicing and RNA degradation.

Thus, several lncRNAs have been shown to directly repress core cell cycle genes expression, like cyclins, *CDKs*, *CKIs* or *RBs* (Figure 13). For example, expression of *CYCD1* is repressed by $lncRNA_{CCND1}$ upon DNA damage, leading to cell cycle arrest. $lncRNA_{CCND1}$ binds to a specific sequence on the CYCD1 promoter and recruits the RNA-binding protein TLS (TRANSLOCATED IN LIPOSARCOMA) that further inhibits CREB-binding protein (CBP) and p300 histone acetyltransferase activities on the repressed target gene (Wang et al., 2008). Another lncRNA, *gadd7* (*growth-arrested DNA damage-inducible gene 7*) participates to prevent cell division by destabilizing the CDK6 transcript. CDK6 mRNA is protected from being degraded by TDP-43 that bind to its 3' untranslated region. Exposure to genotoxic stresses induces the transcription of *gadd7* that will titrate TDP-43, and by consequence release the protection of CDK6 mRNA (Liu et al., 2012). A last remarkable example of cell cycle-related lncRNA function is the transcriptional repression of the CDK inhibitors $p15^{INK4b}$, $p16^{INK4a}$ and ARF (alternative reading frame gene) by *ANRIL* (antisense lncRNA of the INK4 locus). The INK4/ARF locus encodes for three strong tumor suppressor genes and must therefore be highly controlled. *ANRIL* binds to this specific locus and recruits PRC1 and 2 (POLYCOMB REPRESSIVE COMPLEX 1/2) for transcriptional repression by histone modifications (mostly histone H3 lysine K27 methylation) (Kotake et al., 2009; Yap et al., 2011; Achour and Aguilo, 2018).

In the plant field, the knowledge of lncRNAs is still very limited. Some functional examples of plant lncRNAs have been reported such as in the control of flowering time, photomorphogenesis, or hormone signaling (Liu et al., 2015; Ariel et al., 2015). However, their role in the regulation of the cell cycle has not yet been demonstrated.

Small RNAs (sRNAs)

Small RNAs are 20 to 24 nt-long non-coding RNAs that are involved in several cellular mechanisms including antiviral defense, control of transposable elements, and particularly control of gene expression (Ghildiyal and Zamore, 2009). Among these, micro RNAs (miRNA) represents a specific class of endogenously-encoded small RNAs. Through base pair complementarity with the target transcript, they guide the effector complex RISC (RNA-induced silencing complex) to trigger repression of gene expression either by endonucleolytic cleavage or translational inhibition (Krol et al., 2010; Meister, 2013). It has been predicted that more than 50% of the genes are post-transcriptionally controlled by miRNAs in human (Leung and Sharp, 2010). In human, it has been demonstrated that miRNAs are involved in almost every biological process, including the control of the cell cycle and cell fate, and that they play a pivotal role in cell proliferation. By consequence, it is not surprising that misregulation or mutations of miRNAs in mammals are frequently observed in a wide spectrum of cancers (reviewed in Bueno and Malumbres, 2011; Leva et al., 2014). In the following chapter, I will develop the role of small RNAs in regulating gene expression in human as well as in plants.

B. Mechanisms and functions of RNA interference in eukaryotes

1. General principles

RNA silencing (or RNAi) is a cellular process that consists in the inhibition of gene expression in an RNA-dependent manner. RNAi has been observed very early on in *Petunia hybrida* by Napoli and Jorgensen, where the introduction of a transgenic copy of the chalcone synthase gene resulted in the silencing of the endogenous one (Napoli, 1990). Andrew Fire and Craig C. Mello were later awarded by a Nobel Prize in physiology and medicine in 2006 for their work on RNAi in the worm *Caenorhabditis elegans* and especially on the role of small RNA controlling the expression of developmental genes (Fire et al., 1998). Several specialized pathways exist, triggering either transcriptional gene silencing (TGS) or post-transcriptional gene silencing (PTGS). Although they act at different levels, TGS and PTGS RNAi share common features such as formation of double-stranded RNA (dsRNA), small

RNA production by type III RNase activity, and inhibition of gene expression by the RISC complex, that is notably composed of an ARGONAUTE (AGO) effector protein associated to a small RNA. Small RNAs have been classified in different groups in function of their origins, their functions and size. Thus, composition of the RISC and particularly the nature of the small RNA and the AGO protein will condition the mode of action of the complex.

In human, DROSHA and DICER RNases III are involved in a stepwise process for maturation of small RNAs that is initiated in the nucleus and ends up in the cytosol. Plants however have evolved a family of DICER-LIKE proteins (DCL1-4), of which the activity can be redundant, or exclusive to some dsRNA species (Bologna and Voinnet, 2014; Borges and Martienssen, 2015). As mentioned previously, AGO proteins are the central proteins of the RISC complex. Human and Arabidopsis genomes encode respectively 8 and 10 AGOs (Meister, 2013; Poulsen et al., 2013). Some AGOs possess an endonucleolytic activity (or slicer activity) and direct transcript cleavage on sequences that are complementary to the associated small RNA. Other AGOs act as a cargo: they associate with the target and bring additional cofactors that direct either translational inhibition or RNA-dependent DNA methylation (RdDM). Thus, a newly-formed RISC can play a role in endogenous gene expression control if associated with a miRNA, or when associated with a tasiRNA (trans-acting small interfering RNA) in plants, or a phasiRNA (phased small interfering RNA). RISC can also be loaded with transgene or virus-derived exogenous small interfering RNA and therefore act on transgene silencing and anti-viral immunity (Ding, 2010; Martínez de Alba et al., 2013). Finally, a last class of RISC complexes is related to maintenance of heterochromatin and participates to the transcriptional control of genomic repeated regions (Borges and Martienssen, 2015). Below, I will describe some, but not all, classes of known sRNAs.

2. Biogenesis and functions of micro-RNAs

miRNAs originate from genomic DNA and most commonly from intergenic regions. They are transcribed by RNA polymerase II in long capped and polyadenylated transcripts called pri-miRNAs (Lee et al., 2004; Cai et al., 2004; Kim et al., 2011) (Figure 14). In human, pri-miRNA are mostly polycistronic transcripts, forming miRNA clusters (Kim, 2005). For instance, the miR17-92 encodes for six distinct miRNAs (miR-17, miR-18a, miR-19a, miR-

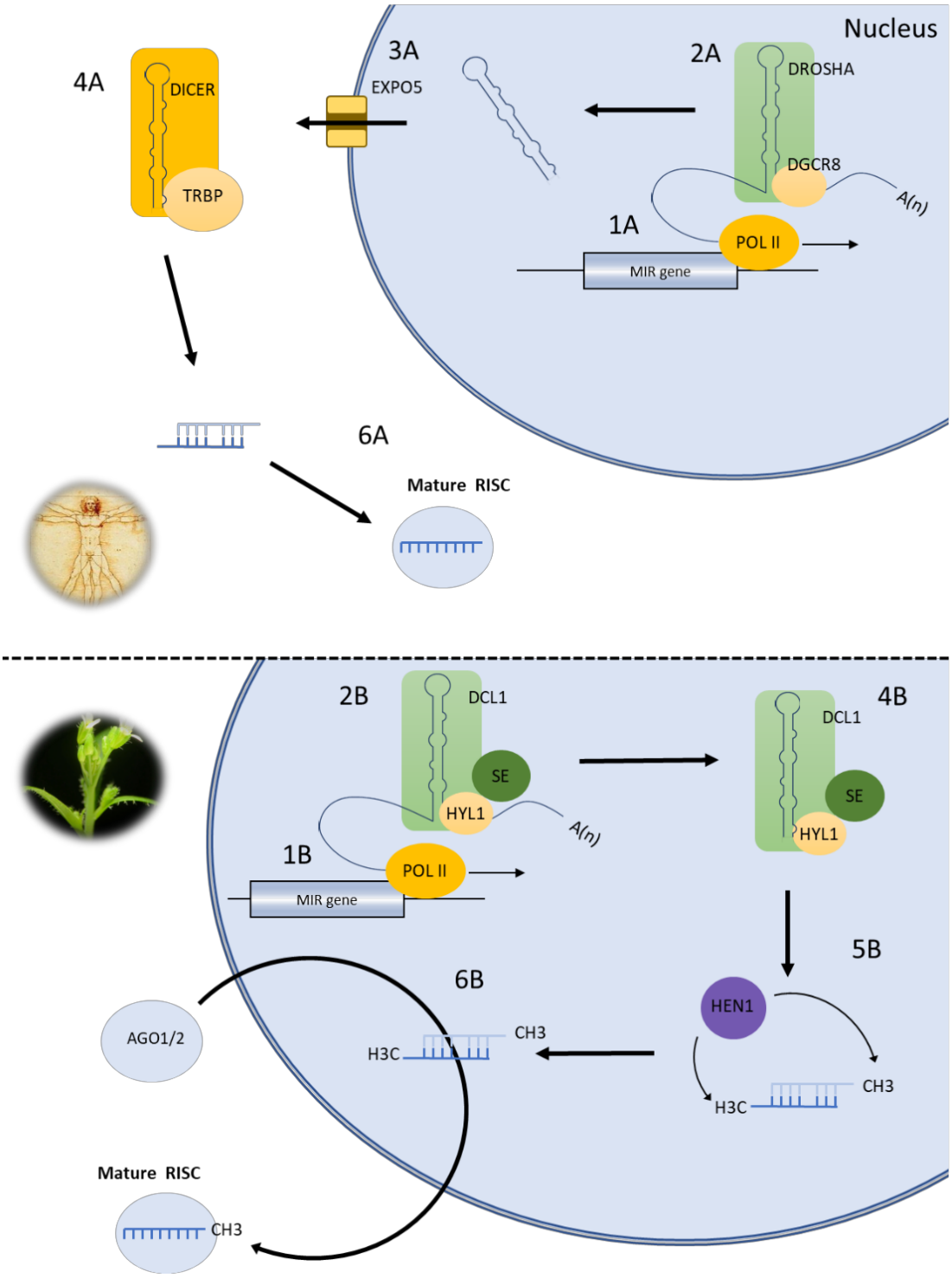

Figure 14 : microRNAs biogenesis in animals and plants.

(1A and 1B) miRNA precursors (pri-miRNA) are first transcribed by the RNA POL II from *MIR* genes in capped and polyadenylated transcripts. **(2A)** animal pri-miRNAs are processed in pre-miRNA by the microprocessor complex, composed of DROSHA and DGCR8. **(3A)** The excised step-loop pre-miRNA is exported in the cytosol by the exportin EXPO5 were the DICER/TRBP complex cleaves it in small RNA duplex **(4A)**. The guide stand of the duplex is further incorporated in AGO proteins to form a mature RISC **(6A)**. **(2B and 4B)** Plant pri-to pre- and pre- to small RNA duplexes processing is a stepwise mechanism that is performed by the same complex composed of the dicer protein DCL1, supported by the double-stranded RNA-binding protein HYL1 and the zinc-finger protein SE. **(5B)** The small RNA duplexes are then 2'-O-methylated by HEN1 to enhance their stability. **(6B)** It has recently been shown that AGO1 reaches the nucleus to load miRNAs. TRBP: TAR RNA-BINDING PROTEIN

20a, miR-19b-1, and miR-92a) (reviewed in Mogilyansky and Rigoutsos, 2013). These pri-miRNA are then processed by type III endoribonucleases. In human, pri-miRNAs are loaded in the nuclear microprocessor complex, composed of the DROSHA RNase and its double-stranded RNA binding cofactor DGCR8 (DIGEORGE SYNDROME CHROMOSOMAL REGION 8) (Lee et al., 2003; Han et al., 2004). Microprocessor activity releases a 60 to 100 nucleotides hairpin-shaped pre-miRNA (Lee et al., 2003; Han et al., 2004). It has been proposed that DGCR8 is required to anchor the microprocessor complex and therefore participate to the correct unbranching of the stem-loop (Han et al., 2004; Gregory et al., 2004). Pre-miRNAs are exported outside the nucleus by EXPO-5 (EXPORTIN-5) (Yi et al., 2003) and processed a second time by DICER RNase III in 21 nt-long miRNA/miRNA* duplex (* stands for passenger strand) (Hutvagner et al., 2010). A non-canonical pathway also exists for miRNAs that are transcribed from coding genes (also called mirtron, for intronic-miRNAs). Excision of the mirtron by the splicing machinery therefore bypasses the activity of the microprocessor complex and is directly processed by DICER (reviewed in Westholm and Lai, 2011).

In contrast to human, only a few polycistronic *MIR* genes have been described in plants (reviewed in Voinnet, 2009; Rogers and Chen, 2013). Plant *MIR* genes mostly encode a unique miRNA. Pri-miRNA are processed by a plant microprocessor-like complex that first releases the stem-loop structure and then cleaves it to form a 21 nt-long miRNA/miRNA* duplex (Figure 14). This process has been proposed to happen in the nucleus and particularly in discrete foci called “dicing bodies” (Fang and Spector, 2007). The plant microprocessor complex is composed of the RNase III DCL1 (DICER-LIKE 1) and two cofactors: the zinc finger protein SE (SERRATE) (Yang et al., 2006) and the double-stranded RNA binding protein HYL1/DRB1 (HYPONASTIC LEAVES 1 or DOUBLE-STRANDED RNA BINDING PROTEIN 1)(Dong et al., 2008; Hiraguri et al., 2005; Han et al., 2004). Plants however lack the DROSHA-like enzymes from metazoans and DCL1 is in charge of both pri-to-pre and pre-to-mature miRNA processing (Kurihara et al., 2006). While, DCL1 alone is able to generate 21 nt miRNA duplexes *in vitro*, it has been shown that SE and HYL1 greatly enhance their production and their correct processing (Kurihara et al., 2006; Dong et al., 2008). Accordingly, mature miRNA abundance is strongly reduced in Arabidopsis *hyl1-/-* mutants and miRNA precursors are accumulating (Kurihara et al., 2006). Before being loaded into AGO proteins, miRNA/miRNA* duplexes are subjected to 2’-O methylation by HEN1 (HUA ENHANCER 1) on their 3’ protruding ends that has been generated by DCL1 cleavage

(Li et al., 2005; Ren et al., 2014) This post-transcriptional modification enhances the stability of the miRNA by preventing polyuridylation by the terminal-uridyltransferase (TUTase) HESO1 (HEN1 SUPPRESSOR 1) (Zhao et al., 2012) and its subsequent degradation by the 3'-5' endoribonuclease SDN1 (SMALL RNA DEGRADING NUCLEASE 1) (Ramachandran and Chen, 2008). Once methylated, the miRNA duplex is loaded into the AGO protein that removes the passenger strand (reviewed in Kobayashi and Tomari, 2016). A recent study in Arabidopsis suggests that the slicer protein AGO1 (ARGONAUTE1) reaches the nucleus to associates with miRNAs, and forms a functional RISC and is then exported by EXPO1 (EXPORTIN 1) to the cytosol to regulate gene expression (Bologna et al., 2018).

Notably, in human and in plants, base pair complementarity was suggested to condition the preference for either slicing or translational inhibition by AGO proteins. Indeed, perfect matches between small RNAs and their target transcripts mainly leads to slicing, while imperfect matches rather trigger translational inhibition. However, the choice between the two activities may also depend on the RISC composition (Ding and Han, 2007). Human AGO2 is the main effector of miRNA-dependent PTGS pathway (Meister, 2013). After the removal of the passenger strand, AGO2 mainly directs translational inhibition, but is also able to slice some target mRNAs. In plants, AGO1 is the main effector protein for miRNAs, though AGO2, 7 and 10 can also associate with miRNAs but are involved in specific cellular processes. Arabidopsis AGO1 loaded with miRNAs mediates both endonucleolytic cleavage (Baumberger and Baulcombe, 2005) and translational repression of target transcripts (Brodersen et al., 2008; Li et al., 2013). AGO proteins and their modes of action will be described in more detail in another section below.

3. Biogenesis and functions of small interfering RNAs (siRNAs)

While miRNAs are processed from imperfect stem-loop precursors transcribed from *MIR* genes, siRNA are excised from endogenous or exogenous, fully complementary, double-stranded RNAs (Borges and Martienssen, 2015). Plant endogenous siRNAs are distributed in two groups: secondary siRNAs and hetsiRNA/rasiRNA (heterochromatic siRNAs or repeat-associated siRNA). Secondary siRNAs include tasiRNAs (trans-acting siRNAs), easiRNAs (epigenetically-activated siRNAs) and natsiRNA (natural antisense siRNAs) (reviewed in Voinnet, 2009; Borges and Martienssen, 2015).

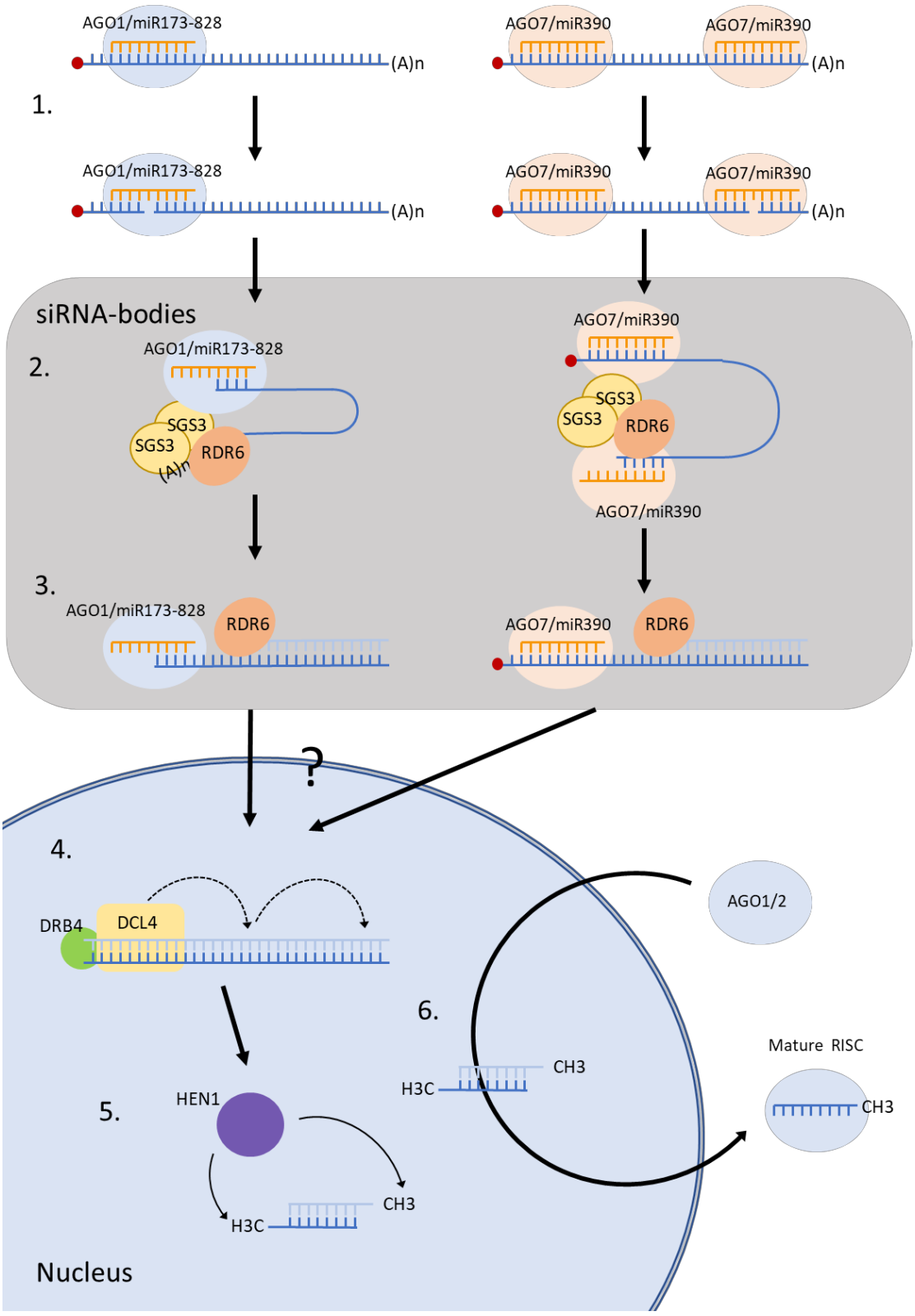

Figure 15 : Biogenesis of secondary trans-acting siRNA (tasiRNAs).

(1) Generation of secondary tasiRNA starts with the cleavage of a precursor transcript by a RISC complex that contain a miRNA bound to AGO1 or AGO7 (miRISCs). **(2)** The cleaved precursor is stabilized by SGS3 that binds directly to the complex and recruits the RNA-dependent RNA polymerase RDR6 to generate the double-stranded RNA molecule (dsRNA) **(3)**. **(4)** The dsRNA is then imported in the nucleus to be processed by the DCL4/DRB4 complex. Small RNA duplexes are generated in phase with the first miRISC-directed cleavage. **(5 and 6)** Like miRNAs, phased small RNA duplexes are subsequently 2'O-methylated and loaded in AGOs.

a. Trans-acting RNAs (tasiRNAs)

In Arabidopsis, four TAS genes have been identified (Vazquez et al., 2004; Peragine et al., 2004; Allen et al., 2005). TAS genes are transcribed by the RNA pol II in 7-methyl guanosine-capped and 3' polyadenylated transcripts. Conversely to pri-miRNAs, tasiRNAs do not harbour any specific foldback structures that can be processed by DCLs. They need a specific processing pathway that involves a primary cleavage by a miRISC and the generation of a double strand RNA molecule by an RNA-dependent RNA polymerase (Figure 15). *TAS1*, *TAS2* and *TAS4* precursors are first cleaved by a RISC composed of AGO1 and miR173 for TAS1 and 2, and miR828 for *TAS4* (Rajagopalan et al., 2006; reviewed in Yoshikawa, 2013). While most of plant miRNAs are 21 nt in size, miRNAs triggering secondary siRNAs are however 22 nt-long. Interestingly, 21 nt-long forms of these miRNAs are not able to generate secondary siRNAs *in vivo* (Cuperus et al., 2010; Chen et al., 2010). A proposed model for generation of tasiRNA is that, upon miRISC cleavage, SGS3 (SUPPRESSOR OF GENE SILENCING 3) associates with AGO1 to protect the 5' phosphate of the generated 3' TAS fragment from exoribonucleases and subsequently, contributes to the recruitment of the RdRP RDR6 to generate the double stranded RNA (Yoshikawa et al., 2013). Generation of tasiRNAs from *TAS1,2* and *4* precursors is commonly called a "one hit" system, since it requires only one cleavage. The case of the *TAS3* precursor is qualified of a "two hits" system (Axtell et al., 2006). Indeed, in this case miR390 is complementary to two different target sites along *TAS3* that are absolutely required for generation of secondary siRNAs. *TAS3* is also unique since it requires the specialized ARGONAUTE protein, AGO7 (Axtell et al., 2006; Montgomery et al., 2008). The final step in this pathway consists in the processing of the double-stranded RNA, in a phase determined by the initial miRNA cleavage site, by DICER-LIKE 4 and DRB4 (DOUBLE-SRANDED RNA BINDING PROTEIN 4) to generate a 21nt tasiRNA population (Gasciolli et al., 2005; Xie et al., 2005; Adenot et al., 2006; Fei et al., 2013).

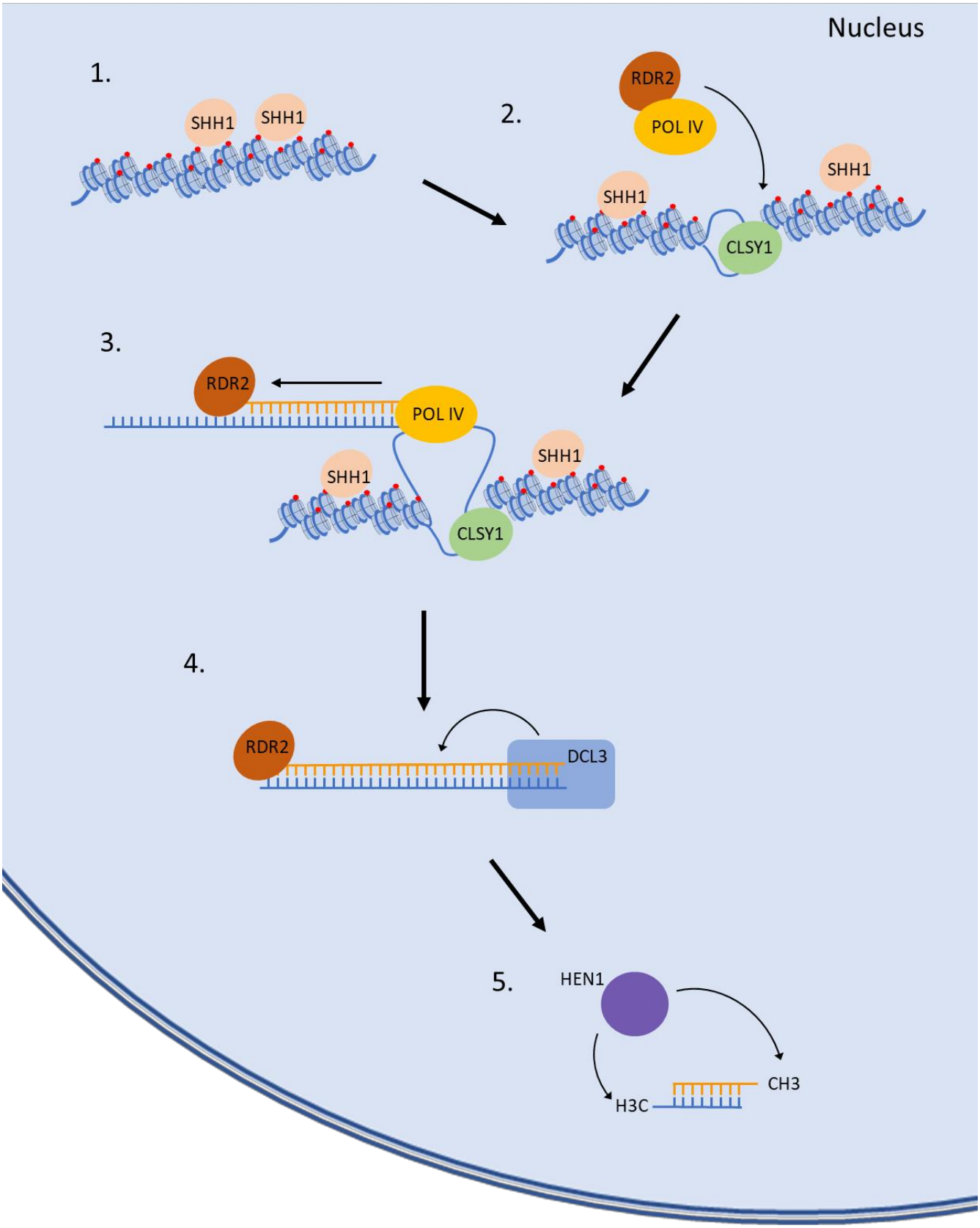

Figure 16 : Heterochromatic siRNAs (hetsiRNAs) biogenesis.

(1) SSH1 is associating with epigenetically silenced regions on the chromatin and recruits the CLSY1 helicase. **(2)** CLSY1 uncoil the condensed chromatin and recruits the RNA POLIV and the RNA-dependent RNA polymerase RDR2 to this specific locus. **(3)** RNA POLIV and RDR2 act jointly to generate the dsRNA molecule that is then processed by DCL3 into 24 nucleotides-long siRNAs duplexes **(4)**. **(5)** Small RNA duplexes are 2'-O methylated by HEN1 prior to be loaded in AGOs. SHH1: SAWADEE HOMEODOMAIN HOMOLOG 1.

b. Heterochromatic siRNAs (hetsiRNAs)

hetsiRNAs represent the most abundant class of small RNAs in the cell (Mi et al., 2008). They are 24 nt-long small RNAs that trigger transcriptional gene silencing (TGS) through RNA-dependent DNA methylation (RdDM) and participate to the maintenance of heterochomatin and silencing of transposable elements (Borges and Martienssen, 2015; Fultz et al., 2015). In plants, hetsiRNA precursors are first transcribed by the plant-specific RNA pol IV (Figure 16). Loss of one of the two main subunits of pol IV, NRPD1 or NRPD2 (NUCLEAR RNA POLYMERASE D1 or 2), abolishes the production of hetsiRNAs resulting in the hypomethylation of loci that are normally silenced (Herr, 2005; Onodera et al., 2005; Kanno et al., 2005). In addition to POLIV, RDR2 (RNA-DEPENDENT RNA POLYMERASE 2) is also essential for hetsiRNA biogenesis (Pontes et al., 2006). Other members of the complex have also been identified, like the CLSY1 helicase (CLASSY1), which mutation affects hetsiRNA biogenesis and the localization of RDR2 (Smith et al., 2007; Law et al., 2011). These observations suggest that the helicase activity of CLSY1 might provide accessibility for the complex to the chromatin. The dsRNA molecule generated by the activity of the pol IV/RDR2 complex is then processed in 24nt-long siRNAs by DCL3 and those small RNAs are then 2'-O-methylated by HEN1 (Xie et al., 2004; Yang et al., 2006b). Finally, hetsiRNAs are loaded in specialized AGOs, mainly AGO4, but also 6 and 9, to perform DNA methylation. Moreover, the 24 nt-associated AGO4 is recruited to DNA and required for methylation through RNA POL V activity (Kanno et al., 2005; Pontier et al., 2005; Lahmy et al., 2009), though this mechanism is not fully understood.

4. tRNA-derived fragments

Transfer RNAs (tRNAs) are housekeeping RNAs that are essential components of the translation machinery (reviewed in Giegé, 2008) (Figure 17A). As many other non-coding RNAs, tRNAs are transcribed as precursor RNAs that undergo several steps of maturation, including 5' leader and 3' trailer cleavage by RNase P and RNase Z, respectively. They are also subjected to several base modifications, such as methylation and pseudo-uridylation that are required for the folding and the recognition of other maturation enzymes. Addition of the CCA motif by a tRNA nucleotidyl-transferase and the loading of the amino acid by aminoacyl

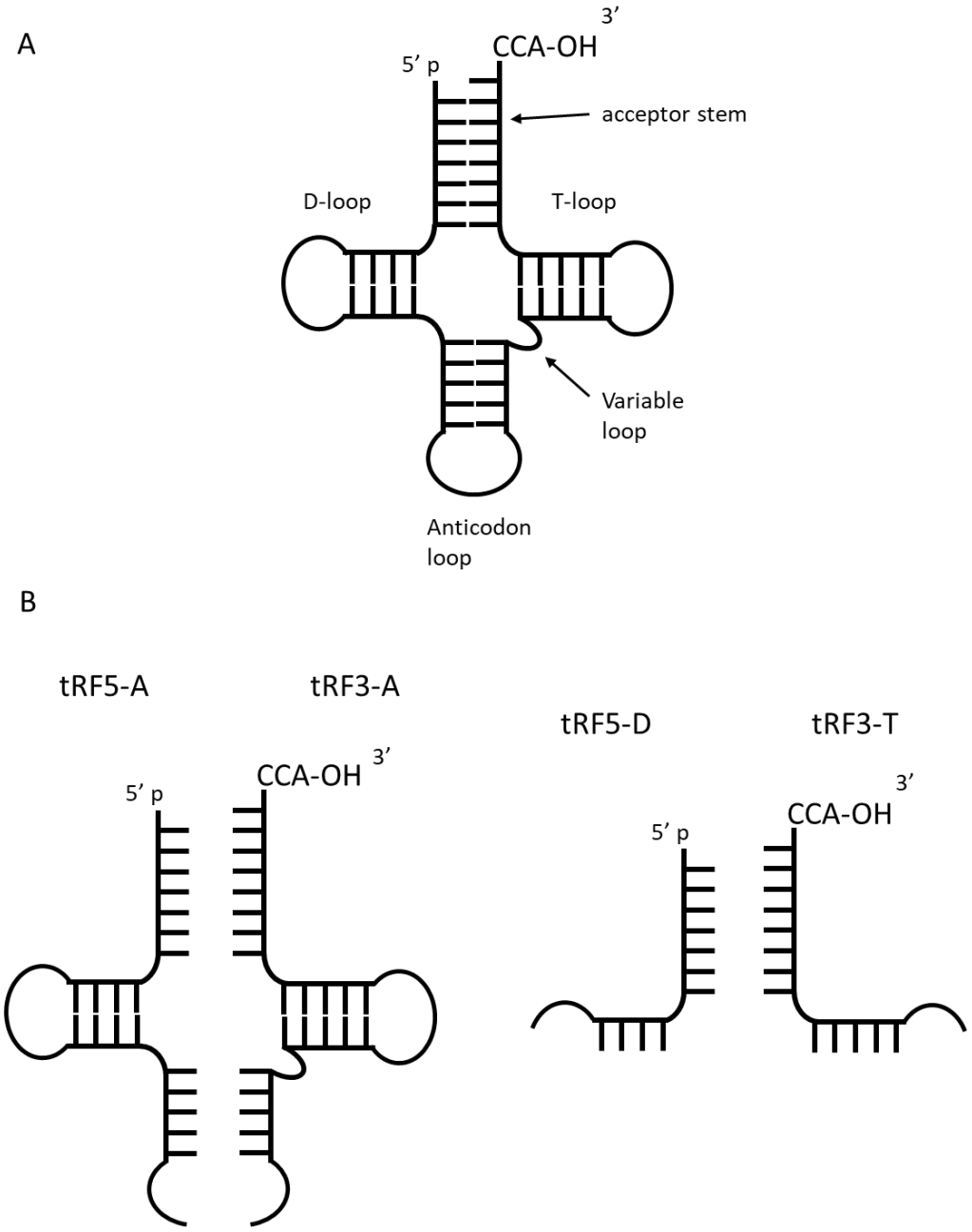

Figure 17 : Secondary structure of transfer RNAs (tRNAs) and tRNA-derived fragments (tRFs).

(A) tRNAs are composed of an acceptor stem that ends with the 3’ CCA motif required for aminoacylation, the D and T-loop, the anticodon loop and a variable loop. the D and T-loop are responsible of the ternary structure of the tRNA. **(B)** tRFs can be generated by endonucleolytic cleavage in the A, D and T loops. Cleavage in the anticodon results in generation of tRNA approximately 33 nucleotides-long tRNA halves, while cleavage in the D or T loop generate around 20 nucleotides tRFs.

tRNA synthetase in 3' are then sequentially performed, leading to the formation of the mature tRNA.

tRNA-derived fragments (tRFs) have been recently identified by high-throughput sequencing approaches in a wide spectrum of eukaryotes, ranging from fission yeast to plants and human (reviewed in Keam and Hutvagner, 2015; Schimmel, 2018). tRFs are generated through endonucleolytic cleavage and are classified in two groups: 30 to 35 nt tRNA-halves, that are the results of cleavage in the anticodon loop, and approximately 20 nt-long small tRFs, generated by cleavage in the T or D loop (Figure 17B). How these cleavages are performed, and what are the enzymes involved in tRFs production is still a matter of debate, but published results support the role of animal DICER and ANGIOGENIN in the generation of at least some tRF species. To assess the question of the biological functions of tRFs, identification of tRF-associated proteins is one of the main concerns in the field. Immunoprecipitations of AGO-bound small RNAs followed by small RNA sequencing highlighted that several AGO, including human AGO1 to 4 and Arabidopsis AGO1, 2, 4 and 7, are able to load tRFs, suggesting a role in transcriptional and post-transcriptional gene silencing (Haussecker et al., 2010; Loss-Morais et al., 2013; Cognat et al., 2017). Indeed, the ability of tRFs to specifically target 3'UTR of mRNAs and repress their translation was demonstrated in multiple cases (Gebetsberger et al., 2012; Sobala and Hutvagner, 2013). Interestingly, some tRFs have been linked to developmental processes including cell proliferation and viability. As an example, the tRF-1001 was found highly accumulated in several types of cancer and siRNA-directed silencing of tRF-1001 prevented proper cell cycle progression by blocking cells in G2 (Lee et al., 2009). By contrast, plant tRFs accumulation is mainly observed in stress conditions, and particularly oxidative stresses, heat and phosphate starvation, suggesting that they might be involved in rapid reprogramming of gene expression in response to diverse external stimuli (Thompson et al., 2008; Hsieh et al., 2010; Wang et al., 2011b; Pandey et al., 2014; Cognat et al., 2017). Interestingly, tRNAs have also been recently connected to genome protection against retrotransposons (reviewed in Martinez, 2018).

A

(Vaucheret, 2008)

B

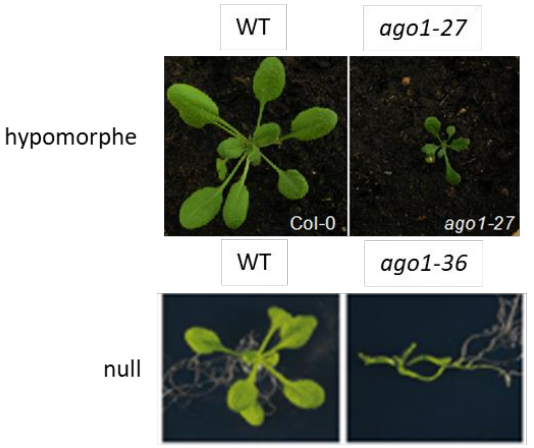

(Baumberger et al., 2005)

C

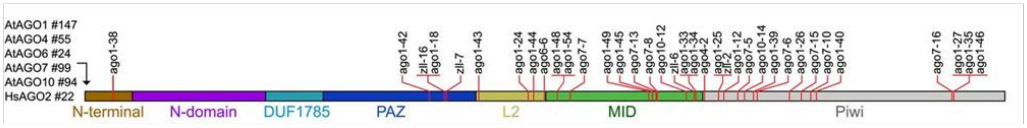

(Poulsen et al. , 2013)

D

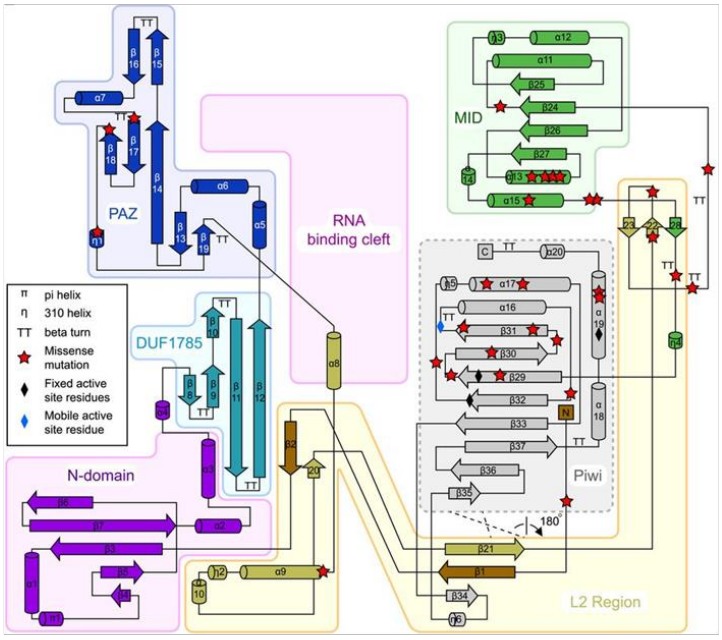

(Poulsen et al. , 2013)

Figure 18 : Plant and human ARGONAUTES features (adapted from Baumberger and Baulcombe, 2005; Vaucheret, 2008; Poulsen et al., 2013).

(A and B) Characteristic phenotypes of Arabidopsis *ago1* mutants. **(C)** Schematic representation of ARGONAUTE domains and position of Arabidopsis ARGONAUTEs missense mutations. (**D**) Diagram representing the spatial organization of human AGO2. Arabidopsis mutations are represented by red stars. AGOs are formed of two lobes that are respectively composed of the N-terminal domain/DUF1785/Paz and MID/PIWI. They are linked by the L2 domain. The small RNA binding pocket is located in-between these two lobes.

5. ARGONAUTE proteins

a. Structural features of ARGONAUTE proteins

Historically, the *ARGONAUTE* gene was first identified in plant, as *ago1-1* to *-6* Arabidopsis mutants were isolated from a EMS (ethyl methanesulfonate)-mutagenized population due to their severe alterations in leaf morphology resembling the tentacles of the little Argonaute squid (Bohmert et al., 1998) (Figure 18B). The structural hallmark of ARGONAUTE (AGO) proteins are three distinct domains: PAZ (PIWI/ARGONAUTE/ZWILLE), MID (MIDDLE) and PIWI (P ELEMENT-INDUCED WIMPY TESTIS) (Figure 18C) (reviewed in Vaucheret, 2008; Poulsen et al., 2013; Meister, 2013). Resolution of the human AGO2 structure revealed that the protein is composed of two lobes (Elkayam et al., 2012; Schirle and MacRae, 2012). These lobes correspond to the N-terminal and C-terminal part of AGO that are respectively composed of N/DUF1785/PAZ domains and the MID/PIWI domains (Figure 18D). Notably, most of Arabidopsis ARGONAUTE mutations recovered from genetic screens are located in the PAZ, MID and PIWI domains, highlighting their importance for AGO function (Figure 18C and D). The PAZ and MID domains confer small RNA-binding properties to AGOs. Structural studies report that the PAZ domain is composed of two subdomains that specifically bind the two nucleotides protruding 3' end of small RNA duplexes (Lingel et al., 2004; Ma et al., 2004), whereas human AGO2 MID domain was shown to interact with the 5' phosphate end of the guide RNA with a specificity for AMP or UMP (adenosine/uridine monophosphate) (Frank et al., 2010; Boland et al., 2011). The PIWI domain resembles the RNase H enzymes and supports the endonucleolytic activity (or slicing) that has been demonstrated for several AGOs (Baumberger and Baulcombe, 2005). The PIWI domain activity is carried out by a conserved catalytic core Asp-Asp-His (DDH) or Asp-Asp-Lys (DDK) (Vaucheret, 2008; Poulsen et al., 2013).

The N-terminal domain is composed of a long non-folded region terminated by a coiled structure followed by a domain of unknown function called DUF1785 (Poulsen et al., 2013). In metazoans, the N-terminal part of the AGO protein seems to be the main driving force for ejection of the passenger strand also called "unwinding" (Kwak and Tomari, 2012). So far, the function of the N-domain and the DUF1785 is still not well understood in plants, partly due to the fact that only few point mutations are available in this region for functional

analysis. Recent work from our laboratory showed that the DUF1785 is required for unwinding perfectly matched siRNA duplexes (Derrien et al., 2018). Moreover, a mutation in the coil domain was identified which affects Arabidopsis AGO1 association to membranes, suggesting a role of the N-terminal coil as membrane-bound protein interaction interface (Brodersen et al, 2012).

Recently, Bologna and colleagues validated the presence of a nuclear export signal (NES) and a nuclear localization signal (NLS) in the N-terminal part of Arabidopsis AGO1 that are involved in the nucleo-cytoplasmic shuttling of the protein (Bologna et al., 2018). They proposed that in the non-loaded form of AGO1, the N-domain is translocated in the small RNA binding cleft, masking the NES and thus allowing the nuclear import of AGO1, presumably for miRNA loading. Once the miRNA is associated to AGO1, the N-terminal domain is released, and the NES is exposed, forcing AGO1 to reach the cytoplasm to perform PTGS.

b. Assembly of mature RISC complexes

In the last decade, many efforts have been put on dissecting the molecular mechanisms behind small RNA loading and small RNA duplexes unwinding in several models, namely human, fruit fly and plants. Typically, the loading of perfectly-matched siRNAs or bulge-containing miRNAs occurs in a similar way. Small RNA loading is an ATP-dependent process that requires intervention of at least two chaperoning proteins: HSC70 (HEATSCHOCK COGNATE 70) and HSP90 (HEATSCHOCK PROTEIN 90) (Kawamata et al., 2009; Iwasaki et al., 2010; Iki et al., 2010). Thus, it was proposed that this process induces conformational changes and therefore provides access to the binding cleft for the small RNA duplex.

Then, passenger strand removal is required prior to repression of target mRNA. The strand selection rule has been deciphered in animal systems, where the strand with the less thermodynamically stable 5' end is favoured as the guide stand (Khvorova et al., 2003; Schwarz et al., 2003). Slicer activity has been shown to participate to ejection of the passenger strand, though, mutations of the PIWI core catalytic residues do not abolish the production of mature RISC complexes (Kawamata et al., 2009). Thus, slicer-dependent and -independent unwinding processes coexist, consistent with the fact that some AGO proteins

lack the slicer activity. As indicated above, the N-terminal part of the human AGO was shown to be required to initiate strand separation or "wedging" (Kwak and Tomari, 2012). In addition, it was recently shown that a mutation in the DUF1785 domain of Arabidopsis AGO1 impairs passenger strand removal of perfectly matched siRNA, severely affecting the production of secondary siRNAs (Derrien et al., 2018).

Overall, our current understanding of the loading process can be summarized as a three-step model: (1) ATP-dependent opening of AGO and small RNA duplex binding, (2) active wedging initiating the opening of the dsRNA of the duplex at the 5' end or the passenger strand, (3) slicer-dependent or -independent unwinding, depending on the slicing activity of the AGO protein and complementarity of the two strands.

c. Plants and Human ARGONAUTEs

The Arabidopsis genome encodes 10 AGO proteins that are distributed in 3 distinct clades: namely AGO1/5/10, the AGO2/3/7 and AGO4/6/8/9 (Vaucheret, 2008). As discussed previously, AGO1 was firstly identified due to its strong developmental phenotype (Figure 18A and B). Indeed mutations in the PAZ, MID or PIWI domain abolished or at least partly reduced AGO1 activity and led to pleiotropic defects, including dwarfism, abnormal leaf and root shapes, and even sterility and lethality in the worst cases (Vaucheret, 2008). Thus, AGO1 is a major regulator of gene expression and it has been shown that it is the principal effector of the miRNA pathway in plant. The closest homolog of AGO1 is AGO10/ZWILLE/PINHEAD. In contrast to AGO1, AGO10 lacks the slicer activity despite the presence of the DDH motif in the PIWI domain (Mallory and Vaucheret, 2009), but is able to perform translational inhibition (Brodersen et al., 2008). AGO10 has been reported to be involved in several processes, including AGO1 post-transcriptional control (Mallory et al., 2009; Zhu et al., 2011). Thus, AGO10 plays a role in the meristem formation and development by sequestering and inducing degradation of miR165/166, hence preventing them to being loaded in AGO1 and perform PTGS (Roodbarkelari et al., 2015; Zhu et al., 2011b; Yu et al., 2017). AGO2 and AGO5 have been both linked to antiviral defense, they were shown to bind to virus-derived small RNAs and *AGO2*- and *AGO5*-silenced plants are more susceptible to virus infection than wild-type plants (reviewed in Alvarado and Scholthof, 2012; Brosseau and Moffett, 2015). In addition, recent studies demonstrated also

the capability of AGO2 to participate to the regulation of gene expression in response to diverse stresses such as virus and bacterial infection and double-strand break DNA damage (Zhang et al., 2011a; Wei et al., 2012; Cao et al., 2014; Fátyol et al., 2016). As we detailed in the section dedicated to small interfering RNAs, AGO7 is a highly specialized ARGONAUTE involved in the generation of Tas3 secondary RNAs and participates to a wide spectrum of auxin-related responses (Allen et al., 2005; Fahlgren et al., 2006; Montgomery et al., 2008; Hobecker et al., 2017). Finally, AGO4, 6 and 9 functions are related to transcriptional gene silencing (reviewed in Mallory and Vaucheret, 2010; Poulsen et al., 2013). Though, they exhibit different expression patterns: while AGO4 is expressed rather ubiquitously, AGO6 and AGO9 are mostly expressed in flowers and seeds and are most likely involved in germ line-specific functions (reviewed in Mallory and Vaucheret, 2010). AGO4, 6 and 9 specifically interact with 24-nt RNAs and AGO4 was shown to bind directly to NRPD1, a subunit of the RNA POL IV, and performs chromatin silencing by RNA-dependent DNA methylation (El-Shami et al., 2007).

In mammals, AGO was initially characterized as EIF2C (EUKARYOTIC INTIATION FACTOR C), as it linked to translation initiation in rabbit reticulocyte lysate (Roy et al., 1988; Zou et al., 1998). Investigating the role of a genomic region that is frequently involved in proliferative diseases, Koesters and colleagues cloned and sequenced the human EIF2C1/AGO1 (Koesters et al., 1999). In human, eight members belonging to the ARGONAUTE family were later discovered (Sasaki et al., 2003). ARGONAUTE proteins are distributed in two groups: AGO proteins, AGO1^{EIF2C1}, AGO2 ^{EIF2C2}, AGO3 ^{EIF2C31} and AGO4 ^{EIF2C4}, that are related to plant AGOs, and PIWI proteins, PIWIL1^{HIWI1}, PIWIL2^{HIWI2}, PIWIL3^{HIWI3} and PIWIL4^{HIWI4}, that share similarity with *Drosophila melanogaster* PIWI proteins. In contrast to AGOs, PIWI are exclusively restricted to the germ lines and were proposed to be responsible of stem cells maintenance and differentiation, as well as transcriptional silencing of transposable elements (Sasaki et al., 2003; Mani and Juliano, 2013). AGO2 is the only catalytically active AGO protein in animals. Slicing activity is required for the processing of miR451 that is not dependent of the canonical DICER pathways and mutation of the catalytic triad DDH leads to post-embryonic lethality, highlighting the essential role of the AGO2 slicing activity (Cheloufi et al., 2010). In addition to its slicer activity, AGO2 shares at least partly redundant functions with AGO1, 3 and 4 by binding miRNAs and performing translational inhibition (Burroughs et al., 2011). Human AGOs also

function in specific nuclear pathways such as double-strand break repair mechanisms and alternative splicing (reviewed in Meister, 2013)

d. Regulation of Argonaute proteins

In plants, prediction of miRNA targets pointed out that AGO1 might be itself regulated in a PTGS-dependent manner (Rhoades et al., 2002; Axtell and Bartel, 2005) and was indeed later validated through 5'-RACE (rapid amplification of cDNA ends) experiments (Vazquez et al., 2004). Expression of a miR168-resistant version of AGO1 causes developmental defects, and even lethality in the most severe cases (Vaucheret et al., 2004). In addition, miR168 accumulation was also found correlated with AGO1 mRNA level (Vaucheret, 2006). These observations suggest a deleterious effect of AGO1 overexpression and support the essential role to regulate AGO1 homeostasis in plants. Another example of such a miRNA-mediated AGO regulation has also been described for AGO2 by the miR403 (Allen et al., 2005). Although the function of the miR403 has not yet been fully investigated in Arabidopsis, overexpression of miR403 was shown to delay flowering, affect leaf morphogenesis and response to abscisic acid treatment in tomato (Zhang et al., 2015).

Although it has been reported that AGO1 alone is able to cleave target RNA *in vitro* (Baumberger and Baulcombe, 2005), it is likely that additional proteins might modulate its activity. For instance, the RNA helicase SDE3, a glycine-tryptophan (GW)-repeat-containing protein interacts with AGO1 and is a facilitator of the sense transgene post-transcriptional gene silencing (S-PTGS) amplification step (Garcia et al., 2012). Moreover a genetic screen based on the suppression of the *sqn* (SQUINT) phenotype, SQUINT being a co-chaperone interacting with HSP90 that is a putative AGO1 regulator (Earley and Poethig, 2011), allowed the identification of the F-box protein FBW2 (Earley et al., 2010). Loss of *FBW2* in several hypomorphic alleles of AGO1 partially restored a wild-type phenotype, whereas overexpression of FBW2 was shown to induce phenotypes similar to AGO1 mutants. Moreover, loss of FBW2 enhances AGO1 protein accumulation, suggesting that FBW2 is an endogenous F-BOX that controls AGO1 homeostasis. This remains however to be formally demonstrated. Interestingly, an example of an F-BOX protein that triggers AGO1 degradation has been already reported in viral context. Thus, the viral protein P0 from poleroviruses interacts with ASK1 (Pazhouhandeh et al., 2006) to highjack an SCF complex and further

triggers AGO1 degradation through the autophagy pathway (Baumberger et al., 2007; Bortolamiol et al., 2007; Derrien et al., 2012). AGO1 P0-targeted degron has recently been identified in the DUF1785 domain (Derrien et al., 2018) and its mutation abolishes AGO1 degradation upon P0 expression. The fact that the mutated AGO1 protein in the DUF1785 domain does not overaccumulate in plants suggests that endogenous ubiquitin ligases might target another motif.

We still know very little about post-translational modifications regulating AGO proteins in plants. In animals, however, this became an expending topic (reviewed in Johnston and Hutvagner, 2011; Meister, 2013). Spectrometry analysis of human AGOs revealed that they are subjected to hydroxylation, and in particular AGO2 and AGO4, (Qi et al., 2008). Furthermore, both the mutation of the enzyme responsible of AGO2 hydroxylation and mutation of the targeted residue led to decreased amount of AGO2, linking hydroxylation to AGO stability. In parallel, several phosphorylation sites have been identified in human AGO2 (Zeng et al., 2008; Rüdel and Meister, 2008). Phosphorylation of AGO2 was shown to participate to localization in processing bodies (P-bodies) (Zeng et al., 2008) and to interfere with small RNA binding (Rüdel et al., 2011). Interestingly, these modifications appear to be induced under stress, suggesting a potential role in the reprogramming of the RISC complex to quickly modulate gene expression. Finally, two recent reports indicate that human AGO2 phosphorylation by CSNK1A1 casein kinase 1 on a cluster of conserved residues (S824-S834) impairs mRNA target association (Golden et al., 2017; Quévillon Huberdeau et al., 2017). The negatively charged phosphates would remove the mRNA from AGO2, and mRNA target is released. Thus, after dephosphorylation, AGO2 could thus be recycled and guided to a new target mRNA or would be degraded.

6. The fate of RISC-targeted transcripts: slicing or translational inhibition

Both plant and animal ARGONAUTEs are able to perform endonucleolytic cleavage or translational inhibition. However, while the slicing activity appears to be the main mode of action in plants, this process happens much more occasionally in animal cells. Whether the RISC is performing slicing or translational repression depends, at least in part, on the base pair complementarity within the miRNA and the target RNA. Perfect or nearly-perfect complementarity leads to slicing, which is in general the case for siRNAs (Figure 19A). Note

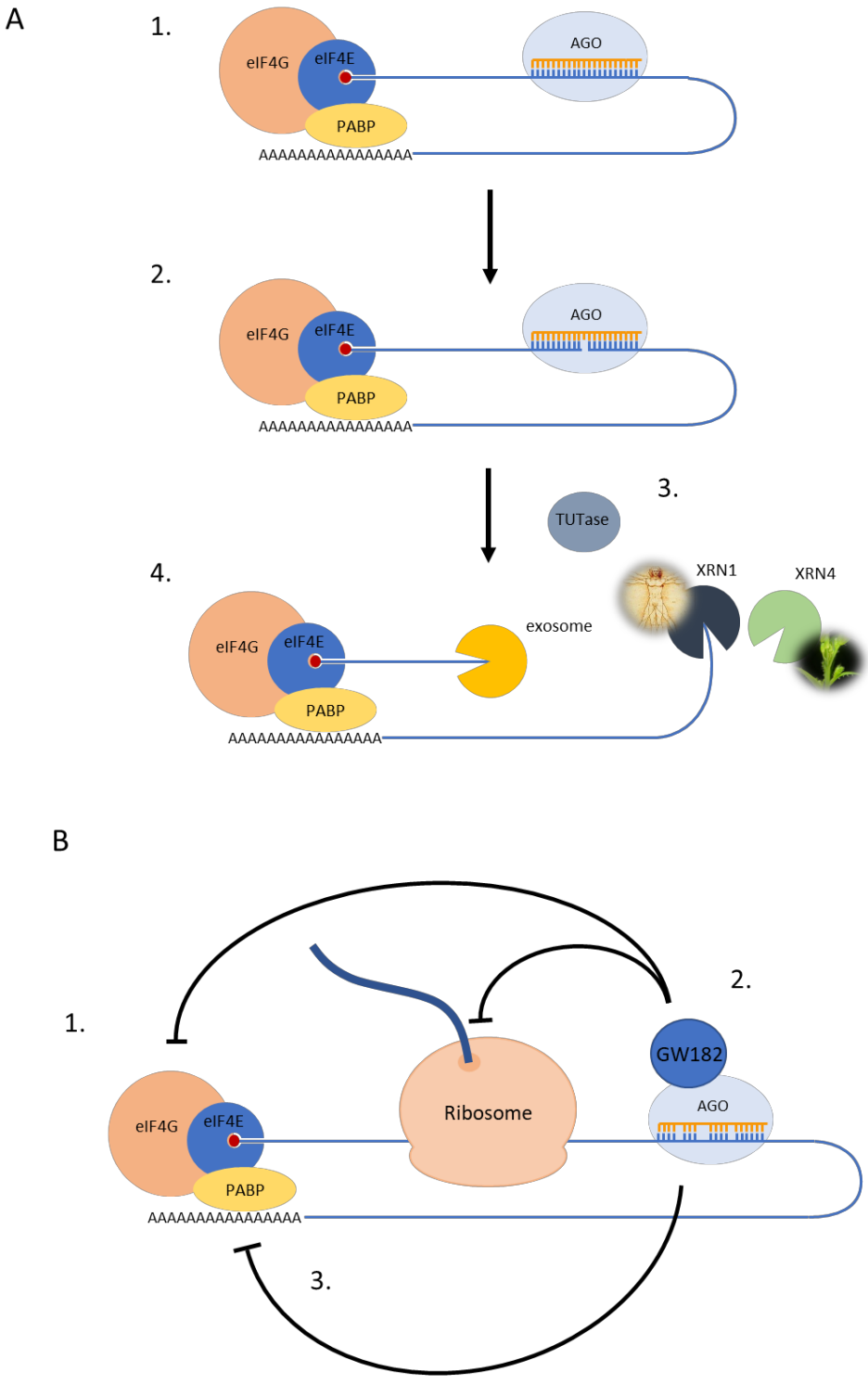

Figure 19 : RISC-mediated slicing and translational repression.

(A) To accomplish post-transcriptional gene silencing, RISC complex must first prime to a target sequence **(1)**. **(2)** Perfect or near-perfect complementarity between small RNA and the target sequence results in endonucleolytic cleave of the target RNA between the position 10 and 11 of the small RNA. Slicing activity leads to the generation of 3'-OH and 5'-monophosphate unprotected end that are subjected by exonucleolytic degradation by the exosome and XRN1/XRN4, respectively **(4)**. **(3)** Note that 3' polyuridylation by terminal-uridyltransferases (TUTases) can accelerate the degradation of the 5' fragment. **(B)** Imperfect small RNA/target RNA hybrids lead to translational repression rather than slicing. In animals, translational repression required the GW-containing protein GW182. Translational repression relies on several mechanisms including **(1)** inhibition of translation initiation, **(2)** inhibition of translation elongation and premature termination and even deadenylation and decapping in animals **(3).**

that plant mRNA cleavage by AGO1-loaded miRNAs occurs essentially in the open reading frame of target mRNAs (Rhoades et al., 2002). Conversely, bulge-containing miRNAs are preferentially involved in translational repression (Figure 19B). In mammals, the minimal sequence complementarity needed for target recognition comprises six to seven nucleotides in position 2 to 7-8, also called seed sequence (Lewis et al., 2003; Bartel, 2009).

In animals, the GW182 protein is essential for translational inhibition (reviewed in Iwakawa and Tomari, 2015). GW182 and miRNA-associated RISC were shown to colocalized in P-bodies, cytosolic foci where it is though that untranslated mRNAs are stored and eventually degraded. A model of translation inhibition suggests a 3 steps process: (1) Inhibition of translation initiation, (2) Inhibition of translation elongation and (3) premature termination (Figure 19B). In such a model, GW182 recruits deadenylase complexes, CCR4-NOT (CARBON CATABOLITE REPRESSOR 4- NEGATIVE ON TATA) and PAN2-PAN3 (POLY (A) NUCLEASE 2-3), to initiate mRNA decay. In parallel, GW182 was shown to provide accessibility of the poly(A) tail to deadenylases by promoting dissociation of PABP (POLY (A)-BINDING PROTEIN). Deadenylation is immediately followed by the removal of the 7-methylguanosine 5' cap by the decapping complex, composed of the catalytic subunit DCP2 (DECAPPING PROTEIN 2) and its cofactor DCP1 and DDX6. Shortened poly(A) tails also allow the recruitment of terminal-uridyltransferases (or TUTase) at the 3' end of RNA. Polyuridylation by TUTases consist in the untemplated adding of uracils in 3' that facilitate the recruitment of 5'-3' degrading enzymes (Aphasizhev et al., 2016; Scheer et al., 2016). In parallel, the decapping complex releases an unprotected 5' monophosphate end that is required to initiate 5' to 3' degradation by the exoribonuclease XRN1 (EXORIBONUCLEASE 1).

First evidences of translational repression mechanisms in plants were highlighted by the work of Brodersen and colleagues (Brodersen et al., 2008) demonstrating that a component of the decapping complex, VCS (VARICOSE), is indeed essential for RNA silencing but does not affect the target mRNA level. In addition, they also showed that the microtubule-severing enzyme KTN1 (KATANIN 1) is required in this process, suggesting that spatial reorganization of the microtubule network may play a role in translational inhibition. In contrast to animals, plants have no GW182 homolog. However, a GW motif-containing protein SUO was identified in a genetic screen based on the accumulation of SPL3 (SQUAMOSA PROMOTER-LIKE 3), a miR156-targeted transcript known to be repressed by translational inhibition (Yang et al., 2012). Besides understanding of structural discrepancies

between GW182 and SUO, whether they are functional homologs is a question that still needs to be investigated. Although VCS and SUO are localized in P-bodies, animal and plant translational repression seem to act, at least partially, in a different way. Thus, the plant RISC is not able to trigger either deadenylation nor mRNA decay (Iwakawa and Tomari, 2013). It was shown that the position of the targeted mRNA sequence influences the mode of action of the plant RISC and that the 5' UTR- and ORF-directed RISC might block the assembly of the initiation complex and translation elongation, presumably by steric hindrance, while the 3'UTR-directed RISC might act like in animal cells (Iwakawa and Tomari, 2013).

Nevertheless, phenotypes of Arabidopsis mutants impaired in translational repression are much less severe than catalytically dead AGO1 mutants, supporting that slicing activity is predominant in plants (Vaucheret, 2008; Baumberger and Baulcombe, 2005; Brodersen et al., 2008; Yang et al., 2012). RISC-mediated cleavage results in the formation of two RNA fragments: the 5' fragment exhibit a 3'-OH extremity and the 3' fragment a 5' monophosphate end that are respectively degraded by the exosome and 5'-3' exoribonuclease XRN4 (Siwaszek et al., 2014; Scheer et al., 2016) (Figure 19A).

7. Human miRNAs functions in cell cycle and cancer

In human, one of the first evidences that miRNAs are involved in cancer emerged with the development of high-throughput sequencing of small RNAs. By analyzing chronic lymphocyte leukemia (CLL) and other tumor samples, Croce and colleagues identified a deletion in the 13q14 locus encoding two miRNAs (miR15 and miR16) that are downregulated or deleted in the majority of CLL (~70%), suggesting that these miRNAs have a potent tumor suppressor activity (Calin et al., 2002). The role of the miR15/miR16 cluster in regulating the expression of cell cycle genes was subsequently demonstrated (reviewed in Bueno and Malumbres, 2011; Leva et al., 2014). Indeed, miR15a and miR16-1 were shown to target a plethora of core cell cycle genes responsible of the G1/S transition including CDK6 and D-type cyclins (Liu et al., 2008b; Wang et al., 2009), and therefore may induce cell cycle arrest. In addition, overexpression of miR16 or introduction of mature miR16 in cell culture is sufficient to abolish cell proliferation (Linsley et al., 2007).

Cell cycle-regulating miRNAs have been extensively studied, notably to develop diagnostic and curative tools in cancer therapy. A large number of miRNA families have been

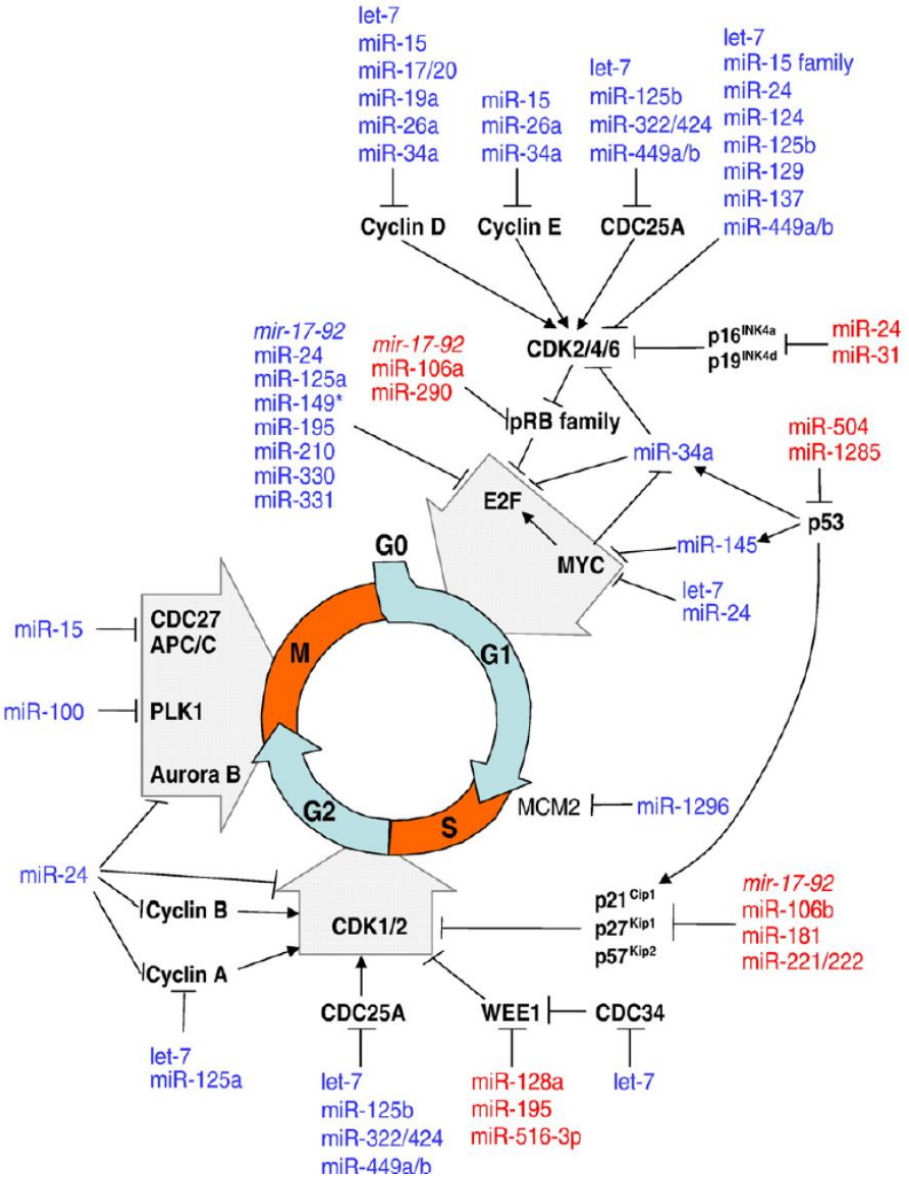

Figure 20 : Human miRNA-mediated cell cycle regulatory network (from Bueno and Malumbres, 2011).

This skim represents an overview of interactions between miRNAs and core cell cycle genes expression. Note that not all indicated miRNAs targets have been validated *in vivo*. miRNAs represented in blue correspond to tumor suppressor miRNAs and thus trigger cell cycle arrest. Red-tagged miRNAs correspond to miRNAs that have oncogenic properties and could promote cell proliferation.

identified as well as their targets. These miRNAs can be categorized in two classes: Oncogenic miRNAs (or OncomiRs) that promote cell proliferation and tumor development, and tumor suppressor miRNAs (or anti-proliferative miRNAs) that induce cell cycle arrest and even apoptosis for some of them (reviewed in Bueno and Malumbres, 2011; Leva et al., 2014). Interestingly, most of miRNA-dependent cell cycle regulation occurs at the G1/S transition. D-type cyclins, that are accumulated upon mitogenic stimuli and, associated with CDK4 and 6, promote cell cycle entry, are not only targeted by miR15 and 16, but also by at least five other miRNAs (reviewed in Bueno and Malumbres, 2011). Overall, a wide spectrum of core cell cycle genes is post-transcriptionally controlled by miRNAs (Figure 20). This includes positive cell cycle regulators, such as CDK2/4 and 6, E2F transcription factors and CDC25 phosphatases, but also inhibitory proteins like RB, $p107^{RBL1}$, $p130^{RBL2}$, CDK inhibitors ($p21^{CIP1}$, $p27^{KIP1}$ and $p57^{KIP2}$) and the tumor suppressor p53. Some miRNAs target genes are also required for progression through mitosis. Among them, B-type cyclins and CDK1, but also the kinase AURORA-B, that plays a crucial role in mitotic spindle attachment to the kinetochore, seem all repressed by miR24 (Lal et al., 2009) (Figure 20). The striking diversity of miRNA targets illustrates a high redundancy of miRNA function, as well as the fact that one miRNA is able to directly repress several functional related transcripts.

While the steady state level of most of the miRNA species remains stable in time, cell cycle-regulating miRNAs are subjected to a rapid turnover in proliferative cells to achieve their function on cell cycle progression. Thus, they are transcriptionally controlled by a set of cell cycle- specific transcription factors such as the proto-oncogene C-MYC, which is a crucial regulator of cell growth, proliferation, differentiation and other associated metabolic processes (Eilers and Eisenman, 2008; reviewed in Miller et al., 2012). C-MYC positively or negatively regulates the expression of a great variety of genes, including core cell cycle genes (S-phase cyclins, $p21^{CIP1}$,$p57^{INK4B}$), but also non-coding RNAs, like ribosomal RNAs, transfer RNAs and miRNAs (reviewed in Krol et al., 2010; Bui and Mendell, 2010; Kenneth and White, 2009). As an example, C-MYC induces the expression of the miR17-92, which inhibits expression of RB and RB-like proteins, and therefore allows expression of G1/S genes (Figure 21A). In addition, some E2Fs transcription factors also activate expression of OncomiRs, while the tumor suppressor p53 induces expression of anti-proliferative miRNAs and particularly miR34a and miR145, that inhibit E2Fs and c-MYC expression, respectively (Figure 20) (Bao et al., 2012; Sachdeva et al., 2009).

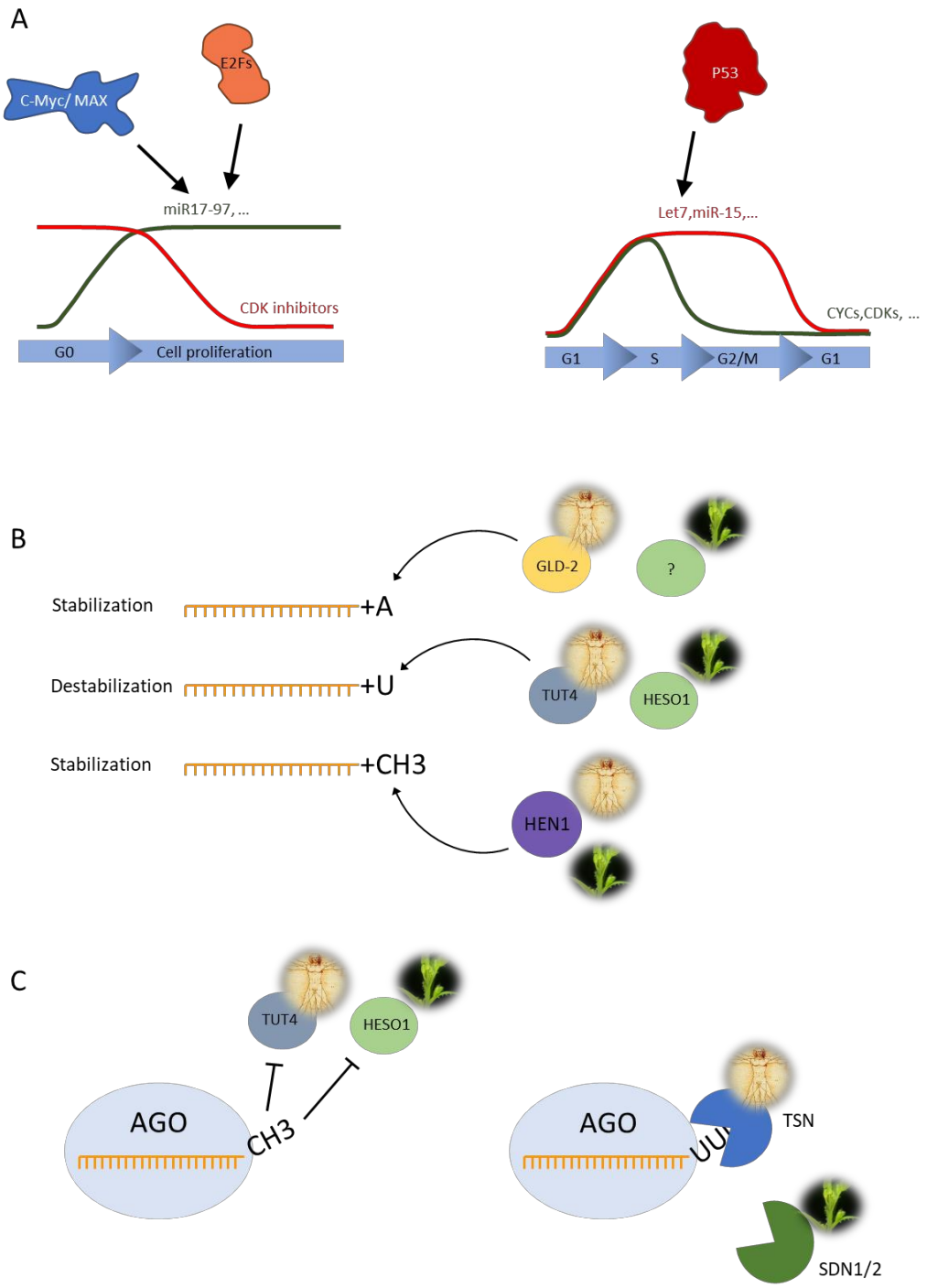

Figure 21 : Cell cycle regulatory miRNAs are highly dynamic.

(A) Upon mitogenic stimuli, proliferative miRNAs levels increase to lower the expression of CDK inhibitors and other inhibitory cell cycle proteins such as pRB. Their levels remain constant as long as proliferative signals are maintained. Some miRNAs are accumulated in a phase specific manner to decrease the expression of regulatory genes and therefore might contribute to trigger cell cycle transitions. Differential accumulation of some miRNAs can be partly explained by the fact that they are under transcriptional control of cell cycle specific transcription factors, including c-MYC, E2Fs and P53. **(B)** miRNAs are subjected to post-transcriptional modifications that affect their stability. Mono or polyadenylation has been observed in animals and plants and stabilizes the miRNA. GLD-2 is the enzyme responsible of miRNA adenylation in human. miRNAs can also be stabilized by HEN1-mediated 2'-O methylation that prevents their uridylation by the human TUT4 and plant HESO1 terminal uridyl-transferases (TUTases). **(C)** miRNA polyuridylation destabilize miRNA accumulation by promoting their degradation by exoribonucleases. The human TSN and Arabidopsis SDN1/2 nucleases can degrade uridylated miRNAs that are loaded in AGO proteins and consequently may contribute to RISC reprogramming.

Transcriptional control is however not sufficient to explain the differential accumulation along the cell cycle of some miRNAs and miRNA turnover is also an active process allowing quick miRNA decay (Figure 21B and C) (reviewed in Krol et al., 2010; Rüegger and Großhans, 2012). For instance, miR29s are tumor suppressors miRNAs that act by upstream relieving p53 inhibition (reviewed in Kriegel et al., 2012). miR29a and miR29b form a cluster and thereby are transcribed and processed the same way. However, miR29b half-life is shorter compared to miR29b (Hwang et al., 2008). In addition, miR29b half-life was shown to be significantly increased in mitotic cells (Hwang et al., 2008), and mutations of two uracil in position 9 and 11 almost totally abolished its degradation (Zhang et al., 2011), highlighting the existence of a cell cycle-specific miRNA decay pathway. Other miRNAs are also continuously accumulated or repressed during cell proliferation, like miR503 (Bueno and Malumbres, 2011). miR503 promotes cell cycle arrest in G1 and differentiation by targeting the CDK-activating phosphatase CDC25A (Sarkar et al., 2010; Llobet-Navas et al., 2014). It has been shown that miR503 accumulation is strongly reduced at G0/G1 transition and is almost not anymore detectable in proliferative cells (Rissland et al., 2011). Unlike miR29b, it is not degraded with a specific timing but it is constitutively unstable, suggesting that variations in miR503 levels are principally the consequences of transcriptional changes (Rissland et al., 2011).

Although cell cycle-regulating miRNAs decay is not fully understood, a recent study showed that the endonuclease TSN (TUDOR STAPHYLOCOCCAL/MICROCOCCAL-LIKE NUCLEASE), that initiates miRNA degradation on loaded AGO2-RISC, promotes G1/S transition, illustrating the fundamental role of miRNA turnover in cell cycle regulation (Elbarbary et al., 2017) (Figure 21C).

8. Small RNA functions in plant development

Nowadays, 428 mature miRNAs have been referenced in miRbase for Arabidopsis (www.miRbase.org). Common experimental strategies used to study miRNA functions and particularly identify their targets rely on several tools: (1) Bioinformatics prediction of miRNA targets (2) genome-wide and/or gene specific transcript analysis, (3) identification of miRNA cleavage products by 5'-RACE and (4) *in vivo* target validation by dominant negative approaches, like miRNA mutations or expression miRNA-resistant versions of the putative

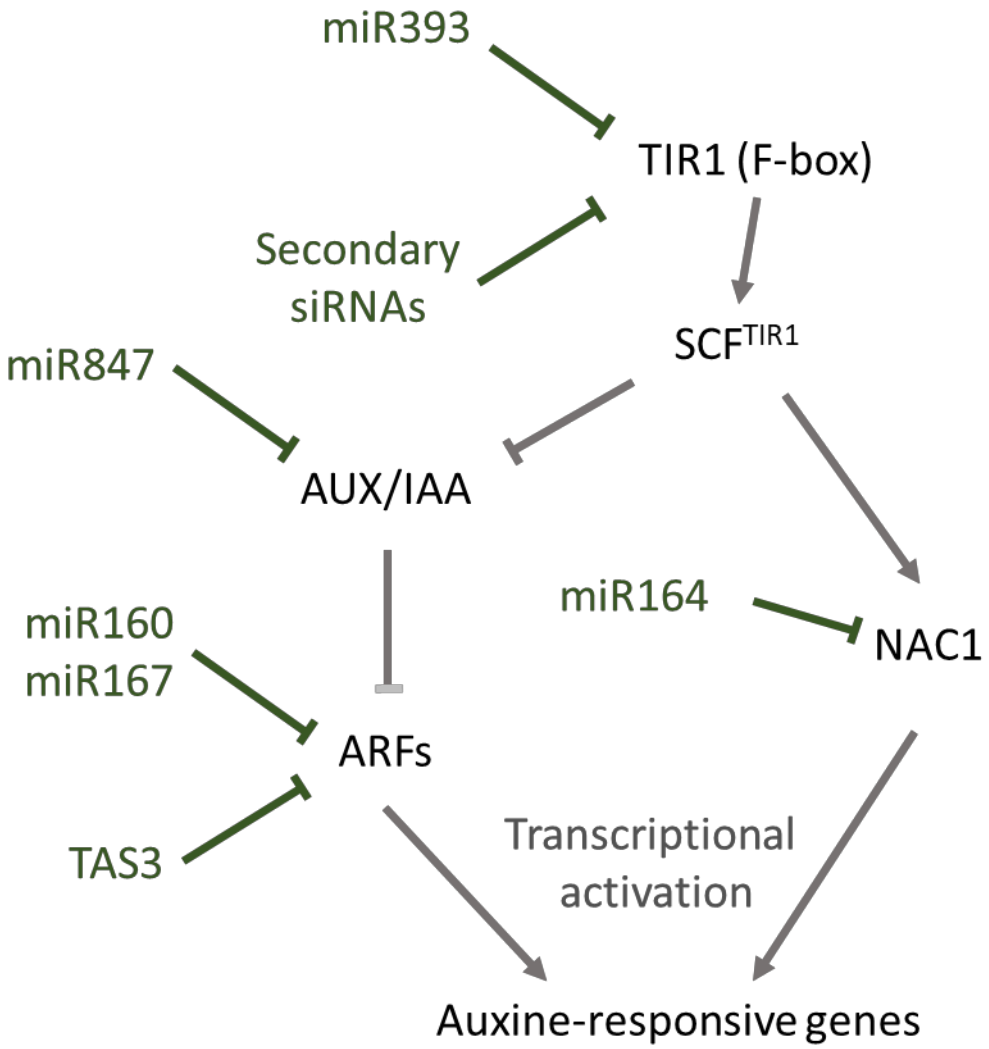

Figure 22 : Small RNAs contribute to the regulation of the auxin signalling pathway.

TIR1 is the F-box protein that associates with the SCF to trigger AUX/IAA polyubiquitination. AUX/IAA are transcriptional repressors that inhibit ARFs transactivation activity. Upon auxin binding to TIR1, the SCF^{TIR1} interacts with AUX/IAAs and triggers their degradation though the 26S proteasome, resulting in the expression of ARF-responsive genes. NAC1 is another transcription factor acting downstream TIR1. In addition to post-translational regulations, auxin signalling is also subjected to post-transcriptional regulations mediated by small RNAs. This process involves both miRNAs and siRNAs. siRNAs are generated through TAS3 targeting ARFs transcription factors and by miR393 induced RDR6 mediated-secondary siRNA generation to repress TIR1.

targets. During the last decade, target predictions in plants were based on nearly perfect complementarity of miRNA/mRNA duplexes, since it was thought that, unlike animals, plant RISC essentially perform slicing rather than translation inhibition (Rhoades et al., 2002; Axtell and Bartel, 2005; Axtell and Meyers, 2018). Most of the plant miRNAs functions are related to plant development, hormone signaling and stress responses (reviewed in Chen, 2005; Voinnet, 2009). In the following section, I will focus on some examples of miRNA functions related to cell proliferation.

a. Post-transcriptional control of auxin signaling

Auxin signaling is essential for plant development and adaptation to stresses. It is involved in both embryogenesis and post-embryonic organ formation and participates to the establishment of polarity and to tropic responses (reviewed in Lavy and Estelle, 2016). At a cellular level, auxin plays a pivotal role in the balance between cell division and cell expansion (reviewed in Perrot-rechenmann, 2010). The first link between RNA silencing and the auxin signaling pathway was highlighted by Sorin and colleagues, showing that Arabidopsis *ago1* null mutants are affected in auxin responses and were insensitive to auxin treatment (Sorin et al., 2005). In addition, loss of *AGO1* was correlated with the overaccumulation of ARF17 (AUXIN-RESPONSE FACTOR 17), a transcription factor involved in activation and repression of auxin-responsive genes. Several ARFs were predicted as putative miRNA targets: miR160 binding sites were identified in ARF10, ARF16 and ARF17 while miR167 was thought to target ARF6 and ARF8 (Rhoades et al., 2002; Axtell and Bartel, 2005) (Figure 22). These miRNAs targets were later validated *in vivo* through genetic approaches (Mallory et al., 2005; Wang et al., 2005; Liu et al., 2007; Wu et al., 2006; Ru et al., 2006).

Other components of the auxin-signaling pathway are also targeted by miRNAs. ARFs transactivation activity is negatively regulated by AUX/IAA transcriptional repressors (reviewed in Lavy and Estelle, 2016) (Figure 22). Activation of auxin-induced genes therefore requires 26S proteasomal degradation of AUX/IAA that is mediated by TIR1/AFB1-3 F-box proteins (TRANSPORT INHIBITOR RESPONSE 1/ AUXIN-RELATED F-BOX PROTEIN 1-3). Thus, miR393 was shown to accumulate in response to auxin treatment and to trigger the inhibition of TIR1/AFBs (Parry et al., 2009; Sunkar and Zhu, 2004; Chen et al., 2011). In

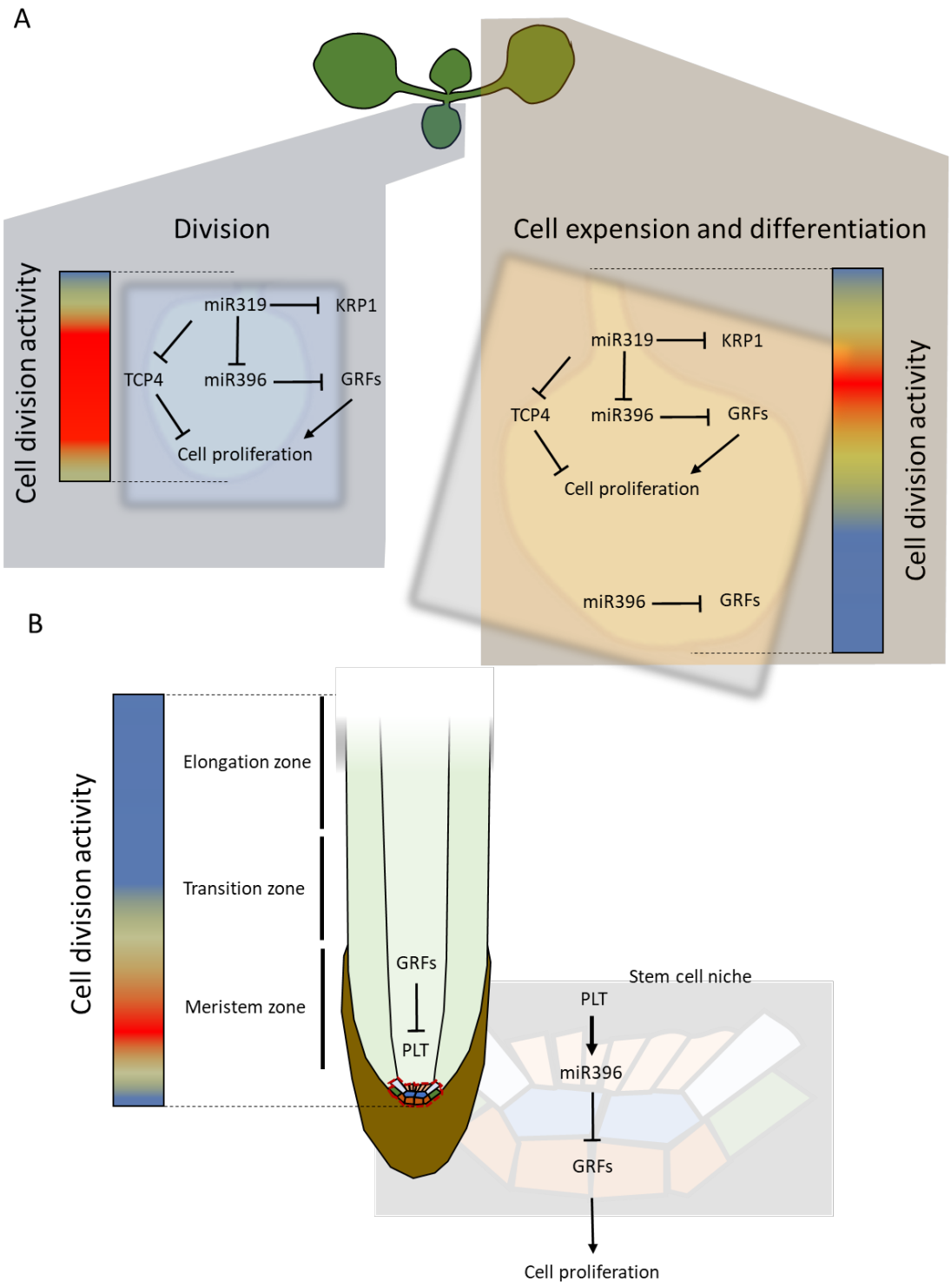

Figure 23 : Control of cell proliferation by miR319 and miR396 in *Arabidopsis thaliana.*

miR319 and miR396 play antagonistic functions in regulating cell proliferation in plants. miR396 targets the transcripts of GRF transcription factors that promote cell proliferation. miR319 is acting upstream of miR396 and represses its accumulation. miR319 also represses the expression of TCP4, a transcription factor that inhibits cell proliferation, and of the CDK inhibitor KRP1. **(A)** In young leaves miR319 is highly expressed to promote cell division. Conversely in older leaves, miR396 is gradually accumulated to repress cell division and promote cell expansion and differentiation. **(B)** In the root apical meristem, the accumulation of miR396 contributes to maintain stem cell niche (SCN) identity. To achieve this, PLETHORA (PLT) promotes miR396 expression, thus lowering GRF accumulation in the SCN. In contrast in the meristematic zone, GRF transcription factors promote intensive cell division activity.

addition, expression of miR393-insensitive mutant of TIR1 induces strong pleiotropic phenotype, suggesting that miR393 plays a key role in a feedback loop to regulate auxin signaling (Figure 22). Interestingly, secondary RNAs are also controlling the auxin pathway, as two members of the ARF family, ARF3 and ARF4, are subjected to post-transcriptional regulation by the *TAS3* locus (Figure 22) (Allen et al., 2005). It has also been shown that miR393-mediated cleavage of TIR1/AFB2 transcripts initiates generation of secondary siRNAs that further target other mRNAs, including all of the four members of the TIR1/AFB clade.

The transcription factor NAC1 (NAC DOMAIN-CONTAINING PROTEIN 1), acting downstream of TIR1 and involved in shoot apical meristem and lateral root formation, is targeted by miR164 (Rhoades et al., 2002; Guo et al., 2005), whereas the IAA28 transcript, encoding a transcriptional repressor belonging to the AUX/IAA family, is degraded by miR847, regulating both cell proliferation in the aerial part and lateral root branching (Wang and Guo, 2015) (Figure 22). In conclusion, small RNA-mediated post-transcriptional regulation of auxin signaling pathways constitutes a complex network responding to diverse stimuli and contributing to plant phenotypic plasticity (reviewed in De-la-Pena et al., 2017).

b. Control of cell proliferation by miR319 and miR396

Despite the fact that no plant miRNA has yet been found to directly target components of the core cell cycle machinery, two miRNAs, miR319 (*jaw*) and miR396 modulate cell proliferation through the control of two classes of transcription factors: TCPs (TEOSINTE BRANCHED 1, CYCLOIDEA, AND PCNA-BINDING FACTOR) and GRFs (GROWTH-REGULATING FACTOR) (Figure 23). Four *jaw* mutant alleles were initially isolated from an enhancer screen due to their developmental alterations, such as serrated abnormal leaf shape and curvature (Weigel et al., 2000). Since no open reading frame was identified near the T-DNA insertion, it was proposed that the mutation might affect a non-protein coding gene (Weigel et al., 2000). Genome-wide transcriptomics analysis revealed that ectopic activation of the *JAW* locus led to a substantial reduction of TCP2, 3, 4, 10 and 24 expression (Palatnik et al., 2003a). RNA blot analysis further demonstrated that the mature product of *JAW* expression is indeed a 21 nt miRNA (later called miR319) and the expected miR319-targeted TCPs were further validated (Palatnik et al., 2003a, 2007; Ori et al., 2007) . The TCP

family is constituted by 24 members and is divided in two classes based on their affinity for different consensus DNA binding sites (Kosugi and Ohashi, 2002). Class I and Class II TCPs are thought to play antagonistic functions in post-embryonic development. TCP4, as well as four other miR319-regulated TCPs, belongs to the Class II. Interestingly, microarray analysis of miR319-resistant TCP4 mutants highlighted the down regulation of more than 1300 genes and many of those were related to cell division and the progression of the cell cycle, including MYBR1R2and R3 transcription factors (Schommer et al., 2014). In parallel, TCP4 was shown to bind directly to the promoter of the CDK inhibitor ICK/KRP1 by chromatin immunoprecipitation and thereby stimulate its expression (Schommer et al., 2014).

TCP4 also activate the expression of miR396, that specifically target seven GRF proteins: GRF1, 2, 3, 4, 7, 8 and 9 (Jones-Rhoades and Bartel, 2004; Rodriguez et al., 2010b). GRF are regulating several plant developmental processes that are linked to cell growth and proliferation, including leaves and root growth, stem elongation, flowering, lipid metabolism in seeds and maintenance of the shoot (SAM) and root apical meristem (RAM) (reviewed in Omidbakhshfard et al., 2015). Rodriguez et al., 2010 showed that GRF2 accumulation pattern, that is normally restricted to proliferating leaves and to the SAM, is extended to the entire aerial part of the plant when a miR396-resistant version of GRF2 (rGRF) is expressed (Figure 23A). In parallel, miR396 overexpression significantly decreases rosette area and cell number, suggesting that cell proliferation is impaired. miR396 is also involved in the maintenance of the RAM (Figure 23B). The RAM is composed of the meristematic zone, that carries most of the cell division activity and provides cells for proper root development, and the stem cell niche (SCN), that includes the quiescent center (QC) and the initials. While the principal function of the QC is to maintain the stem cell identity of the neighbouring cells, initials are essential for root patterning, as they give rise to the different root cell layers (reviewed in Petricka et al., 2012). Hence, maintenance of the SCN is crucial for root development. Three major transcription factors have been involved in SCN identity: SHORTROOT (SHR), SCARECROW (SCR) and PLETHORA (PLT). Interestingly, miR396 expression is restricted to the SCN and depends on PLT (Rodriguez et al., 2015). in contrast, GRFs are strongly accumulated in the meristematic zone but absent from the SCN and both miR396 overexpression and expression of the miR396-resistant (rGRF) affects meristem organization, size, and mitotic activity. Based on these observations, the authors proposed that miR396 contributes to maintain low division rate of the SCN in the root meristem and thereby

controlling the transition between the SCN and the meristematic zone (Rodriguez et al., 2015).

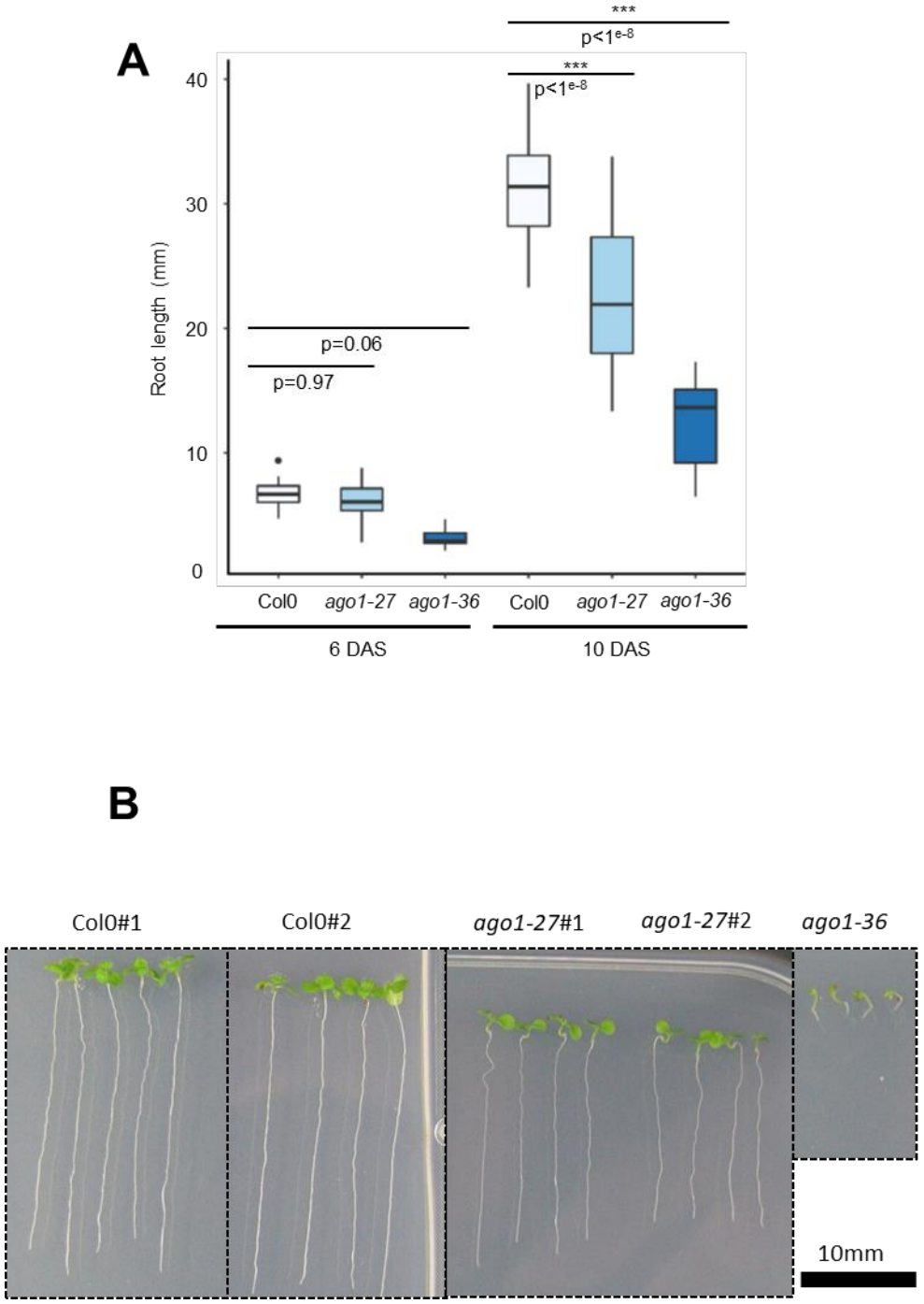

Figure 24: Loss of *AGO1* affects root development.

(A) Root length measurement of wild type plants compared to *ago1* mutant plants indicated in mm. Roots were measured at 6 and 10 days after stratification (DAS) for >30 seedlings. ANOVA test were performed for each genotype compared to WT, indicating significant differences ($p<0.05$). The (***) symbol highlights comparison for which $p<0.001$. **(B)** Phenotype of wild type plants compared to *ago1* mutants on 10 DAS seedlings. Seedlings were grown on vertical plates and 4 of each genotype were randomly selected for more clarity. #1 and #2 correspond to different seed stock. Bar: 10 mm.

Results

A. AGO1 depletion affects Arabidopsis cell division and root meristem activity

1. Arabidopsis *ago1* mutants are impaired in root developments

In Arabidopsis, *ago1* null mutants exhibit a severe morphological phenotype affecting leaf shape and polarity, along with defects in meristem identity and function (Bohmert et al., 1998; Morel et al., 2002; Kidner and Martienssen, 2004, 2005). To better characterize these defects in plant development, I first analyzed the primary root growth of two different mutant alleles of *AGO1*. The Arabidopsis *ago1-27* mutant has been isolated from a genetic suppressor screen (Morel et al., 2002). *ago1-27* mutation is located is the PIWI domain and results in a reduced activity of the protein. I also tested the strong *ago1-36* allele that correspond to a T-DNA insertion (salk_087076) in the PAZ domain, leading to the expression of a truncated protein (Baumberger and Baulcombe, 2005) and therefore can be considered as a null allele. I already found a slight reduction in the root length of the hypomorphic *ago1-27* allele, while this phenotype was severely compromised in the strong *ago1-36* mutant (Figure 24). Because root development largely relies on the function of the root meristem, I investigated its structural organization by confocal microscopy using propidium iodide (PI) cell wall staining. In wild type Arabidopsis root meristem, cells are well organized in a characteristic pattern. The quiescent center is surrounded by the initials, forming the SCN that give rise to the different cell layers of the meristematic zone (Figure 25).

In the *ago1-27* background, only a subset of the observed roots exhibit defects in meristem organization. In addition, those defects seem to be restricted to the SCN and do not affect the upper layers. Conversely, the root patterning is completely lost in *ago1-36* (Figure 25). We conclude that *AGO1* is required for proper root development. These observations are consistent with the published data that have already linked the miRNA pathway to the maintenance of stem cell identity in the root meristem. However, the QC and the initials have low cell division rate and most of the cell division activity is carried out by upper cells. Interestingly, both hypomorphic and strong *ago1* mutants are affected in the SCN organization, while phenotypes that are related to cell cycle defects, such as a decrease in cell number coupled to an increase of cell size, are only present in the strong *ago1-36* mutants.

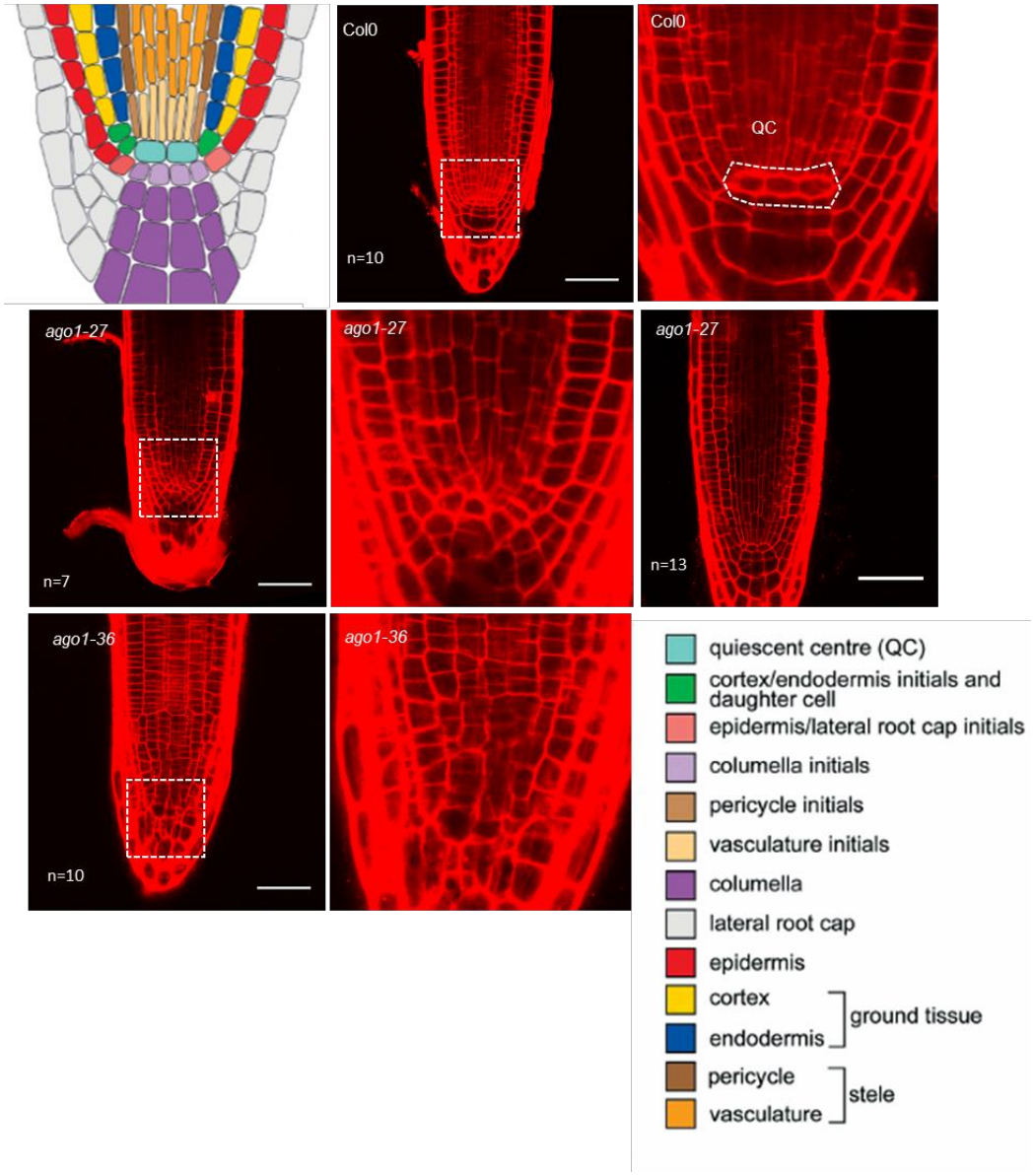

Figure 25: *ago1* mutants exhibit altered root meristem patterning (The figure illustrating the different cell types in the RAM is from Stahl et al., 2005).

Representative wild type and mutant root tips of 6-days old seedlings. The skim represents the different cell layers that constitute the root apical meristem (RAM) in Arabidopsis (adapted from Stahl and Simon, 2005). The middle column represents close-up views of the quiescent center (QC). The n value represents the number of plant observed. Roots were counterstained with propidium iodide (red signal). Bars = 50 µm.

2. AGO1 is required for the maintenance of the root meristem

It is possible that the defects in root meristem activity described above might find their origin already during the embryo development. Indeed, mutations in genes encoding miRNA pathway components, like DCL1, cause pattern formation defects leading, in the worse cases, to embryonic lethality (Nodine and Bartel, 2010; Vashisht and Nodine, 2014). To confirm that AGO1 is essential to maintain the root meristem activity post-embryonically, I took advantage of an Arabidopsis transgenic line engineered in the lab, in which it is possible to induce AGO1 degradation upon chemical induction of P0 with β-estradiol (XVE:P0-myc). In this line, β-estradiol treatment induces the expression of the viral protein P0 from Turnip yellows virus (TuYV), which is a potent viral suppressor of silencing. P0 carries an F-box motif and is able to highjack a SCF complex to form a fully functional E3 ligase (Figure 26A). By interacting with AGO1, it triggers its degradation in the vacuole, presumably though AGO1 polyubiquitinylation (Derrien et al., 2018 and references therein).

Thus, I germinated the P0-inducible line on MS medium supplemented with or without β-estradiol in order to induce P0 expression. Upon P0 induction, the root length was significantly reduced compared to the untreated seedling (Figure 26B and C). Because P0 triggers the degradation of several, if not all plant AGOs (Baumberger et al., 2007; Derrien et al., 2018), the phenotypes we observed might not be exclusively due to the loss of AGO1. To evaluate the contribution of only AGO1, I also induced P0 expression in the *ago1-57* genetic background. The *ago1-57* mutation is located in the DUF1785 domain of AGO1 and abolishes its interaction with P0 (Derrien et al., 2018). By inducing P0 in *ago1-57*, we are then able to uncouple the effects of AGO1 depletion from the loss of other AGO proteins. The strong effect of P0 on root growth was significantly suppressed in *ago1-57* (Figure 26B and C), indicating that this phenotype is largely dependent on AGO1 (and thus likely on miRNAs) and not on other AGO proteins.

To further dissect the phenotype caused by loss of AGO1, I analyzed the length of the root meristem of P0-induced compared to untreated seedlings. To do so, I imaged at least 20 root tips for each genotype using PI staining. I then measured the distance between the QC and the first cell of the cortex that undergoes cell expansion (Figure 27). I was able to detect a decrease of the root meristem length in XVE:P0-myc after six days of β-estradiol treatment,

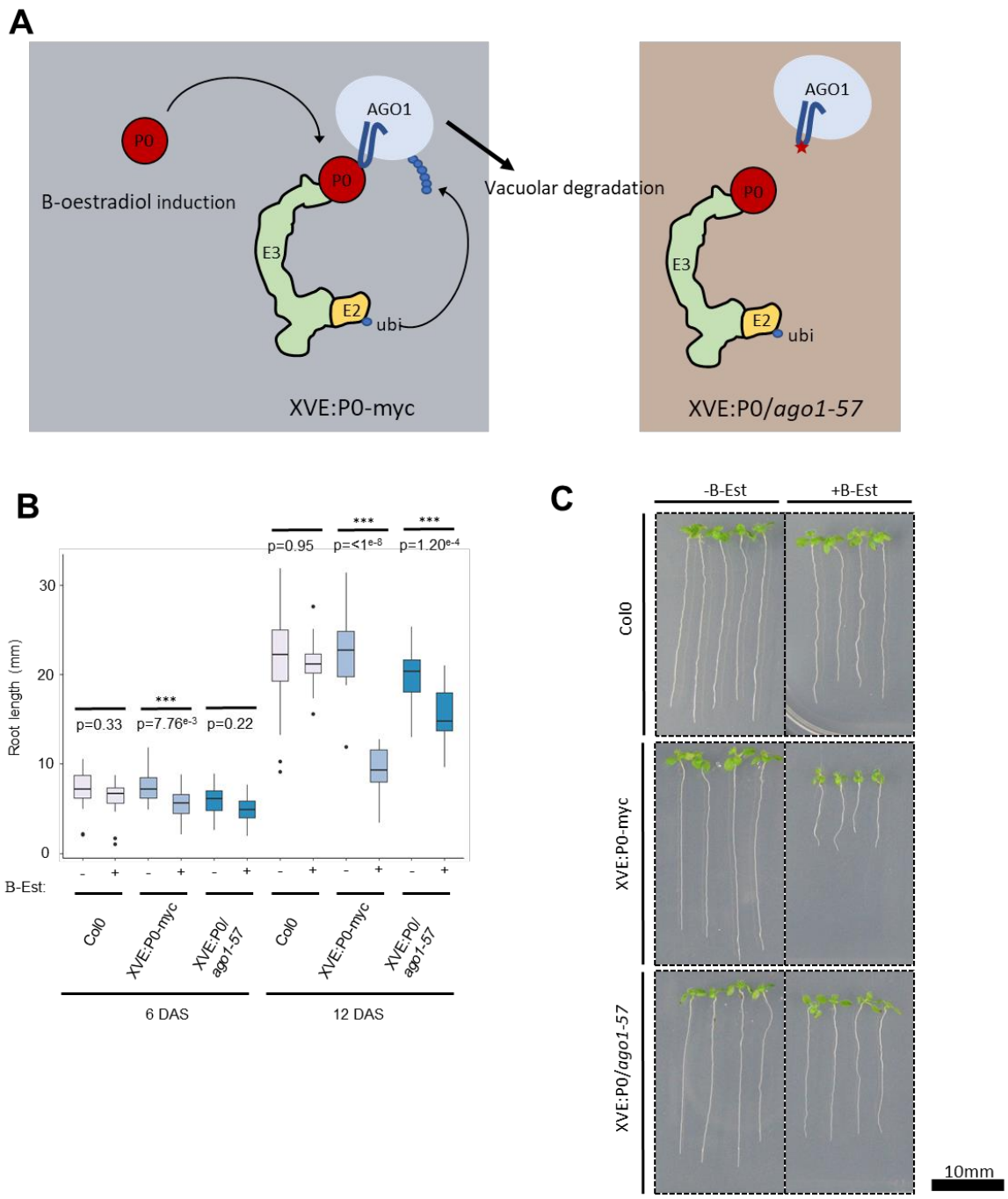

Figure 26: Post-embryonic depletion of AGO1 affects root development.

(A) Mechanism for P0-depedent AGO1 degradation in XVE:P0-myc and XVE:P0/*ago1-57* transgenic Arabidopsis lines. Upon B-estradiol treatment, P0 is induced and highjacks an SCF complex. P0 then interact with AGO1 to trigger its polyubiquitination and its subsequent degradation through a vacuolar process. In the *ago1-57* genetic background, a residue essential for P0 interaction is mutated abolishing AGO1-57 degradation. **(B)** Root length measurements in mm of wild type plants compared to P0-inducible line and P0-insensitive *ago1-57* mutants. Seedling were germinated with (+) or without (-) β-estradiol (10 µM) to induce P0 expression. Measurement were done at 6 and 12 days after stratification (DAS) on >30 seedlings. ANOVA tests were performed, indicating significant differences ($p<0.05$). The (***) symbol highlight comparison for which $p<0.001$. **(C)** Phenotype of wild type plants compared to XVE:P0-myc and XVE:P0/*ago1-57* on 10 DAS seedlings with or without B-estradiol induction. Seedlings were grown on vertical plates and 4 of each genotype were randomly selected for illustration. Bar: 10mm.

while XVE:P0 in *ago1-57* background showed no obvious differences between induced and non-induced conditions. In addition, root meristem measurements were no more possible after 12 days of induction, as induced the XVE:P0-myc lines recapitulate the phenotype of strong *ago1-36* mutants. From these experiments, we conclude that AGO1 is indeed required for proper root development and contributes to the maintenance of the root meristem. An overall decrease of the cell division activity might explain that the root meristem is gradually consumed upon AGO1 degradation. We next wondered whether cells arrest at a specific cell cycle stage.

3. Loss of AGO1 affects cell proliferation in the root apical meristem

To confirm that loss of AGO1 indeed affects cell cycle activity in the root tip and investigate whether it would block cell division at a specific cell cycle phase, I transformed both XVE:P0-myc and XVE: P0 (*ago1-57*) lines with two lines expressing fluorescent cell cycle markers: pHTR2:CDT1a(C3)-GFP and pCYCB1.2::CYCB1.2 (dBox)-GFP (Figure 28A). The pHTR2:CDT1a(C3)-GFP construct consists of an S phase specific promoter from a histone 3 gene that drives the expression of the C-terminal part of the replication factor CDT1a, that is subjected to 26S proteasome-mediated degradation in late G2 (Yin et al., 2014). By fusing it to GFP, it is possible to identify cell that are in S/G2. On the other end, the CYCB1.2 is known to accumulate starting from G2 and be quickly degraded later by the APC/C at the exit of mitosis (Donnelly et al., 1999). By consequence, expression of the unstable motif (DBox) of CYCB1.2 under the control of its own promoter is sufficient to highlight cells that undergo mitosis.

I then performed confocal imaging of root tips of doubly homozygous seedlings to compare cell cycle marker distribution with or without P0 induction. In untreated conditions, S/G2 marker is widely expressed in the root meristem and particularly in adjacent cells belonging to the same cell layer (referred as S phase synchronized cells) (Hayashi et al., 2013). As mitosis is a highly transient event, G2/M marker expression is only restricted to only few cells. Upon P0 induction, the number of cells expressing both S/G2 and G2/M markers dramatically decreased (Figure 28B) and correlates with a progressive disorganization of the root tip. Inversely, cell cycle activity was maintained when expressing P0 in *ago1-57* mutant background even after 10 days of induction. At this point, I conclude

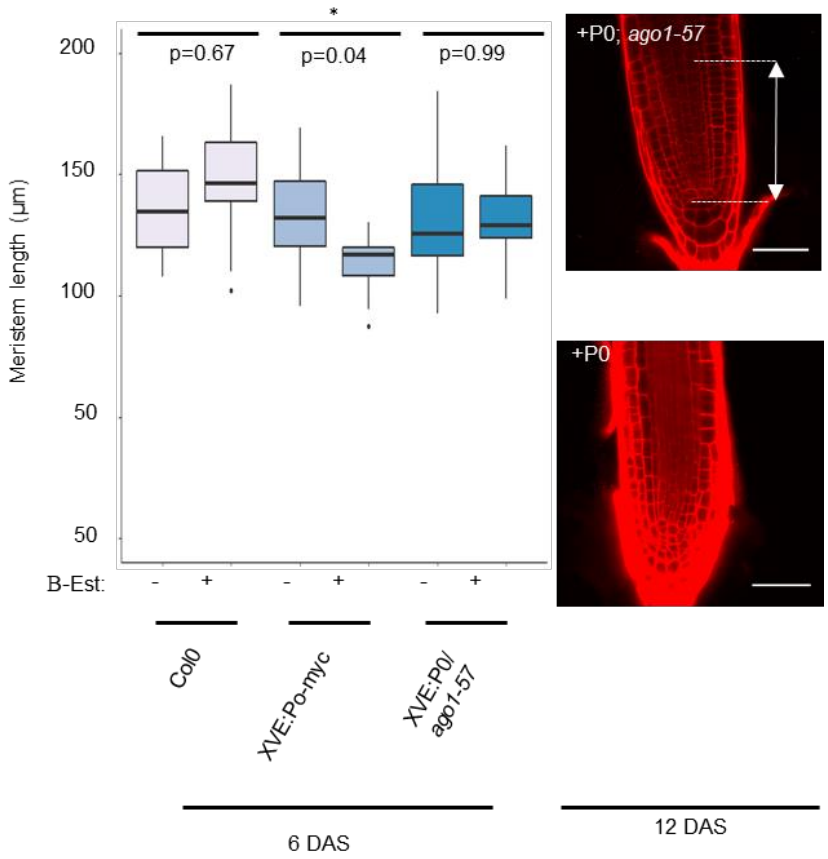

Figure 27: Post-embryonic depletion of AGO1 affects root meristem length and organization.

Root-meristem size indicated in µm of wild-type plants compared to the indicated genotypes. Cortex meristematic cells showing no sign of differentiation were counted. Values are meristem length of 6 DAS seedlings germinated with (+) or without (-) β-estradiol (10 µM). Anova test were performed, indicating significant differences ($p<0.05$). The (*) symbol highlights comparison for which $0.01<p<0.05$. Right panels are primary root tips of XVE:P0-myc and XVE:P0-myc (ago1-57) after 12 days of P0 induction. Roots were counterstained with propidium iodide (red signal). Arrows indicate the length of the meristematic zone (from the QC to the first elongating cell of the cortex). Bars = 50 µm.

that AGO1 activity is required to maintain normal cell proliferation in the Arabidopsis root meristem, but, as both cell cycle markers were repressed similarly, AGO1 depletion does not seem to distinctly lead to a specific cell cycle phase arrest.

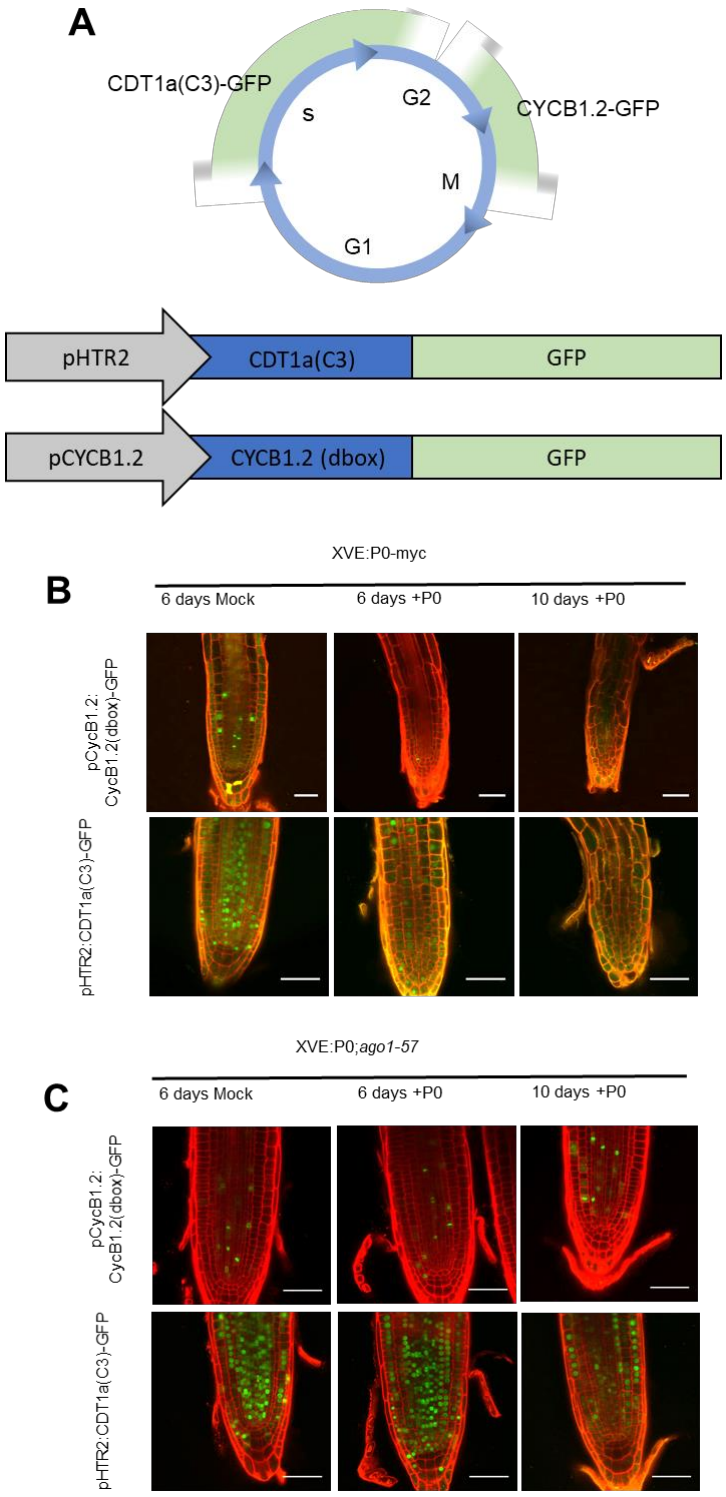

Figure 28: AGO1 is required for the maintenance of cell cycle activity in the root meristem.

(A) To evaluate the cell cycle activity upon AGO1 depletion, two fluorescent cell cycle markers were transformed in XVE:P0-myc and XVE:P0/*ago1-57* transgenic lines. pHTR2:CDT1a(C)-GFP construct is expressed from G1/S transition to early G2 while pCYCB1.2:CYCB1.2-GFP is expressed in late G2 and then degraded in telophase. **(B)** Confocal laser scanning images of primary root tips of XVE:P0-myc and XVE:P0-myc (*ago1-57*) lines expressing the indicated cell cycle markers without and after 6 and 10 days of P0 induction with β-estradiol (10 µM). Bars=50 µM.

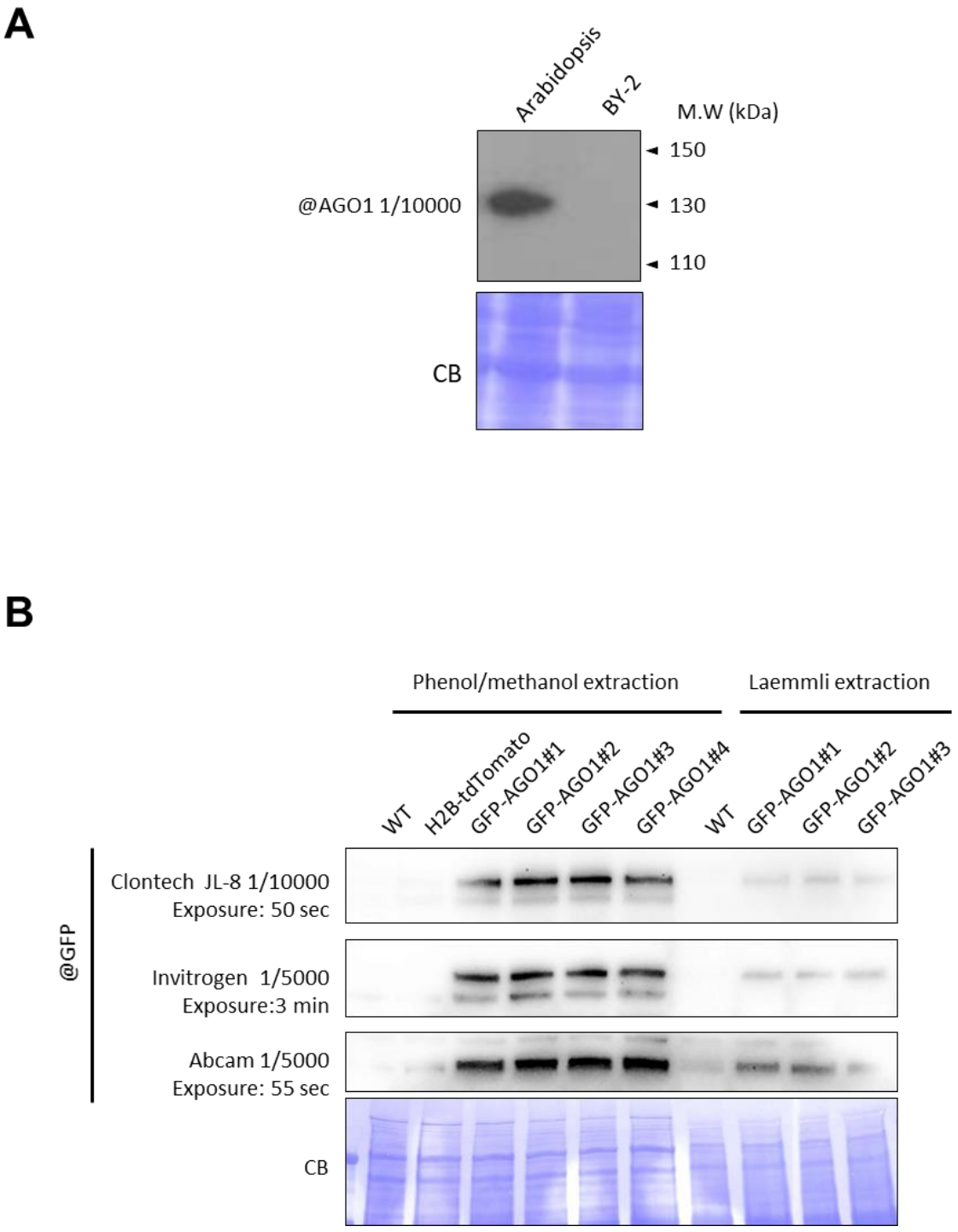

Figure 29: Protocol to optimize AGO1 immunodetection from BY-2 cell suspension.

(A) Attempt to detect endogenous AGO1 from BY-2 tobacco cells on wester-blot using a commercial rabbit polyclonal antibody raised against Arabidopsis AGO1. Proteins were extracted from Arabidopsis seedling and BY2 cells using the same buffer (Laemmli 1X) **(B)** Optimization of the protein extraction protocol in order to detect GFP-AGO1 from transgenic BY-2 cell suspension. Classical Laemmli 1X extraction and Phenol/methanol precipitation were challenged by SDS-PAGE. 30µg of total protein were loaded on a 7% Tris-Glycine acrylamide gel. WT and H2B-tdTomato expressing BY2 cells were used as negative control. #1, #2, #3 and #4 correspond to 4 different BY2 clonal cell suspension cultures. Three commercial anti-GFP antibodies were tested. The concentration and time of exposure are indicated. Coomassie blue (CB) staining was used as a loading control.

B. AGO1 regulation in synchronized BY-2 cells

To address more specifically the question of the regulation and function of AGO1 during the cell cycle, it is essential to adopt an experimental setup where cells can be sufficiently enriched in the specific cell cycle phases. Synchronizable systems have already been extensively used in the past for cell cycle studies. This generally requires undifferentiated, highly proliferative cell suspensions. Hence, yeast and human HeLa cells are well suited for these experiments. In the plant field, *Chlamidomonas reinhardtii,* Arabidopsis and Tobacco BY-2 cell suspensions have been commonly used for cell cycle synchronization. While Arabidopsis is the best characterized plant model organisms, the tobacco BY-2 cell suspension is offering a much better synchronization efficiency and the possibility to biochemically monitor AGO1 steady state level at all cell cycle phases. Note that *Nicotiana tabacum* (tobacco) is an allotetraploid organism that originates from the hybridization of *Nicotiana sylvestris* and *Nicotiana tomentosiformis* about 200,000 years ago. Until recently, its genome was poorly annotated due to its size (4.5Gb) and its high complexity (70% of repeats), but more recent efforts have significantly improved this issue (Sierro et al., 2014; Edwards et al., 2017). Thus, I decided to move to BY-2 cells to study AGO1 regulation and function over the cell cycle in this system.

1. Generation of transgenic GFP-AGO1 BY-2 cell suspension and detection optimization

I first checked whether it was possible to detect endogenous AGO1 in BY-2 cells using the commercially available anti-AGO1 antibody from Arabidopsis. Unfortunately, this was not the case (Figure 29A). Thus, to be able to detect and later purify AGO1 from BY-2 cells, I transformed the cell suspension with a construct allowing expression of a GFP-fused Arabidopsis AGO1 under the control of its own promoter (pAGO1:GFP-AGO1). This construct encodes a functional AGO1 protein that was shown to complement several *ago1* mutant alleles in Arabidopsis (Derrien et al., 2012). Such a functional AGO1 fluorescent protein will also permit to study its subcellular localization during the cell cycle.

Among the different transgenic clonal cell suspension generated, I was unable to find some with high GFP-AGO1 expression levels, thus the optimization of the protein extraction protocol for GFP-AGO1 immunodetection was critical. Therefore, I compared the quick

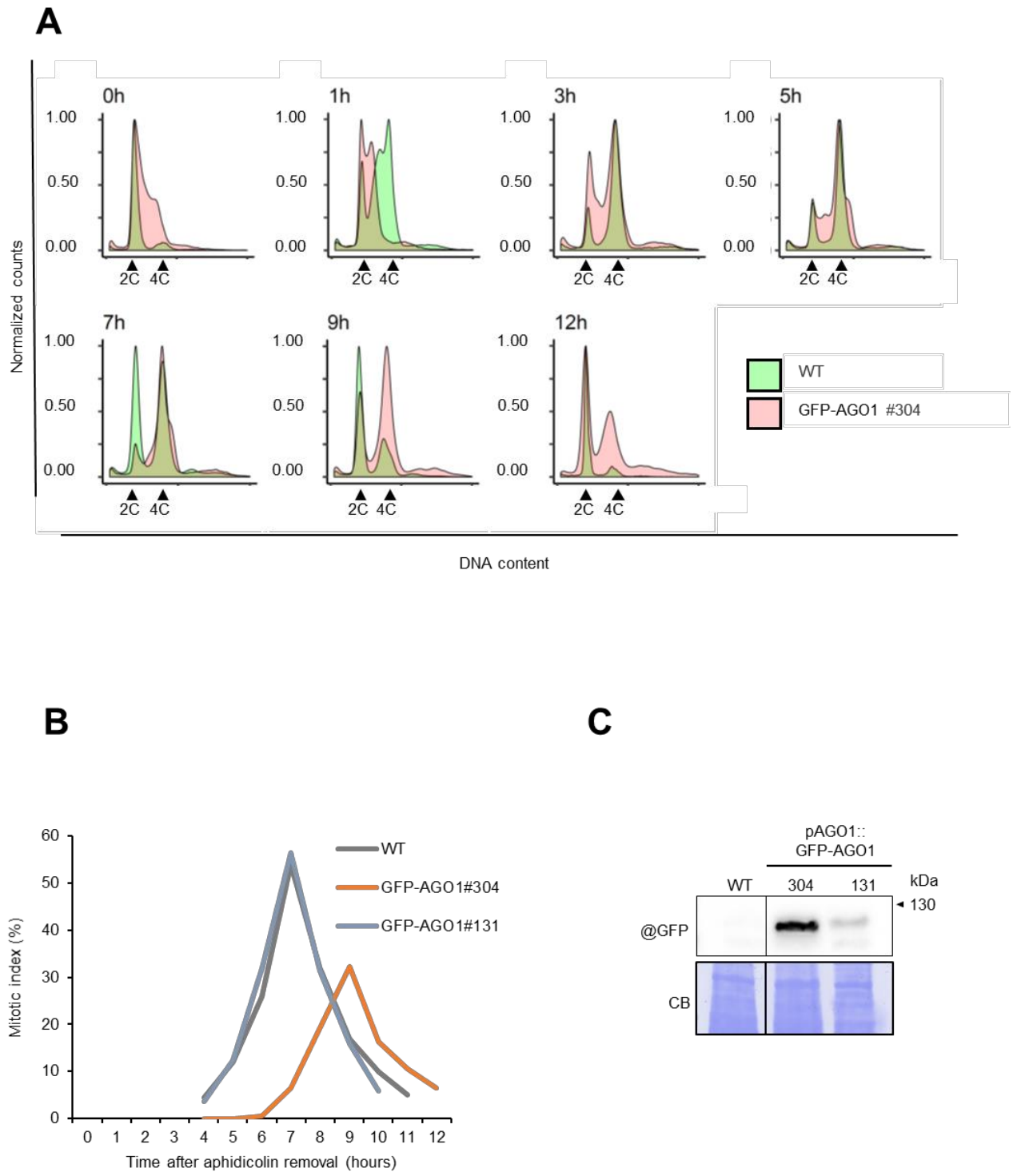

Figure 30: Too high GFP-AGO1 expression affects cell cycle progression in synchronized clonal BY-2 cell suspensions.

(A) DNA content measurements of synchronized cell nuclei by flow cytometry at the indicated time points after aphidicolin removal. Arrows represents 2C and 4C DNA contents. **(B) The** graph represents the mitotic index of a wild type and two GFP-AGO1 expressing cell lines, indicating the percentage of observed dividing cells at a given time point. **(C) Western** blot showing the accumulation level of GFP-AGO1 protein in the two indicated cell lines compared to the non-transformed wild type cell line. Coomassie blue (CB) staining was used as a loading control.

protein extraction protocol (Laemmli method) usually used in our laboratory for Arabidopsis protein extracts with a phenol extraction followed by methanol precipitation protocol. By using the phenol extraction method, I could observe a significant increase of GFP-AGO1 detection on SDS-PAGE (polyacrylamide gel electrophoresis) for the same amount of total protein loaded on the gel (Figure 29B).

2. Lines selection for synchronization experiments

Next, I then synchronized different GFP-AGO1 expressing BY-2 clonal cell lines following a protocol previously published by Nagata and Kumagai and further adapted in our laboratory (Nagata and Kumagai, 1999; Criqui et al., 2000). It consists in chemically blocking dividing cells in S phase using aphidicolin, which is a DNA polymerase inhibitor produced by the fungus *Nigrospora sphaerica.* Briefly, stationary phase cells are subcultured in a fresh medium supplemented with aphidicolin and treated for 24 hours. I then performed extensive washes to remove aphidicolin and allow S-phase synchronized cells to undergo cell cycle progression. Every hour, cell samples were harvested for protein and RNA extraction, and also to monitor the ploidy level by flow cytometry and to determine the percentage of cells in mitosis by microscopy (indicated as mitotic index).

By comparing different GFP-AGO1 expressing BY-2 cell lines to a wild type (non-transformed) cell line, I observed that at high expression level of the GFP-AGO1 transgene, cell cycle progression was significantly delayed (Figure 30). In addition, high expression of GFP-AGO1 affects also the synchrony level, precluding the possibility to assess high quality synchronization experiments. Thus, I selected a clonal BY-2 cell line with a moderate GFP-AGO1 expression level (referred as line #131) for biochemical analysis and kept a high GFP-AGO1 expression line (referred as line # 304) for microscopy imaging experiments, where high synchronization efficiency is less crucial but however requires a sufficient amount of protein for detection.

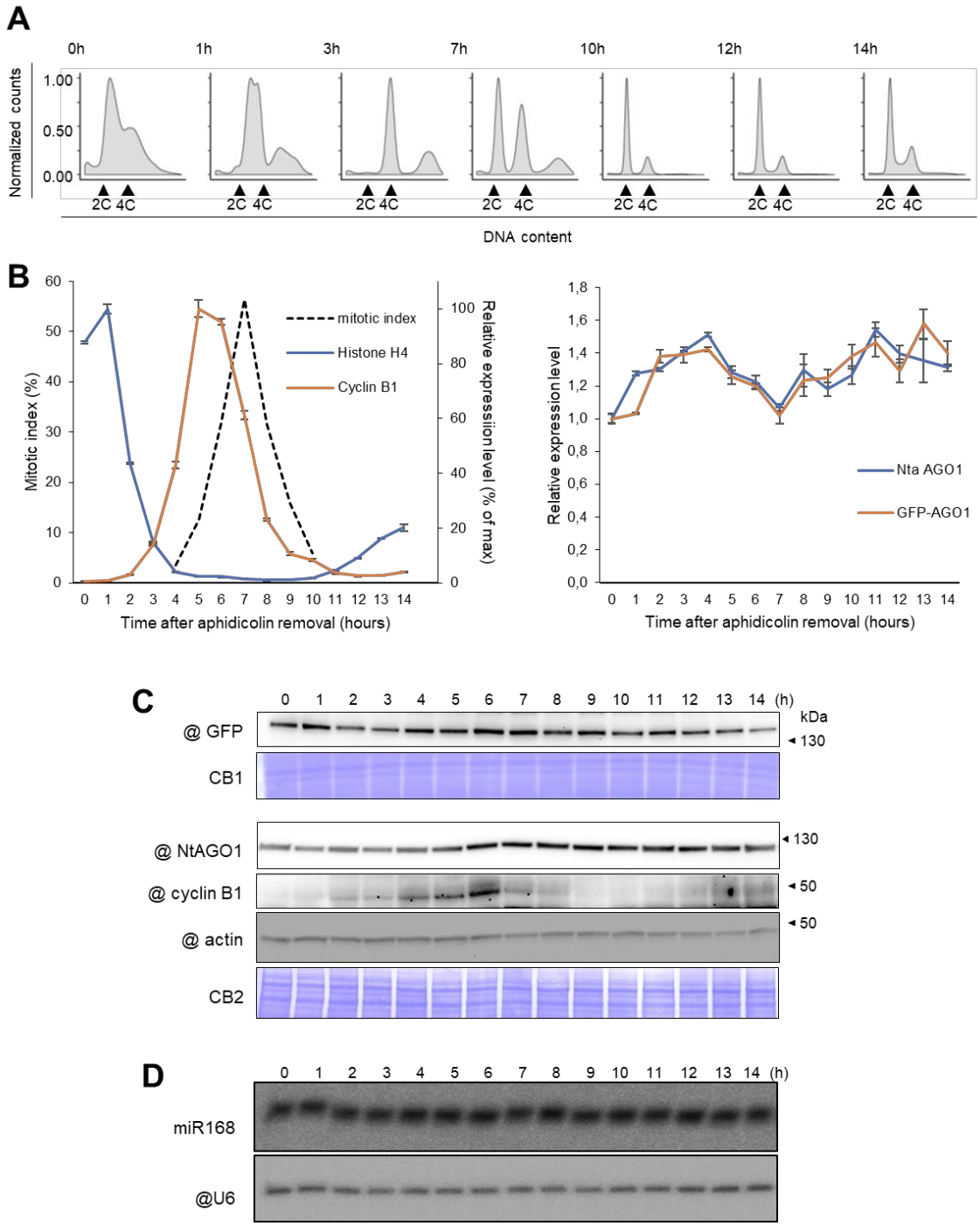

Figure 31: Accumulation pattern of AGO1 mRNA and protein in synchronized BY2 cells.

(A) DNA content measurements of synchronized cell nuclei by flow cytometry at different time points. **(B)** Transcript analysis of gene expression by q-RT PCR. The left panel represents the transcript accumulation of the cell cycle regulated genes histone H4 and Cyclin B1 used to monitor S-phase and G2/M, respectively. The dashed line represents the mitotic index determined by the counting of dividing cells. The right panel show the transcript level of both endogenous AGO1 and GFP-AGO1. qRT-PCR values represent the mean +/- the standard error of 3 technical replicates. **(C)** Accumulation of endogenous AGO1 and GFP-AGO1 protein levels at different time points of the synchronization experiment. 30 µg of total proteins were separated by 4-16% gradient SDS-PAGE for GFP-AGO1 (Coomassie Blue stain CB1) and for endogenous AGO1 (Coomassie Blue stain CB2). Antibodies against cyclin B1 and actin were respectively used as G2/M phase marker and loading control. **(D)** Northern blot showing the steady state accumulation of the micro-RNA miR168a-h. A probe against U6 snRNA was used as loading control. Total RNA samples were separated on a 15% 0.5X TBE 8 M urea gel.

3. AGO1 steady state level remains constant during cell cycle progression

Using the line with a moderate GFP-AGO1, I was able to reach synchrony levels up to 57 percent in mitosis (Figure 31). Based on qRT-PCR analysis of cell cycle regulated genes and on ploidy level, I determined the time points of the different cell cycle phases (Figure 31A and B). S phase starts from 1 hour after aphidicolin removal to 3 hours, where almost all cells already reached the 4C DNA content. G2 is following and ends at 5-6 hours with the mitotic index that is suddenly increasing to reach a peak at 7 hours. G1 spreads from 10 hours to 12 hours before a second S-phase starts. Note that at 10h and 12h most of the cells have a 2C DNA content but a non-negligible number of cells, representing around 25% of the total counts, are in 4C indicating that the synchrony level drops significantly after mitosis.

During cell cycle progression, the GFP-AGO1 protein was detected at all time points of the cell cycle without important fluctuations (Figure 31C). Only a slight, but reproducible increase of the protein steady state level was observed during mitosis. Interestingly, we could obtain from the laboratory of Professor József Burgyán (Agricultural Biotechnology Institute, Hungary) an aliquot of an antibody raised against the *N. benthamiana* AGO1 (Csorba et al., 2010). Blotting my protein samples with this antibody revealed a pattern of AGO1 accumulation similar to the GFP-AGO1 (Figure 31C). By contrast, as expected, cyclin B1 protein level only accumulated during G2/M, rapidly decreased at the time of the peak in the mitotic index (6h) and reached background levels at the exit of mitosis (9 h). Similarly to the level of AGO1 protein, the accumulation of its transcript (Figure 31B) or of miRNA168, that negatively regulates its expression (Vaucheret et al., 2004), did also not significantly change during the cell cycle (Figure 31D). Thus, we can conclude that AGO1 expression level remains overall constant along the cell cycle.

Since I was able to detect slight and reproducible increase in AGO1 protein level during mitosis, I wanted to test whether a higher level of synchrony would strengthen this effect. To do so, I performed a dual-step synchronization as described by Kumagai and colleagues (Kumagai-Sano et al., 2007) . Dual-step synchronization consists in first blocking cells in S phase with aphidicolin. After the release of this inhibition, the cell cycle is followed until first prophases can be observed under the microscope, corresponding to approximately 5% of the mitotic index. At this point, the medium is supplemented with propyzamide, which is a microtubule assembly inhibitor, thus preventing mitotic spindle assembly and triggering a mitotic checkpoint. Cells are treated so during four hours before we perform washings with

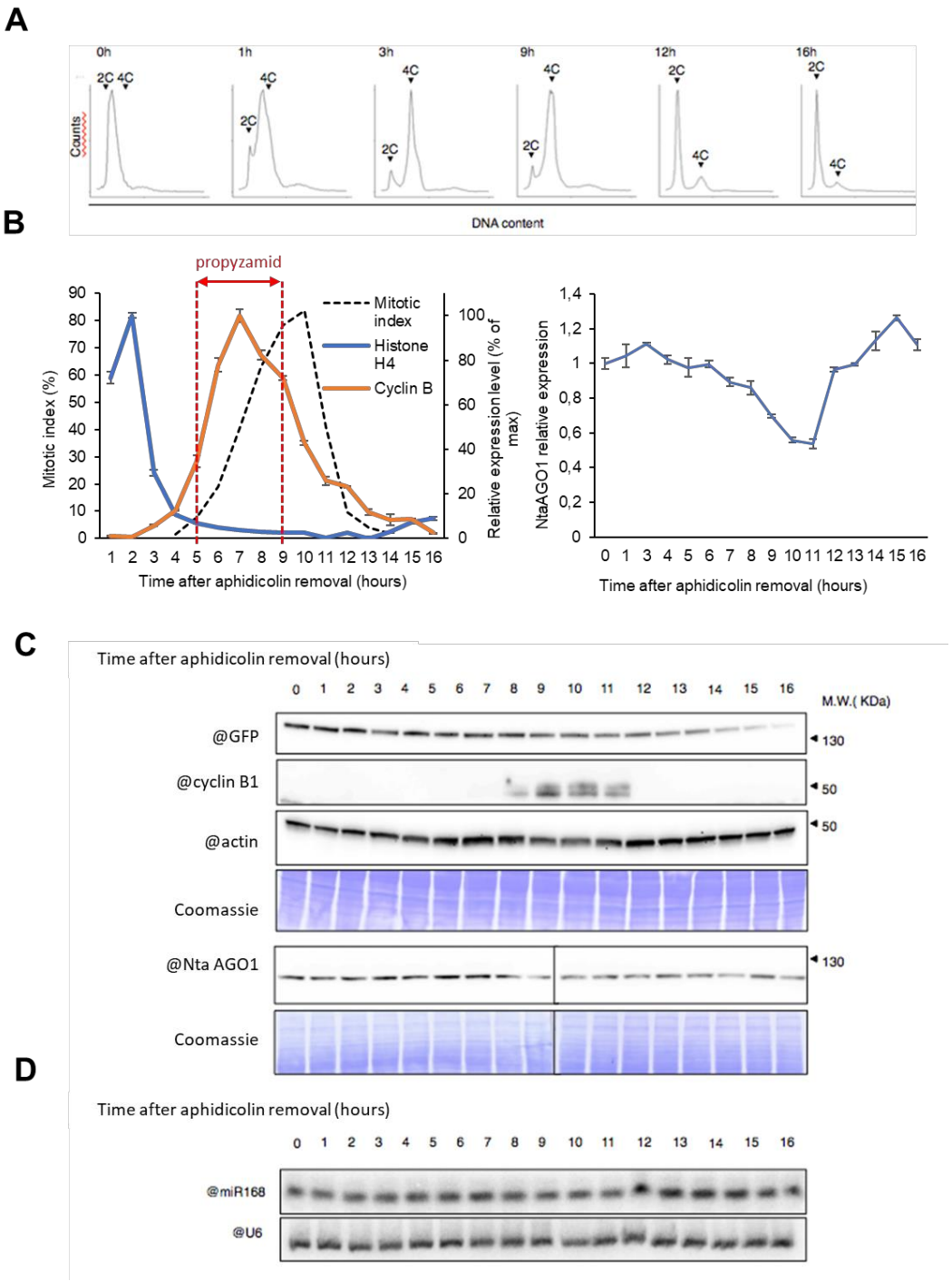

Figure 32: Analysis of AGO1 steady state level from dual-step synchronization experiment.

(A) DNA content measurements of synchronized cell nuclei by flow cytometry at different time points. **(B)** Transcript analysis of gene expression by q-RT PCR. The left panel represents the transcript accumulation of the cell cycle regulated genes histone H4 and Cyclin B1 used to monitor S-phase and G2/M, respectively. The dashed line represents the mitotic index determined by the counting of dividing cells. The right panel show the transcript level of endogenous AGO1. qRT-PCR values represent the mean +/- the standard error of 3 technical replicates. **(C)** Accumulation of endogenous AGO1 and GFP-AGO1 protein levels at different time points of the synchronization experiment. 30 micrograms of total proteins were separated by 4-16% gradient SDS-PAGE for GFP-AGO1 (Coomassie Blue stain CB1) and for endogenous AGO1 (Coomassie Blue stain CB2). Antibodies against cyclin B1 and actin were respectively used as G2/M phase marker and loading control. **(D)** Northern blot showing the steady state accumulation of the micro-RNA miR168a-h. A probe against U6 snRNA was used as loading control. Total RNA samples were separated on a 15% 0.5X TBE 8 M urea gel.

fresh medium to counteract drug effects and by consequence allowing cells to complete mitosis. By performing dual-step synchronization assays, I was able to reach about 83% of mitotic index (Figure 32B). Interestingly, the accumulation level of the cyclin B1 transcript is not really affected by propyzamide treatment and is only delayed of 1 hour compared to the aphidicolin-only treatment. The cyclin B1 protein level however is detected up to 1 hour after the release of the propyzamide inhibition, illustrating that mitotic checkpoint was activated and that APC/C was most likely not able to trigger mitotic exit.

When checking the steady state level of both GFP-AGO1 and endogenous AGO1 on western blot, I was able to detect variations during cell cycle progression (Figure 32C). However, I never succeed to reproduce exactly the same pattern of accumulation in the three different dual-step synchronization experiments I have performed. While dual-step synchronization allows very high synchrony level, several points can be criticized concerning the reproducibility of the experiment and might explain why these experiments were not conclusive. As propyzamide inhibit microtubule polymerization, it might affect a wide spectrum of cellular processes in addition to mitotic spindle assembly. Moreover, I observed that, even though more than 80% of the cells were able to go through mitosis after propyzamide removal, a significant number of cells exhibited chromatin defect such as lagging chromosomes and formation of micronuclei. From this experiment, I was also initially expecting to reach a better synchrony level in the last S phase compared to aphidicolin synchronization, to see whether GFP-AGO1 protein level is fluctuating in a cell cycle periodic manner. Despite a much higher mitotic index, entry in the S phase was greatly delayed and the synchrony level was even lower to what I usually obtained with aphidicolin synchronization.

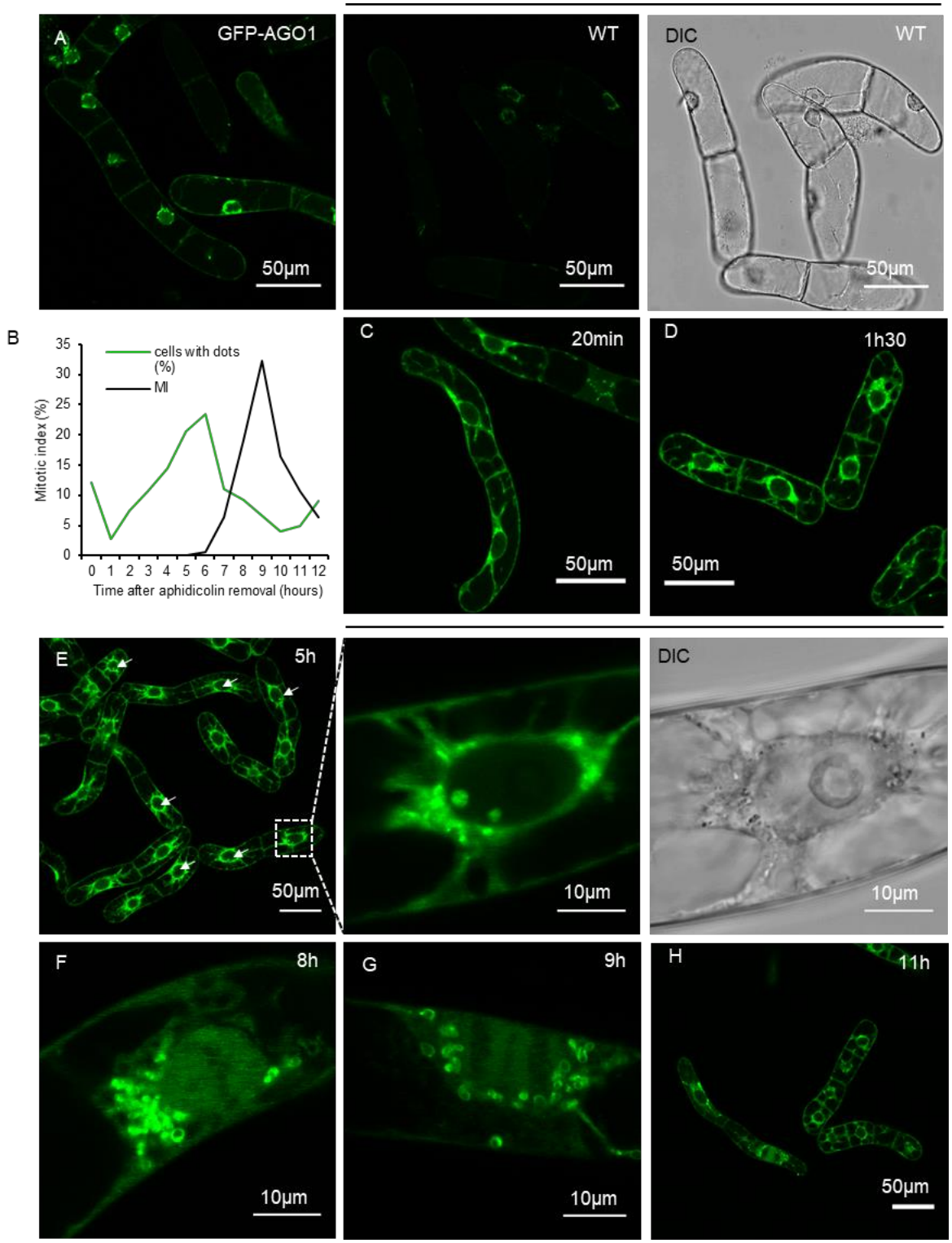

Figure 33: Subcellular localization of GFP-AGO1 in BY-2 tobacco cell suspension.

(A) Confocal laser imaging of GFP-AGO1 and non-transformed wild BY2 cell lines. GFP detection represented in green was acquired in the 500-550 nm band (excitation: 480 nm). The DIC panel corresponds to the bright field imaging. **(B-G)** Subcellular localization of GFP-AGO1 in synchronized cell culture. **(B)** Graph representing the mitotic index (MI) of the synchronization experiment used for imaging. The green line represents the percentage of cells exhibiting GFP-AGO1 nuclear foci. **(C-G)** Panels showing different confocal acquisitions of the synchronization experiment at the indicated time points (after aphidicolin removal). Arrows highlight the presence of nuclear foci.

4. AGO1 localizes to different cellular bodies in synchronized BY-2 cells

I then assessed the question of the subcellular localization of GFP-AGO1. Due to the low expression level of GFP-AGO1 in BY-2 cells, its detection was a challenging part of the project. For me, the main issue of BY-2 cells was the presence of plastids in the periphery of the nucleus that exhibit high autofluorescence level and therefore made the identification of cytosolic GFP-AGO1 foci difficult (Figure 32A). A method for diminishing the signal-to-noise ratio might be the use of spectral imaging and linear unmixing techniques that consists in establishing the emission spectrum of plastids in non-transformed cells and subtracting it from the signal of GFP-AGO1 expressing lines. This process is commonly used to split emission spectrum from two overlapping fluorescent markers but can be applied to background fluorescence. However, compared to conventional confocal imaging, spectral acquisition requires high fluorescent and by consequence, might be the limiting factor to image GFP-AGO1 expressing cells.

Despite these difficulties, I was able to determine the localization of GFP-AGO1 at the sub-cellular level at the different time points of the cell cycle. Thus, the GFP-AGO1 fusion protein was found predominantly in the cytosol of asynchronous cells, as previously reported in Arabidopsis root cells (Derrien et al., 2012), but was also present, in the nuclear compartment (Figure 33A). The background signal in non-transformed BY-2 cells using the same confocal settings is also shown (middle panel; the right panel showing the corresponding DIC image).

I next synchronized BY-2 cells and imaged GFP-AGO1 at different cell cycle phases (Figure 33B-H). During S-phase the GFP-AGO1 signal was mainly enriched in the cytosol (Figure 33C-D). Interestingly during G2, I observed the GFP-AGO1 signal also in larger nuclear bodies (of ~2-6 μm) distinct from nucleoli (Figure 33E). Further quantifications showed that the number of cells that contain these bodies is increasing during S and G2 and drop significantly when the mitotic index starts to increase, suggesting a cell cycle-dependent periodic accumulation of GFP-AGO1 nuclear foci (Figure 33B).

In mitotic cells, despite a slightly higher accumulation of GFP-AGO1 protein level (Figure 31C), the fluorescence signal was clearly excluded from condensed chromosomes of mitotic cells (Figure 33F-G). To confirm this observation, I transformed the GFP-AGO1 clonal cell suspension with a construct expressing histone H2B fused to tdTomato, which

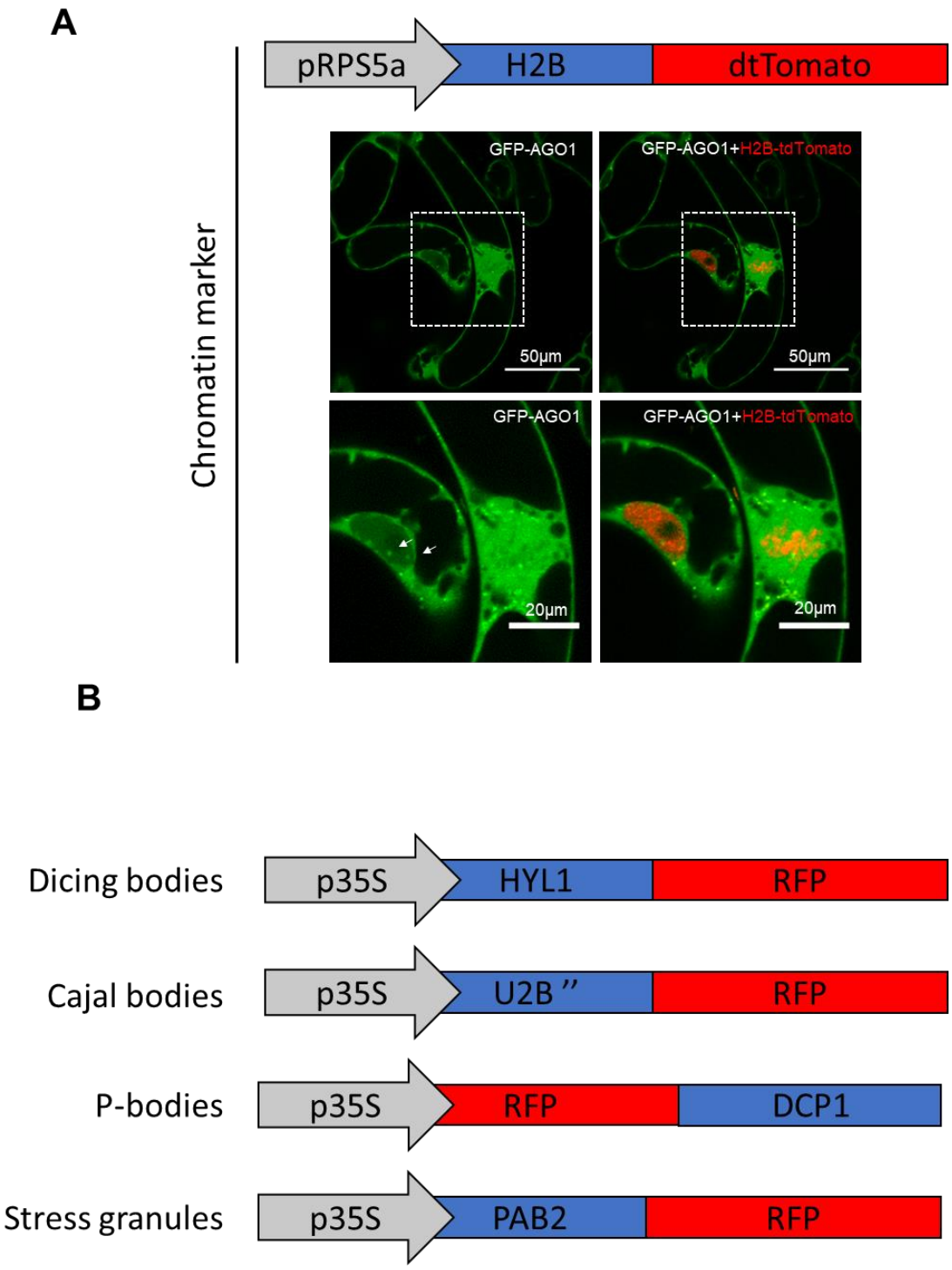

Figure 34: Identification of GFP-AGO1 containing bodies.

(A) Confocal laser imaging of cells expressing GFP-AGO1 and the chromatin marker pRPS5:H2B-tdTomato. The panels below are close-up views of the area delimited by the dashed squares on the upper panels. No colocalization was observe between GFP-AGO1 and pRPS5:H2B-tdTomato on condensed chromatin. Both proteins also do not seem to co-localize in nuclear foci. **(B)** Constructs that are currently engineered to be transformed in GFP-AGO1 expressing lines in order to identify the nature of GFP-AGO1 nuclear and cytosolic bodies.

once incorporated into chromatin allows visualization of nuclear events. Hence, the dual localization of both fluorescent proteins in mitotic cells indicates no substantial overlap between them on condensed chromatin and GFP-AGO1 nuclear bodies (Figure 34). Finally, after mitotic exit, cells in G1 show again a predominant cytosolic distribution of the GFP-AGO1 protein (Figure 33H). From these observations, I conclude that GFP-AGO1 exhibits a complex subcellular localization pattern with foci in both the nucleus and cytosol, supporting the existence of pools of RISCs that may play distinct functions along the cell cycle.

In order to address the question of the identity of both nuclear and cytosolic GFP-AGO1 foci, I plan to transform GFP-AGO1 expressing BY-2 cells with fluorescent nuclear and cytosolic compartment markers. Thus, I am currently engineering a series of constructs to image cellular structures of interest (Figure 34B), which I will describe below. For instance, the double-stranded RNA binding protein HYL1 is a component of the plant microprocessor complex, and together with the zinc finger protein SE and DCL1 contribute to the biogenesis of miRNAs in discrete nuclear foci called dicing bodies. Using bimolecular fluorescent complementation assays, Fang and colleagues already demonstrated that AGO1 interacts with HYL1 in Arabidopsis dicing bodies (Fang and Spector, 2007), presumably to load the processed small RNA duplex in the RISC. Hence, HYL-RFP marker is undoubtedly a priority. Nuclear localization was also shown for AGO4. Immunolocalization experiments already revealed that a pool of AGO4 is located in specific nuclear bodies called Cajal bodies (Li et al., 2006, 2008). Cajal bodies have been linked to RNA metabolism and are involved in biogenesis and maturation of small nuclear ribonucleoproteins but also to the replication-dependent transcription of histone mRNAs (Ma, 2000). In addition, the size and number of Cajal bodies is highly dynamic during cell cycle and they reach their maximum size and number during Gap phases. Given that, I will also generate the U2B”-RFP construct that will localize in the plant Cajal bodies.

Finally, I wish also to investigate the presence of AGO1 in cytosolic bodies that are related to the RNA metabolism (Figure 34B). The decapping protein DCP1 is a component of a type of cytosolic ribonucleoprotein (RNP) bodies called P-Bodies. Purification and proteomic analysis of P-bodies in human cell cultures showed that proteins involved in RNA decay, decapping and also AGO proteins are present in P-bodies to repress gene expression, presumably by storing RNAs and consequently preventing their translation (reviewed in Maldonado-Bonilla, 2014). Like P-bodies, stress granules are RNP bodies also constituted by pools of untranslated mRNAs (reviewed in Protter and Parker, 2016). However, P-bodies and

stress granules differ by their protein composition. Stress granules are composed of RNA binding proteins, polyA-binding proteins (including PAB2) and other translation initiation factors. Because the overall gene expression is known to be highly dynamic during the cell cycle, it will be interesting to see whether these bodies have a dynamic pattern during the plant cell cycle progression and whether they colocalize with a pool of AGO1.

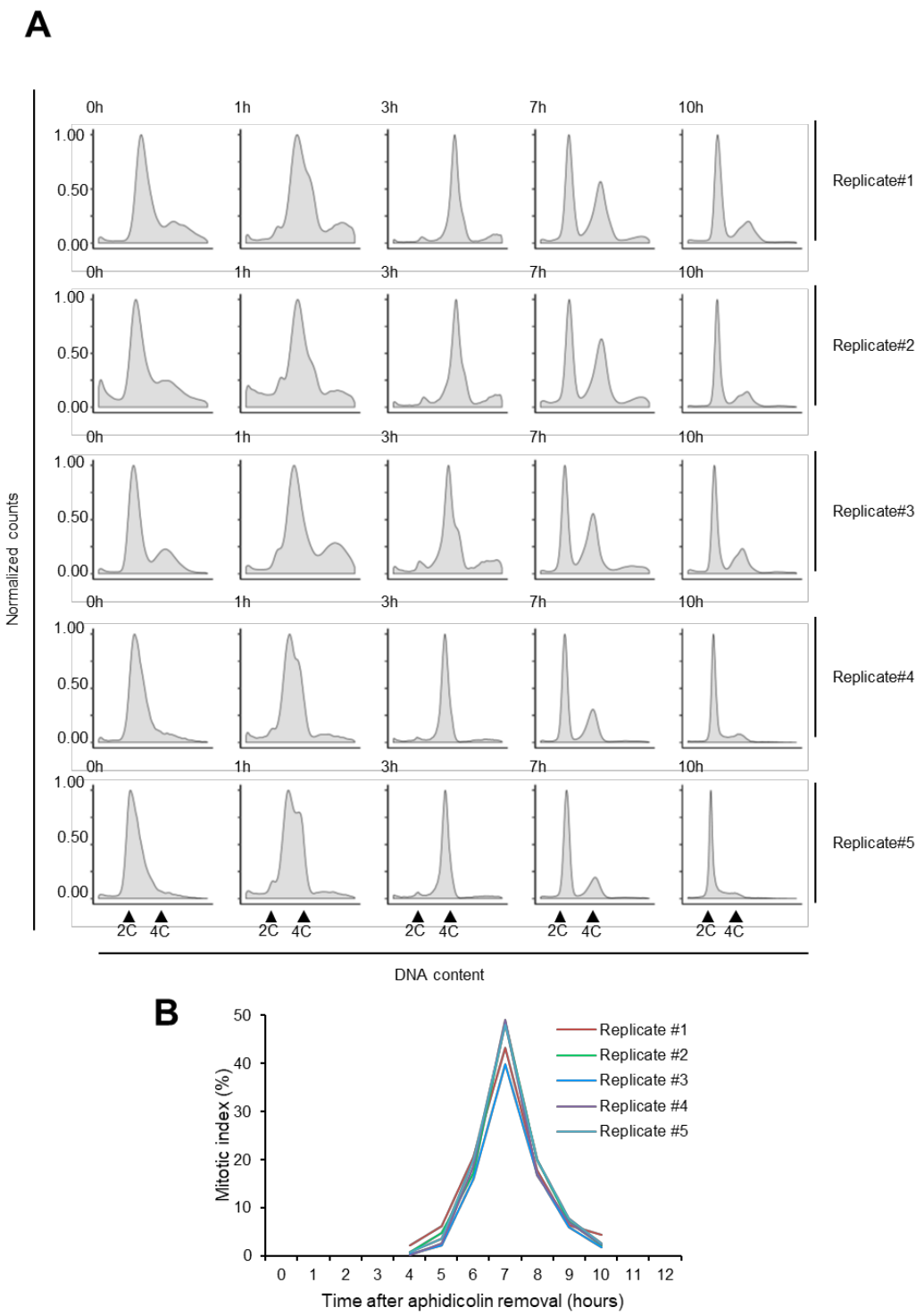

Figure 35: Quality control of the synchronization experiments used for high-throughput sequencing.

(A) DNA content measurements of synchronized cell nuclei by flow cytometry at the indicated time points after aphidicolin removal. Arrows represents 2C and 4C DNA contents. **(B)** The graph represents the mitotic index for the five synchronization replicates, indicating the percentage of dividing cells at a given time point

C. Differential gene expression in synchronized BY-2 cells

I the following chapter, I address the question of the function of AGO1 related to gene expression during cell cycle. To reach a global view of total RNA, total small RNAs and AGO1-associated small RNAs at key points of the cell cycle, I performed five independent synchronization experiments (hereafter called replicate 1 to 5) using a clonal BY-2 cell suspension with a moderate expression level of GFP-AGO1. Flow cytometry measurements of DNA contents and monitoring mitotic indexes, revealed that all five synchronization experiments were highly reproducible in the timing of the different cell cycle phases and their level of synchrony (Figure 35). For each experiment, I collected RNA and protein samples for S, G2, M and G1 phases (at 1, 3, 7 and 10 hours after aphidicolin removal, respectively).

1. Transcriptomic analysis of synchronized BY-2

Focus on genes regulated specifically in relation to the cell cycle requires transcriptomic data from synchronized cells. While deep RNA sequencing of synchronized animal cells is routine, this is not the case for higher plants. A microarray dataset of synchronized Arabidopsis cell suspension has been previously published by Menges and colleagues (Menges et al., 2005). In this article, they reported the differential expression of many cell cycle regulated genes for both aphidicolin treated and carbon starved synchronized cell suspensions. However, the synchrony level of Arabidopsis cell suspension is well below what can be achieved with BY-2 cells. Thus, we performed RNA sequencing on synchronized BY-2 samples to get a better transcriptome data set and be able to detect even subtle changes in gene expression during cell cycle. We performed RNA-seq (Fasteris, Switzerland) of three biological replicates to identify differentially expressed genes, comparing S, G2, M and G1 phases (Supplemental Table 1). From this sequencing experiment, we were able to get more than 20 million reads per libraries where about 75% were matching the last version of the tobacco genome published by Edwards and colleagues (Edwards et al., 2017). In addition, only less 5% of reads matched on abundant non-coding RNAs, such as ribosomal or transfer RNAs, underlying the high sequencing depth of our dataset. I then checked whether our 3 different biological replicates were reproducible. To do so, I performed principal component analysis (PCA). PCA revealed that the libraries were indeed well separated and were clustered

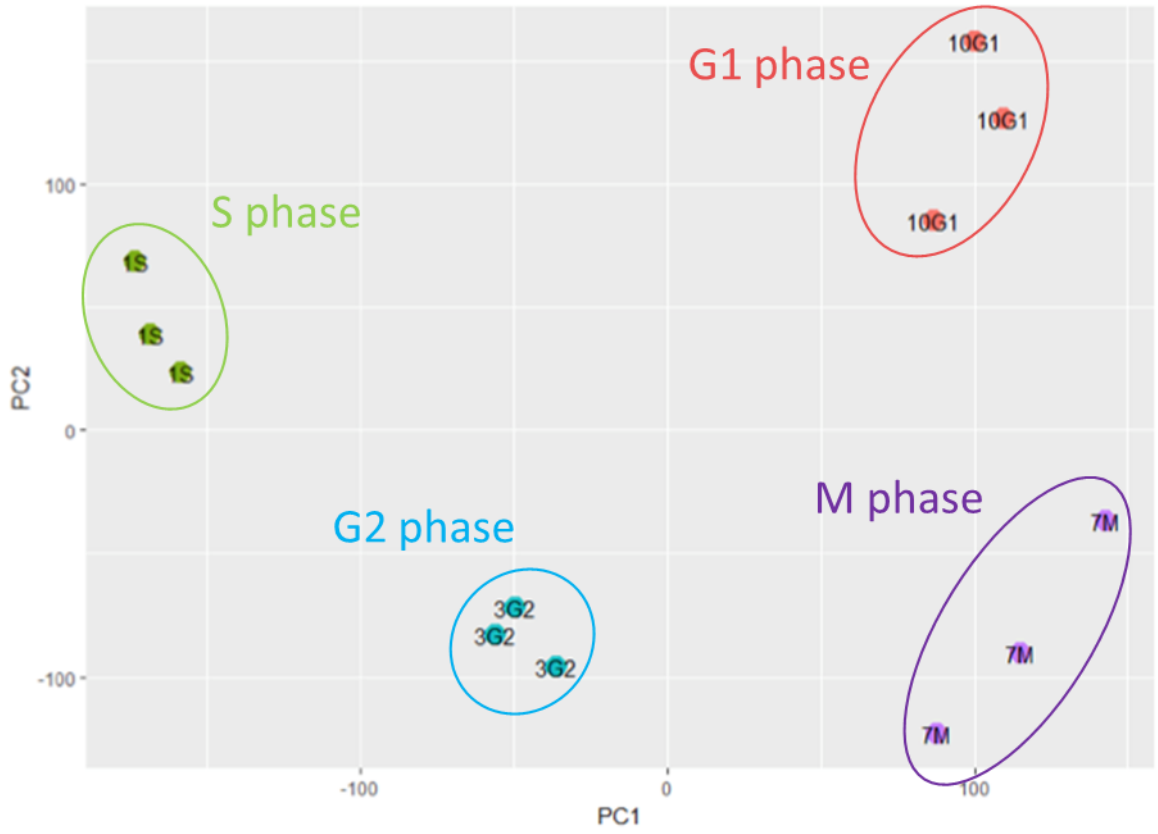

Figure 36: Variability of RNA seq libraries.

Principal component analysis (PCA) of 12 RNA-libraries composed of 3 biological replicates and 4 cell cycle phase time points (S, G2, M, G1). All libraries are well clustered by cell cycle phases, underlying the high reproducibly of the three biological replicates. PC1 and PC2: Principal component 1 and 2.

by cell cycle phases (Figure 36). Given that, we conclude that our replicates were highly reproducible and therefore we expected to get a high number of differentially expressed genes between different cell cycle phases.

Out of the 69500 genes identified in the tobacco genome (Edwards et al., 2017), we were able to detect 66753 (96%). Among those, we identified a total of 23060 differentially expressed (DE) transcripts corresponding to 13623 genes with a functional annotation (see RNaseq.xls file). The number of DE genes is variable depending on the comparison, going from 6737 to 14771 DE genes in M/G1 and S/M comparisons respectively (Figure 37A-B). However, the ratio of down- and up-regulated genes seems to be maintained in each cell cycle phase, always around a 50%. For instance, by comparing S-phase and M-phase, 7295 genes were upregulated and 7476 downregulated (Figure 37A-B). However, if we consider only the DE genes with a fold change of 5 or higher, we can observe a change in the expression trend, where a high percentage of the DE genes are upregulated in M and G1 phases, and downregulated in S and G2 (Figure 37B)

For a better understanding of the RNA-seq data structure, we performed a soft clustering analysis using Mfuzz package. Soft clustering groups together genes that have a similar expression pattern, providing insights in gene function and networks. Here we divided our DE dataset, containing more than 23000 genes, into 16 different clusters (Figure 37C and Figure 38). We were able to observe very distinct expression patterns, mostly due to the highly dynamic transcription. The two most abundant clusters where cluster 11 and cluster 6, which present a single peak of expression during phases M and S, respectively. Genes included in cluster 6 are involved in chromatin assembly and organization, receptor mediated endocytosis, and phosphorylation. Among these genes, those with the highest expression in S phase are not surprisingly histones. Genes included in cluster 11 are enriched in cellular component movement, cytoskeleton organization and intercellular protein transport. I checked also whether component of the RNA silencing pathways, from small RNA biogenesis (including DCLs) to effectors AGOs, are differentially expressed. However, no significant difference was found, indicating that the transcriptional control of the RNA silencing machinery is not subjected to important variations over the cell cycle.

Next, we conducted a Gene Ontology (GO) analysis on the DE genes by using the Panther software. As expected, gene categories related to cell cycle functions such as DNA replication, chromosome segregation and mitotic processes including cytokinesis are well represented (Figure 37D). In addition, a significant number of DNA repair and DNA damage

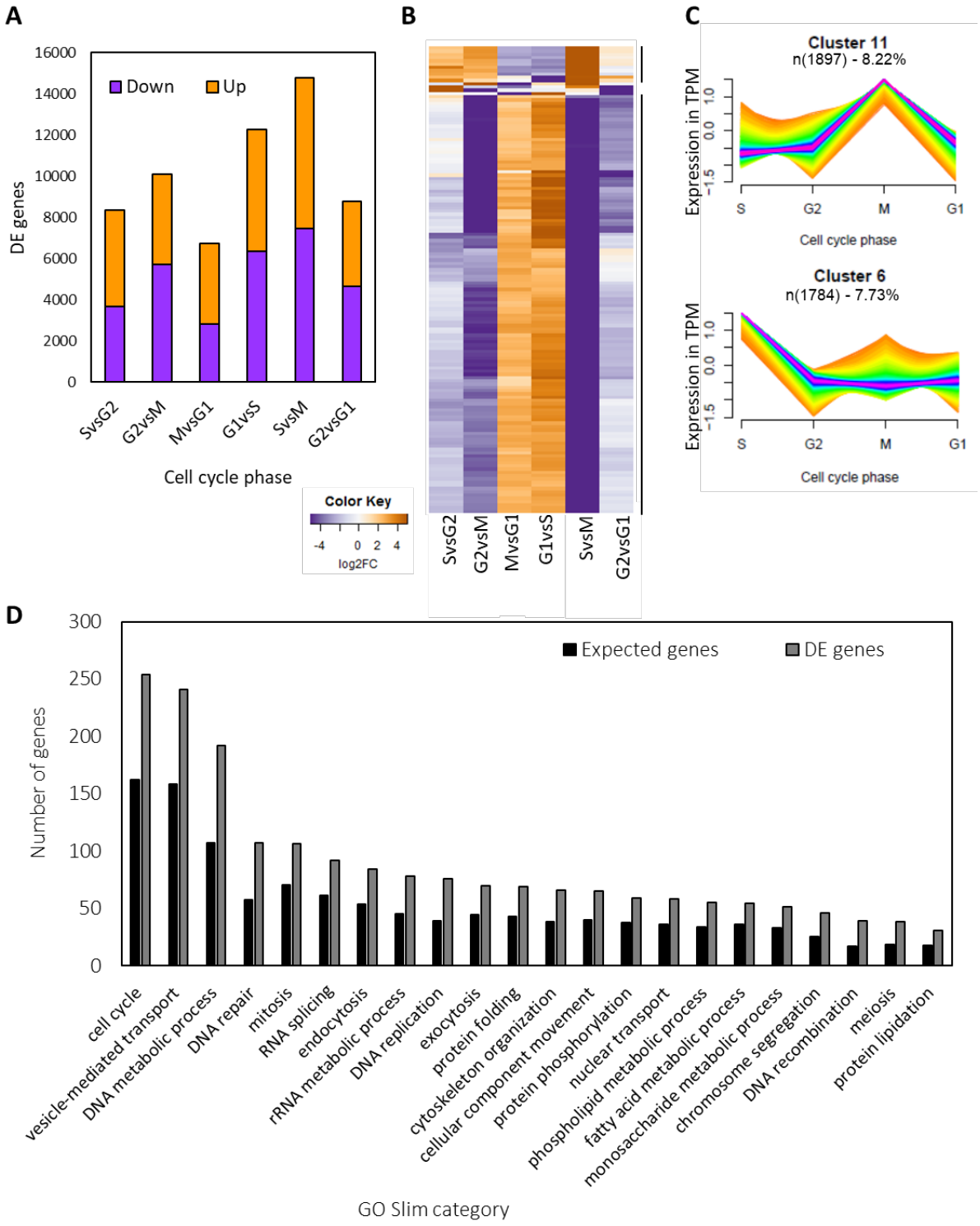

Figure 37: RNA-seq analysis on synchronized BY-2 cells.

(A) Summary of differentially expressed genes, down- and up-regulated genes are represented in purple and orange, respectively. **(B)** Heatmap representation of differentially regulated genes with a fold change bigger or equal to 5. **(C)** Representation of the two most abundant clusters. **(D)** GO Slim categories representing the biological function of differentially expressed genes. Here are only represented GO categories with more than 1.5x representation fold change.

signaling genes were also induced. These genes might be expressed during replication to prevent and repair replication errors. However, aphidicolin treatment is already known to induce replicative stresses, thus, expression of some factors of the DNA repair machinery might actually be a consequence of the aphidicolin treatment rather than be related to cell cycle. Note that homologs for all core cell cycle genes established in Arabidopsis have been identified and most of them are DE along the cell cycle regulation (see cell_cycle.xls file). To the best of our knowledge, this dataset provides the most exhaustive analysis of cell cycle regulated genes in eudicots.

2. Expression and targets of miRNAs in synchronized BY-2 cells

As hundreds of different transcripts show highly dynamic accumulation and decay patterns, I questioned whether some small RNAs might be involved in their regulation. Thus, I performed deep-sequencing analyses on total small RNAs and GFP-AGO1-associated small RNAs on the different cell cycle phases. In the following section, I will detail the protocol that I developed to purify AGO1-associated small RNAs and how I tried to optimize its purity.

a. RNA immunoprecipitation of GFP-AGO1 associated small RNA

As discussed previously, the necessary low GFP-AGO1 expression in BY-2 cells (as high expression affects the cell cycle) and the weak solubility of the AGO1 protein in denaturing extraction buffers were already technical locks for GFP-AGO1 detection. This was also a limit for GFP-AGO1 immunoprecipitation (IP) as GFP-AGO1 solubility was even lower in non-denaturing IP buffer. Thus, I adapted a protocol used in the lab and published in Derrien et al., 2012, that was designed for anti-AGO1 co-immunoprecipitation of small RNA from Arabidopsis crude extracts. I choose to use anti-GFP nanobodies coupled to magnetic beads instead of anti-AGO1 polyclonal rabbit antibodies in order to minimize non-specific binding. In a protocol developed for purification of AGO1 and AGO4 -associated small RNA prior to deep sequencing, Wang and colleagues (Wang et al., 2011) were using higher salt and

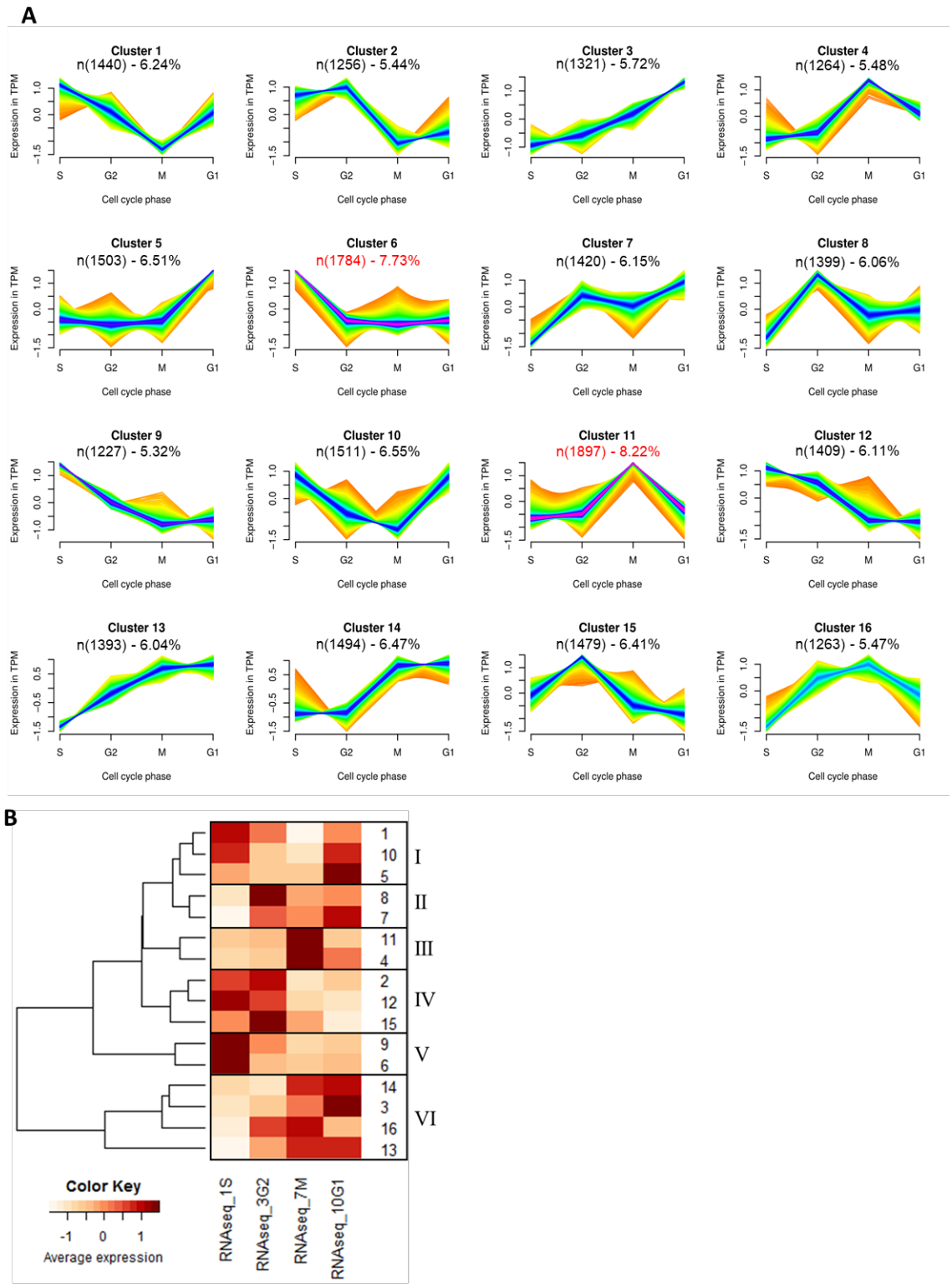

Figure38.

Figure 38: Clustering of differentially expressed genes from RNA-seq libraries.

(A) Soft clustering of the 23060 DE expressed genes using the Mfuzz package form R program. The number of cluster was manually chosen to get the best fit. The n value indicates the number of gene belonging to the corresponding cluster. **(B)** Heatmap representing the average gene expression by clusters for each cell cycle phases. Clusters ae organized in subgroups with similar expression patterns.

detergent concentration (300 mM NaCl, 0.2% triton-X100) and adding reducing agents (5 mM DTT), underlying the robust interaction between AGO1 and small RNAs.

By changing these three parameters, I was able to efficiently purify both GFP-AGO1 and control GFP from BY-2 cell crude extracts (Figure 39A). As a first quality control, I checked the efficiency of small RNA recovery by blotting a probe designed against the tobacco miR168a-h. The miR168 was enriched in the GFP-AGO1 fraction whereas it was absent from the control GFP IP fraction (Figure 39A), thus validating the experimental setup. To go further, I also analyzed the profile of immunoprecipitated RNAs using capillary electrophoresis. By doing this, I obtained a precise view of the purified small RNAs separated by size (Figure 39B). RNA recovered from GFP and GFP-AGO1 IPs exhibit similar profiles and 20-24 nt small RNAs but as aimed their quantities were significantly enriched in the GFP-AGO1 IPs. Surprisingly however, 20-24 nt small RNAs represent only a small fraction of the purified pools of RNA. By contrast, a high proportion of about 40 to 150 nt-long RNAs were detected in both IPs, representing a contamination by abundant non-coding RNAs that could affect the quality of the libraries.

With this in mind, I wished to improve the purity of immunoprecipitated RNAs using a dual-step technique described by Wang and colleagues (Wang et al., 2011). They performed a first round of purification by size exclusion chromatography, followed by immunoprecipitation on pooled fractions that contain the RISC complex. With the same extraction conditions that have been used for single-step IPs, I extracted and separated total protein from BY-2 extract on gel filtration column. GFP-AGO1 was mainly detected in the fraction 13 to 17 (Figure 40A). This column was previously calibrated using standards with known molecular weight. Thus, I estimated that fraction 13 to 17 correspond to a size of approximately 150 kDa corresponding to the monomeric GFP-AGO1. I checked whether small RNAs were present is AGO1-containing fractions. RNA blot using the anti-miR168 probe revealed that a pool of miRNAs was still associated to AGO1, while a significant amount (about the half) was most likely unbound small RNAs.

I then performed anti-GFP immunoprecipitation on pooled 13 to 17 fractions and analyzed it by Western-blot. GFP-AGO1 was successfully enriched in the IP fraction but to a lesser extent than what has been achieved using the singe-step IP protocol (Figure 40B). Capillary electrophoresis profiles showed that RNA purified from dual-step IP were ranged from about 10 to 60 nt, meaning than most of the contaminating RNAs has been removed during the process. However, even though the input volume has been significantly increased

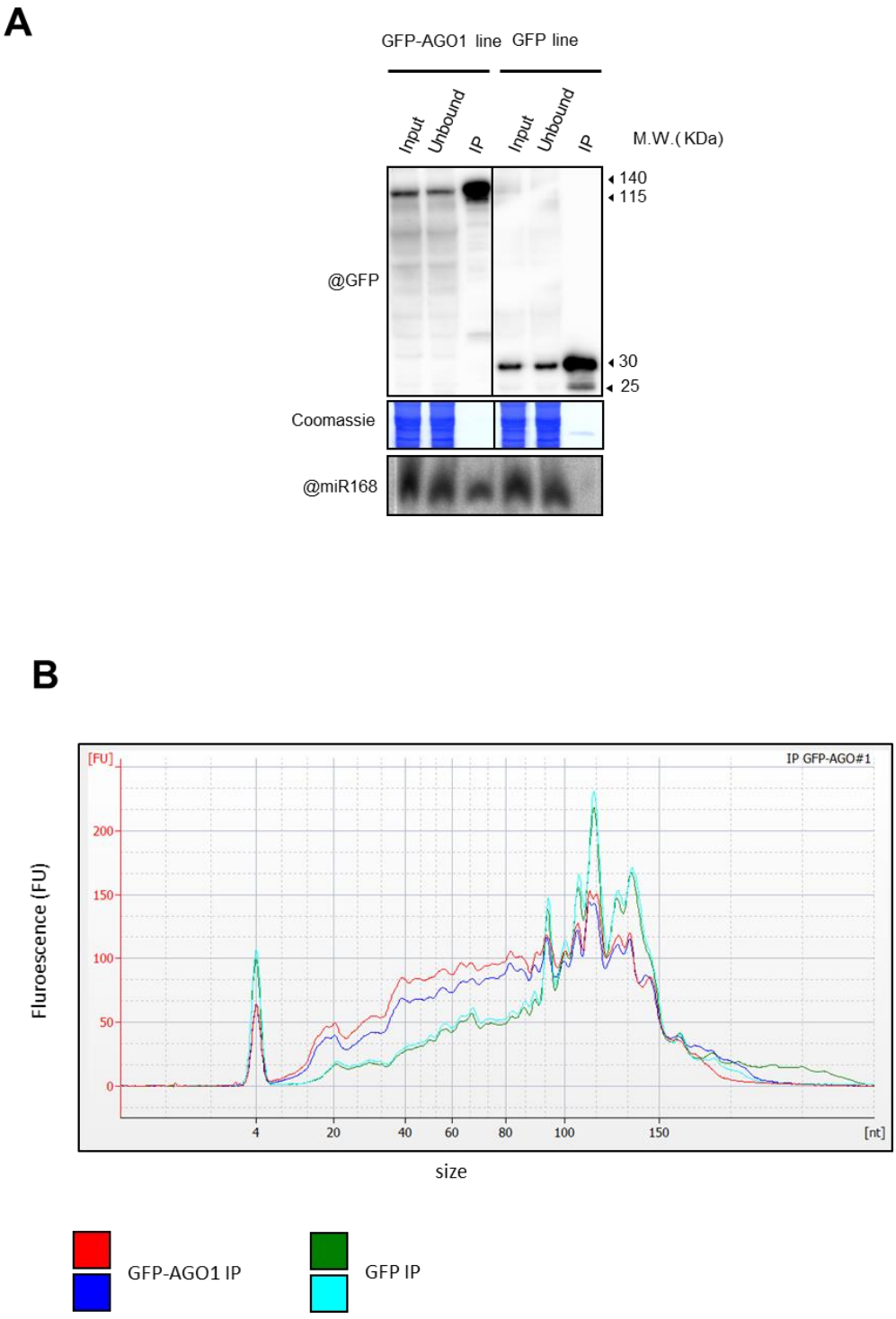

Figure 39: RNA-immunoprecipitation (RIP) of GFP-AGO1 loaded small RNAs in BY-2 tobacco cell suspension.

(A) Anti-GFP nanobodies coupled to magnetic beads were used for immunoprecipitation from asynchronous BY2 cells expressing GFP-AGO1 or as a control GFP alone (a dexamethasone-inducible GFP line) at 3 days of culture. GFP-AGO1 and GFP proteins were separated on a 4-16% gradient SDS-PAGE. Total RNA and Immunoprecipitated RNA were separated on a 15% 0.5X TBE 8M urea gel. A probe against miR168 was used to detect miRNAs enrichment in IP fractions. **(B)** Analysis of copurified small RNAs. Half of IP fraction was used for capillary electrophoresis. Samples are loaded 2 times each on the chip to minimize technical variations. 4 nucleotides spikes are added as a standard for estimating the sample RNA quantity.

compared to single-step IP, I was not able to get an acceptable quantity of purified RNA to generate small RNA libraries (Figure 40C). Given that, we finally decided to validate the single-step IP protocol to purify small RNAs from synchronized BY-2 samples.

b. Identification of differentially expressed small RNAs from synchronized BY-2 cells

Next, I performed total and AGO1-associated (with the single-step IP protocol) small RNA sequencing (Fasteris, Switzerland) of five biological replicates at S, G2, M and G1 phases of the cell cycle (Supplemental Table 1). As expected, we observed a typical Solanaceae size distribution of small RNAs in total RNA samples (Figure 41A), where 24-mers are the most abundant class of sRNA, followed by 22- and 21-mers. In contrast, the AGO1-associated small RNAs were strongly enriched in 21 and 22 nt sRNAs (Mallory and Vaucheret, 2010) (Figure 41B). To further investigate the distribution of sRNAs, we quantified along the cell cycle the accumulation of their different classes, including miRNAs, tasiRNAs, hetsiRNAs and tRFs (Figure 42A). hetsiRNAs represented the most abundant category in total RNA samples, while miRNAs represented the most abundant category in AGO1-IP samples. Overall, there were no significant differences between the cell cycle phases for small RNAs distributions.

For miRNA identification we used the workflow presented in Supplemental Figure 1. A total of 312 different mature miRNAs, belonging to 103 different miRNA families (see smallRNA.xls file), were identified in this study, including the already annotated miRNAs deposited in miRBase and also newly predicted miRNAs. These represent a total of 221 distinct sequences. Most of them (215/221) were present in both, total RNA and AGO1-IP samples.

Among those, we found 10 and 3 miRNAs DE in total RNA and AGO1-IP samples, respectively (Figure 42B). Most of the DE microRNAs had a cell cycle phase-specific accumulation. Thus, six miRNAs show a higher expression during the G2 phase, while only a single miRNA, miR168a-5p, was specific to M phase (Figure 42C). Two newly identified miRNAs (miR-33-3p and miR-12-5p) and two others (miR6147a-3p and miR479) were more abundant in the G1 phase. Additionally, miR390-3p and miR482-5p are accumulating at higher level during S phase (Figure 42C). Note that in the AGO1-IP samples, we only found DE miRNAs when comparing opposite phases of the cell cycle (S/M and G2/G1). Overall,

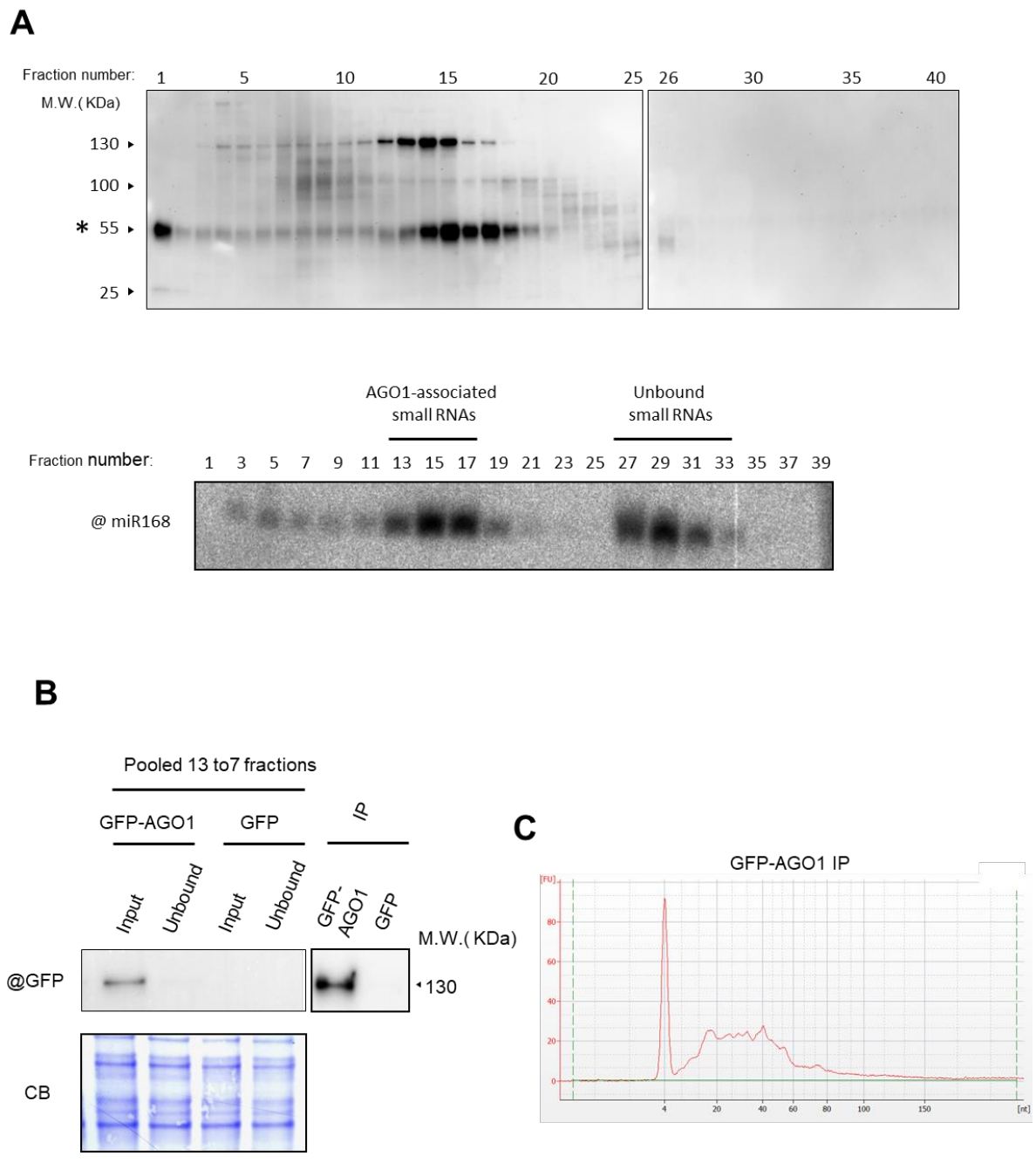

Figure 40: Attempt to improve RNA immunoprecipitation (RIP) specificity by two-step purification.

(A) GFP-AGO1 was extracted from asynchronous BY-2 cell suspension using the RIP buffer used previously for the single-step IP protocol. Total proteins were then separated by size exclusion chromatography on a gel filtration column. 1/4th of each fraction was precipitated and loaded on a 7% Tris-Glycine acrylamide gel. GFP-AGO1 was detected using anti-GFP rabbit polyclonal primary antibody. To check whether small RNAs are still associated to AGO1, RNAs were extracted from 1/4th of each fraction and were separated on a 15% 0.5XTBE 8M urea gel. A probe against miR168 was used as a representative miRNA to detect small RNAs. **(B)** Control RIP experiment on pooled 13 to 17 fractions containing the monomeric form of GFP-AGO1. Anti-GFP nanobodies coupled to magnetic beads were used for immunoprecipitation on GFP-AGO1. Proteins were separated on a 7% Tris-Glycine SDS-PAGE. **(C)** Analysis of copurified small RNAs. 1/2 of IP fraction was used for capillary electrophoresis and the 4 nucleotides spike was added as a standard for estimating sample RNA quantity.

this data indicates that only a few miRNAs show a DE pattern when comparing contiguous cell cycle phases and therefore might gradually damper gene expression rather than quickly shut it down.

c. miRNA target identification

We next asked what are the targets of the abundant miRNAs identified in our analysis and even more interestingly, whether some targets are cell cycle-regulated transcripts. To address this question, we generated PARE (parallel analysis of RNA ends) libraries for three biological replicates of each phase of the cell cycle (Supplemental Table 3). PARE-seq consists in sequencing uncapped 5' monophosphate RNA fragments that results of endonucleolytic cleavage by AGO proteins (German et al., 2008; Zhai et al., 2014). The procedure to generate PARE libraries can be briefly summarized as following: (1) 3' mRNA fragment purification using polyT oligonucleotides coupled to magnetic beads. (2) 5' adapter ligation on uncapped RNAs. (3) Reverse transcription. (4) To minimize the number of sequencing cycles, cDNAs are digested with *Mme1*, generating 20 bp signature fragments. (5) 3' adapter ligation. (6) libraries amplification by PCR prior to sequencing. In contrast to the previous sequencing that has been outsourced (Fasteris, Switzerland), PARE-seq has been performed by our collaborator P. Baldrich of the team of Blake C. Meyers (Danforth plant science center/ Washington university in St-Louis, USA). PARE-seq was performed on the same three biological replicates as used for RNA-seq (Supplemental Table 3).

To minimize sample variability, we focused on miRNA-target pairs present in all biological replicates and supported with robust evidence of cleavage (i.e. a sPARTA-defined class $\leq$ 3) (see PARE_libraries.xls file). Thus, we found 571 unique miRNA-target pairs considering all samples, corresponding to 88 different miRNAs and 123 different genes (Figure 43A). Among those, we found a core subset of miRNAs and their respective target genes that appears to be present in all phases of the cell cycle. This includes 197 miRNA-target pairs, involving 63 miRNAs from 19 families, and 42 target genes (Figure 43A). The majority of these targets encode transcription factors (TFs) such as AP2/ERF (APETALA 2/ETHYLEN RESPONSE FACTOR) , MYB, Scarecrow and GRF. The elevated number of TFs targeted by miRNAs in all phases of the cell cycle supports the idea of a miRNA-mediated second layer of fine control of transcription during the cell cycle. The second

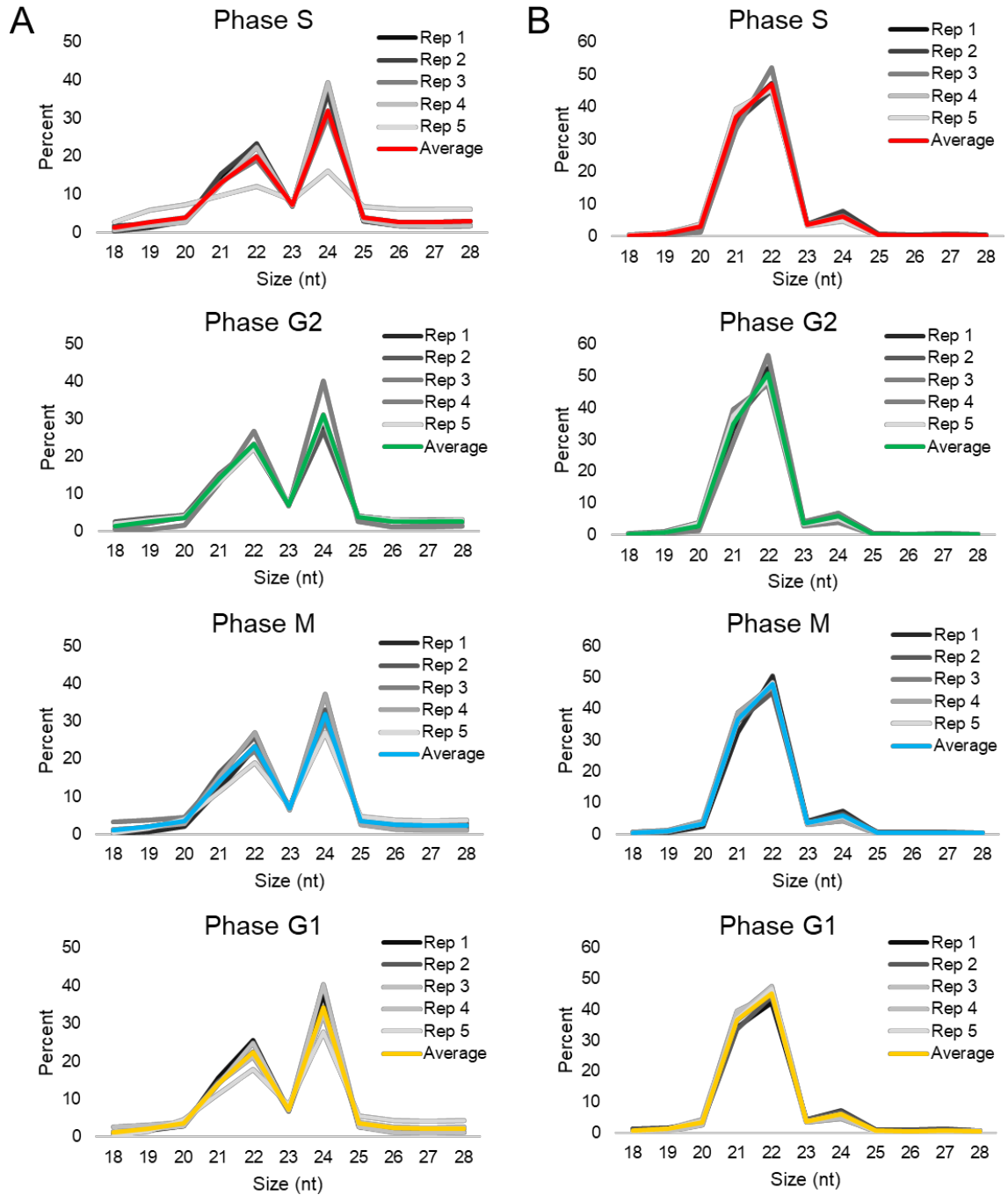

Figure 41: Size distribution of small RNAs.

Percentage of each small RNA size category is represented for each library corresponding to different phases of the cell cycle. In each graph, five replicates are represented in different greys and the average is represented in color. The *x-axis* indicates the small RNA nucleotide size and the *y-axis* indicates its proportion. **(A)** Size distribution for total small RNA libraries. **(B)** Size distribution for AGO1 IP small RNA libraries.

biggest group of target genes are disease resistance proteins. Several studies have already pointed to surprising connections between the cell cycle and some disease resistance genes, which are still poorly understood (reviewed in Eichmann and Schäfer, 2015). Our results suggest that miRNAs may damper their expression in proliferating cells. Finally, there were also a few miRNAs that target F-box domain containing transcripts, including AUXIN SIGNALING F-BOX 2.

We also observed several phase specific miRNA-target pairs, miRNA-target pairs that were only found in one phase of the cell cycle (Figure 43A; see PARE_libraries.xls file). For example, the miR6019 family targets DUF688 only in G2 Phase, miRC-13 targeting RNA-DIRECTED DNA METHYLATION 3 was only present in M phase, and miR530 and miR6145a targeting NOB1 (NIN1 BINDING PROTEIN) Zn-ribbon-like (D-site 20S pre-rRNA nuclease) and DUF1985 respectively, were only present in G1 phase.

In contrast to the situation in mammals, plant miRNAs do not target any of the core cell cycle gene. They may however indirectly contribute to cell proliferation by targeting some important regulators such as transcription factors that might act upstream to modulate transcription of core cell cycle genes. For instance, we found that miR164, targeting the NAC TF CUC2 (Cup Shaped Cotyledon 2), and miR160, targeting ARFs (Auxin response factors), are not present in G2 phase. CUC2 promotes the generation of auxin response maxima and therefore could release ARF repression, triggering downstream auxin signaling components such as CYCA and CDKB. These genes are known to be involved in the control of G2/S and S/G1 transitions.

3. Differential accumulation of tRFs in synchronized BY-2 cells

Beside miRNAs, we did not identify any DE tasiRNAs or hetsiRNAs in these datasets. It has been shown that tRNA-derived Fragments (tRFs) can form a complex with Ago proteins and may play important cellular functions (Shigematsu and Kirino, 2015; Martinez, 2018). With that in mind, we investigated if there were any DE tRFs in our samples. None of the tRFs derived from the 1,529 tRNAs analyzed show any DE in total sRNA samples. However, we found tRFs originating from 67 different tRNAs that are DE in the AGO1-IP samples (Supplemental Figure 2). These tRFs come from 14 different types of tRNAs (Figure 44A). Interestingly, each DE tRF-producing tRNA was associated with a different phase of the cell

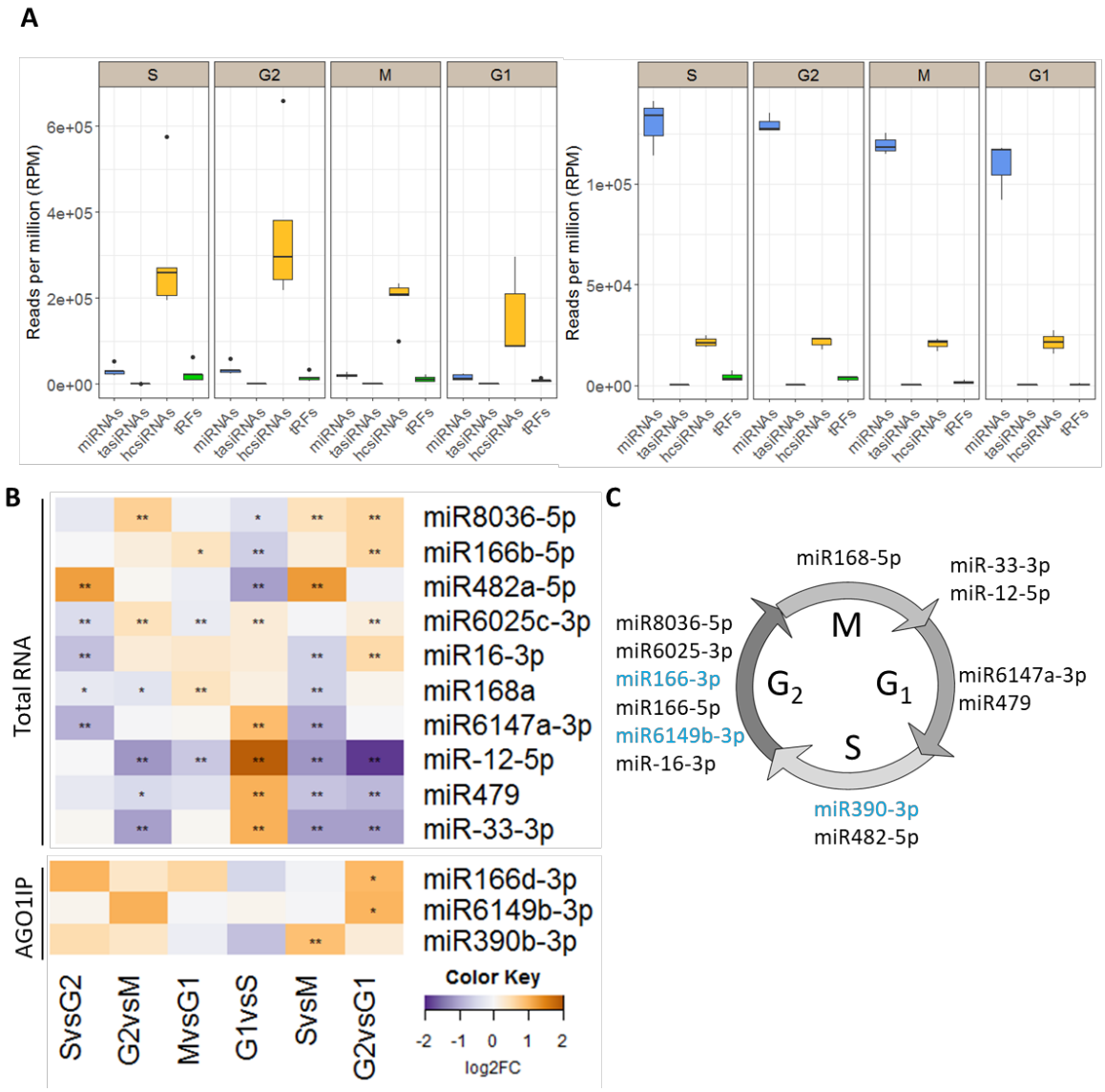

Figure 42: Small RNAs distribution and differentially accumulating miRNAs along the cell cycle.

(A) small RNA abundance per category. The left and right panels represent the five biological replicates of total small RNA samples and three biological replicates of AGO1 IP small RNA samples, respectively. The x-axis represents the different small RNA categories included in this study and the y-axis represents the abundance (RPM) **(B)** microRNA fold change accumulation (in log2 scale) for the differentially expressed microRNAs (*q-value≤0.05 **q-value≤0.01). **(C)** High abundant miRNAs in each phase of the cell cycle phases. In Black are miRNAs identified in total RNA samples and in blue, those identified in AGO1 IP samples.

cycle, with the exception of G1 phase, which did not accumulate high levels of DE tRFs (Figure 44B). To further characterize the role of the DE tRFs during the cell cycle, we analyzed their size and sequence. These DE tRFs had a size distribution pattern different from all tRFs (Figure 44C), with a higher abundance at 19 nt. These DE 19-mers share a conserved sequence (Figure 44D) and lacked the CCA or polyU signatures typical of the 3' end of the tRNA, and thus are classified as 5'-end tRFs ("tRFs-5"). At present it is still unclear what are the targets of these tRFs, if any.

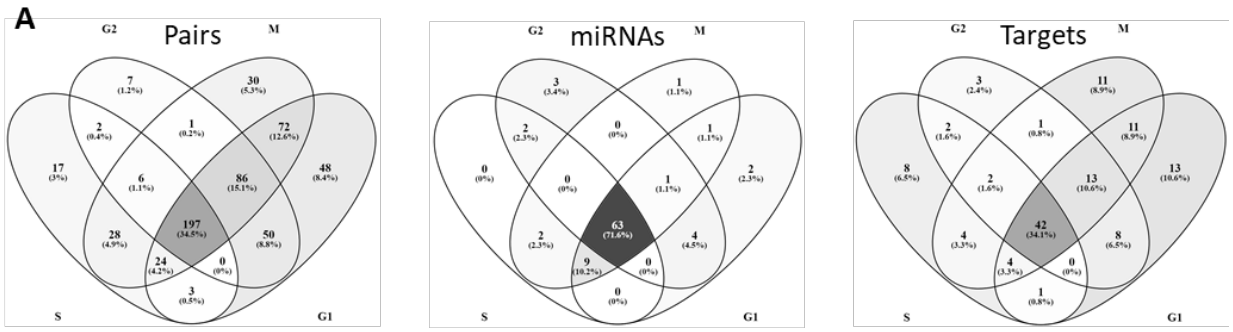

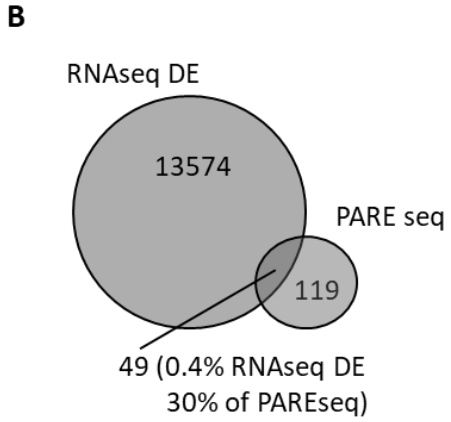

Figure 43: Analysis of PARE libraries from Synchronized BY-2 cells.

(A) Vein diagram of identified PARE signatures and miRNA present in the different cell cycle phases. While most of the miRNA and PARE signatures are found in all libraries, some are exclusively restricted to specific cell cycle phases. **(B)** Vein diagram showing the overlap between identified PARE signatures and the 13574 DE genes with a functional annotation found in RNA-seq data. Only a small subset of DE genes is detected in PARE libraries suggesting that other mechanisms than slicing are responsible of cell cycle dependent RNA turnover in plants.

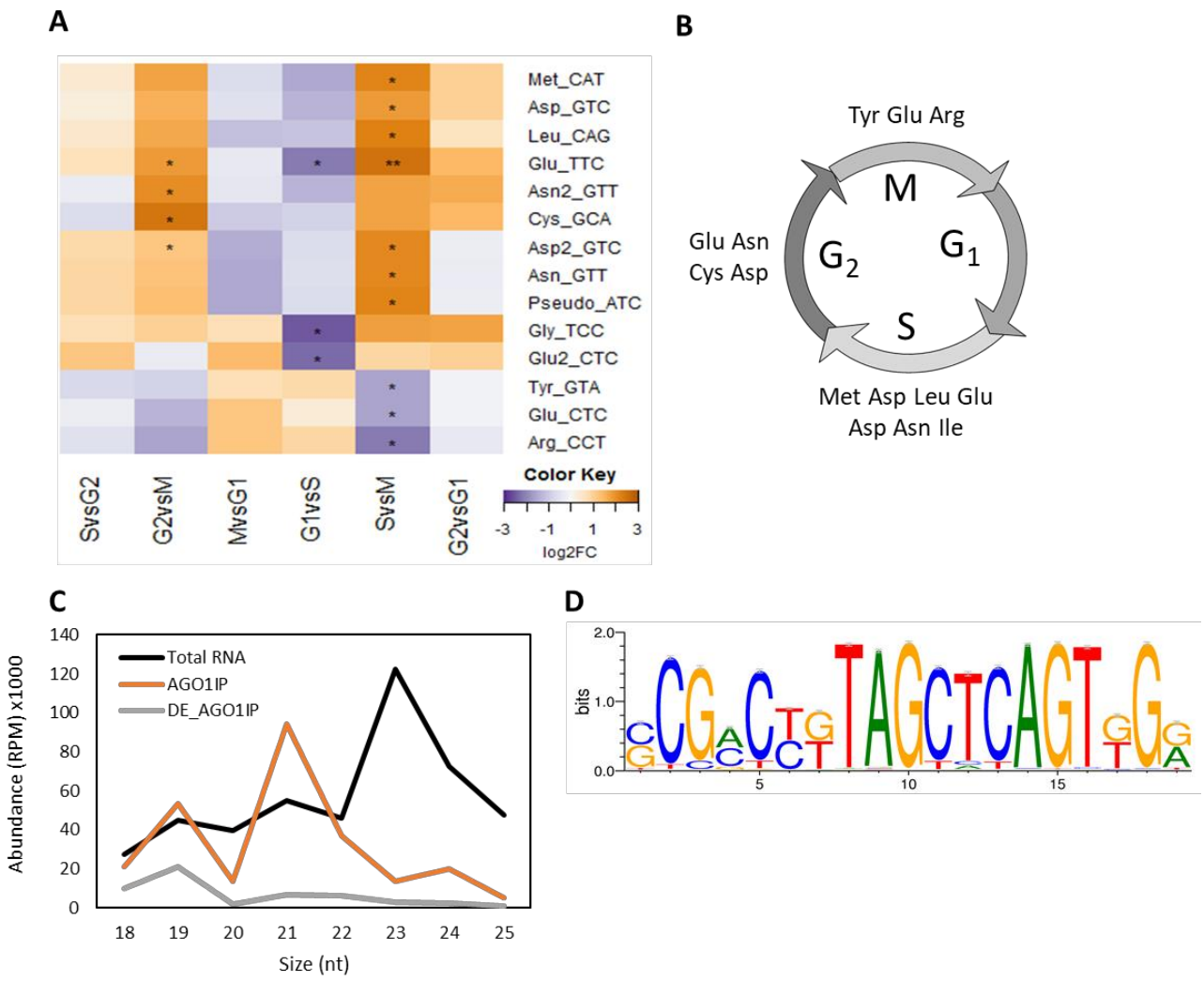

Figure 44: tRFs and cell cycle.

(A) tRF fold change accumulation (in log2 scale) for the differentially expressed tRNA-derived small RNAs (*q-value≤0.05 **q-value≤0.01). **(B)** Highly abundant tRNAs with DE fragments in each phase of the cell cycle. **(C)** Size distribution of tRFs abundance in different samples. In black are total RNA samples, in red are represented all AGO1 IP samples and in grey only the DE tRFs from AGO1 IP samples. **(D)** Logo representation of the most abundant size category (19mers) of the DE tRFs of AGO1 IP samples.

Discussion and some perspectives

In mammalian cells, the role of AGO proteins and miRNAs in the regulation of core cell cycle genes mRNAs is already well established (Bueno and Malumbres, 2011). This has been extensively described in the Introduction. However, in plants, the situation was unclear despite the fact that defects in miRNA biogenesis or in PTGS impact on cell proliferation. The objectives of my thesis were to investigate the regulation and function of AGO1, the major effector of the Arabidopsis miRNA pathway, in the cell cycle control and to identify small RNAs that could regulate cell cycle progression. During my thesis, I demonstrated that AGO1 is essential for the maintenance of cell division in proliferative tissues. I could also show that in contrast to mammals AGO1 does not seem to control the expression of the core cell cycle genes. I also established the repertoire of small RNAs during the cell cycle and I will discuss how some associated to AGO1 may participate in gene expression during the cell cycle. Finally, in a last chapter, I will present some perspectives of my work that deserve attention to be studied in the future.

A. Plant miRNAs control only a small set of DE cell cycle gene in plants

In plants, miRNAs inhibit gene expression by guiding AGO1, likely as part of a RISC complex, to complementary mRNA targets to promote their degradation or represses their translation. The genome of *Arabidopsis thaliana* contains more than 300 miRNA genes, which have been grouped into families, and some of them play crucial roles during development (Jones-Rhoades et al., 2006). Whether plant miRNAs control directly cell division was at present unclear, but mutations affecting miRNA biogenesis and action can lead to altered cell divisions and cell proliferation at different developmental stages and organs in Arabidopsis.

For instance, it has been shown that miR159 targets DUO1 (DUO POLLEN 1), a transcription factor that induces CYCB1;1 expression during male gametophyte development (Zheng et al., 2011). Interestingly, the APC/C, a E3 ubiquitin ligase involved in the turnover of mitotic Cyclins by the proteasome, plays also a role in miR159 biogenesis and could thus contribute to DUO1 repression leading to reduced CYCB1;1 transcription at least in the male

gametophyte. Several other reports have also highlighted the essential role of miRNAs at different stages of embryogenesis. Thus, mutation of *DICER-LIKE 1 (DCL1)* alters embryogenesis at the globular stage showing abnormal cell divisions throughout the suspensor and hypophysis (Schwartz et al., 1994; Nodine and Bartel, 2010). Moreover, *dcl1* mutation fails to establish vascular primordia and ground tissue initials, implying miRNAs in the majority of early embryonic cell differentiation events (Nodine and Bartel, 2010). Similarly, aberrant patterns of cell division and cell expansion during embryogenesis have also been identified in mutants of Arabidopsis *SERRATE (SE)* and *HYPONASTIC LEAVES 1 (HYL1)*, that both cooperate with DCL1 for miRNA biogenesis (Grigg et al., 2009; Armenta-Medina et al., 2017). Accordingly, loss of function of *AGO1* and its closely related *AGO10*, also lead to aberrant cellular divisions during early embryogenesis and defects in polarity (Lynn et al., 1999; Moussian et al., 1998). The molecular basis of altered embryogenesis, pattern formation and abnormal cell divisions is however not yet well understood. Although, *dcl1* mutant exhibit altered auxin responses (Grigg et al., 2009; Nodine and Bartel, 2010; Seefried et al., 2014) and several miRNAs target AUXIN RESPONSE FACTORs (ARFs) (Jones-Rhoades and Bartel, 2004; discussed in Armenta-Medina et al., 2017), a causal link between auxin signaling and defects of embryogenesis in these mutants has not been established. At present, only miR156-mediated repression of the two redundant SQUAMOSA PROMOTER BINDING PROTEIN-LIKE (SPL) transcription factors (SPL10 and SPL11) could explain at least partially the *dcl1* embryo patterning defects (Nodine and Bartel, 2010). Indeed, this work proposed that miR156 might repress the precocious expression of SPLs to avoid a too premature differentiation of the embryo.

Besides embryogenesis, miRNAs have also been shown to control cell proliferation in leaf and root tissues. One of these miRNAs is miR847 that positively regulates meristematic competence and cell proliferation by targeting the mRNA of the auxin/indole acetic acid (Aux/IAA) repressor-encoding gene IAA28 for cleavage (Wang and Guo, 2015). Interestingly ectopic expression of miR847 increases the expression of cell cycle genes as well as the neoplastic activity of leaf cells. It was proposed that the auxin-dependent induction of miR847 may upregulate auxin signaling by clearing the IAA28 mRNA and thus contribute to determine the duration of cell proliferation and lateral organ growth in Arabidopsis. Another important miRNA during leaf morphogenesis is miR319 that targets several Arabidopsis TCPs (TCP2, 3, 4, 10 and 24), belonging to class II TCPs, and is proposed to promote the arrest of the cell cycle (Palatnik et al., 2003b; Nicolas and Cubas, 2016). Thus, it was shown

that increased expression of miR319 causes the degradation of these TCPs and a crinkled leaf phenotype due to excess cell proliferation at the leaf margin similar of *tcp* loss-of-function mutants ((Palatnik et al., 2003; Schommer et al., 2008). These studies revealed that even a slight increase in TCP4 significantly reduces cell proliferation, while a high TCP4 level strongly reduces the expression of G2-M phase cell cycle genes (Schommer et al., 2014). TCP4 could act in at least two ways (Schommer et al., 2014). First, it could directly act on the cell cycle by activating the Cyclin-Dependent Kinase Inhibitor 1 (ICK1)/KIP RELATED PROTEIN1 (KRP1). Second, TCP4 also activates MIR396b that represses cell proliferation. The miR396 family is encoded by two genes, MIR396a and MIR396b, and regulates the expression of transcription factors belonging to the GROWTH-REGULATING FACTOR (GRF) class (Rodriguez et al., 2010; Debernardi et al., 2012). GRF activity is required for cell proliferation in developing leaves, and its repression by miR396 attenuates cell proliferation and lead to a decrease in the expression of cell cycle genes such as CYCLIN B1 (Rodriguez et al., 2010). miR396 plays also important function in the determination of the architecture of the root meristem. There it was shown that PLETHORA (PLT) activates MIR396 in the stem cells to repress GRFs and thus inhibit cell division in the SCN (Rodriguez et al., 2015). Conversely, GRFs repress PLT and putative other stem cell-promoting genes in proliferating transit-amplifying cells, which is essential for the progression of the cell cycle and the orientation of cell division. Recently, another study reported that mutants of *MIR159* genes developed a larger root meristem, likely by enhanced activity of one of its targets, MYB65, which promotes cell cycle progression (Xue et al., 2017).

In all those reported cases, none of these miRNAs directly target core cell cycle genes. In all these cases, the cell cycle is indirectly controlled in a developmental context by miRNAs targeting transcription factors, which positively or negatively impact on cell proliferation in various tissues. Our analysis of miRNAs expression at different stages of the cell cycle and their identified targets further support this assumption, as only a small proportion of the cell cycle DE genes showed miRNA-target pairs and none of them correspond to core cell cycle genes (Figure 42 B; see PARE_libraries.xls file). Moreover, P0-mediated depletion of AGO1 in the root apical meristem impairs meristem size and cell division activity but does not block cells at a specific stage of the cell cycle (Figure27). This situation is very different from metazoans (see Introduction) for which the transcription of some miRNAs is cell cycle regulated and miRNAs target numerous cell cycle transcripts at different cell cycle stages. A possible explanation of such a difference is that the mode of

action of RISC in gene silencing differs between plant and animals. Even though plant AGO1 is also able to perform translational repression, most of its gene silencing activity consists in slicing the target transcript. As this process requires a perfect or near-perfect complementarity between a miRNA and its mRNA target, it might preclude the possibility that a unique miRNA targets a wide spectrum of genes (i.e. CYCs, CDKs,..), as it is the case in mammals (Bueno and Malumbres, 2011). Nevertheless, plant miRNAs might actually control indirectly core cell cycle genes activation by modulating the expression of specific transcription factors. Even though two miRNAs among the 13 DE expressed miRNA were predicted to target transcription factors (Figure 42 B, see PARE_libraries.xls file), further analysis are needed to determine whether they are involved in the transcriptional control of cell cycle genes.

In animals, the large majority of cell cycle miRNAs are particularly targeting G1/S transition but also the G0/G1 transition, corresponding to cell cycle re-entry (Bueno and Malumbres, 2011). Using aphidicolin synchronization we are not able to study this G0/G1 transition. To address this issue additional experiments would be required. For example, it would be interesting to compare the level of the abundant and/or DE miRNAs identified in synchronized cells to BY-2 cells at the saturation phase of the culture or even cells that have been depleted in sugar and hormone-depleted cells.

At the cellular level, the presence of large GFP-AGO1 nuclear bodies in the nucleus during cell cycle suggests that AGO1 is somehow involved in a cellular process during cell division. As the interaction between AGO1 and HYL1 have already been shown in the nucleus (Fang and Spector, 2007), the most evident explanation is that AGO1 might associates with the plant microprocessor complex to load nascent miRNAs and thus contributes to RISC reprogramming. This activity might be particularly strong during the G2 phase of the cell cycle where these bodies are the most prominent. However, we cannot exclude that these bodies might contain correspond to other functional domains of AGO1 and other types of AGO1-associated small RNAs. To further address the question of the function of the nuclear pool of AGO1 and particularly during cell cycle, AGO1 immunoprecipitation on purified nuclei from synchronized samples might be helpful to identify proteins and RNAs associated to these nuclear AGO1 foci.

While the role of AGO1 on cell cycle control needs further investigation, I also observed that a high GFP-AGO1 expression in the BY-2 cell suspension was affecting cell cycle progression in synchronized samples (Figure 30). Interestingly, delay in the G2/M transition has also been observed in *S. pombe* that overexpress the amino-terminal part of

S.pombe AGO1. In fission yeast, AGO1 has also been linked to cell cycle (Carmichael et al., 2004; Stoica et al., 2006). Indeed, yeast *ago1* mutants are impaired in chromatin maintenance and fail to properly segregate sister chromatids during mitosis (Provost et al., 2002; Hall et al., 2003; Volpe, 2002). Yeast AGO1 has been shown to directly interact with 14-3-3 proteins involved in cell cycle regulation (Stoica et al., 2006). In addition, overexpression of yeast AGO1 results in the inhibition of CDC25 nuclear import, leading to the accumulation of Tyr15 phosphorylated form of CDC2 (Stoica et al., 2006). However, *S. pombe* AGO1 mode of action largely differs from human AGO2 and Arabidopsis AGO1, as it is essentially involved in chromatin maintenance and only contributes to transcriptional gene silencing of a subset of genes. Whether Arabidopsis *ago1* mutants exhibit chromatin-related defects would be interesting to further examine. For instance, analyzing the chromatin integrity in Arabidopsis *ago1* mutant backgrounds and looking more particularly for chromatids missegregation in dividing cells represent some possible perspectives.

B. Plant miRNAs repress defense genes during the cell cycle

By contrast with animals, plant do not possess adaptive immune system but evolved an innate immunity system and a systemic defense against pathogens (reviewed in Jones and Dangl, 2006). This immunity system is subdivided in two mechanisms. One uses PRRs (pattern recognition receptors) transmembrane proteins to detect microbial or pathogen-associated molecular patterns (MAMPS or PAMPS) and induces PTI (PAMPS-triggered immunity) responses aiming to stop pathogens before they infect the cells. The other involves NB-LRR (nucleotide-binding leucine-rich repeat protein) that senses pathogen effectors in the cells and usually induces HR (Hypersensitive cells death response). Upon pathogen infection, plants also activate SAR (systemic acquired resistance) through the diffusion of signal molecules, such as salicylic acid, from the site of infection to the whole plant (Durrant and Dong, 2004).

The molecular links between the cell cycle and defense responses in plants are still not well understood. Microarray data from synchronized Arabidopsis cell suspension revealed that some resistance genes are differentially expressed during the cell cycle with a peak of expression either in S or M phase (Menges et al., 2005), and we identified also 100 of those DE resistance genes from our RNA-seq libraries. More recently, it has been shown that cell

cycle mis-regulation can lead to the activation of disease resistance genes (Bao et al., 2013). For instance, overexpression of OSD1 (OMISSION OF SECOND DIVISION 1) or UVI4 (UV-B-INSENSITIVE 4), two negative regulators of the APC/C, results in the expression of the defense marker gene PR1 and confers resistance to virulent pathogens. Conversely, loss of these two proteins, as well as the APC10 subunit or the CCS52 APC/C coactivator, lead to enhanced susceptibility to bacterial infection. In addition, the *cdkb1;1* mutant suppresses *osd1* phenotype and loss of the resistance gene SNC1 (SUPPRESSOR OF *npr1-1* CONSTITUTIVE 1) abolishing pathogen resistance conferred by *osd1* mutation. On the other hand, plant pathogens and beneficial symbionts can also modulate the cell cycle activity by inducing or suppressing cell cycle gene expression. For example, infection by the root-nematode *Meloidogyne incognita* induces expression of the early nodulin ENOD40 and the APC/C subunit CCS52a and promote galls formation in *Medicago trunculata* (Favery et al., 2002). In addition, overexpression of NOD40 results in activation a wide range of genes, including cyclin D3, that might enhance cell proliferation in galls.

Taken together, these data suggest that the balance between cell proliferation and defense against pathogens might, a least partly, involves regulation of core cell cycle genes. In our total small RNA libraries, we identify three miRNAs, among the 13 DE miRNAs, that target NB-LRR genes (Figure 42 B and see PARE_libraries.xls file). For now, the biological significance of this cell cycle-dependent regulation of resistance genes is still unclear. However, one could speculate that these genes are repressed upon mitogenic stimuli to promote cell proliferation. Thus, the cell cycle and defense gene expression programs may antagonize each other and small RNAs could be involved in this regulation.

C. A novel class of tRNA-derived fragments

By contrast to other small RNAs, tRFs abundance was surprisingly different between total small RNAs and AGO1 associated small RNAs libraries. This suggest that tRFs biogenesis is most likely constant during cell cycle, while loading in AGO of at least some tRFs must somehow be cell cycle-regulated. It is already known that some plant tRFs accumulate in a wide range of stresses including oxidative stresses (Thompson et al., 2008) and UV stresses (Gebetsberger et al., 2012) that induce deleterious effects such as DNA damage. Interestingly some tRFs that are differentially accumulated in our libraries originate

from the tRNAs that are also processed upon oxidative stresses, and particularly the tRNA-Arg (CCT) and the tRNA-Glu (CTC) (Figure 43 A). In addition, 11 tRFs among the 14 DE tRFs appear to be enriched in S and G2, suggesting that they might be involved in DNA replication processes. However, whether this accumulation is related to the cell cycle or caused by aphidicolin-induced replicative stress remains to be determined.

Interestingly, almost all of the 19-mer tRFs associated to AGO1 have a G or a C in 5' (Figure 43D) while it has been already reported that AGO1 has a preference for a U or a A in 5' (Wang et al., 2011). This might explain why tRFs represent such a small subset of AGO1-associated small RNAs. Moreover, the presence of G/C in tRFs 5' end might also affect the stability of the RISC complex and therefore explain why we have detected high fold changes for AGO1-associated tRFs while other small RNAs remains overall unchanged during cell cycle. However, the biological significance of these DE tRFs, as well as their mode of action remain to be determined. To further examine whether tRFs are able to trigger mRNA slicing while associated with RISC complex, we will look for PARE signatures that can match with tRFs sequences. However, available data are more in favor of a slicing-independent mechanism. Indeed, some tRFs have already been shown to induce translational inhibition (Gebetsberger et al., 2012; Sobala and Hutvagner, 2013). For example, Val-tRF from the archaea *Haloferax volcanii* associates to the small ribosomal subunit and is able to inhibit protein synthesis by interfering with peptide bond formation, presumably to fine tune overall protein synthesis in response to several stresses. In addition, Sobala and Hutvagner described a similar tRF-mediated translational inhibition mechanism in HeLa cells (Sobala and Hutvagner, 2013). They also showed that the 3' "GG" dinucleotide is essential for this function. Interestingly, this motif was highly represented in our AGO1-associated tRFs sequences (Figure 43D), suggesting that, at least of a subset of these tRFs might act in a similar way. To determine whether DE tRFs are indeed involved in translational repression, looking for tRFs enrichment in polysomal fraction could be an interesting experiment to perform.

Finally, we did not detect any 3'- end TRFs in our libraries. However, tRNAs, as other housekeeping non-coding RNAs, undergo several steps of base modifications to ensure proper folding. Among these modifications, the N-1-methyladenosine in the T-arm is misread by reverse transcriptase, resulting in the incorporation of mismatched dNTPs. Thus, as we mapped the small RNA libraries on the tobacco genome without allowing any mismatch, we

would certainly have missed this class of tRFs and we will further need to remap the libraries allowing at least one mismatch.

D. How cell cycle genes could be post-transcriptionally controlled in plants?

From my results, I concluded that PTGS is not responsible of the highly dynamic changes of core cell cycle transcript abundance during cell division. While transcriptional control has been already well characterized in eukaryotes, it is however not enough to explain why some transcripts quickly disappear at cell cycle phase transitions. In *S. cerevisiae,* a specific RNase has been shown to be involved in cell cycle regulation. The MRP (MITOCHONDRIAL RNA PROCESSING) endoribonuclease is a ribonucleoproteic RNase composed of an RNA coded by *NME1* (NUCLEAR MITOCHONDRIAL ENDONUCLEASE 1) and at least nine proteins, with height of those that are shared with the yeast nuclear RNase P. Interestingly, mutations in the *NME1* gene or in *SNM1*, that encodes a RNA-binding subunit, both result in a delay of the exit from mitosis, characterized by cells blocked in telophase (Cai et al., 2002). These defects were not associated to misfunction of the APC/C directly, but to overaccumulation of the cyclin *CLB2* transcript. Thus, in addition to APC/C mediated degradation of the CLB2 protein, *CLB2* mRNA degradation by a specific ribonuclease is required to ensure the correct timing of exit from mitosis. *In vitro* experiments further demonstrated that MRP directly affects the *CLB2* transcripts by cleaving its 5' UTR (Gill et al., 2004). These researchers proposed a hypothetical model where *CLB2* mRNAs are subjected to MRP cleavage in late mitosis, releasing an unprotected 5' monophosphate and are then degraded by the 5'-3' exoribonuclease XRN1. More recently, Trcek and colleagues showed that yeast *CLB2* mRNA and *SWI5* mRNA, that codes for M phase specific transcription factors, are bound to the cell cycle regulatory kinase DBF2 (DUMPBELL FORMER 2) (Trcek et al., 2011), whose activity is promoted in anaphase by its dephosphorylation (Toyn and Johnston, 1994). Following their model, DFB2 is recruited to the promoter region of these genes and transcriptionally associates with the newly synthetized transcript. Then, depending on the phosphorylation state of DFB2, DFB2 might itself participate to the stability of the messenger or recruit deadenylating complexes to trigger 3'->5' degradation by the exosome. In the animal field, poly (A) tails have been shown to be important for RNA stability and also for cap-dependent translation (reviewed in Weill et al.,

2012). Interestingly polyadenylation and deadenylation are also regulating expression of core cell cycle genes during cell cycle. For example, B1 cyclin from Xenopus oocytes is strongly deadenylated in S phase, leading to its translational silencing, whereas it is polyadenylated in M phase (Groisman et al., 2002). This process involves CPEB (CPE-BINDING PROTEIN) and MASKIN proteins that prevents recruitment of poly (A) polymerases in S phase and inhibits formation of the pre-initiation complex. In M phase, Aurora kinase phosphorylates CPEB, and thus allows polyadenylation and assembly of the pre-initiation complex, presumably by inactivating CPEB/MASKIN. Interestingly, genome wide analysis of poly(A) tail length on synchronized human cells highlighted that even though the overall poly (A) length remains constant during cell cycle, a subset of genes exhibit dramatic poly(A) tail length changes between S and M phases (Park et al., 2016). Gene ontology revealed that these genes are mainly involved in cell cycle regulation, microtubules cytoskeleton, ubiquitin ligase activity and DNA binding. The most striking example is CDK1, for which the mean poly (A) tail length is ranging from 80 nt in M phase to 3 nt in S phase. In addition, ribosome profiling confirmed that transcript with short poly (A) tails of less than 20 nt (that correspond to the minimal length for PABP binding) are depleted from polysomal fractions, supporting that these genes are translationally silenced in a cell cycle phase-specific fashion. Note that this study also pointed out the bias created during generation of RNA-seq libraries. Indeed, mRNA are first purified using poly(T) oligonucleotides coupled to magnetic beads, excluding purification of deadenylated mRNA. However, studies already demonstrated that deadenylated mRNAs do not systematically undergo RNA degradation but can be stored as translationally silenced RNA. Thus, we have to keep in mind that our RNA-seq libraries do not reflect the overall mRNA abundance but only the pool of mRNA that can be translated.

Other strategies have been also developed to control translation of core cell cycle genes, for example, the yeast cyclin *CLN3* mRNA, possess a upstream open reading frame in its 5' UTR that interferes with its translation (Kronja and Orr-Weaver, 2011) and require the eIF4E homologue CDC33 protein to promote G1/S transition. In human, Cyclin E1 mRNA exhibit a long 5' UTR with GC-rich sequence that are supposed to alter ribosome scanning during translation initiation. Proper Cyclin E1 translation during G1/S transition is facilitated by the action of the human DEAD-box helicase DDX3 that might be required to unwind 5' UTR secondary structures (Kronja and Orr-Weaver, 2011).

To our knowledge, none of those mechanisms have been described in plants so far. But, among the 23000 DE genes found in our RNA seq libraries, I identified more than 70

DEAD-box helicases with respectively 2 and 1 that peak in S and M phases, as well as 4 DE eIF4E-like proteins. I-might be interesting to determine whether these proteins play important functions in the regulation of the cell cycle in plants. First, one would need to examine their promoter sequences for E2F-binding or MSA binding elements. Moreover, our efficient synchronizable BY-2 cell suspension could be also useful for identification of RNA-associated proteins by gene candidate approach. For example, it is possible to incubate in vitro transcribed-biotinylated core cell cycle mRNAs with synchronized cell extract and then identify copurified proteins in mass spectrometry. Finally, a recent study described a method to purify GFP-labelled P-bodies from human cell cultures using fluorescence-activated particle sorting (Hubstenberger et al., 2017). These researchers performed proteomics and RNA-seq analysis on these purified P-bodies (containing translational silenced transcripts), providing insights on their composition. Moreover, gene ontology revealed that a significant number of genes enriched in P-bodies are involved in cell division, suggesting that this method is robust enough to investigate cell cycle-related events. Thus, it might be possible to use this technique on synchronized BY-2 samples to identify the proteins that are involved in post-transcriptional regulation of core cell cycle gene expression.

Material and methods

A. Material

1. Bacterial strains

a. *Escherichia coli*

E.coli, TOP10 (Invitrogen) were used for plasmid amplification. This strain carries a mutated *recA* recombinase to minimize recombination events between plasmids and bacterial DNA.

Genotype: *F- mcrA Δ(mrr-hsdRMS-mcrBC) Φ80lacZΔM15 Δ lacX74 recA1 araD139 Δ(araleu)7697 galU galK rpsL (StrR) endA1 nupG*

E.coli, DB3.1 (Invitrogen) were used for propagating empty Gateway vectors containing the *ccdB* gene. *ccdB* gene encodes a protein that interferes with the bacterial gyrase. DB3.1 strain carries the gyrA462 allele that confers the resistance to the *ccdB* gene.

Genotype: *gyrA462 endA1 Δ(sr1-recA) mcrB mrr hsdS20 glnV44 (=supE44) ara14 galK2 lacY1 proA2 rpsL20 xyl5 leuB6 mtl1*

b. *Agrobacterium tumefaciens*

A.tumefaciens, GV3101 (PMP90) were used for Arabidopsis transformation. It carries chromosomal resistance to rifampicin. Gentamycin resistance is conferred by the disarmed Ti (Tumor inducing) plasmid PMP90 that encodes *vir* genes required for T-DNA transfer.

A.tumefaciens LBA4404 were used for efficient transformation of tobacco BY-2 cell suspension. This strain harbors the disarmed Ti plasmid pAL 4404 that contains the *vir* genes, required for T-DNA transfer.

2. Plant material

All *Arabidopsis thaliana* plants are in Columbia-0 accession genetic background (Col-0). Arabidopsis thaliana mutant allele *ago1-36* was previously described in Baumberger and Baulcombe, 2005. The T-DNA insertion line originates from the salk collection (salk_087076 line) and results in expression of a truncated protein missing PAZ and PIWI domains. *ago1-27* mutant allele was isolated from a EMS-mutagenized population (Morel et al., 2002). *ago1-27* mutation consists in glycine to serine substitution at position 758 in the PIWI domain. *ago1-57* was described in Derrien et al., 2018. *ago1-57* allele was isolated in the lab of Pascal Genschik (IBMP, France) from an EMS suppressor genetic screen based on the stabilization of AGO1 protein level upon P0 induction with β-estradiol. The point mutation induced by EMS leads to a glycine to aspartic acid substitution in position 371, located in the DUF1785 domain. *ago1-57* mutant line carries the XVE:P0 construct that allows induction of P0 expression upon β-estradiol treatment (Derrien et al., 2018).

Col-0 and ago1 mutants lines were transformed with the pHTR2:CDT1a (C3)-GFP (Yin et al., 2014) and pCYCB1;2::CYCB1.2(DBox)-eGFP constructs and double homozygous transgenic plants for both transgenes were selected and used for further experiments.

3. Tobacco BY-2 cell suspension

Tobacco BY-2 cells suspension has been established in 1972 by Japan Tobacco, Inc from callus induced on *Nicotiana tabacum* cultivar Bright Yellow-2 seedlings (reviewed in Nagata et al., 1992). This line has been selected among 40 other cell suspensions of Nicotiana species for their high proliferative rate, providing a good plant model to study cell cycle, comparable to human HeLa cells.

4. Plasmids

The pGREENII pAGO1: GFP-AGO1 construct is described in Derrien et al., 2012. This binary vector encodes a functional GFP-AtAGO1 protein that complements *ago1-11* and *ago1-27* arabidopsis mutants. Promoter and 5'UTR sequences were amplified from 1654 bp

upstream the ATG and AGO1 cDNA (including the 3'UTR) was fused in 5' to eGFP coding sequence. pGREENII confers resistance to Basta for plant selection. As this selection cannot be efficiently used for BY-2 cells transformation, pAGO1: GFP-AGO1 DNA sequence was transferred to a binary vector with kanamycin resistance using gateway cloning. Thus, pAGO1:GFP-AGO1 construct was first clone in a pDONR^{TM} 221 and then recombined with pKGW. Vector maps are shown in supplemental figure 3.

All vectors and primers used for cloning are listed in supplemental table 4 and 5, respectively.

5. Chemicals and antibiotics used for bacterial and plant selection

Chemicals and antibiotics used for bacterial and plant selection are listed below with their corresponding working concentrations:

			Final concentration (µg/ml)	
	Soluble in	Stock solution (mg/ml)	Bacteria	Plants/ BY-2 cells
Cefotaxime	Water	250	500	
Carbenicillin	Water	200	100-500	
Kanamycin	Water	100	50	50
Tetracyclin	Ethanol	12,5	12,5	
Gentamycin	Water	100	50	
Spectinomycin	Water	100	100	
Streptomycin	Water	30	30	
Chloroamphenicol	Ethanol	30	30	
Rifampicin	DMSO	100	50	
Hygromycin	Water	500		30
Basta/glufosinate	Water	10		10

Note that cefotaxime and carbenicillin have been used at a concentration of 500 µg/ml only to kill Agrobacteria after BY-2 cells transformation.

B. Methods

1. Protocols related to cloning and bacterial transformation

a. Genomic DNA extraction (Doyle and Doyle, 1987)

CTAB buffer: 2% cetyl trimethylammonium bromide, 1% polyvinyl pyrrolidone, 100 mM Tris-HCl, 1.4 M NaCl, 20 mM EDTA

CAI solution: chloroform:24 volumes, Isoamyl alcohol 1volume

About 100 mg of liquid nitrogen-frozen plant tissue are grinded with 1.7-2.1 mm glass beads and resuspended in 500 µl CTAB buffer by vortexing thoroughly. Lysates are then incubated at 60°C for 30 minutes. Following incubation, samples are clarified by centrifugation at maximum speed for 15 minutes. Supernatant is then collected and mixed with 1 volume of CAI and vortexed. Samples are centrifuged, and aqueous phase is collected. DNA is precipitated by adding 1 volume of cold isopropanol and incubating at -20°C for 20 minutes. DNA is pelleted by centrifugation at maximum speed for 20 minutes. Pellets are washed twice with cold 70% Ethanol and air dried until pellets became colorless. They are finally resuspended in PCR-grade water or 10 mM Tris pH 8. Pellets may need warming to dissolve. DNA concentration is measured on a Nanodrop spectrometer (ThermoFisher Scientific).

b. DNA amplification by PCR

Polymerase chain reaction (PCR) is performed for DNA amplification for cloning purpose and bacterial colony screening. Taq Phusion master mix (FinnZymes) is used for high-fidelity DNA amplification while Gotaq DNA polymerase (Promega) and Phire 2 DNA polymerase (ThermoFisher Scientific) was used for other applications.

PCR conditions are listed below:

	Phusion 2X mix	Phire 2	Gotaq
Total volume	50 µl	20 µl	25 µl
Foward primer (10µM)	1 µl	1 µl	0.5 µl
Reverse primer (10µM)	1 µl	1 µl	0.5 µl
dNTP (10mM)		0,4 µl	0.5 µl
Buffer		5X: 4 µl	5X: 5µl+2µl $MgCl_2$ (10 mM)
DNA polymerase		0,1 µl	0.125 µl
Master mix	2X: 25 µl		
DNA matrix	10 ng vector/up to 200 ng genomic DNA		

PCR programs are listed below:

	Phusion	Phire 2	Gotaq
Initial Denaturation	2 min 98 °C	30 sec 98°C	2 min 95°C
Denaturation	15 sec	5 sec 98°C	30 sec 95°C
Priming	15-30 sec	5 sec	30 sec
Elongation	30 sec/kb 72°C	15 sec/kb 72°C	1 min/kb 72°C
Final elongation	5 min 72°C	1 min 72°C	5 min 72°C

The number of PCR cycle is generally comprised between 30 and 35.

c. DNA analysis

TAE (Tris-Acetate EDTA) : 40 mM Tris-Acetate, 0.1 mM EDTA

Amplified PCR fragment and vectors are analyzed by agarose gel electrophoresis on 1X TAE agarose gel (0.8% to 2% Agarose). DNA is stained with ethidium bromide and revealed on a UV transilluminator. Amplified vectors are then sequenced at the IBMP sequencing platform by the sanger method.

d. Gateway cloning (Invitrogen)

PEG solution: 30% PEG 8000, 30 mM $MgCl_2$

Tris-EDTA buffer (TE) : 10 mM Tris HCl pH 8, 1 mM EDTA

All the constructs were generated using Gateway technology. PCR products are purified by PEG precipitation as followed. Water is added to the PCR reaction up to a volume of 200 µl. 100 µl of PEG solution is added to a final concentration of 10% PEG, 10 mM $MgCl_2$ and vortexed thoroughly. The sample is then centrifuged at maximum speed for 20 minutes at room temperature. The supernatant is discarded (pellets might not be visible). Pellet is resuspended in 20 µl. 5 µl of purified PCR fragment are loaded on agarose gel to verify its presence and concentration.

BP clonase and LR clonase reaction are incubated overnight at 25°C. Reaction conditions are listed below:

BP clonase reaction		LR clonase reaction	
Purified PCR product	5 µl	Entry vector	150 ng
pDONR221	150 ng	Destination vector	150 ng
BP clonase	1 µl	LR clonase	1 µl
TE buffer	up to 10 µl	TE buffer	up to 10µl

BP clonase and LR clonase reactions are treated with 1µl Proteinase K (Invitrogen) for 10 minutes at 37°C prior to bacterial transformation.

e. Plasmid purification

GTE buffer: 50 mM glucose, 25 mM Tris HCl pH8, 10 mM EDTA, 0.1 mg/ml RNase A (stored at 4°C)

Lysis buffer: 0.2 N NaOH, 2% SDS (freshly prepared)

Neutralization buffer: 3 M CH_3CO_2K, 1.8 M formic acid

CAI solution : Chloroform : 24 volumes, Isoamyl alcohol : 1volume

2.5 ml of overnight *E. coli* culture is pelleted by centrifugation at 3500 rpm for 10 minutes and resuspended in 250 µl of GTE buffer. 250 µl of lysis buffer are added, tubes are gently mixed by hand and incubated at room temperature for 5 minutes maximum. Lysis is immediately stopped by adding 250 µl of neutralization buffer and gently mixing tubes again. Debris are pelleted at maximum speed for 10 minutes and the supernatant is mixed with 1 volume of CAI solution. Phases are separated by centrifugation at maximum speed for 15 minutes and aqueous phase is precipitated at -20°C with 1 volume of cold isopropanol for 20 minutes. Plasmid DNA is then pelleted by centrifugation at maximum speed for 20 minutes and washed 2 times with 70% ethanol. Pellets are air dried and resuspended in 50 µl bidistilled water or 25 mM Tris HCl pH8. Nucleic acid dosage is performed using NanoDrop spectrophotometer (ThermoFisher Scientific).

f. Bacterial transformation

LB (Luria Bertini) medium: 10 g/L bacto-tryptone, 5 g/L yeast extract, 5 g/L NaCL, pH 7.2

YEB medium: 5 g/L beef extract, 1 g/L yeast extract, 5 g/L peptone, 5 g/L sucrose, 20 mM $MgSO_4$ (added after autoclaving) pH 7.4

Preparation of thermocompetent *E. coli* cells

A 5 ml preculture is inoculated with *E. coli* cells and grown overnight at 37°C in liquid LB medium. 250 ml of LB medium in one-liter Erlenmeyer is then inoculated with the entire preculture and grown at 37°C until the optical density at 600 nm reaches 0.7. The following steps are then done at 4°C in sterile conditions. Cells are centrifuged at 5000xg for 15 minutes and washed two times with cold 0.1 M $CaCl_2$. They are resuspended in 50ml of 0.1 M $CaCl_2$ and incubated at 4°C overnight. Cells are then centrifuged as previously and resuspended in 3 ml of cold 0.1 M $CaCl_2$, 15% glycerol solution before being divided in 50 µl aliquots. Aliquots can be directly used for high efficiency transformation or are frozen in liquid nitrogen and stored at -80°C.

Preparation of electrocompetent *A.tumefaciens* cells

10 ml of YEB supplemented with necessary antibiotics are inoculated with GV3101 (PMP90) or LBA 4404 agrobacterium strain and grown overnight at 28°C in dark on a shaker (180 rpm). 250 ml of YEB medium supplemented with antibiotics in one-liter Erlenmeyer are

inoculated with the preculture and grown at 28°C until the optical density at 600 nm reaches 0.6. The following steps are then done at 4°C in sterile conditions. Cells are centrifuged at 5000xg for 15 minutes and washed 3 times with cold sterile water and resuspended in 10% glycerol before being divided in 50µl aliquots. Aliquots can be directly used for high efficiency transformation or are frozen in liquid nitrogen and stored at -80°C.

E.coli heat shock transformation

Competent *E.coli* cells, stored at -80°C, are thawed on ice. DNA that needs to be amplified (10 ng of vector or 5 µl of BR/LR clonase reaction) is gently mixed with the cells and incubated on ice for 20 minutes. Cells are then transferred to a heated bath at 42°C for 45 seconds and immediately chilled on ice for 2 minutes. 500 µl of LB medium are added and cells are incubated 20 minutes at 37°C. 250 µl of cells are finally plated on solid LB medium (1,5 % agar) supplemented with the appropriate antibiotics and incubated for overnight at 37°C. List of used antibiotics and concentration for bacterial selection is described above in material section.

A.tumefaciens transformation by electroporation

Competent *A.tumefaciens* cells, stored at -80°C, are thawed on ice. 10 ng of vector are gently mixed in a microtube and then transferred in an ice-chilled electroporation cuvette and electroporated at 2500 V, 400 Ohm resistance, 0.25 µF, $\tau \pm 3.8$ ms on a Gene pulser (BioRad) apparatus. Cells are transferred in 500 µl of LB medium and incubated for 1 hour at 28°C. Finally, 250 µl of cells are plated on solid LB medium with antibiotics and incubated at 28°C for 36 to 48 hours. List of used antibiotics and concentration for bacterial selection is described above in material section.

2. Protocols related to *Arabidopsis thaliana*

a. Culture conditions

Plants were cultivated in growth chambers following two conditions:

- 16h light/8h dark photoperiod, temperature: 21/18°C, 80% humidity for long-day culture

- 8h light /16h dark photoperiod, temperature: 21/18°C, 80% humidity for short-day culture

For *in vitro* culture, seeds are sterilized as followed:

- 2X 70% Ethanol, 0.05%TWEEN 20 (Sigma-Aldrich); 3minutes each (can be extended to 10 minutes)
- 1X 96% Ethanol; 1 minute

Murashige and Skoog (MS) medium: MS with micro and macro elements M0255 (KALYS), 10 g/L sucrose, pH 5.8

Sterilized seeds are sawn of MS medium (0.8% or 1% agar) and stratified 2 days at 4°C in dark conditions. Seeds are then germinated in growth chambers with the following culture conditions:

- 16h light/8h dark photoperiod, temperature: 21/18°C, 80% humidity

b. Agrotransformation of Arabidopsis plants

T-DNA plant transformation are performed with "floral dip" method as described in Clough and Bent, 1998. Transgenic plants were obtained by transformation of XVE:P0-myc and XVE:P0/*ago1-5*7 lines with the following constructs:

- pGWB650 pCYCB1.2:CYCB1.2(dBox)-eGFP
- pGWB650 pHTR2:CDT1a(C3)-eGFP

Heterozygous T1 transformants were selected on soil using glufosinate/Basta selection. Mono-insertion homozygous lines (representing 75% resistance in T2, 100% resistance in T3) were selected *in vitro* and used for analyses.

c. Root length analysis

Sterilized seeds are sawn of solid MS medium (1% agar) without sucrose and stratified 2 days at 4°C. Seeds are then germinated on vertical plates in growth chambers with the classical *in*

vitro culture conditions described above. Seedlings are imaged at 6 and 10 days after stratification (DAS), and root length is measured using ImageJ software. Anova statistical tests are performed using R software.

d. Imaging of Arabidopsis root tips

Propidium iodide (PI) staining solution: 80 µg/ml propidium iodide (Sigma-Aldrich), solubilized in water (stored at 4°C in dark)

Primary roots of 6, 10 or 12 DAS Arabidopsis seedlings grown on vertical plates are mounted on microscopy slides with PI staining solution. Settings that has been used for imaging root tips are described below in the section related to microscopy.

e. Induction of gene expression with β-estradiol

β-estradiol stock solution: 10 mM β-estradiol in DMSO (Stored at -20°C in dark)

For β-estradiol treatment, sterilized seeds are sawn on solid MS medium (0.8 or 1% Agarose) without sucrose supplemented with 10 µM β-estradiol and grown as described in the section related to culture conditions.

3. Protocols related to BY-2 cell suspension

a. Growth conditions (see Nagata et al., 1992)

BY-2 medium: Murashige and Skoog MO222 (KALYS), 30 g/L sucrose, 1 mg/L Thyamine, 200 mg/L 2,4D, 200 mg/ml KH_2PO_4, 100 mg/L Myoinositol, pH 5.8

BY-2 cells are grown in the dark at 23-25°C under agitation (120 rpm). BY-2 cell suspension must be subcultured weekly. 1.5 ml of 7-day-old saturated BY-2 culture are inoculated in 80 ml of fresh sterile BY-2 liquid medium.

b. Transient expression in BY-2 cell

Before stable transformation, constructs are transitory expressed by biolistic for validation. 1mg of tungsten beads is sterilized in ethanol and centrifuged. Supernatant is discarded, and beads are resuspended in 17 µl of 50% glycerol. 4 µg of vector are added to the mix, and tubes are vortexed. 16.5 µl of 2 M CaCl2 and 7.5 µl of 1 M spermidine are added while still vortexing. Tubes are incubated 20 minutes a room temperature. Beads are then washed 2 times with ethanol and air dried for 5 minutes. Beads are finally resuspended in 12 µl of ethanol. 5 ml of 3 to 4-day-old BY-2 cell suspension are vacuum-filtered on filter paper and transferred on solid BY-2 medium. Cells are then bombarded with a homemade helium particle inflow gun with 12 µl of coated beads at -0.7 bar of pressure. Cells are kept in classical growth conditions until observation on a microscope.

c. Transformation with *A.tumefaciens*

YEB medium: 5 g/L beef extract, 1 g/L yeast extract, 5 g/L peptone, 5 g/L sucrose, 20 mM $MgSO_4$ (added after autoclaving) pH 7.4

Bacterial resuspension solution: 10 mM $MgSO_4$, 10 µM acetosyringone (sterile, freshly prepared)

Previously transformed LBA4404 agrobacterium strains are cultured overnight in YEB medium at 28°C supplemented with antibiotics required for selection. Bacteria are then pelleted and resuspended in sterile 10 mM $MgSO_4$. Bacterial suspension is supplemented with 10 µM acetosyringone for 1 hour to activate virulence. 80 ml of 3 to 4-day-old BY-2 cells are then divided in 3 ml aliquots in sterile 24 well plates and inoculated with 100 µl of bacterial solution in each well. Cells are cocultured at 23-25°C in dark for 36 hours under mild agitation (50 rpm). Cells are then pooled in 50 ml tubes and centrifuged at 800 rpm for 3 minutes. Supernatant is discarded, and cells are gently resuspended in fresh medium. This step is repeated 3 times. Cells are then supplemented with appropriate antibiotics for selection of transformants and 10 ml aliquots are plated on Petri dishes containing solid selective solid BY-2 medium (0.8% agar). Petri dishes are sealed with Micropore adhesive and kept in dark

at 23-25°C. 3 to 4-week-old calli are put in 20 ml of liquid BY-2 medium and then cocultured weekly in 80 ml. Selection pressure is maintained for at least 2 weeks. List of used antibiotics and concentration for plant selection is mentioned above in the material section.

d. Cell cycle synchronization

Aphidicolin stock solution: 10 mg/ml aphidicolin (Sigma-Aldrich, Santa Cruz) in DMSO, stored at -80°C for 6 months maximum (or freshly prepared)

Propyzamide stock solution: 6 mM propyzamide (Sigma-Aldrich) in DMSO, stored at -20°C

BY-2 medium: described above

Washing solution: 40 g/L sucrose, freshly prepared and tempered to 25°C

Single step synchronization (see Nagata and Kumagai, 1999; Criqui et al., 2000)

10 ml of an 8-day-old saturated BY-2 cell suspension are inoculated in 90 ml of fresh BY-2 liquid medium supplemented with aphidicolin (Sigma-Aldrich, Santa Cruz) to a final concentration of 5 mg/L and kept at 25°C in the dark in shaking incubator (120 rpm). To release aphidicolin inhibition, cells are washed 10 times on 48 µm nylon mesh with tempered washing solution for 10 minutes and then washed at least 1 time with 100ml of BY-2 medium. Cell are then resuspended in 100 ml of BY-2 medium. The whole procedure should not exceed 15 minutes. Cells are then kept under classical culture and aliquots are harvested every hour for protein and RNA extraction, flow cytometry, mitotic index measurement after DAPI staining (see below) or GFP fluorescence confocal imaging (detailed later in the microscopy section).

Dual-step synchronization (see Kumagai-Sano et al., 2007)

Dual-step synchronization is performed as the single step synchronization procedure until cells reach 5% of mitotic index. Propyzamide is then added to a final concentration of 3 µM. After 4 hours of propyzamide treatment, cells are washed thoroughly for 15 minutes as described previously to remove aphidicolin.

Flow cytometry measurement

Ploidy measurement by flow cytometry was performed using Cystain UV precise P kit (PARTEC). 1 ml of vacuum-filtered synchronized BY-2 culture is frozen on liquid nitrogen and chopped in 200 µl of nuclei extraction buffer with a razor blade for approximately 2 minutes. 800 µl of nuclei staining solution is added and samples are gently homogenized and filtered on a CellTrics 30 µM disposable filter (PARTEC). Prepared samples are analyzed on Attune flow cytometer (Applied Biosciences) using the following parameters:

Acquisition volume	500 µl
Flow	100 µl/min
Laser	405 nm 50 mW
Detection wavelength	410-450 nm
PMT gain VL1	1350 mv
PMT gain SSC	4500 mv
PMT gain FSC	2400 mv

Flow cytometry data are exported from Attune software in FCS format and analyzed using the following R packages: FlowCore, FlowViz, ggPlot2 and cowPlot.

Mitotic index measurements

DAPI solution: 0.2 mg/L 2,4-Dichlorophenoxyacetic acid (DAPI), 2% Triton X-100 (Sigma-Aldrich)

50 µl of DAPI solution are added to 500 µl of synchronized BY-2 cells, homogenized and put on ice for 5 minutes. Mitotic and interphasic cells are counted on a Nikon E800 microscope using x400 magnification (x40/0.75 Nikon Plan Fluor, x10 ocular) and Nikon UV-2A filter; excitation wavelength: 330-380 nm (band-pass); dichromatic mirror cut-on wavelength 400 nm (long-pass); barrier filter wavelength: 420 nm cut-on (long-pass). A minimum of 500 cells are counted. The mitotic index represents the percentage of cells in M phase (pro-meta-ana- and telophase) in the analyzed population.

4. Protocols related to RNA analysis

a. RNA extraction from BY-2 cell suspension

2 ml of BY-2 cell suspension are vacuum filtered and frozen in liquid nitrogen. Cell are first grinded with 1.7-2.1 mm glass beads using a Silamat grinding apparatus (Ivoclar Vivadent) and resuspended in 800 µl of Tri-reagent (Sigma-Aldrich). Microtubes are incubated 3 minutes under strong agitation. 200 µl of Chloroform (Sigma-Aldrich) are added and microtubes are again vortexed for 3 minutes. Phases are separated by centrifugation at maximum speed for 15 minutes. Aqueous phase is recovered and incubated for 1 hour at -20°C with 1 volume of cold Isopropanol. RNA is then precipitated by centrifugation at maximum speed for 20 minutes at 4°C. Pellet are washed twice with 1 ml of 70% ethanol and air dried until they became colorless. RNA pellets are finally resuspended in 50 µl of RNase-free water and dosed using Nanodrop spectrophotometer (ThermoFisher Scientific).

b. Northern blot for small RNA detection

Loading buffer: 99.9% deionized formamide, 0.01% bromophenol blue (Sigma-Aldrich), 0.05% Xylene Cyanol blue (Sigma-Aldrich)

10X TBE buffer (Tris Borate EDTA): 89 mM Tris, 89 mM boric acid, 2 mM EDTA, pH 7.5

20X SSC buffer (Saline sodium citrate): 3M NaCl, 300mM $C_6H_5Na_3O$; $2H_20$, pH 7.2

EDC crosslinking buffer: 0.16 M l-ethyl-3-(3-dimethylaminopropyl) carbodiimide (EDC) (Sigma-Aldrich), 0.13 M 1-methylimidazole, pH 8

Methylene blue staining buffer: 0.04% methylene blue (Sigma-Aldrich), 0.5 M $NaCH_3COO$ pH 5.2

Mild stringency washing buffer: 2X SSC, 2% SDS

High stringency washing buffer: 1X SSC 1% SDS

Sample preparation

20 µg of total RNA are first standardized to identical volumes to minimize migration variation. Loading buffer is then added to reach a final concentration of 60% formamide. Samples are denatured at 95°C for 5 minutes and immediately chilled on ice before loading on gel.

Electrophoresis and transfer of RNA

RNA samples are separated on a 15% acrylamide, 0.5X TBE, 8 M urea gel prior samples loading, acrylamide gels are preheated for 30 minutes at 15 W. Gel is then run at 3 W for 30 minutes followed by approximately 4 hours at 15 W in 0.5X TBE. After electrophoresis, RNA loading is checked by ethidium bromide coloration. Separated RNAs are transferred on Amersham Hybond-NX nylon membrane (GE Healthcare-Life Sciences) for 1h30 at 400 mA in 0.5X TBE.

Chemical crosslinking (see Pall et al., 2007)

Membranes are put on a Whatman paper imbibed with freshly prepared EDC-crosslinking buffer, sealed in a bag (the transferred face must be upside) and incubated 1 hour at 60°C. membranes can be rinsed with demineralized water and RNA quality can be verified with methylene blue staining buffer.

5' radio-labelling of oligonucleotides

DNA oligonucleotides complementary to miR168 and U6 RNA were 5' end-labelled with [γ-32P]ATP using T4 polynucleotide kinase (PNK) (Promega). Reaction conditions are listed below:

Total volume	20 µl
Buffer A	2 µl
DNA oligonucleotide (10µM)	1 µl
[γ-P32]ATP	25 µCi (2,5 µl)
T4 PNK	1,5 µl
H_20	13 µl

PNK reaction is incubated at 37°C for 1 hour.

Radio-labelled probes were then purified from non-incorporated γ-32P using Microspin G-25 column (GE Healthcare-Life Sciences).

Hybridization

Crosslinked membranes are incubated 2 hours in 15ml of PerfectHyb hybridization buffer (Sigma-Aldrich) at 42°C and then incubated overnight with the radio-labelled probes. Membranes are finally washed 2 times with mild stringency buffer and high stringency buffer for 15 minutes at 50°C before exposure.

c. Quantitative real-time PCR (qRT-PCR)

2 µg of total RNAs samples are frist treated with DNase I (ThermoFisher Scientific). cDNAs are reverse transcribed using High-capacity cDNA Reverse Transcription Kit (Applied Bioscience). cDNAs are further diluted 10 times prior to qRT-PCR. qRT-PCR is performed using LigthCycler 480 SYBR Green I Master mix (Roche) on a LigthCycler 480 apparatus (Roche) following constructor recommendations.

Primers used for qRT-PCR on BY-2 tobacco cell suspension cDNAs are listed below:

Gene	Forward primer (5'->3')	Reverse primer (5'->3')	Type
Ubiquitin-conjugating enzyme E2 (Ntubc2)	CTGGACAGCAGACTGACATC	CAGGATAATTTGCTGTAACAGATTA	Reference
Protein phosphatase 2A (PP2A)	GTGAAGCTGTAGGGCCTGAGC	CATAGGCAGGCACCAAATCC	Reference
L25 ribosomal protein	CCCCTCACCACAGAGTCTGC	AAGGGTGTTGTTGTCCTCAATCTT	Reference
Histone H4	GAAAGGGAGGCAAGGGATTA	CACGTAATACCTTACGGTGTCG	Target
CYCB1 (NtaCyc29)	TGGGCTCCTGAGGTCAAT	ATTCATCAACCCCAGCTC	Target g
Arabidopsis AGO1	CGGTGGACAGAAGTGGGAAT	GGTCGAGAAGTGCCCTGAAT	Target
AGO1	CATTTGGCAGCTTTCCGTGCTC	TGCGCTTGTGACTGATCCACTG	Target

5. Protocols related to protein analysis

a. Protein extraction from BY-2 cell suspension

Rapid protein extraction

4X Laemmli buffer: 200 mM Tris HCl pH 6.8, 8% SDS, 40% glycerol 0.04% bromophenol blue, 3% β-mercaptoethanol (freshly added)

Approximately 100 mg of frozen plant tissue (or vaccum-filtered BY-2 cells) are grinded with glass beads and immediately resuspended in 300 µl of hot 1X Laemmli buffer. Samples are then denatured at 95°C for 2 minutes. Debris are eliminated by centrifugation at maximum speed for 15 minutes.

Phenol extraction

Extraction buffer (EB): 0.7 M saccharose, 500 mM Tris HCl pH 8, 5 mM EDTA pH 8, 100 mM NaCl, 2% β-mercaptoethanol and complete mini protease inhibitor (Roche) must be added extemporaneously.

Resuspension buffer (RS): 10% glycerol, 3% SDS, 62.3 mM Tris HCl pH8

4X Loading buffer (WB): 40%, 16% SDS, 250 mM Tris HCl pH 8, 20% β-mercaptoethanol (must be added extemporaneously)

2 ml of BY-2 cell suspension are vaccum-filtered and frozen in liquid nitrogen. Cell are first grinded with glass beads, resuspended in 600 µl EB buffer and vortexed. 600 µl of biophenol pH8 are added and vortexed again. Samples are then centrifuged at maximum speed for 5 minutes and aqueous phase is precipitated overnight with 5 volumes of methanol/100 mM ammonium acetate at -20°C. Microtubes are centrifuged at maximum speed for 20 minutes in order to pellet proteins. Pellets are washed 2 times with chilled methanol and air dried for 30 seconds maximum. Pellet are resuspended in 75 µl of RB buffer by vortexing. When pellets are completely dissolved, 25 µl of WB buffer are added and samples are heated 2 minutes at 60°C (usually 95°C, but 60°C is best suited for GFP-AGO1 detection).

b. Protein quantification

Amidoblack solution: 10% acetic acid, 90% methanol, 0.05% naphtol blue (Sigma-Aldrich)

Washing solution: 10% acetic acid, 90% ethanol

190 µl of bidistilled water are added to 10µl of total protein extracts and vortexed. 1 ml of Amidoblack solution is then added and mixed by hand. Tubes are centrifuged at maximum speed for 15 minutes and the supernatant is discarded. Pellets are rinsed with washing solution and centrifuged again at maximum speed for 15 minutes. When the supernatant has been removed and the pellets are dry, they are resuspended in 1 ml of 0,2 N Sodium hydroxide solution (NaOH). 200 µl are used for measuring optical density at 630 nm. Protein concentration is calculated according to a BSA (bovine serum albumin) standard curve.

c. Immunodetection by Western blot

Tris-Glycine electrophoresis buffer: 25 mM Tris Base, 250 mM glycine, 0.1% SDS

Transfer buffer: 25 mM Tris base, 192 mM glycine, 15% ethanol

TBST-T (Tris-buffered saline-Tween) buffer: 20 mM Tris base, 150 mM NaCl, 0.1% Tween20 (Sigma-Aldrich) pH 7.4

Staining solution: 89.9% ethanol, 10% acetic acid, 0.05% Coomassie blue (Sigma-Aldrich)

Destaining solution: 30% ethanol, 10% acetic acid

Total protein extract and immunoprecipitated proteins were separated by SDS-PAGE. Acrylamide gels are prepared as described in Sambrook et al., 1989 (book) using Mini-Protean III (BioRad) casting system. Frozen protein samples are thawed at 40°C for 2 minutes and loaded on 7% Tris-glycine gels or gradient 4-16% Tris-glycine Criterion TGX precast gels (BIORAD). Protein are first migrated at 50 V until the migration front reaches the resolving gel and are then migrated at 100 V. For Criterion TGX gels, migration was done at 200 V for 20 minutes. Protein separated on gel are then transferred on previously activated

Immobilon-P PVDF membrane (GE Healthcare-Life Sciences) at 400 mA for 1h15. Transferred membranes are rinsed with TBS-T and incubated with 5% milk TBS-T for 20 minutes at room temperature. Membranes are incubated in 5% milk TBS-T with primary antibody for 2 hours at room temperature or overnight at 4°C. Membranes are rinsed 3 times with TBS-T, 5 minutes each and incubated for 1 hour in 5% milk TBS-T with secondary antibody at room temperature. Membrane is washed 3 times, as done previously and revealed using Clarity chemoluminescent substrate (BIORAD). Total proteins can be stained with Coomassie blue solution. To enhance contrast, membranes are washed with destaining solution

Antibodies and dilutions are listed below:

Primary antibodies					
Reference	Immunogen	Clonality	Host	Dilution	Company/reference
JL-8	GFP	Monoclonal	Mouse	1/2000	Takara Bio Clontech
A11122	GFP	Polyclonal	Rabbit	1/5000	ThermoFisher Scientific
ab290	GFP	Polyclonal	Rabbit	1/5000	Abcam
AS09 527	Arabidopsis AGO1	Polyclonal	Rabbit	1/10000	Agrisera
AS16 3141	Actin	Monoclonal	Mouse	1/20000	Agrisera
	Tobacco CYCB1	Polyclonal	Rabbit	1/1000	Criqui et al., 2000
	Tobacco AGO1	Polyclonal	Rabbit	1/10000	J. Burgyan's lab, Hungary
Secondary antibodies					
Reference	Reactivity	Host	Label	Dilution	Company
A16104	Rabbit	Goat	HRP (horseradish peroxydase)	1/10000	ThermoFisher Scientific
A16072	Mouse	Goat	HRP (horseradish peroxydase)	1/10000	ThermoFisher Scientific

d. <u>RNA immunoprecipitation of AGO1-associated small RNAs</u>

Extraction buffer (EB): 50 mM Tris HCl 7.5, 300 mM NaCl, 10% glycerol, 5 mM MgCl2, 0.5% Triton X-100 (Sigma-Aldrich), 5 mM DTT, complete mini protease inhibitors (Roche)

Washing buffer (WB): same as EB but without DTT and protease inhibitors

4X Loading buffer: 40%, 16% SDS, 250 mM Tris HCl pH 8, 20% β-mercaptoethanol (must be added extemporaneously)

The whole procedure must be done at 4°C, except for RNA and protein elution.

Sample preparation

At least 1.25 g of frozen BY-2 cells are grinded in a nitrogen chilled mortar. 3 volumes of cold EB buffer are added to the frozen powder and mixed gently until it is thawed completely. Crude extracts are incubated for 30 minutes on a rotary shaker (5 rpm) and debris are eliminated by centrifugation at maximum speed for 15 minutes in a pre-chilled rotor.

Magnetic beads preparation

50 µl GFP-trap (Chromotek) magnetic beads are used for each sample. Microtubes are place on a magnetic stand and supernatant is discarded when beads are completely sedimented. Beads are then rinsed with 1 ml of cold WB and incubated at 4°C on a rotary shaker for 5 minutes. This step is repeated 3 times. Finally, the beads are resuspended in 50 µl of WB buffer.

Incubation and Washings

3 ml of cleared crude extracts are incubated in a 15 ml tube with 50 µl of washed magnetic beads. Tubes are placed on a rotary shaker for 1 hour. 15 ml tubes are then centrifuged 2 minutes at 3000 rpm. Beads are resuspended in 1 ml of EB and transferred in microtubes. Samples are then washed 4 times as described for magnetic beads preparation. In parallel, 150 µl of input fraction and unbound fraction are kept as control and denatured 2 minutes at 95°C with 50 µl of 4X loading buffer.

RNA and protein elution

Supernatant is discarded on a magnetic rack and beads are resuspended in 50 µl of WB. 800 µl of TriReagent (Sigma-Aldrich) are added to 45 µl of beads. Microtubes are incubated 1 minutes under strong agitation. 200 µl of Chloroform (Sigma-Aldrich) are added and microtubes are again vortexed for 3 minutes. Phases are separated by centrifugation at maximum speed for 15 minutes. Aqueous phase is recovered and incubated for 12 hours at -20°C with 1 volume of cold isopropanol. RNAs are then precipitated by centrifugation at maximum speed for 20 minutes at 4°C. Pellet are washed 2 times with 1 ml of 70% ethanol and air dried until they became colorless. RNA pellets are finally resuspended in 50 µl of ultrapure water (Sigma-Aldrich). For protein extraction, 15 µl of WB buffer are added to the remaining 5 µl of beads and 4X loading buffer was added to a final concentration of 1X. Samples are then denatured for 2 minutes at 95°C.

e. Size exclusion chromatography

Extraction Buffer (EB): 50 mM Tris HCl 7.5, 300 mM NaCl, 10% glycerol, 5 mM MgCl2, 0.5% Triton X-100 (Sigma-Aldrich), 5 mM DTT, complete mini protease inhibitors (Roche)

Chromatography buffer (CB): same as EB but without Glycerol, DTT and protease inhibitors

Sample preparation

5 g of frozen BY-2 cell are grinded in a nitrogen chilled mortar. 3 volumes of cold EB buffer are added to the frozen powder and mixed gently until it is thawed completely. Crude extracts are incubated for 30 minutes on a rotary shaker (5 rpm) and debris are eliminated by centrifugation at maximum speed for 15 minutes in a pre-chilled rotor. Lysate is then filtered on a 0.22 μM filter.

Gel filtration

The entire procedure is done at 4°C.

Gel filtration was performed on AKTA PURE (GE Healthcare-Life Sciences) FPLC (Fast protein liquid chromatography apparatus) equipped with Superdex 200 16/60 HiLoad gel filtration column (GE Healthcare-Life Sciences). The column is preliminary equilibrated with 240 ml (2X column volume) of CB buffer. Cleared crude BY-2 extract is entirely injected and separated with 200 ml of CB (more than 1.5X column volume) at 0.2 ml/min. 2 ml fractions were collected and processed for RNA and protein extraction as described previously.

6. Confocal Microscopy

Confocal microscopy was performed on a LEICA TCS SP8 laser scanning microscope (Leica Microsystem) using the following objectives:

Designation	Magnification	Numeric aperture	Immersion
HCX APO CS 20X	X20	0,7	AIR
HC PL APO CS2 40X	X40	1,1	WATER
HC PL APO CS2 63X	X63	1,4	OIL

Microscopy settings for Arabidopsis thaliana and BY-2 samples are listed below:

Plant material	BY-2		*Arabidopsis thaliana*	
Protein	GFP-AGO1	H2B-tdTomato	GFP-tagged proteins	Propidium Iodide
Laser	Argon	DSSP	Argon	DSSP
Excitation	480 nm-approx. 20%	561 nm-approx. 1%	480 nm-approx. 2%	561 nm-approx. 1%
Emission	500-550 nm	575-650 nm	500-550 nm	600-630 nm
Pinhole	1,5-2	1,5-2	1	1
PMT-HYD gain	340%	100%	100%	50-100%

Microscopy images are processed using the FigureJ software.

7. Libraries preparation and high-throughput sequencing

Libraries were prepared from total and AGO1 immunoprecipitated RNAs for each key step of the cell cycle. Cells in S, G2, M and G1 phases were harvested from synchronized BY-2 samples at 1,3,7 and 10 hours after aphidicolin removal, respectively. RNA libraries and small RNA libraries were prepared by Fasteris company (Swiss). RNA quality was assessed using Bioanalyzer (Agilent) capillary electrophoresis and Qubit (ThermoFisher Scientific) fluorometer. For mRNA libraries, 1µg of total RNA was used following TruSeq stranded mRNA kit (Illumina) instructions. Libraries were sequenced (2X75bp) on a HiSeq 4000 (Illumina) apparatus. For small RNA libraries, 1µg of total RNA of the whole immunopurified RNA samples was used following protocol of the TruSeq Small RNA library preparation kit (Illumina). Libraires were sequenced (1x50bp) on a HiSeq 2500 (Illumina) apparatus. PARE libraries were prepared in collaboration with the laboratory of professor Blake C. Meyers (Danforth plant science center, St Louis, USA) following the protocol described in (Zhai et al., 2014). PARE libraries were sequenced (1x50bp) on a HiSeq2500 (Illumina) apparatus by Delaware Biotechnology Institute (DE, USA). All the small RNA,

RNA and PARE sequences will be deposited in the National Centre for Biotechnology Information (NCBI) Gene Expression Omnibus (GEO).

8. Bioinformatic analysis

Sequencing data quality was assed using FastQC. Reads were processed by removing the adaptor sequences using Trimmomatic (Bolger et al., 2014) and mapped to the *Nicotiana tabacum* genome version 4 (Edwards et al., 2017), (https://solgenomics.net/organism/Nicotiana_tabacum/genome), using Bowtie (Langmead and Salzberg, 2012).

For sRNAs, a modified version of miREAP was used as described in (Arikit et al., 2014) for miRNA prediction. Only miRNA precursors with reads present in both arms and mature miRNAs 21nt or 22nt-long were selected. New miRNA candidates were then used for homology search using miRBase v22 (Kozomara and Griffiths-Jones, 2014), with a maximum of 4 nucleotides difference. To analyse heterochromatic siRNAs, we first ran RepeatMasker (http://www.repeatmasker.org) using the Viridiplantae RepBase database (http://www.girinst.org/repbase) as library. For RNa-seq, analyses were performed using the HISAT2 and StringTie as described in (Pertea et al., 2016). Clustering analysis was done using MFuzz v3.6 and gene ontology analysis was performed by using the Arabidopsis orthologs and PANTHER v11 (Mi et al., 2017). PARE libraries were analyzed using sPARTA (Kakrana et al., 2014). Three biological replicates of each cell cycle phase were used as starting material. Only miRNA-target pairs present in all biological replicates, with a score of 3 or lower, were considered for further analysis. All statistical analysis were performed using DESeq2 (Love et al., 2014).

Supplemental figures

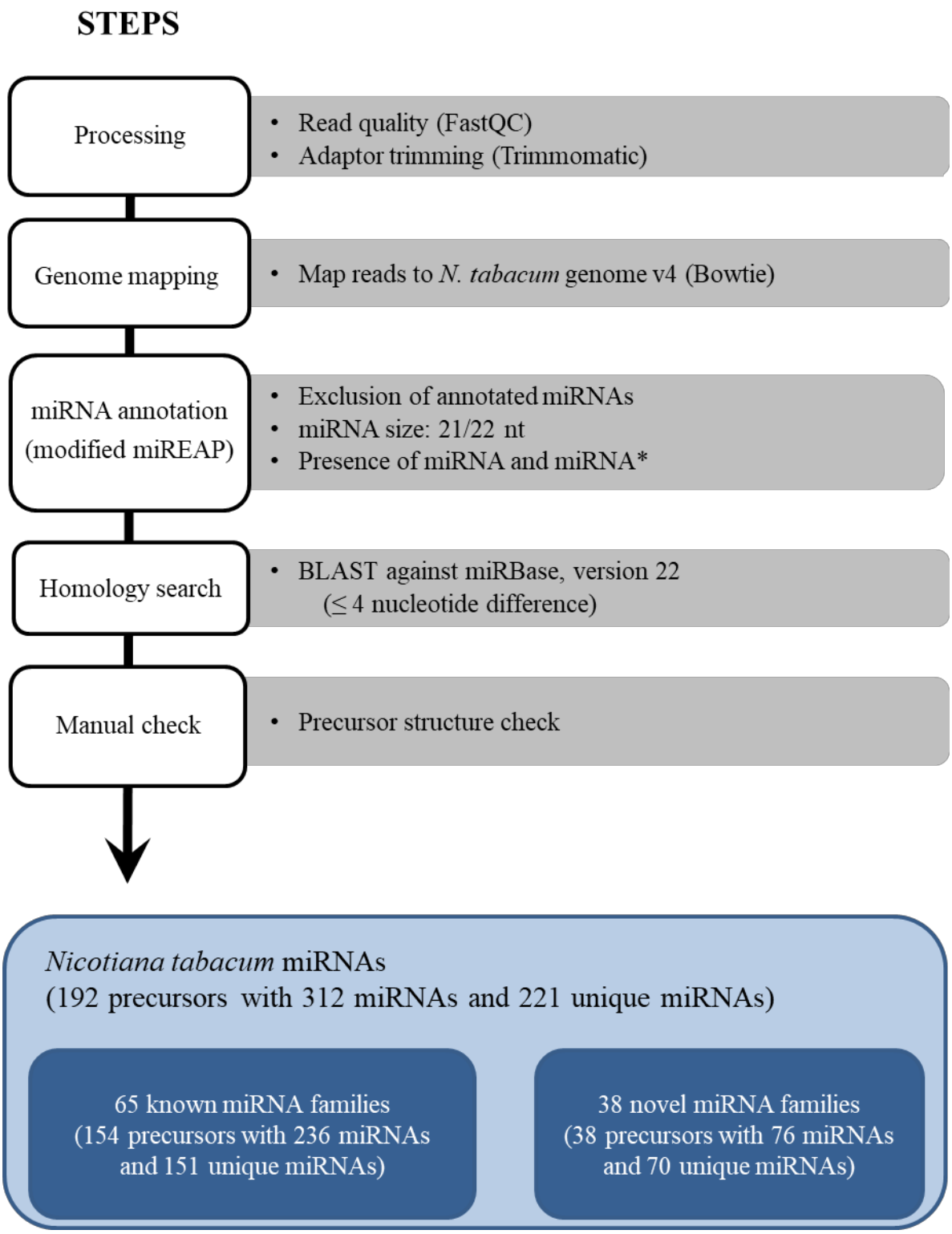

Supplemental Figure 1 : Workflow for small RNA identification from BY-2 libraries

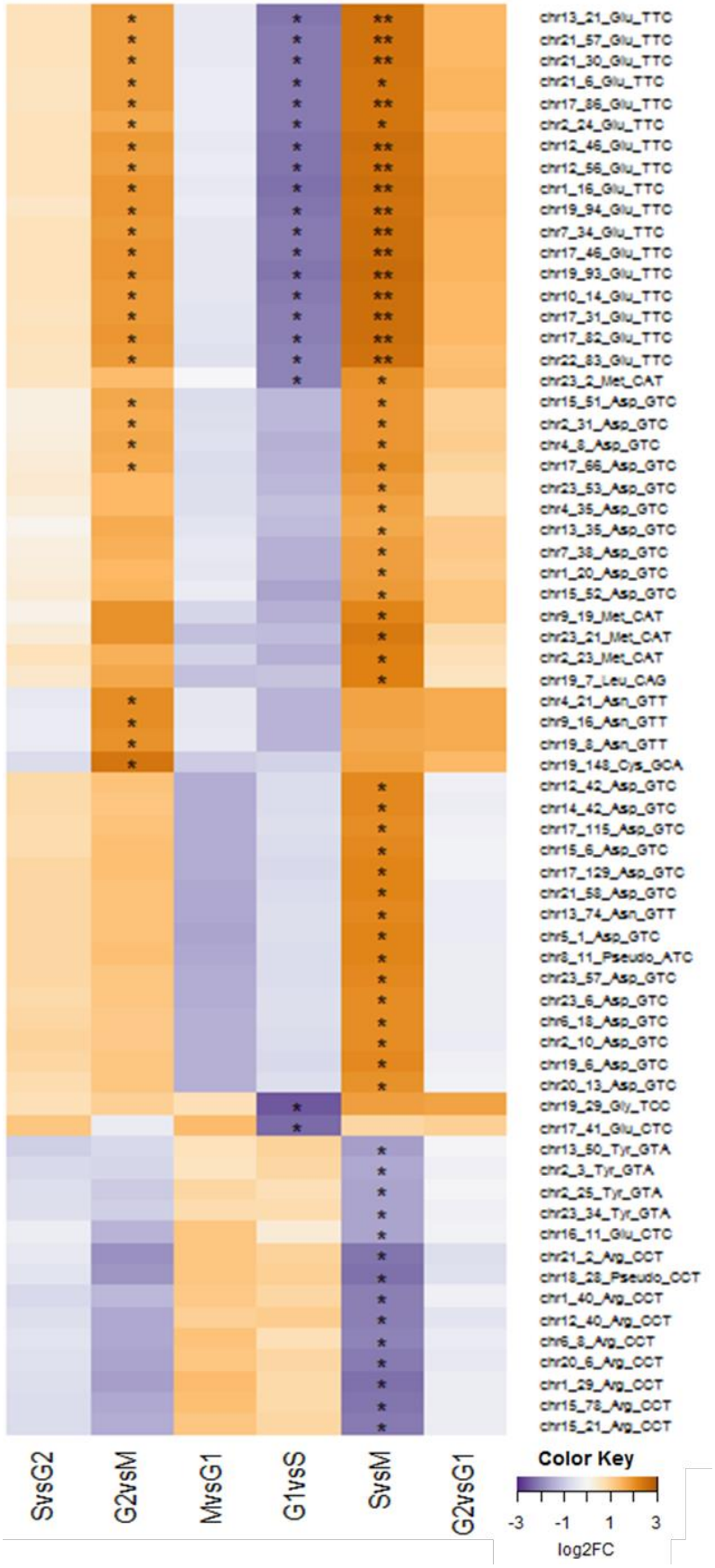

Supplemental Figure 2 : Heatmap of differentially expressed tRFs in AGO1 IP libraries

(*q-value≤0.05 ; **q-value≤0.01)

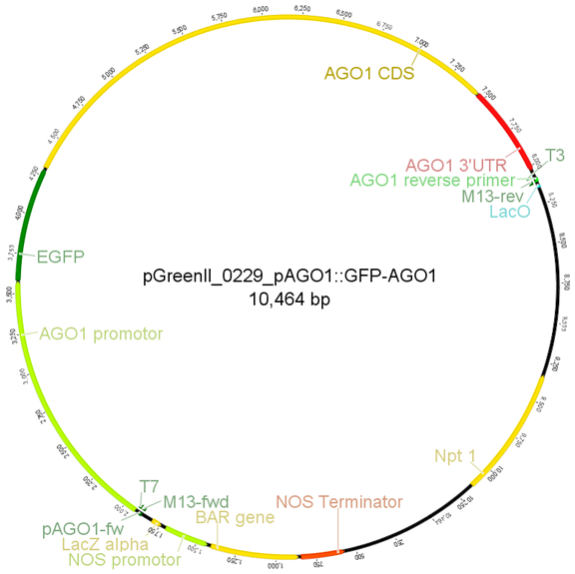

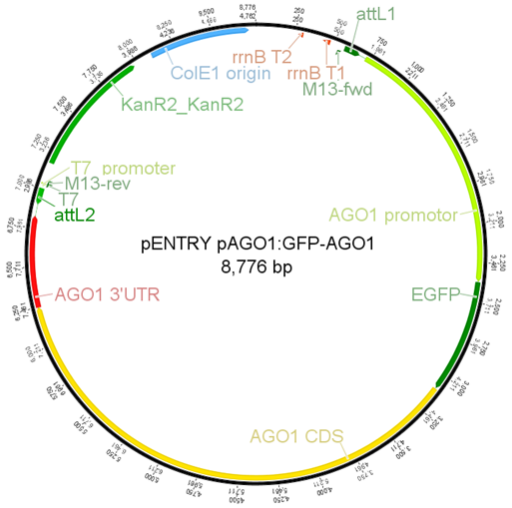

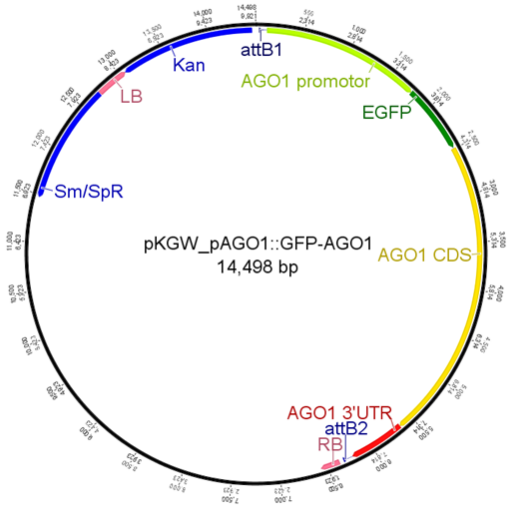

Supplemental Figure 3: Maps of vector carrying pAGO1:GFP-AGO1 construct.

pAGO1:GFP-AGO1 construct was amplified from the pGREEN II binary vector that carries the Basta resistance in plant. The construct was cloned in a pDONR221 vector and transferred to a pKGW (conferring kanamycin resistance in plant) binary vector using Gateway cloning. pKGW-pAGO1:GFP-AGO1 was then used to express GFP-AGO1 in tobacco BY-2 cell suspension).

Supplemental tables

			Total sequences	Clean Sequences		Genome matched reads		t/r/s n/s noRNA matched reads
Total RNA	Phase S	Rep 1	25,261,213	24,906,429	(98.60%)	18,815,918	(75.55%)	366,272
		Rep 2	27,654,112	27,252,068	(98.55%)	20,535,473	(75.35%)	329,497
		Rep 3	19,442,435	19,162,684	(98.56%)	14,427,804	(75.29%)	67,454
	Phase G2	Rep 1	29,602,898	29,255,343	(98.83%)	21,912,814	(74.9%)	376,803
		Rep 2	24,271,572	23,950,128	(98.67%)	17,930,340	(74.87%)	309,676
		Rep 3	27,209,924	26,792,516	(98.47%)	20,130,859	(75.14%)	94,691
	Phase M	Rep 1	22,704,393	22,342,160	(98.40%)	16,918,011	(75.72%)	268,637
		Rep 2	31,794,316	31,326,162	(98.53%)	23,742,753	(75.79%)	793,301
		Rep 3	27,426,192	27,039,417	(98.59%)	20,417,465	(75.51%)	81,001
	Phase G1	Rep 1	22,501,475	22,172,030	(98.54%)	16,744,177	(75.52%)	257,910
		Rep 2	20,504,973	20,149,664	(98.27%)	15,179,295	(75.33%)	262,574
		Rep 3	26,158,026	25,855,361	(98.84%)	19,419,831	(75.11%)	59,422

Supplemental Table 1 : Counts of total reads and mapped reads per RNA seq libraries.

			Total sequences	Genome matched reads	Distinct genome matched reads	t/r/sn/snoRNA matched reads
Total RNA	Phase S	Rep 1	15,831,347	11,020,964	3,179,460	111,297
		Rep 2	22,487,637	15,611,036	4,002,493	149,338
		Rep 3	23,754,822	16,960,336	3,615,497	393,825
		Rep 4	46,598,703	32,821,878	7,337,438	396,444
		Rep 5	60,247,557	48,409,873	4,943,774	1,024,247
	Phase G2	Rep 1	23,635,985	16,448,861	4,355,828	107,248
		Rep 2	23,841,850	16,830,891	3,988,754	246,736
		Rep 3	22,135,501	15,855,904	3,541,476	234,422
		Rep 4	49,159,711	34,468,489	8,058,486	197,544
		Rep 5	50,529,983	38,155,157	6,097,906	581,084
	Phase M	Rep 1	22,759,408	16,261,095	3,491,576	294,152
		Rep 2	22,961,401	16,283,177	3,748,283	166,219
		Rep 3	22,843,303	16,532,414	3,276,305	227,687
		Rep 4	49,414,871	34,167,344	7,187,488	263,675
		Rep 5	57,879,829	42,958,699	6,649,403	770,535
	Phase G1	Rep 1	23,852,357	17,400,653	3,323,541	270,707
		Rep 2	24,386,060	18,057,521	3,182,326	180,781
		Rep 3	23,340,967	16,747,779	3,452,736	279,724
		Rep 4	66,198,411	45,467,882	9,124,051	762,415
		Rep 5	53,588,918	39,707,210	6,840,669	355,569
AGO1 IP RNA	Phase S	Rep 1	23,818,840	16,732,251	1,639,495	12,243
		Rep 2	23,552,491	16,175,384	1,689,596	56,515
		Rep 3	21,423,891	14,787,108	1,358,965	27,266
		Rep 4	52,391,500	35,055,836	2,562,998	220,973
		Rep 5	47,903,203	33,637,160	2,721,452	72,849
	Phase G2	Rep 1	2,135,694	663,083	63,860	3,124
		Rep 2	5,238,321	2,215,001	104,755	10,209
		Rep 3	19,874,906	13,846,102	1,377,605	60,677
		Rep 4	34,119,124	23,111,895	2,036,417	43,626
		Rep 5	51,058,629	35,899,360	3,098,323	68,033
	Phase M	Rep 1	10,025,190	6,782,163	492,560	11,649
		Rep 2	2,485,835	1,337,031	138,006	6,796
		Rep 3	20,149,003	14,214,640	1,428,323	5,231
		Rep 4	53,645,132	37,864,774	2,854,585	32,254
		Rep 5	45,186,142	31,787,379	2,552,767	75,938
	Phase G1	Rep 1	22,307,761	15,636,022	1,604,474	15,684
		Rep 2	11,124,265	7,420,233	498,879	8,940
		Rep 3	19,305,417	13,412,036	1,235,929	15,900
		Rep 4	60,916,794	43,334,391	2,870,476	35,545
		Rep 5	54,742,923	39,035,635	3,256,536	37,547

Supplemental Table 2 : Counts of total reads and mapped reads per small-RNA seq libraries.

			Total sequences	Genome matched reads		Distinct genome matched reads	t/r/sn/snoRNA matched reads
Total RNA	Phase S	Rep 1	14,647,205	9,738,524	(66.49%)	4,269,658	21573
		Rep 2	14,718,547	9,667,797	(65.68%)	4,510,998	31490
		Rep 3	13,837,696	9,308,550	(67.27%)	3,704,141	86109
	Phase G2	Rep 1	26,025,903	16,815,427	(64.61%)	6,409,021	23117
		Rep 2	16,053,096	10,714,399	(66.74%)	4,800,217	43213
		Rep 3	14,764,149	9,888,052	(66.97%)	4,019,360	65528
	Phase M	Rep 1	14,548,786	9,872,981	(67.86%)	4,347,503	29512
		Rep 2	14,711,219	9,857,899	(67.01%)	4,637,904	49753
		Rep 3	19,993,156	13,635,670	(68.2%)	5,652,963	53843
	Phase G1	Rep 1	27,916,891	18,493,549	(66.24%)	6,761,313	46671
		Rep 2	19,015,537	12,736,768	66.98%)	5,603,500	51656
		Rep 3	16,967,175	11,555,300	68.1%)	5,184,845	43230

Supplemental Table 3 : Counts of total reads and mapped reads per PARE seq libraries.

			Selection					
Vector name	**Accession**	**Vector backbone**	**In bacteria**	**In plant**	**Designation**	**Used for**	**Primers**	**Provenance/reference**
pENTRY pAGO1:GFP-AGO1	AT1G48410	pDONR221	Kanamycin		Entry clone/ AGO1 promoter;AGO1 cDNA; 3'UTR, N-ter fusion to eGFP	cloning	3,4	designed in the lab
pCYCB1.2:CYCB1.2	AT5G06150	pDONR221	Kanamycin		Entry clone/cell cycle marker C-ter fusion	cloning		designed in the lab
pHTR2:CDT1a(C3)	AT2G31270	pDONR221	Kanamycin		Entry clone/cell cycle marker C-ter fusion	cloning		designed in the lab
pENtry U2B"	AT2G30260	pDONR221	Kanamycin		Entry clone/U2B" CDS for C-ter fusion	cloning	25,26	designed in the lab
pENTRY DCP1	AT1G08370	pDONR207	Gentamycin		Entry clone/DCP1 CDS for N-ter fusion	cloning		D.Gagliardi lab, IBMP
pENTRY PAB2	AT4G34110	pDONR207	Gentamycin		Entry clone/ PAB2 CDS for C-ter fusion	cloning		D.Gagliardi lab, IBMP
pENTRY HYL1	AT1G09700	pDONR221	Kanamycin		Entry clone/HYL1 genomic sequence for C-ter fusion	cloning	27,28	designed in the lab
pGREENII pAGO1:GFP-AGO1	AT1G48410	pGREENII	Kanamycin	Basta	Binary vector/ GFP-AGO1 expression	cloning		Derrien et al., 2012
pKGW pAGO1:GFP-AGO1	AT1G48410	pKGW	Spectinomycin	Kanamycin	Binary vector/ GFP-AGO1 expression	BY-2 transformation		designed in the lab
pRPS5a:H2B-tdTomato	At1G07790	pMDC99	Kanamycin	Hygromycin	Binary vector/histone H2B chromatin marker; C-ter fusion to tdTomato	BY-2 transformation		Adachi et al., 2011
pGWB pCYCB1.2:CYCB.2-eGFP	AT5G06150	pGWB650	Spectinomycin	Basta	Binary vector/ M-phase cell cycle marker; C-ter fusion to eGFP	Arabidopsis transformation		designed in the lab
pGWB pHTR2:CDT1a(C3)-eGFP	AT2G31270	pGWB650	Spectinomycin	Basta	Binary vector/S-phase cell cycle marker; C-ter fusion to eGFP	Arabidopsis transformation		designed in the lab
pH7 U2B"-RFP	AT2G30260	pH7RWG2	Spectinomycin	Hygromycin	Binary vector/Cajal bodies marker; C-ter fusion to RFP	BY-2 transformation		designed in the lab
pH7 RFP-DCP1	AT1G08370	pH7WGR2	Spectinomycin	Hygromycin	Binary vector/Dicing bodies marker; N-ter fusion to RFP	BY-2 transformation		designed in the lab
pH7 PAB2-RFP	AT4G34110	pH7RWG2	Spectinomycin	Hygromycin	Binary vector/Stress granules marker; C-ter fusion to RFP	BY-2 transformation		designed in the lab
pH7 HYL1-RFP	AT4G34110	pH7RWG2	Spectinomycin	Hygromycin	Binary vector/Dicing bodies marker; C-ter fusion to RFP	BY-2 transformation		designed in the lab
Empty vectors								
pDONR221			Kanamycin		Empty donor vector	cloning		Invitrogen
pH7WGR2			Spectinomycin	Hygromycin	Empty binary vector/35S promoter, N-ter fusion to RFP	cloning		VIB, Belgium
pH7RWG2			Spectinomycin	Hygromycin	Empty binary vector/35S promoter, C-ter fusion to RFP	cloning		VIB, Belgium
pGWB650			Spectinomycin	Basta	Empty binary vector/No promoter, C-ter fusion to eGFP	cloning		RIKEN, Japan
pKGW			Spectinomycin	Kanamycin	Empty binary vector/No promoter	cloning		VIB, Belgium

Supplemental Table 4 : List of vectors used for cloning and gene expression in Arabidopsis and BY-2 cells.

Primer number	Designation	Sequence (5'->3')	Used for
1	M13-fw	TGTAAAACGACGGCCAGT	sequencing/cloning
2	M13-rv	CATGGTCATAGCTGTTTCCTG	sequencing/cloning
3	AttB1-AGO1-fw	GGGGACAAGTTTGTACAAAAAAGCAGGCTTAACGACGGCCAGTGAATTGTAATACGA	Gateway cloning pAGO1:GFP-AGO1
4	AttB2-AGO1-rv	GGGGACCACTTTGTACAAGAAAGCTGGGTAGCTATGACCATGATTACGCCAAGCT	Gateway cloning pAGO1:GFP-AGO2
5	AGO1-seq-fw1	ACCAAGGAAGAGGAAGAGGA	AGO1 sequencing
6	AGO1-seq-fw2	TTACCTGACCAACTGTGTTC	AGO1 sequencing
7	AGO1-seq-fw3	CTTGTAAGTCTCAGCTGGTT	AGO1 sequencing
8	AGO1-seq-fw4	AAGTGACTCATCGAGGAAAC	AGO1 sequencing
9	AGO1-seq-fw5	ATGCTCAAGAGTTTGGCATC	AGO1 sequencing
10	AGO1-seq-fw6	ATGCTCTATCTAGGCGGAT	AGO1 sequencing
11	AGO1-seq-fw7	CCGTAGATCAACTGGGCAT	AGO1 sequencing
12	AGO1-seq-fw8	TGTAGGCACTGTTGTGGACTCT	AGO1 sequencing
13	AGO1-seq-fw9	AGGGCTCGATTCTACATGGA	AGO1 sequencing
14	AGO1-seq-rv1	TCCTCTTCCTCTTCCTTGGT	AGO1 sequencing
15	AGO1-seq-rv2	GAACACAGTTGGTCAGGTAA	AGO1 sequencing
16	AGO1-seq-rv3	AACCAGCTGAGACTTACAAG	AGO1 sequencing
17	AGO1-seq-rv4	GTTTCCTCGATGAGTCACTT	AGO1 sequencing
18	AGO1-seq-rv5	GATGCCAAACTCTTGAGCAT	AGO1 sequencing
19	AGO1-seq-rv6	ATCCGCCTAGATAGAGCAT	AGO1 sequencing
20	AGO1-seq-rv7	ATGCCCAGTTGATCTACGG	AGO1 sequencing
21	AGO1-seq-rv8	AGAGTCCACAACAGTGCCTACA	AGO1 sequencing
22	AGO1-seq-rv9	TCCATGTAGAATCGAGCCCT	AGO1 sequencing
23	AttB1-CYCB1.2-fw	GGGGACAAGTTTGTACAAAAAAGCAGGCTTAAGACTTACTCTGATCTTCAACGCCAA	Gateway cloning pCYCB1:CYCB1.2 (dBox)
24	AttB2-CYCB1.2-rv	GGGGACCACTTTGTACAAGAAAGCTGGGTACTTAGGTGACATCGCTACTTCCTT	Gateway cloning pCYCB1:CYCB1.2 (dBox)
25	AttB1-U2B"-fw	GGGACAAGTTTGTACAAAAAAGCAGGCTATGTTAACGGCAGATATACCACC	Gateway cloning U2B" CDS
26	AttB2-U2B"-rv	GGGGACCACTTTGTACAAGAAAGCTGGGTTTTCTTGGCGAAAGAGATGAC	Gateway cloning U2B" CDS
27	AttB1-HYL1-fw	GGGACAAGTTTGTACAAAAAAGCAGGCTTAATGACCTCCACTGATGTTTCCTC	Gateway cloning HYL1 genomic sequence
28	AttB2-HYL1-rv	GGGGACCACTTTGTACAAGAAAGCTGGGTATGCGTGGCTTGCTTCTGTCT	Gateway cloning HYL1 genomic sequence

Supplemental Table 5 : Primers used for cloning and sequencing.

References

Achour, C. and Aguilo, F. (2018). Long non-coding RNA and Polycomb: an intricate partnership in cancer biology. Front. Biosci. **23**: 2106–2132.

Adachi, S., Minamisawa, K., Okushima, Y., Inagaki, S., Yoshiyama, K., and Kondou, Y. (2011). Programmed induction of endoreduplication by DNA double-strand breaks in Arabidopsis. Proc. Natl. Acad. Sci. **108**: 10004–10009.

Adenot, X., Elmayan, T., Lauressergues, D., Boutet, S., Bouché, N., Gasciolli, V., and Vaucheret, H. (2006). DRB4-Dependent TAS3 trans-Acting siRNAs Control Leaf Morphology through AGO7. Curr. Biol. **16**: 927–932.

Allen, E., Xie, Z., Gustafson, A.M., and Carrington, J.C. (2005). microRNA-Directed Phasing during Trans -Acting siRNA Biogenesis in Plants. Cell **121**: 207–221.

Alvarado, V.Y. and Scholthof, H.B. (2012). AGO2: A New Argonaute Compromising Plant Virus Accumulation. Front. Plant Sci. **2**: 1–6.

Anders, L., Ke, N., Hydbring, P., Choi, Y.J., Widlund, H.R., Chick, J.M., Zhai, H., Vidal, M., Gygi, S.P., Braun, P., and Sicinski, P. (2011). A Systematic Screen for CDK4/6 Substrates Links FOXM1 Phosphorylation to Senescence Suppression in Cancer Cells. Cancer Cell **20**: 620–634.

Andersen, S.U., Buechel, S., Zhao, Z., Ljung, K., Novak, O., Busch, W., Schuster, C., and Lohmann, J.U. (2008). Requirement of B2-Type Cyclin-Dependent Kinases for Meristem Integrity in Arabidopsis thaliana. Plant Cell Online **20**: 88–100.

Aphasizhev, R., Suematsu, T., Zhang, L., and Aphasizheva, I. (2016). Constructive edge of uridylation-induced RNA degradation. RNA Biol. **13**: 1078–1083.

Araki, S., Ito, M., Soyano, T., Nishihama, R., and Machida, Y. (2004). Mitotic cyclins stimulate the activity of c-Myb-like factors for transactivation of G2/M phase-specific genes in tobacco. J. Biol. Chem. **279**: 32979–32988.

Ariel, F., Romero-Barrios, N., Jégu, T., Benhamed, M., and Crespi, M. (2015). Battles and hijacks: Noncoding transcription in plants. Trends Plant Sci. **20**: 362–371.

Arikit, S., Xia, R., Kakrana, A., Huang, K., Zhai, J., Yan, Z., Valdés-López, O., Prince, S., Musket, T.A., Nguyen, H.T., Stacey, G., and Meyers, B.C. (2014). An Atlas of Soybean Small RNAs Identifies Phased siRNAs from Hundreds of Coding Genes. Plant Cell Online **26**: 4584–4601.

Armenta-Medina, A., Lepe-Soltero, D., Xiang, D., Datla, R., Abreu-Goodger, C., and Gillmor, C.S. (2017). Arabidopsis thaliana miRNAs promote embryo pattern formation beginning in the zygote. Dev. Biol. **431**: 145–151.

Axtell, M.J. and Bartel, D.P. (2005). Antiquity of MicroRNAs and Their Targets in Land Plants. Plant Cell **17**: 1658–1673.

Axtell, M.J., Jan, C., Rajagopalan, R., and Bartel, D.P. (2006). A Two-Hit Trigger for siRNA Biogenesis in Plants. Cell **127**: 565–577.

Axtell, M.J. and Meyers, B.C. (2018). Revisiting Criteria for Plant MicroRNA Annotation in the Era of Big Data. Plant Cell **30**: 272–284.

Bao, J., Li, D., Wang, L., Wu, J., Hu, Y., Wang, Z., Chen, Y., Cao, X., Jiang, C., Yan, W., and Xu, C. (2012). MicroRNA-449 and MicroRNA-34b/c function redundantly in murine testes by targeting E2F transcription factor-retinoblastoma protein (E2F-pRb) pathway. J. Biol. Chem. **287**: 21686–21698.

Bao, Z., Yang, H., and Hua, J. (2013). Perturbation of cell cycle regulation triggers plant immune response via activation of disease resistance genes. Proc. Natl. Acad. Sci. **110**: 2407–2412.

Bartel, D.P. (2009). MicroRNAs: Target Recognition and Regulatory Functions. Cell **136**: 215–233.

Baumberger, N. and Baulcombe, D.C. (2005). Arabidopsis ARGONAUTE1 is an RNA Slicer that selectively recruits microRNAs and short interfering RNAs. Proc. Natl. Acad. Sci. **102**: 11928–11933.

Baumberger, N., Tsai, C.H., Lie, M., Havecker, E., and Baulcombe, D.C. (2007). The Polerovirus Silencing Suppressor P0 Targets ARGONAUTE Proteins for Degradation. Curr. Biol. **17**: 1609–1614.

Berckmans, B. and De Veylder, L. (2009). Transcriptional control of the cell cycle. Curr. Opin. Plant Biol. **12**: 599–605.

Berry, L.D. and Gould, K.L. (1996). Novel alleles of cdc13 and cdc2 isolated as suppressors of mitotic catastrophe in Schizosaccharomyces pombe. Mol. Gen. Genet. **251**: 635–646.

Berthet, C., Aleem, E., Coppola, V., Tessarollo, L., and Kaldis, P. (2003). Cdk2 Knockout Mice Are Viable. Curr. Biol. **13**: 1775–1785.

Berthet, C., Klarmann, K.D., Hilton, M.B., Suh, H.C., Keller, J.R., Kiyokawa, H., and Kaldis, P. (2006). Combined Loss of Cdk2 and Cdk4 Results in Embryonic Lethality and Rb Hypophosphorylation. Dev. Cell **10**: 563–573.

Besson, A., Dowdy, S.F., and Roberts, J.M. (2008). CDK Inhibitors: Cell Cycle Regulators and Beyond. Dev. Cell **14**: 159–169.

Bohmert, K., Camus, I., Bellini, C., Bouchez, D., Caboche, M., and Banning, C. (1998). AGO1 defines a novel locus of Arabidopsis controlling leaf development. EMBO J. **17**: 170–180.

Boland, A., Huntzinger, E., Schmidt, S., Izaurralde, E., and Weichenrieder, O. (2011). Crystal structure of the MID-PIWI lobe of a eukaryotic Argonaute protein. Proc. Natl. Acad. Sci. **108**: 10466–10471.

Bolger, A.M., Lohse, M., and Usadel, B. (2014). Trimmomatic: A flexible trimmer for Illumina sequence data. Bioinformatics **30**: 2114–2120.

Bologna, N.G., Iselin, R., Abriata, L.A., Sarazin, A., Pumplin, N., Jay, F., Grentzinger, T., Dal Peraro, M., and Voinnet, O. (2018). Nucleo-cytosolic Shuttling of ARGONAUTE1 Prompts a Revised Model of the Plant MicroRNA Pathway. Mol. Cell **69**: 709–719.

Bologna, N.G. and Voinnet, O. (2014). The Diversity, Biogenesis, and Activities of Endogenous Silencing Small RNAs in *Arabidopsis*. Annu. Rev. Plant Biol. **65**: 473–503.

De Bondt, H.L., Rosenblatt, J., Jancarik, J., Jones, H.D., Morgan, D.O., and Kim, S.H. (1993). Crystal structure of cyclin-dependent kinase 2. Nature **363**: 595–602.

Booher, R.N., Holman, P.S., and Fattaey, A. (1997). Human Myt1 is a cell cycle-regulated kinase that inhibits Cdc2 but not Cdk2 activity. J. Biol. Chem. **272**: 22300–22306.

Borges, F. and Martienssen, R.A. (2015). The expanding world of small RNAs in plants. Nat. Rev. Mol. Cell Biol. **16**: 727–741.

Bortolamiol, D., Pazhouhandeh, M., Marrocco, K., Genschik, P., and Ziegler-Graff, V. (2007). The Polerovirus F Box Protein P0 Targets ARGONAUTE1 to Suppress RNA Silencing. Curr. Biol. **17**: 1615–1621.

Boudolf, V., Barrôco, R., Engler, J.D.A., Verkest, A., Naudts, M., Inzé, D., Veylder, L. De, The, S., Cell, P., and Apr, N. (2016). B1-Type Cyclin-Dependent Kinases Are Essential for the Formation of Stomatal Complexes in Arabidopsis thaliana. Plant Cell **16**: 945–955.

Boudolf, V., Inzé, D., and De Veylder, L. (2006). What if higher plants lack a CDC25 phosphatase? Trends Plant Sci. **11**: 474–479.

Brodersen, P. and Sakvarelidze-achard, L. (2012). Isoprenoid biosynthesis is required for miRNA function and affects membrane association of ARGONAUTE 1 in Arabidopsis. Proc. Natl. Acad. Sci. **109**: 1778–1783.

Brodersen, P., Sakvarelidze-Achard, L., Bruun-Rasmussen, M., Dunoyer, P., Yamamoto, Y.Y., Sieburth, L., and Voinnet, O. (2008). Widespread Translational Inhibition by Plant miRNAs and siRNAs. Science . **320**: 1185–1190.

Brosseau, C. and Moffett, P. (2015). Functional and Genetic Analysis Identify a Role for Arabidopsis ARGONAUTE5 in Antiviral RNA Silencing. Plant Cell **27**: 1742–1754.

Brown, N.R., Noble, M.E., Endicott, J. a, and Johnson, L.N. (1999). The structural basis for specificity of substrate and recruitment peptides for cyclin-dependent kinases. Nat. Cell Biol. **1**: 438–443.

Bueno, M.J. and Malumbres, M. (2011). MicroRNAs and the cell cycle. Biochim. Biophys. Acta - Mol. Basis Dis. **1812**: 592–601.

Bui, T. V. and Mendell, J.T. (2010). Myc: Maestro of MicroRNAs. Genes and Cancer **1**: 568–575.

Burroughs, A.M., Ando, Y., De Hoon, M.J.L., Tomaru, Y., Suzuki, H., Hayashizaki, Y., and Daub, C.O. (2011). Deep-sequencing of human argonaute-associated small RNAs provides insight into miRNA sorting and reveals argonaute association with RNA fragments of diverse origin. RNA Biol. **8**: 158–177.

Cai, T., Aulds, J., Gill, T., Cerio, M., and Schmitt, M.E. (2002). The Saccharomyces cerevisiae RNase mitochondrial RNA processing is critical for cell cycle progression at the end of mitosis. Genetics **161**: 1029–1042.

Cai, X., Hagedorn, C.H., and Cullen, B.R. (2004). Human microRNAs are processed from capped, polyadenylated transcripts that can also function as mRNAs. RNA **10**: 1957–1966.

Calin, G.A. et al. (2002). Frequent deletions and down-regulation of micro- RNA genes miR15 and miR16 at 13q14 in chronic lymphocytic leukemia. Proc. Natl. Acad. Sci. **99**: 15524–15529.

Callis, J. (2014). The Ubiquitination Machinery of the Ubiquitin System. Arab. B. **12**: e0174.

Cánepa, E.T., Scassa, M.E., Ceruti, J.M., Marazita, M.C., Carcagno, A.L., Sirkin, P.F., and Ogara, M.F. (2007). INK4 proteins, a family of mammalian CDK inhibitors with novel biological functions. IUBMB Life **59**: 419–426.

Cao, M., Du, P., Wang, X., Yu, Y.-Q., Qiu, Y.-H., Li, W., Gal-On, A., Zhou, C., Li, Y., and Ding, S.-W. (2014). Virus infection triggers widespread silencing of host genes by a distinct class of endogenous siRNAs in *Arabidopsis*. Proc. Natl. Acad. Sci. **111**: 14613–14618.

Carmichael, J.B., Provost, P., Ekwall, K., and Hobman, T.C. (2004). Ago1 and Dcr1, Two Core Components of the RNA Interference Pathway, Functionally Diverge from Rdp1 in Regulating Cell Cycle Events in Schizosaccharomyces pombe. Mol. Biol. Cell **15**: 1425–1435.

Chang, L. and Barford, D. (2014). Insights into the anaphase-promoting complex: A molecular machine that regulates mitosis. Curr. Opin. Struct. Biol. **29**: 1–9.

Cheloufi, S., Dos Santos, C.O., Chong, M.M.W., and Hannon, G.J. (2010). A dicer-independent miRNA biogenesis pathway that requires Ago catalysis. Nature **465**: 584–589.

Chen, H.-M., Chen, L.-T., Patel, K., Li, Y.-H., Baulcombe, D.C., and Wu, S. (2010). 22-nucleotide RNAs trigger secondary siRNA biogenesis in plants. Proc. Natl. Acad. Sci. **107**: 15269–15274.

Chen, X. (2005). microRNA biogenesis and function in plants. FEBS Lett. **579**: 5923–5931.

Chen, Z., Bao, M., Sun, Y., Yang, Y., Xu, X., Wang, J., Han, N., Bian, H., and Zhu, M. (2011). Regulation of auxin response by miR393-targeted transport inhibitor response protein 1 is involved in normal development in Arabidopsis. Plant Mol. Biol. **77**: 619–629.

Chi, Y., Welcker, M., Hizli, A.A., Posakony, J.J., Aebersold, R., and Clurman, B.E. (2008). Identification of CDK2 substrates in human cell lysates. Genome Biol. **9**: 1–12.

Ciechanover, A., Orian, A., and Schwartz, A.L. (2000). Ubiquitin-mediated proteolysis: Biological regulation via destruction. BioEssays **22**: 442–451.

Clough, S.J. and Bent, A.F. (1998). Floral dip : a simplified method for Agrobacterium-mediated transformation of Arabidopsis thaliana. Plant J. **16**: 735–743.

Cognat, V., Morelle, G., Megel, C., Lalande, S., Molinier, J., Vincent, T., Small, I., Duchêne, A.-M., and Maréchal-Drouard, L. (2017). The nuclear and organellar tRNA-derived RNA fragment population in Arabidopsis thaliana is highly dynamic. Nucleic Acids Res. **45**: 3460–3472.

Costa, R.H. (2005). FoxM1 dances with mitosis. Nat. Cell Biol. **7**: 108–110.

Criqui, M.C., Parmentier, Y., Derevier, A., Shen, W.H., Dong, A., and Genschik, P. (2000). Cell cycle-dependent proteolysis and ectopic overexpression of cyclin B1 in tobacco BY2 cells. Plant J. **24**: 763–773.

Cuperus, J.T., Carbonell, A., Fahlgren, N., Garcia-ruiz, H., Burke, R.T., Takeda, A., Sullivan, C.M., Gilbert, S.D., Montgomery, T. a, and Carrington, J.C. (2010). Unique fonctionality of 22 nt miRNAs in triggering RDR3-dependent siRNA biogenesis from target transcripts in Arabidopsis. Mol. Cell **17**: 997–1003.

Dahiya, A., Wong, S., Gonzalo, S., Gavin, M., and Dean, D.C. (2001). Linking the Rb and Polycomb pathways. Mol. Cell **8**: 557–568.

Damagnez, V., Makela, T.P., and Cottarel, G. (1995). Schizosaccharomyces pombe Mop1-Mcs2 is related to mammalian CAK. EMBO J. **14**: 6164–6172.

De-la-Pena, C., Nic-Can, G.I., Avilez-Montalvo, J., Cetz-Chel, J.E., and Loyola-Vargas, V.M. (2017). The Role of MiRNAs in Auxin Signaling and Regulation During Plant Development. Plant Epigenetics

Debernardi, J.M., Rodriguez, R.E., Mecchia, M.A., and Palatnik, J.F. (2012). Functional Specialization of the Plant miR396 Regulatory Network through Distinct MicroRNA–Target Interactions. PLoS Genet. **8**: e1002419.

Derrien, B., Baumberger, N., Schepetilnikov, M., Viotti, C., De Cillia, J., Ziegler-Graff, V., Isono, E., Schumacher, K., and Genschik, P. (2012). Degradation of the antiviral component ARGONAUTE1 by the autophagy pathway. Proc. Natl. Acad. Sci. **109**: 15942–15946.

Derrien, B., Clavel, M., Baumberger, N., Iki, T., Sarazin, A., Hacquard, T., Ponce, M.R., Ziegler-Graff, V., Vaucheret, H., Micol, J.L., Voinnet, O., and Genschik, P. (2018). A Suppressor Screen for AGO1 Degradation by the Viral F-Box P0 Protein Uncovers a Role for AGO DUF1785 in sRNA Duplex Unwinding. Plant Cell **30**: 1–22.

Desai, D., Wessling, H.C., Fisher, R.P., and Morgan, D.O. (1995). Effects of phosphorylation by CAK on cyclin binding by CDC2 and CDK2. Mol. Cell. Biol. **15**: 345–350.

Dick, F.A. and Rubin, S.M. (2013). Molecular mechanisms underlying RB protein function. Nat. Rev. Mol. Cell Biol. **14**: 297–306.

Ding, L. and Han, M. (2007). GW182 family proteins are crucial for microRNA-mediated gene silencing. Trends Cell Biol. **17**: 411–416.

Ding, S.W. (2010). RNA-based antiviral immunity. Nat. Rev. Immunol. **10**: 632–644.

Dong, Z., Han, M.-H., and Fedoroff, N. (2008). The RNA-binding proteins HYL1 and SE promote accurate in vitro processing of pri-miRNA by DCL1. Proc. Natl. Acad. Sci. **105**: 9970–9975.

Donnelly, P.M., Bonetta, D., Tsukaya, H., Dengler, R.E., and Dengler, N.G. (1999). Cell cycling and cell enlargement in developing leaves of Arabidopsis. Dev. Biol. **215**: 407–419.

Doyle, J.J. and Doyle, J.L. (1987) A rapid DNA isolation procedure for small quantities of fresh leaf tissue. Phyt. Bull., **19:** 11-15.

Dubois, M., Selden, K., Bediée, A., Rolland, G., Baumberger, N., Noir, S., Bach, L., Lamy, G., Granier, C., and Genschik, P. (2018). SIAMESE-RELATED1 Is Regulated Posttranslationally and Participates in Repression of Leaf Growth under Moderate Drought. Plant Physiol. **176**: 2834–2850.

Ducommun, B., Brambilla, P., Félix, M.A., Franza, B.R., Karsenti, E., and Draetta, G. (1991). Cdc2 Phosphorylation Is Required for Its Interaction With Cyclin. EMBO J. **10**: 3311–9.

Durrant, W.E. and Dong, X. (2004). Systemic Acquired Resistance. Annu. Rev. Phytopathol. **42**: 185–209.

Earley, K., Smith, M.R., Weber, R., Gregory, B.D., and Poethig, R.S. (2010). An endogenous F-box protein regulates ARGONAUTE1 in Arabidopsis thaliana. Silence **1**: 1–10.

Earley, K.W. and Poethig, R.S. (2011). Binding of the cyclophilin 40 ortholog SQUINT to Hsp90 protein is required for SQUINT function in Arabidopsis. J. Biol. Chem. **286**: 38184–38189.

Edwards, K.D. et al. (2017). A reference genome for Nicotiana tabacum enables map-based cloning of homeologous loci implicated in nitrogen utilization efficiency. BMC Genomics **18**: 1–14.

Eichmann, R. and Schäfer, P. (2015). Growth versus immunity-a redirection of the cell cycle? Curr. Opin. Plant Biol. **26**: 106–112.

Eilers, M. and Eisenman, R.N. (2008). Myc ' s broad reach. Genes Dev. **22**: 2755–2766.

El-Shami, M., Pontier, D., Lahmy, S., Braun, L., Picart, C., Vega, D., Hakimi, M.-A., Jacobsen, S.E., Cooke, R., and Lagrange, T. (2007). Reiterated WG/GW motifs form functionally and evolutionarily conserved ARGONAUTE-binding platforms in RNAi-related components. Genes Dev. **21**: 2539–2544.

Elbarbary, R.A., Miyoshi, K., Myers, J.R., Du, P., Ashton, J.M., Tian, B., and Maquat, L.E. (2017). Tudor-SN – mediated endonucleolytic decay of human cell microRNAs promotes G 1 /S phase transition. Science . **862**: 859–862.

Elkayam, E., Kuhn, C.-D., Tocilj, A., Haase, A.D., Greene, E.M., Hannon, G.J., and Joshua-Tor, L. (2012). The Structure of Human Argonaute-2 in Complex with miR-20a. Cell **150**: 100–110.

Evans, T., Rosenthal, E.T., Youngblom, J., Distel, D., and Hunt, T. (1983). Cyclin: A protein specified by maternal mRNA in sea urchin eggs that is destroyed at each cleavage division. Cell **33**: 389–396.

Fahlgren, N., Montgomery, T.A., Howell, M.D., Allen, E., Dvorak, S.K., Alexander, A.L., and Carrington, J.C. (2006). Regulation of AUXIN RESPONSE FACTOR3 by TAS3 ta-siRNA Affects Developmental Timing and Patterning in Arabidopsis. Curr. Biol. **16**: 939–944.

Fang, Y. and Spector, D.L. (2007). Identification of Nuclear Dicing Bodies Containing Proteins for MicroRNA Biogenesis in Living Arabidopsis Plants. Curr. Biol. **17**: 818–823.

Fátyol, K., Ludman, M., and Burgyán, J. (2016). Functional dissection of a plant Argonaute. Nucleic Acids Res. **44**: 1384–1397.

Favery, B., Complainville, A., Vinardell, J.M., Lecomte, P., Vaubert, D., Mergaert, P., Kondorosi, A., Kondorosi, E., Crespi, M., and Abad, P. (2002). The endosymbiosis-induced genes ENOD40 and CCS52a are involved in endoparasitic-nematode interactions in Medicago truncatula. Mol. Plant. Microbe. Interact. **15**: 1008–1013.

Fei, Q., Xia, R., and Meyers, B.C. (2013). Phased, Secondary, Small Interfering RNAs in Posttranscriptional Regulatory Networks. Plant Cell **25**: 2400–2415.

Ferreira, P.C.G., Hemerly, A.S., Villarroel, R., Van Montagu, M., and Inze, D. (1991). The Arabidopsís Functional Homolog of the p34 cdc2 Protein Kinase. Plant Cell **3**: 531–540.

Fesquet, D., Labbé, J.C., Derancourt, J., Capony, J.P., Galas, S., Girard, F., Lorca, T., Shuttleworth, J., Dorée, M., and Cavadore, J.C. (1993). The MO15 gene encodes the catalytic subunit of a protein kinase that activates cdc2 and other cyclin-dependent kinases (CDKs) through phosphorylation of Thr161 and its homologues. EMBO J. **12**: 3111–3021.

Fire, A., Xu, S., Montgomery, M.K., Kostas, S.A., Driver, S.E., and Mello, C.C. (1998). Potent and specific genetic interference by double-stranded RNA in caenorhabditis elegans. Nature **391**: 806–811.

Fischer, M. and Müller, G.A. (2017). Cell cycle transcription control: DREAM/MuvB and RB-E2F complexes. Crit. Rev. Biochem. Mol. Biol. **52**: 638–662.

Fisher, R.P. and Morgan, D.O. (1994). A novel cyclin associates with M015/CDK7 to form the CDK-activating kinase. Cell **78**: 713–724.

Frank, F., Sonenberg, N., and Nagar, B. (2010). Structural basis for 5′-nucleotide base-specific recognition of guide RNA by human AGO2. Nature **465**: 818–822.

Fultz, D., Choudury, S.G., and Slotkin, R.K. (2015). Silencing of active transposable elements in plants. Curr. Opin. Plant Biol. **27**: 67–76.

Garcia, D., Garcia, S., Pontier, D., Marchais, A., Renou, J.P., Lagrange, T., and Voinnet, O. (2012). Ago Hook and RNA Helicase Motifs Underpin Dual Roles for SDE3 in Antiviral Defense and Silencing of Nonconserved Intergenic Regions. Mol. Cell **48**: 109–120.

Gasciolli, V., Mallory, A.C., Bartel, D.P., and Vaucheret, H. (2005). Partially redundant functions of arabidopsis DICER-like enzymes and a role for DCL4 in producing trans-Acting siRNAs. Curr. Biol. **15**: 1494–1500.

Gautier, J., Minshull, J., Lohka, M., Glotzer, M., Hunt, T., and Maller, J.L. (1990). Cyclin is a component of maturation-promoting factor from Xenopus. Cell **60**: 487–494.

Gautier, J., Norbury, C., Lohka, M., Nurse, P., and Maller, J. (1988). Purified maturation-promoting factor contains the product of a Xenopus homolog of the fission yeast cell cycle control gene cdc2+. Cell **54**: 433–439.

Gebetsberger, J., Zywicki, M., Künzi, A., and Polacek, N. (2012). tRNA-Derived Fragments Target the Ribosome and Function as Regulatory Non-Coding RNA in Haloferax volcanii. Archaea **2012**: 1–11.

Genschik, P., Marrocco, K., Bach, L., Noir, S., and Criqui, M.C. (2014). Selective protein degradation: A rheostat to modulate cell-cycle phase transitions. J. Exp. Bot. **65**: 2603–2615.

German, M.A. et al. (2008). Global identification of microRNA-target RNA pairs by parallel analysis of RNA ends. Nat. Biotechnol. **26**: 941–946.

Ghildiyal, M. and Zamore, P.D. (2009). Small silencing RNAs: An expanding universe. Nat. Rev. Genet. **10**: 94–108.

Giegé, R. (2008). Toward a more complete view of tRNA biology. Nat. Struct. Mol. Biol. **15**: 1007–1014.

Gill, T., Cai, T., Aulds, J., Wierzbicki, S., Mark, E., and Schmitt, M.E. (2004). RNase MRP Cleaves the CLB2 mRNA To Promote Cell Cycle Progression : Novel Method of mRNA Degradation RNase MRP Cleaves the CLB2 mRNA To Promote Cell Cycle Progression : Novel Method of mRNA Degradation. Mol. Cell. Biol. **24**: 945–953.

Glotzer, M., Murray, A.W., and Kirschner, M.W. (1991). Cyclin is degraded by the ubiquitin pathway. Nature **349**: 132–138.

Golden, R.J. et al. (2017). An Argonaute phosphorylation cycle promotes microRNA-mediated silencing. Nature **542**: 197–202.

Gregory, R.I., Yan, K.P., Amuthan, G., Chendrimada, T., Doratotaj, B., Cooch, N., and Shiekhattar, R. (2004). The Microprocessor complex mediates the genesis of microRNAs. Nature **432**: 235–240.

Grigg, S.P., Galinha, C., Kornet, N., Canales, C., Scheres, B., and Tsiantis, M. (2009). Repression of Apical Homeobox Genes Is Required for Embryonic Root Development in Arabidopsis. Curr. Biol. **19**: 1485–1490.

Groisman, I., Jung, M.-Y., Sarkissian, M., Cao, Q., and Richter, J.D. (2002). Translational control of the embryonic cell cycle. Cell **109**: 473–483.

Guo, H., Xie, Q., Fei, J., and Chua, N. (2005). MicroRNA Directs mRNA Cleavage of the Transcription Factor NAC1 to Downregulate Auxin Signals for Arabidopsis Lateral Root Development. Plant Cell **17**: 1376–1386.

Gusti, A., Baumberger, N., Nowack, M., Pusch, S., Eisler, H., Potuschak, T., De Veylder, L., Schnittger, A., and Genschik, P. (2009). The Arabidopsis thaliana F-box protein FBL17 is essential for progression through the second mitosis during pollen development. PLoS One **4**: e4780.

Gutierrez, C. (2009). The Arabidopsis cell division cycle. Arab. B. **7**: e0120.

Haga, N., Kato, K., Murase, M., Araki, S., Kubo, M., Demura, T., Suzuki, K., Muller, I., Voss, U., Jurgens, G., and Ito, M. (2007). R1R2R3-Myb proteins positively regulate cytokinesis through activation of KNOLLE transcription in Arabidopsis thaliana. Development **134**: 1101–1110.

Haga, N., Kobayashi, K., Suzuki, T., Maeo, K., Kubo, M., Ohtani, M., Mitsuda, N., Demura, T., Nakamura, K., Jurgens, G., and Ito, M. (2011). Mutations in MYB3R1 and MYB3R4 Cause Pleiotropic Developmental Defects and Preferential Down-Regulation of Multiple G2/M-Specific Genes in Arabidopsis. Plant Physiol. **157**: 706–717.

Hall, I.M., Noma, K.-I., and Grewal, S.I.S. (2003). RNA interference machinery regulates chromosome dynamics during mitosis and meiosis in fission yeast. Proc. Natl. Acad. Sci. U. S. A. **100**: 193–8.

Han, J., Lee, Y., Yeom, K., Kim, Y.-K., Jin, H., and Kim, V.N. (2004). The Drosha-DGCR8 complex in primary microRNA processing. Genes Dev. **18**: 3016–3027.

Han, M.-H., Goud, S., Song, L., and Fedoroff, N. (2004). The Arabidopsis double-stranded RNA-binding protein HYL1 plays a role in microRNA-mediated gene regulation. Proc. Natl. Acad. Sci. **101**: 1093–1098.

Haussecker, D., Huang, Y., Lau, A., Parameswaran, P., Fire, A.Z., and Kay, M. a (2010). Human tRNA-derived small RNAs in the global regulation of RNA silencing. RNA **16**: 673–695.

Havens, C.G. and Walter, J.C. (2011). Mechanism of CRL4Cdt2, a PCNA-dependent E3 ubiquitin ligase. Genes Dev. **25**: 1568–1582.

Hayashi, K., Hasegawa, J., and Matsunaga, S. (2013). The boundary of the meristematic and elongation zones in roots: endoreduplication precedes rapid cell expansion. Sci. Rep. **3**: 1-8.

Herr, a J. (2005). RNA Polymerase IV Directs Silencing of Endogenous DNA. Science . **308**: 118–120.

Van Den Heuvel, S. and Dyson, N.J. (2008). Conserved functions of the pRB and E2F families. Nat. Rev. Mol. Cell Biol. **9**: 713–724.

Higa, L.A., Banks, D., Wu, M., Kobayashi, R., Sun, H., and Zhang, H. (2006). L2DTL/CDT2 interacts with the CUL4/DDB1 complex and PCNA and regulates CDT1 proteolysis in response to DNA damage. Cell Cycle **5**: 1675–1680.

Hiraguri, A., Itoh, R., Kondo, N., Nomura, Y., Aizawa, D., Murai, Y., Koiwa, H., Seki, M., Shinozaki, K., and Fukuhara, T. (2005). Specific interactions between Dicer-like proteins and HYL1/DRB-family dsRNA-binding proteins in Arabidopsis thaliana. Plant Mol. Biol. **57**: 173–188.

Hirai, H., Roussel, M.F., Kato, J.Y., Ashmun, R.A., and Sherr, C.J. (1995). Novel INK4 proteins, p19 and p18, are specific inhibitors of the cyclin D-dependent kinases CDK4 and CDK6. Mol. Cell. Biol. **15**: 2672–2681.

Hobecker, K.V., Reynoso, M.A., Bustos-Sanmamed, P., Wen, J., Mysore, K.S., Crespi, M., Blanco, F.A., and Zanetti, M.E. (2017). The MicroRNA390/TAS3 Pathway Mediates Symbiotic Nodulation and Lateral Root Growth. Plant Physiol. **174**: 2469–2486.

Holt, L.J., Tuch, B.B., Villén, J., Johnson, A.D., Gygi, S.P., and Morgan, D.O. (2010). Insights into evolution. Science . **325**: 1–11.

Horton, L.E. and Templeton, D.J. (1997). The cyclin box and C-terminus of cyclins A and E specify CDK activation and substrate specificity. Oncogene **14**: 491–498.

Hsieh, L.C., Lin, S.I., Kuo, H.F., and Chiou, T.J. (2010). Abundance of tRNA-derived small RNAs in phosphate-starved Arabidopsis roots. Plant Signal. Behav. **5**: 537–539.

Hubstenberger, A. et al. (2017). P-Body Purification Reveals the Condensation of Repressed mRNA Regulons. Mol. Cell **68**: 144–157.

Hutvagner, G., McLachlan, J., Pasquinelli, A.E., lint, E., Tuschl, T., and Zamore, P.D. (2010). A Cellular Function for the RNA-Interference Temporal RNA Small let-7 Enzyme Dicer in the Maturation of the . Science . **293**: 1–6.

Hwang, H.-W., Wentzel, E.A., and Mendell, J.T. (2008). A hexanucleotide element directs microRNA nuclear import. Science . **321**: 652–653.

Iki, T., Yoshikawa, M., Nishikiori, M., Jaudal, M.C., Matsumoto-Yokoyama, E., Mitsuhara, I., Meshi, T., and Ishikawa, M. (2010). In vitro assembly of plant RNA-induced silencing complexes facilitated by molecular chaperone HSP90. Mol. Cell **39**: 282–291.

Ito, M. (1998). A Novel cis-Acting Element in Promoters of Plant B-Type Cyclin Genes Activates M Phase Specific Transcription. Plant Cell **10**: 331–342.

Ito, M., Araki, S., and Matsunaga, S. (2001). G2 / M-Phase – Specific transcription during the plant cell cycle Is mediated by c-Myb – like transcription factors. Plant Cell **13**: 1891–1905.

Iwakawa, H. oki and Tomari, Y. (2013). Molecular insights into microRNA-mediated translational repression in plants. Mol. Cell **52**: 591–601.

Iwakawa, H. oki and Tomari, Y. (2015). The Functions of MicroRNAs: mRNA Decay and Translational Repression. Trends Cell Biol. **25**: 651–665.

Iwakawa, H., Shinmyo, A., and Sekine, M. (2006). Arabidopsis CDKA;1, a cdc2 homologue, controls proliferation of generative cells in male gametogenesis. Plant J. **45**: 819–831.

Iwasaki, S., Kobayashi, M., Yoda, M., Sakaguchi, Y., Katsuma, S., Suzuki, T., and Tomari, Y. (2010). Hsc70/Hsp90 chaperone machinery mediates ATP-dependent RISC loading of small RNA duplexes. Mol. Cell **39**: 292–299.

Jackson, S. and Xiong, Y. (2009). CRL4s: the CUL4-RING E3 ubiquitin ligases. Trends Biochem. Sci. **34**: 562–570.

Jin, J., Arias, E.E., Chen, J., Harper, J.W., and Walter, J.C. (2006). A Family of Diverse Cul4-Ddb1-Interacting Proteins Includes Cdt2, which Is Required for S Phase Destruction of the Replication Factor Cdt1. Mol. Cell **23**: 709–721.

Johnston, M. and Hutvagner, G. (2011). Posttranslational modification of Argonautes and their role in small RNA-mediated gene regulation. Silence **2**: 1-4.

Jones-Rhoades, M.W. and Bartel, D.P. (2004). Computational identification of plant MicroRNAs and their targets, including a stress-induced miRNA. Mol. Cell **14**: 787–799.

Jones-Rhoades, M.W., Bartel, D.P., and Bartel, B. (2006). MicroRNAs and their regulatory roles in plants. Annu. Rev. Plant Biol. **57**: 19–53.

Jones, J.D.G. and Dangl, J.L. (2006). The plant immune system. Nature **444**: 323–329.

Jouannet, V., Moreno, A.B., Elmayan, T., Vaucheret, H., Crespi, M.D., and Maizel, A. (2012). Cytoplasmic Arabidopsis AGO7 accumulates in membrane-associated siRNA bodies and is required for ta-siRNA biogenesis. EMBO J. **31**: 1704–1713.

Joubès, J., Chevalier, C., Dudits, D., Heberle-Bors, E., Inzé, D., Umeda, M., and Renaudin, J.-P. (2000). CDK-related protein kinases in plants. Plant Mol. Biol. **43**: 607–620.

Kakrana, A., Hammond, R., Patel, P., Nakano, M., and Meyers, B.C. (2014). SPARTA: A parallelized pipeline for integrated analysis of plant miRNA and cleaved mRNA data sets, including new miRNA target-identification software. Nucleic Acids Res. **42**: 1–13.

Kalin, T. V., Ustiyan, V., and Kalinichenko, V. V. (2011). Multiple faces of FoxM1 transcription factor: Lessons from transgenic mouse models. Cell Cycle **10**: 396–405.

Kamura, T., Hara, T., Matsumoto, M., Ishida, N., Okumura, F., Hatakeyama, S., Yoshida, M., Nakayama, K., and Nakayama, K.I. (2004). Cytoplasmic ubiquitin ligase KPC regulates proteolysis of p27Kip1 at G1 phase. Nat. Cell Biol. **6**: 1229–1235.

Kanno, T., Huettel, B., Mette, M.F., Aufsatz, W., Jaligot, E., Daxinger, L., Kreil, D.P., Matzke, M., and Matzke, A.J.M. (2005). Atypical RNA polymerase subunits required for RNA-directed DNA methylation. Nat. Genet. **37**: 761–765.

Kawamata, T., Seitz, H., and Tomari, Y. (2009). Structural determinants of miRNAs for RISC loading and slicer-independent unwinding. Nat. Struct. Mol. Biol. **16**: 953–960.

Keam, S. and Hutvagner, G. (2015). tRNA-Derived Fragments (tRFs): Emerging New Roles for an Ancient RNA in the Regulation of Gene Expression. Life **5**: 1638–1651.

Kenneth, N.S. and White, R.J. (2009). Regulation by c-Myc of ncRNA expression. Curr. Opin. Genet. Dev. **19**: 38–43.

Khvorova, A., Reynolds, A., and Jayasena, S.D. (2003). Functional siRNAs and miRNAs exhibit strand bias. Cell **115**: 209–216.

Kidner, C.A. and Martienssen, R.A. (2004). Spatially restricted microRNA directs leaf polarity through ARGONAUTE1. Nature **428**: 81–84.

Kidner, C.A. and Martienssen, R.A. (2005). The developmental role of microRNA in plants. Curr. Opin. Plant Biol. **8**: 38–44.

Kim, H.J., Oh, S.A., Brownfield, L., Hong, S.H., Ryu, H., Hwang, I., Twell, D., and Nam, H.G. (2008). Control of plant germline proliferation by SCF^{FBL17} degradation of cell cycle inhibitors. Nature **455**: 1134–1137.

Kim, V.N. (2005). MicroRNA biogenesis: Coordinated cropping and dicing. Nat. Rev. Mol. Cell Biol. **6**: 376–385.

Kim, Y.J., Zheng, B., Yu, Y., Won, S.Y., Mo, B., and Chen, X. (2011). The role of Mediator in small and long noncoding RNA production in Arabidopsis thaliana. EMBO J. **30**: 814–822.

Kipreos, E.T. and Pagano, M. (2000). The F-box protein family. Genome Biol. **1**: 1–7.

Kitagawa, M., Kitagawa, K., Kotake, Y., Niida, H., and Ohhata, T. (2013). Cell cycle regulation by long non-coding RNAs. Cell. Mol. Life Sci. **70**: 4785–4794.

Kobayashi, H. and Tomari, Y. (2016). RISC assembly: Coordination between small RNAs and Argonaute proteins. Biochim. Biophys. Acta - Gene Regul. Mech. **1859**: 71–81.

Kobayashi, K. et al. (2015a). Transcriptional repression by MYB3R proteins regulates plant organ growth. EMBO J. **34**: 1992–2007.

Kobayashi, K., Suzuki, T., Iwata, E., Magyar, Z., Bögre, L., and Ito, M. (2015b). MYB3Rs, plant homologs of Myb oncoproteins, control cell cycle-regulated transcription and form DREAM-like complexes. Transcription **6**: 106–111.

Koesters, R., Adams, V., Betts, D., Moos, R., Schmid, M., Siermann, A., Hassam, S., Weitz, S., Lichter, P., Heitz, P.U., Von Knebel Doeberitz, M., and Briner, J. (1999). Human eukaryotic initiation factor EIF2C1 gene: cDNA sequence, genomic organization, localization to chromosomal bands 1p34-p35, and expression. Genomics **61**: 210–218.

Komaki, S. and Schnittger, A. (2017). The Spindle Assembly Checkpoint in Arabidopsis Is Rapidly Shut Off during Severe Stress. Dev. Cell **43**: 172–185.

Kosugi, S. and Ohashi, Y. (2002). DNA binding and dimerization specificity and potential targets for the TCP protein family. Plant J. **30**: 337–348.

Kotake, Y., Nakagawa, T., Kitagawa, K., Suzuki, S., Liu, N., Kitagawa, M., and Xiong, Y. (2009). Long non-coding RNA ANRIL is required for the PRC2 recruitment to and silencing of $p15^{INK4B}$ tumor suppressor gene. Oncogene **6**: 247–253.

Kozomara, A. and Griffiths-Jones, S. (2014). MiRBase: Annotating high confidence microRNAs using deep sequencing data. Nucleic Acids Res. **42**: 68–73.

Kravtsova-Ivantsiv, Y. et al. (2015). KPC1-mediated ubiquitination and proteasomal processing of nf-κb1 p105 to p50 restricts tumor growth. Cell **161**: 333–347.

Kriegel, A.J., Liu, Y., Fang, Y., Ding, X., and Liang, M. (2012). The miR-29 family: genomics, cell biology, and relevance to renal and cardiovascular injury. Physiol. Genomics **44**: 237–244.

Krol, J., Loedige, I., and Filipowicz, W. (2010). The widespread regulation of microRNA biogenesis, function and decay. Nat. Rev. Genet. **11**: 597–610.

Kronja, I. and Orr-Weaver, T.L. (2011). Translational regulation of the cell cycle: When, where, how and why? Philos. Trans. R. Soc. B Biol. Sci. **366**: 3638–3652.

Kumagai-Sano, F., Hayashi, T., Sano, T., and Hasezawa, S. (2007). Cell cycle synchronization of tobacco BY-2 cells. Nat. Protoc. **1**: 2621–2627.

Kumar, N. et al. (2015). Functional Conservation in the SIAMESE-RELATED Family of Cyclin-Dependent Kinase Inhibitors in Land Plants. Plant Cell **27**: 3065–3080.

Kumar, N. and Larkin, J.C. (2017). Why do plants need so many cyclin-dependent kinase inhibitors? Plant Signal. Behav. **12**: 1–4.

Kurihara, Y., Takashi, Y., and Watanabe, Y. (2006). The interaction between DCL1 and HYL1 is important for efficient and precise processing of pri-miRNA in plant microRNA biogenesis. Rna **12**: 206–212.

Kurita, K., Sakamoto, T., Yagi, N., Sakamoto, Y., Ito, A., Nishino, N., Sako, K., Yoshida, M., Kimura, H., Seki, M., and Matsunaga, S. (2017). Live imaging of H3K9 acetylation in plant cells. Sci. Rep. **7**: 1–9.

Kwak, P.B. and Tomari, Y. (2012). The N domain of Argonaute drives duplex unwinding during RISC assembly. Nat. Struct. Mol. Biol. **19**: 145–151.

Kwon, Y.T. and Ciechanover, A. (2017). The Ubiquitin Code in the Ubiquitin-Proteasome System and Autophagy. Trends Biochem. Sci. **42**: 873–886.

Lahmy, S., Pontier, D., Cavel, E., Vega, D., El-Shami, M., Kanno, T., and Lagrange, T. (2009). PolV(PolIVb) function in RNA-directed DNA methylation requires the conserved active site and an additional plant-specific subunit. Proc. Natl. Acad. Sci. **106**: 941–946.

Lal, A. et al. (2009). miR-24 Inhibits Cell Proliferation by Targeting E2F2, MYC, and Other Cell-Cycle Genes via Binding to "Seedless" 3′UTR MicroRNA Recognition Elements. Mol. Cell **35**: 610–625.

Langmead, B. and Salzberg, S.L. (2012). Fast gapped-read alignment with Bowtie 2. Nat. Methods **9**: 357–359.

Laoukili, J., Kooistra, M.R.H., Brás, A., Kauw, J., Kerkhoven, R.M., Morrison, A., Clevers, H., and Medema, R.H. (2005). FoxM1 is required for execution of the mitotic programme and chromosome stability. Nat. Cell Biol. **7**: 126–136.

Lavy, M. and Estelle, M. (2016). Mechanisms of auxin signaling. Development **143**: 3226–3229.

Lechner, E., Achard, P., Vansiri, A., Potuschak, T., and Genschik, P. (2006). F-box proteins everywhere. Curr. Opin. Plant Biol. **9**: 631–638.

Lee, Y., Ahn, C., Han, J., Choi, H., Kim, J., Yim, J., Lee, J., Provost, P., Radmark, O., Kim, S., and Kim, V. (2003). The nuclear RNase III Drosha initates microRNA processing. Nature **425**: 415–419.

Lee, Y., Kim, M., Han, J., Yeom, K.-H., Lee, S., Baek, S.H., and Kim, V.N. (2004). MicroRNA genes are transcribed by RNA polymerase II. EMBO J. **23**: 4051–4060.

Lee, Y.S., Shibata, Y., Malhotra, A., and Dutta, A. (2009). A novel class of small RNAs: tRNA-derived RNA fragments (tRFs). Genes Dev. **23**: 2639–2649.

Van Leene, J. et al. (2010). Targeted interactomics reveals a complex core cell cycle machinery in Arabidopsis thaliana. Mol. Syst. Biol. **6:** 1-12.

Van Leene, J., Boruc, J., De Jaeger, G., Russinova, E., and De Veylder, L. (2011). A kaleidoscopic view of the Arabidopsis core cell cycle interactome. Trends Plant Sci. **16**: 141–150.

Leung, A.K.L. and Sharp, P.A. (2010). MicroRNA Functions in Stress Responses. Mol. Cell **40**: 205–215.

Leva, G. Di, Garofalo, M., and Croce, C.M. (2014). microRNAs in cancer. Annu Rev Pathol **9**: 287–314.

Lewis, B.P., Shih, I.H., Jones-Rhoades, M.W., Bartel, D.P., and Burge, C.B. (2003). Prediction of Mammalian MicroRNA Targets. Cell **115**: 787–798.

Li, C.F., Henderson, I.R., Song, L., Fedoroff, N., Lagrange, T., and Jacobsen, S.E. (2008). Dynamic regulation of ARGONAUTE4 within multiple nuclear bodies in Arabidopsis thaliana. PLoS Genet. **4**.

Li, C.F., Pontes, O., El-Shami, M., Henderson, I.R., Bernatavichute, Y. V., Chan, S.W.L., Lagrange, T., Pikaard, C.S., and Jacobsen, S.E. (2006). An ARGONAUTE4-Containing Nuclear Processing Center Colocalized with Cajal Bodies in Arabidopsis thaliana. Cell **126**: 93–106.

Li, J., Tian, H., Yang, J., and Gong, Z. (2016). Long Noncoding RNAs Regulate Cell Growth, Proliferation, and Apoptosis. DNA Cell Biol. **35**: 459–470.

Li, J., Yang, Z., Yu, B., Liu, J., and Chen, X. (2005). Methylation protects miRNAs and siRNAs from a 3′-end uridylation activity in Arabidopsis. Curr. Biol. **15**: 1501–1507.

Li, S. et al. (2013). MicroRNAs inhibit the translation of target mRNAs on the endoplasmic reticulum in arabidopsis. Cell **153**: 562–574.

Li, X., Zhao, Q., Liao, R., Sun, P., and Wu, X. (2003). The SCF^{Skp2} ubiquitin ligase complex interacts with the human replication licensing factor Cdt1 and regulates Cdt1 degradation. J. Biol. Chem. **278**: 30854–30858.

Lingel, A., Simon, B., Izaurralde, E., and Sattler, M. (2004). Nucleic acid 3'-end recognition by the Argonaute2 PAZ domain. Nat. Struct. Mol. Biol. **11**: 576–577.

Linsley, P.S. et al. (2007). Transcripts Targeted by the MicroRNA-16 Family Cooperatively Regulate Cell Cycle Progression. Mol. Cell. Biol. **27**: 2240–2252.

Liu, J. et al. (2008a). Targeted Degradation of the Cyclin-Dependent Kinase Inhibitor ICK4/KRP6 by RING-Type E3 Ligases Is Essential for Mitotic Cell Cycle Progression during Arabidopsis Gametogenesis. Plant Cell Online **20**: 1538–1554.

Liu, P., Montgomery, T.A., Fahlgren, N., Kasschau, K.D., Nonogaki, H., and Carrington, J.C. (2007). Repression of AUXIN RESPONSE FACTOR10 by microRNA160 is critical for seed germination and post-germination stages. Plant J. **52**: 133–146.

Liu, Q., Fu, H., Sun, F., Zhang, H., Tie, Y., Zhu, J., Xing, R., Sun, Z., and Zheng, X. (2008). miR-16 family induces cell cycle arrest by regulating multiple cell cycle genes. Nucleic Acids Res. **36**: 5391–5404.

Liu, X., Hao, L., Li, D., Zhu, L., and Hu, S. (2015). Long Non-coding RNAs and Their Biological Roles in Plants. Genomics, Proteomics Bioinforma. **13**: 137–147.

Liu, X., Li, D., Zhang, W., Guo, M., and Zhan, Q. (2012). Long non-coding RNA gadd7 interacts with TDP-43 and regulates Cdk6 mRNA decay. EMBO J. **31**: 4415–4427.

Llobet-Navas, D. et al. (2014). The MicroRNA 424/503 Cluster Reduces CDC25A Expression during Cell Cycle Arrest Imposed by Transforming Growth Factor in Mammary Epithelial Cells. Mol. Cell. Biol. **34**: 4216–4231.

London, N. and Biggins, S. (2014). Signaling dynamics in the spindle checkpoint response. Nat. Rev. Mol. Cell Biol. **15**: 736–747.

Loss-Morais, G., Waterhouse, P.M., and Margis, R. (2013). Description of plant tRNA-derived RNA fragments (tRFs) associated with argonaute and identification of their putative targets. Biol. Direct **8**: 1–6.

Love, M.I., Huber, W., and Anders, S. (2014). Moderated estimation of fold change and dispersion for RNA-seq data with DESeq2. Genome Biol. **15**: 1–21.

Luo, R.X., Postigo, A.A., and Dean, D.C. (1998). Rb interacts with histone deacetylase to repress transcription. Cell **92**: 463–473.

Lynn, K., Fernandez, A., Aida, M., Sedbrook, J., Tasaka, M., Masson, P., and Barton, M.K. (1999). The PINHEAD/ZWILLE gene acts pleiotropically in Arabidopsis development and has overlapping functions with the ARGONAUTE1 gene. Development **126**: 469–481.

Ma, J.B., Ye, K., and Patel, D.J. (2004). Structural basis for overhang-specific small interfering RNA recognition by the PAZ domain. Nature **429**: 318–322.

Ma, T. (2000). Cell cycle-regulated phosphorylation of p220NPAT by cyclin E/Cdk2 in Cajal bodies promotes histone gene transcription. Genes Dev. **14**: 2298–2313.

Magyar, Z., Bögre, L., and Ito, M. (2016). DREAMs make plant cells to cycle or to become quiescent. Curr. Opin. Plant Biol. **34**: 100–106.

Major, M.L., Lepe, R., and Costa, R.H. (2004). Forkhead Box M1B Transcriptional Activity Requires Binding of Cdk-Cyclin Complexes for Phosphorylation-Dependent Recruitment of p300 / CBP Coactivators. Society **24**: 2649–2661.

Maldonado-Bonilla, L.D. (2014). Composition and function of P bodies in Arabidopsis thaliana. Front. Plant Sci. **5**: 1–11.

Mallory, A. and Vaucheret, H. (2010). Form, function, and regulation of ARGONAUTE proteins. Plant Cell **22**: 3879–89.

Mallory, A.C., Bartel, D.P., and Bartel, B. (2005). MicroRNA-Directed Regulation of Arabidopsis AUXIN RESPONSE FACTOR17 Is Essential for Proper Development and Modulates Expression of Early Auxin Response Genes. Plant Cell **17**: 1360–1375.

Mallory, A.C., Hinze, A., Tucker, M.R., Bouché, N., Gasciolli, V., Elmayan, T., Lauressergues, D., Jauvion, V., Vaucheret, H., and Laux, T. (2009). Redundant and Specific Roles of the ARGONAUTE Proteins AGO1 and ZLL in Development and Small RNA-Directed Gene Silencing. PLoS Genet. **5**: e1000646.

Mallory, A.C. and Vaucheret, H. (2009). ARGONAUTE 1 homeostasis invokes the coordinate action of the microRNA and siRNA pathways. EMBO Rep. **10**: 521–526.

Malumbres, M. (2014). Cyclin-dependent kinases. Genome Biol. **15**: 1–10.

Malumbres, M., Sotillo, R., Santamaría, D., Galán, J., Cerezo, A., Ortega, S., Dubus, P., and Barbacid, M. (2004). Mammalian cells cycle without the D-type cyclin-dependent kinases Cdk4 and Cdk6. Cell **118**: 493–504.

Mani, S.R. and Juliano, C.E. (2013). Untangling the web: The diverse functions of the PIWI/piRNA pathway. Mol. Reprod. Dev. **80**: 632–664.

Margottin-Goguet, F., Hsu, J.Y., Loktev, A., Hsieh, H.M., Reimann, J.D.R., and Jackson, P.K. (2003). Prophase destruction of Emi1 by the $SCF^{\beta TrCP}$/Slimbubiquitin ligase activates the anaphase promoting complex to allow progression beyond prometaphase. Dev. Cell **4**: 813–826.

Marti, A., Wirbelauer, C., Scheffner, M., and Krek, W. (1999). Interaction between ubiquitin – protein ligase SCF SKP2 and E2F-1 underlies the regulation of E2F-1 degradation. Nat. Cell Biol. **1**: 14–19.

Martínez de Alba, A.E., Elvira-Matelot, E., and Vaucheret, H. (2013). Gene silencing in plants: A diversity of pathways. Biochim. Biophys. Acta - Gene Regul. Mech. **1829**: 1300–1308.

Martinez, G. (2018). tRNA-derived small RNAs: New players in genome protection against retrotransposons. RNA Biol. **15**: 170–175.

Masui, Y. and Markert, C. (1971). Cytoplasmic control of nuclear behavior during meiotic maturation of frog oocytes. J. Exp. Zool. **177**: 129–146.

Meister, G. (2013). Argonaute proteins: Functional insights and emerging roles. Nat. Rev. Genet. **14**: 447–459.

Menges, M., De Jager, S.M., Gruissem, W., and Murray, J.A.H. (2005). Global analysis of the core cell cycle regulators of Arabidopsis identifies novel genes, reveals multiple and highly specific profiles of expression and provides a coherent model for plant cell cycle control. Plant J. **41**: 546–566.

Mi, H., Huang, X., Muruganujan, A., Tang, H., Mills, C., Kang, D., and Thomas, P.D. (2017). PANTHER version 11: expanded annotation data from Gene Ontology and Reactome pathways, and data analysis tool enhancements. Nucleic Acids Res. **45**: 183–189.

Mi, S. et al. (2008). Sorting of Small RNAs into Arabidopsis Argonaute Complexes Is Directed by the 5′ Terminal Nucleotide. Cell **133**: 116–127.

Miller, D.M., Thomas, S.D., Islam, A., Muench, D., and Sedoris, K. (2012). c-Myc and cancer metabolism. Clin. Cancer Res. **18**: 5546–5553.

Mocciaro, A. and Rape, M. (2012). Emerging regulatory mechanisms in ubiquitin-dependent cell cycle control. J. Cell Sci. **125**: 255–263.

Mogilyansky, E. and Rigoutsos, I. (2013). The miR-17/92 cluster: A comprehensive update on its genomics, genetics, functions and increasingly important and numerous roles in health and disease. Cell Death Differ. **20**: 1603–1614.

Montgomery, T.A., Howell, M.D., Cuperus, J.T., Li, D., Hansen, J.E., Alexander, A.L., Chapman, E.J., Fahlgren, N., Allen, E., and Carrington, J.C. (2008). Specificity of ARGONAUTE7-miR390 Interaction and Dual Functionality in TAS3 Trans-Acting siRNA Formation. Cell **133**: 128–141.

Morel, J., Godon, C., Mourrain, P., Feuerbach, F., and Proux, F. (2002). Fertile Hypomorphic. Plant Cell **14**: 629–639.

Morgan, D.O. (1997). CYCLIN-DEPENDENT KINASES : Engines , Clocks , and Microprocessors. Annu. Rev. Cell Dev. Biol. **13**: 261–291.

Moussian, B., Schoof, H., Haecker, A., Jürgens, G., and Laux, T. (1998). Role of the ZWILLE gene in the regulation of central shoot meristem cell fate during Arabidopsis embryogenesis. EMBO J. **17**: 1799–1809.

Musa, J., Aynaud, M.-M., Mirabeau, O., Delattre, O., and Grünewald, T.G. (2017). MYBL2 (B-Myb): a central regulator of cell proliferation, cell survival and differentiation involved in tumorigenesis. Cell Death Dis. **8**: e2895.

Nagata, T. and Kumagai, F. (1999). Plant cell biology through the window of the highly synchronized tobacco BY-2 cell line. Methods Cell Sci. **21**: 123–127.

Nagata, T., Nemoto, Y., and Hasezawa, S. (1992). Tobacco BY-2 Cell Line as the "HeLa" Cell in the Cell Biology of Higher Plants. International Review of Cytology.**132**: 1–30.

Nakayama, K. (2000). Targeted disruption of Skp2 results in accumulation of cyclin E and p27Kip1, polyploidy and centrosome overduplication. EMBO J. **19**: 2069–2081.

Napoli, C. (1990). Introduction of a Chimeric Chalcone Synthase Gene into Petunia Results in Reversible Co-Suppression of Homologous Genes in trans. Plant Cell Online **2**: 279–289.

Ness, S.A. (2003). Myb protein specificity: Evidence of a context-specific transcription factor code. Blood Cells, Mol. Dis. **31**: 192–200.

Nicolas, M. and Cubas, P. (2016). TCP factors: New kids on the signaling block. Curr. Opin. Plant Biol. **33**: 33–41.

Nieuwland, J., Menges, M., and Murray, J.A.H. (2007). The Plant Cyclins. Cell Cycle Control Plant Dev. **32**: 31–61.

Nishitani, H., Lygerou, Z., and Nishimoto, T. (2004). Proteolysis of DNA replication licensing factor Cdt1 in S-phase is performed independently of Geminin through its N-terminal region. J. Biol. Chem. **279**: 30807–30816.

Nodine, M.D. and Bartel, D.P. (2010). MicroRNAs prevent precocious gene expression and enable pattern formation during plant embryogenesis. Genes Dev. **24**: 2678–2692.

Noir, S., Marrocco, K., Masoud, K., Thomann, A., Gusti, A., Bitrian, M., Schnittger, A., and Genschik, P. (2015). The Control of *Arabidopsis thaliana* Growth by Cell Proliferation and Endoreplication Requires the F-Box Protein FBL17. Plant Cell **27**: 1461–1476.

Nowack, M.K., Grini, P.E., Jakoby, M.J., Lafos, M., Koncz, C., and Schnittger, A. (2006). A positive signal from the fertilization of the egg cell sets off endosperm proliferation in angiosperm embryogenesis. Nat. Genet. **38**: 63–67.

Nurse, P., Masui, Y., and Hartwell, L. (1998). Understanding the cell cycle. Nat. Med. **4**: 1103–1106.

Omidbakhshfard, M.A., Proost, S., Fujikura, U., and Mueller-roeber, B. (2015). Growth-Regulating Factors (GRFs): A Small Transcription Factor Family with Important Functions in Plant Biology. Mol. Plant **8**: 998–1010.

Onodera, Y., Haag, J.R., Ream, T., Nunes, P.C., Pontes, O., and Pikaard, C.S. (2005). Plant nuclear RNA polymerase IV mediates siRNA and DNA methylation- dependent heterochromatin formation. Cell **120**: 613–622.

Ori, N. et al. (2007). Regulation of LANCEOLATE by miR319 is required for compound-leaf development in tomato. Nat. Genet. **39**: 787–791.

Palatnik, J.F., Allen, E., Wu, X., Schommer, C., Schwab, R., Carrington, J.C., and Weigel, D. (2003). Control of leaf morphotgenesis by microRNAs. Nature **425**: 257–263.

Palatnik, J.F., Wollmann, H., Schommer, C., Schwab, R., Boisbouvier, J., Rodriguez, R., Warthmann, N., Allen, E., Dezulian, T., Huson, D., Carrington, J.C.C., and Weigel, D. (2007). Sequence and Expression Differences Underlie Functional Specialization of Arabidopsis MicroRNAs miR159 and miR319. Dev. Cell **13**: 115–125.

Pall, G.S., Codony-Servat, C., Byrne, J., Ritchie, L., and Hamilton, A. (2007). Carbodiimide-mediated cross-linking of RNA to nylon membranes improves the detection of siRNA, miRNA and piRNA by northern blot. Nucleic Acids Res. **35**: e60.

Pandey, R., Joshi, G., Bhardwaj, A.R., Agarwal, M., and Katiyar-Agarwal, S. (2014). A Comprehensive Genome-Wide Study on Tissue-Specific and Abiotic Stress-Specific miRNAs in Triticum aestivum. PLoS One **9**: e95800.

Park, J.E., Yi, H., Kim, Y., Chang, H., and Kim, V.N. (2016). Regulation of Poly(A) Tail and Translation during the Somatic Cell Cycle. Mol. Cell **62**: 462–471.

Pazhouhandeh, M., Dieterle, M., Marrocco, K., Lechner, E., Berry, B., Brault, V. r., Hemmer, O., Kretsch, T., Richards, K.E., Genschik, P., and Ziegler-Graff, V. r. (2006). F-box-like domain in the polerovirus protein P0 is required for silencing suppressor function. Proc. Natl. Acad. Sci. **103**: 1994–1999.

Peragine, A., Yoshikawa, M., Wu, G., Albrecht, H.L., and Poethig, R.S. (2004). SGS3 and SGS2/SDE1/RDR6 are required for juvenile development and the production of trans-acting siRNAs in Arabidopsis. Genes Dev. **3**: 2368–2379.

Peres, A. et al. (2007). Novel plant-specific cyclin-dependent kinase inhibitors induced by biotic and abiotic stresses. J. Biol. Chem. **282**: 25588–25596.

Perrot-Rechenmann, C. (2010). Cellular Responses to Auxin: Division versus Expansion. Cold Spring Harb. Perspect. Biol. **2**: a001446.

Pertea, M., Kim, D., Pertea, G.M., Leek, J.T., and Salzberg, S.L. (2016). Transcript-level expression analysis of RNA-seq experiments with HISAT , StringTie and Ballgown. Nat. Protoc. **11**: 1650–1667.

Peters, J.M. (2006). The anaphase promoting complex/cyclosome: A machine designed to destroy. Nat. Rev. Mol. Cell Biol. **7**: 644–656.

Petricka, J.J., Winter, C.M., and Benfey, P.N. (2012). Control of Arabidopsis Root Development. Annu. Rev. Plant Biol. **63**: 563–590.

Petroski, M.D. and Deshaies, R.J. (2005). Function and regulation of cullin-RING ubiquitin ligases. Nat. Rev. Mol. Cell Biol. **6**: 9–20.

Pines, J. and Hunter, T. (1991). Human cyclins A and B1 are differentially located in the cell and undergo cell cycle-dependent nuclear transport. J. Cell Biol. **115**: 1–17.

Pontes, O., Li, C.F., Nunes, P.C., Haag, J., Ream, T., Vitins, A., Jacobsen, S.E., and Pikaard, C.S. (2006). The Arabidopsis Chromatin-Modifying Nuclear siRNA Pathway Involves a Nucleolar RNA Processing Center. Cell **126**: 79–92.

Pontier, D., Yahubyan, G., Vega, D., Bulski, A., Saez-Vasquez, J., Hakimi, M.A., Lerbs-Mache, S., Colot, V., and Lagrange, T. (2005). Reinforcement of silencing at transposons and highly repeated sequences requires the concerted action of two distinct RNA polymerases IV in Arabidopsis. Genes Dev. **19**: 2030–2040.

Porceddua, A., De Veylder, L., Hayles, J., Van Montagu, M., Inze, D., and Mironov, V. (1999). Mutational analysis of two Arabidopsis thaliana cyclin-dependent kinases in fission yeast. Febs Lett. **446**: 182–188.

Poulsen, C., Vaucheret, H., and Brodersen, P. (2013). Lessons on RNA silencing mechanisms in plants from eukaryotic argonaute structures. Plant Cell **25**: 22–37.

del Pozo, J.C., Boniotti, M.B., and Gutierrez, C. (2002). Arabidopsis E2Fc Functions in Cell Division and Is Degraded by the Ubiquitin-SCF AtSKP2 Pathway in Response to Light. Society **14**: 3057–3071.

Protter, D.S.W. and Parker, R. (2016). Principles and Properties of Stress Granules. Trends Cell Biol. **26**: 668–679.

Provost, P., Silverstein, R.A., Dishart, D., Walfridsson, J., Djupedal, I., Kniola, B., Wright, A., Samuelsson, B., Radmark, O., and Ekwall, K. (2002). Dicer is required for chromosome segregation and gene silencing in fission yeast cells. Proc. Natl. Acad. Sci. **99**: 16648–16653.

Qi, H.H., Ongusaha, P.P., Myllyharju, J., Cheng, D., Pakkanen, O., Shi, Y., Lee, S.W., Peng, J., and Shi, Y. (2008). Prolyl 4-hydroxylation regulates Argonaute 2 stability. Nature **455**: 421–424.

Quévillon Huberdeau, M. et al. (2017). Phosphorylation of Argonaute proteins affects mRNA binding and is essential for microRNA-guided gene silencing *in vivo*. EMBO J. **36**: 2088–2106.

Rajagopalan, R., Vaucheret, H., Trejo, J., and Bartel, D.P. (2006). A diverse and evolutionarily fluid set of microRNAs in Arabidopsis thaliana. Genes Dev. **20**: 3407–3425.

Ralph, E., Boye, E., and Kearsey, S.E. (2006). DNA damage induces Cdt1 proteolysis in fission yeast through a pathway dependent on Cdt2 and Ddb1. EMBO Rep. **7**: 1134–1139.

Ramachandran, V. and Chen, X. (2008). Degradation of microRNAs by a family of exoribonucleases in Arabidopsis. Science . **321**: 1490–1492.

Ramirez-parra, E., Gutierrez, C., and Investigaciones, C.S. De (2008). Role of E2F transcription factors in plant cell physiology and development. **661**: 1–15.

Reitsma, J.M., Liu, X., Reichermeier, K.M., Moradian, A., Sweredoski, M.J., Hess, S., and Deshaies, R.J. (2017). Composition and Regulation of the Cellular Repertoire of SCF Ubiquitin Ligases. Cell **171**: 1326–1339.

Ren, G., Xie, M., Zhang, S., Vinovskis, C., Chen, X., and Yu, B. (2014). Methylation protects microRNAs from an AGO1-associated activity that uridylates 5' RNA fragments generated by AGO1 cleavage. Proc. Natl. Acad. Sci. **111**: 6365–6370.

Ren, H., Santner, A., Pozo, J.C. Del, Murray, J.A.H., and Estelle, M. (2008). Degradation of the cyclin-dependent kinase inhibitor KRP1 is regulated by two different ubiquitin E3 ligases. Plant J. **53**: 705–716.

Rhoades, M.W., Reinhart, B.J., Lim, L.P., Burge, C.B., Bartel, B., and Bartel, D.P. (2002). Prediction of Plant MicroRNA Targets. Cell **110**: 513–520.

Rissland, O.S., Hong, S.J., and Bartel, D.P. (2011). MicroRNA Destabilization Enables Dynamic Regulation of the miR-16 Family in Response to Cell-Cycle Changes. Mol. Cell **43**: 993–1004.

Rodriguez, R.E., Ercoli, M.F., Debernardi, J.M., Breakfield, N.W., Mecchia, M.A., Sabatini, M., Cools, T., De Veylder, L., Benfey, P.N., and Palatnik, J.F. (2015). MicroRNA miR396 Regulates the Switch between Stem Cells and Transit-Amplifying Cells in Arabidopsis Roots. Plant Cell **27**: 3354–3366.

Rodriguez, R.E., Mecchia, M. a, Debernardi, J.M., Schommer, C., Weigel, D., and Palatnik, J.F. (2010). Control of cell proliferation in Arabidopsis thaliana by microRNA miR396. Development **137**: 103–112.

Rogers, K. and Chen, X. (2013). Biogenesis, Turnover, and Mode of Action of Plant MicroRNAs. Plant Cell **25**: 2383–2399.

Roodbarkelari, F., Du, F., Truernit, E., and Laux, T. (2015). ZLL/AGO10 maintains shoot meristem stem cells during Arabidopsis embryogenesis by down-regulating ARF2-mediated auxin response. BMC Biol. **13**: 1–12.

Roy, A.L., Chakrabarti, D., Datta, B., Hileman, R.E., and Gupta, N.K. (1988). Natural mRNA is required for directing Met-tRNAf binding to 40S ribosomal subunits in animal cells: involvement of Co-eIF-2A in natural mRNA-directed initiation complex formation. Biochemistry **27**: 8203–8209.

Ru, P., Xu, L., Ma, H., and Huang, H. (2006). Plant fertility defects induced by the enhanced expression of microRNA 167. Cell Res. **16**: 457–465.

Rüdel, S. and Meister, G. (2008). Phosphorylation of Argonaute proteins: regulating gene regulators: Figure 1. Biochem. J. **413**: e7–e9.

Rüdel, S., Wang, Y., Lenobel, R., Körner, R., Hsiao, H.H., Urlaub, H., Patel, D., and Meister, G. (2011). Phosphorylation of human Argonaute proteins affects small RNA binding. Nucleic Acids Res. **39**: 2330–2343.

Rüegger, S. and Großhans, H. (2012). MicroRNA turnover: When, how, and why. Trends Biochem. Sci. **37**: 436–446.

Russo, a a, Jeffrey, P.D., and Pavletich, N.P. (1996). Structural basis of cyclin-dependent kinase activation by phosphorylation. Nat. Struct. Biol. **3**: 696–700.

Sachdeva, M., Zhu, S., Wu, F., Wu, H., Walia, V., Kumar, S., Elble, R., Watabe, K., and Mo, Y.-Y. (2009). p53 represses c-Myc through induction of the tumor suppressor miR-145. Proc. Natl. Acad. Sci. **106**: 3207–3212.

Sambrook, J., E. F. Fritsch, and T. Maniatis. (1989). Molecular cloning: a laboratory manual, 2nd ed. Cold Spring Harbor Laboratory, Cold Spring Harbor, N.Y.

Sansam, C.L., Shepard, J.L., Lai, K., Ianari, A., Danielian, P.S., Amsterdam, A., Hopkins, N., and Lees, J.A. (2006). DTL / CDT2 is essential for both CDT1 regulation and the early G2 / M checkpoint. Genes Dev. **20**: 3117–3129.

Santamaría, D., Barrière, C., Cerqueira, A., Hunt, S., Tardy, C., Newton, K., Cáceres, J.F., Dubus, P., Malumbres, M., and Barbacid, M. (2007). Cdk1 is sufficient to drive the mammalian cell cycle. Nature **448**: 811–815.

Sarkar, S., Dey, B.K., and Dutta, A. (2010). MiR-322/424 and -503 are induced during muscle differentiation and promote cell cycle quiescence and differentiation by down regulation of Cdc25A. Mol. Biol. Cell **21**: 2138–2149.

Sasaki, T., Shiohama, A., Minoshima, S., and Shimizu, N. (2003). Identification of eight members of the Argonaute family in the human genome. Genomics **82**: 323–330.

Satyanarayana, A., Berthet, C., Lopez-Molina, J., Coppola, V., Tessarollo, L., and Kaldis, P. (2008). Genetic substitution of Cdk1 by Cdk2 leads to embryonic lethality and loss of meiotic function of Cdk2. Development **135**: 3389–3400.

Scheer, H., Zuber, H., De Almeida, C., and Gagliardi, D. (2016). Uridylation Earmarks mRNAs for Degradation… and More. Trends Genet. **32**: 607–619.

Schimmel, P. (2018). RNA Processing and Modifications: The emerging complexity of the tRNA world: Mammalian tRNAs beyond protein synthesis. Nat. Rev. Mol. Cell Biol. **19**: 45–58.

Schirle, N.T. and MacRae, I.J. (2012). The Crystal Structure of Human Argonaute2. Science . **336**: 1037–1040.

Schmid, M., Davison, T.S., Henz, S.R., Pape, U.J., Demar, M., Vingron, M., Schölkopf, B., Weigel, D., and Lohmann, J.U. (2005). A gene expression map of Arabidopsis thaliana development. Nat. Genet. **37**: 501–506.

Schnittger, A., Weinl, C., Bouyer, D., Schobinger, U., and Hulskamp, M. (2003). Misexpression of the Cyclin-Dependent Kinase Inhibitor ICK1/KRP1 in Single-Celled Arabidopsis Trichomes Reduces Endoreduplication and Cell Size and Induces Cell Death. Plant Cell Online **15**: 303–315.

Schommer, C., Debernardi, J.M., Bresso, E.G., Rodriguez, R.E., and Palatnik, J.F. (2014). Repression of cell proliferation by miR319-regulated TCP4. Mol. Plant **7**: 1533–1544.

Schommer, C., Palatnik, J.F., Aggarwal, P., Chételat, A., Cubas, P., Farmer, E.E., Nath, U., and Weigel, D. (2008). Control of jasmonate biosynthesis and senescence by miR319 targets. PLoS Biol. **6**: 1991–2001.

Schubert, S., Horstmann, S., Bartusel, T., and Klempnauer, K.H. (2004). The cooperation of B-Myb with the coactivator p300 is orchestrated by cyclins A and D1. Oncogene **23**: 1392–1404.

De Schutter, K., Joubes, J., Cools, T., Verkest, A., Corellou, F., Babiychuk, E., Van Der Schueren, E., Beeckman, T., Kushnir, S., Inze, D., and De Veylder, L. (2007). Arabidopsis WEE1 Kinase Controls Cell Cycle Arrest in Response to Activation of the DNA Integrity Checkpoint. Plant Cell Online **19**: 211–225.

Schwartz, B.W., Yeung, E.C., and Meinke, D.W. (1994). Disruption of morphogenesis and transformation of the suspensor in abnormal suspensor mutants of Arabidopsis. Development **120**: 3235–3245.

Schwarz, D.S., Hutvágner, G., Du, T., Xu, Z., Aronin, N., and Zamore, P.D. (2003). Asymmetry in the assembly of the RNAi enzyme complex. Cell **115**: 199–208.

Seefried, W.F., Willmann, M.R., Clausen, R.L., and Jenik, P.D. (2014). Global Regulation of Embryonic Patterning in Arabidopsis by MicroRNAs. Plant Physiol. **165**: 670–687.

Sengupta, S. and Henry, R.W. (2015). Regulation of the retinoblastoma-E2F pathway by the ubiquitin-proteasome system. Biochim. Biophys. Acta - Gene Regul. Mech. **1849**: 1289–1297.

Serrano, M., Hannon, G.J., and Beach, D. (1993). A new regulatory motif in cell-cycle control causing specific inhibition of cyclin D/CDK4. Nature **366**: 704–707.

Shen, W.H. (2002). The plant E2F-Rb pathway and epigenetic control. Trends Plant Sci. **7**: 505–511.

Shigematsu, M. and Kirino, Y. (2015). tRNA-derived short non-coding RNA as interacting partners of argonaute proteins. Gene Regul. Syst. Bio. **9**: 27–33.

Shimotohno, A. (2004). The Plant-Specific Kinase CDKF;1 Is Involved in Activating Phosphorylation of Cyclin-Dependent Kinase-Activating Kinases in Arabidopsis. Plant Cell Online **16**: 2954–2966.

Sierro, N., Battey, J.N.D., Ouadi, S., Bakaher, N., Bovet, L., Willig, A., Goepfert, S., Peitsch, M.C., and Ivanov, N. V (2014). The tobacco genome sequence and its comparison with those of tomato and potato. Nat. Commun. **5**: 1-9.

Siwaszek, A., Ukleja, M., and Dziembowski, A. (2014). Proteins involved in the degradation of cytoplasmic mRNA in the major eukaryotic model systems. RNA Biol. **11**: 1122–1139.

Smith, L.M., Pontes, O., Searle, I., Yelina, N., Yousafzai, F.K., Herr, A.J., Pikaard, C.S., and Baulcombe, D.C. (2007). An SNF2 Protein Associated with Nuclear RNA Silencing and the Spread of a Silencing Signal between Cells in Arabidopsis. Plant Cell Online **19**: 1507–1521.

Sobala, A. and Hutvagner, G. (2013). Small RNAs derived from the 5′ end of tRNA can inhibit protein translation in human cells. RNA Biol. **10**: 553–563.

Sorin, C., Busell, J.D., Camus, I., Ljung, K., Kowalczyk, M., Geiss, G., McKhann, H., Garcion, C., Vaucheret, H., Sandberg, G., and Bellini, C. (2005). Auxin and Light Control of Adventitious Rooting in Arabidopsis Require ARGONAUTE1. Plant Cell **17**: 1343–1359.

Starostina, N.G. and Kipreos, E.T. (2012). Multiple degradation pathways regulate versatile CIP/KIP CDK inhibitors. Trends Cell Biol. **22**: 33–41.

Stahl, Y. and Simon, R. (2005). Plant stem cell niches. Int. J. Dev. Biol. **49**: 479–489.

Stevens, C. and La Thangue, N.B. (2003). E2F and cell cycle control: A double-edged sword. Arch. Biochem. Biophys. **412**: 157–169.

Stoica, C., Carmichael, J.B., Parker, H., Pare, J., and Hobman, T.C. (2006). Interactions between the RNA Interference Effector Protein Ago1 and 14-3-3 Proteins: consequences for cell cycle progression. J. Biol. Chem. **281**: 37646–37651.

Strausfeld, U., Labbé, J.C., Fesquet, D., Cavadore, J.C., Picard, A., Sadhu, K., Russell, P., and Dorée, M. (1991). Dephosphorylation and activation of a p34cdc2/cyclin B complex in vitro by human CDC25 protein. Nature **351**: 242–245.

Sunkar, R. and Zhu, J. (2004). Novel and Stress-Regulated MicroRNAs and Other Small RNAs from Arabidopsis. Plant Cell **16**: 2001–2019.

Tanaka, Y., Patestos, N.P., Maekawa, T., and Ishii, S. (1999). B-myb is required for inner cell mass formation at an early stage of development. J Biol Chem **274**: 28067–28070.

Tateishi, Y., Matsumoto, A., Kanie, T., Hara, E., Nakayama, K., and Nakayama, K.I. (2012). Development of mice without Cip/Kip CDK inhibitors. Biochem. Biophys. Res. Commun. **427**: 285–292.

Thompson, D.M., Lu, C., Green, P.J., Thompson, D.M., Lu, C., Green, P.J., and Parker, R.O.Y. (2008). tRNA cleavage is a conserved response to oxidative stress in eukaryotes tRNA cleavage is a conserved response to oxidative stress in eukaryotes. RNA **14**: 2095–2103.

Toyn, J.H. and Johnston, L.H. (1994). The Dbf2 and Dbf20 protein kinases of budding yeast are activated after the metaphase to anaphase cell cycle transition. EMBO J. **13**: 1103–1113.

Trcek, T., Larson, D.R., Moldón, A., Query, C.C., and Singer, R.H. (2011). Single-molecule mRNA decay measurements reveal promoter-regulated mRNA stability in yeast. Cell **147**: 1484–1497.

Tsunematsu, T., Arakaki, R., Yamada, A., Ishimaru, N., and Kudo, Y. (2015). The Non-Canonical Role of Aurora-A in DNA Replication. Front. Oncol. **5**: 1–7.

Tsutsui, T., Hesabi, B., Moons, D.S., Pandolfi, P.P., Hansel, K.S., Koff, A., and Kiyokawa, H. (1999). Targeted Disruption of CDK4 Delays Cell Cycle Entry with Enhanced p27 Kip1 Activity. Mol. Cell. Biol. **19**: 7011–7019.

Umeda, M., Shimotohno, A., and Yamaguchi, M. (2005). Control of cell division and transcription by cyclin-dependent kinase-activating kinases in plants. Plant Cell Physiol. **46**: 1437–1442.

Vashisht, D. and Nodine, M.D. (2014). MicroRNA functions in plant embryos. Biochem. Soc. Trans. **42**: 352–357.

Vaucheret, H. (2008). Plant ARGONAUTES. Trends Plant Sci. **13**: 350–358.

Vaucheret, H. (2006). Post-transcriptional small RNA pathways in plants: Mechanisms and regulations. Genes Dev. **20**: 759–771.

Vaucheret, H., Vazquez, F., Crété, P., and Bartel, D.P. (2004). The action of ARGONAUTE1 in the miRNA pathway and its regulation by the miRNA pathway are crucial for plant development. Genes Dev. **18**: 1187–1197.

Vazquez, F., Gasciolli, V., Crété, P., and Vaucheret, H. (2004). The nuclear dsRNA binding protein HYL1 is required for microRNA accumulation and plant development, but not posttranscriptional transgene silencing. Curr. Biol. **14**: 346–351.

Verkest, a, de O. Manes, C.-L.-, Vercruysse, S., Maes, S., van der Schueren, E., Beeckman, T., Genschik, P., Kuiper, M., Inze, D., and De Veylder, L. (2005). The Cyclin-Dependent Kinase Inhibitor KRP2 Controls the\nOnset of the Endoreduplication Cycle during Arabidopsis\nLeaf Development through Inhibition of Mitotic CDKA;1\nKinase Complexes W. Plant Cell **17**: 1723–1736.

De Veylder, L., Beeckman, T., and Inzé, D. (2007). The ins and outs of the plant cell cycle. Nat. Rev. Mol. Cell Biol. **8**: 655–665.

De Veylder, L., Joubès, J., and Inzé, D. (2003). Plant cell cycle transitions. Curr. Opin. Plant Biol. **6**: 536–543.

Vierstra, R.D. (2009). The ubiquitin-26S proteasome system at the nexus of plant biology. Nat. Rev. Mol. Cell Biol. **10**: 385–397.

Voinnet, O. (2009). Origin, Biogenesis, and Activity of Plant MicroRNAs. Cell **136**: 669–687.

Volpe, T. (2002). Regulation oh heterochromatic silencing and histone H3 Lysine-9 by RNAi. Science . **297**: 1833–1837.

Wang, F., Fu, X.D., Zhou, Y., and Zhang, Y. (2009). Down-regulation of the cyclin E1 oncogene expression by microRNA-16-1 induces cell cycle arrest in human cancer cells. BMB Rep **42**: 725–730.

Wang, H., Zhang, X., Liu, J., Kiba, T., Woo, J., Ojo, T., Hafner, M., Tuschl, T., Chua, N.-H., and Wang, X.-J. (2011). Deep sequencing of small RNAs specifically associated with Arabidopsis AGO1 and AGO4 uncovers new AGO functions. Plant J. **67**: 292–304.

Wang, J. and Guo, H. (2015). Cleavage of INDOLE-3-ACETIC ACID INDUCIBLE28 mRNA by MicroRNA847 Upregulates Auxin Signaling to Modulate Cell Proliferation and Lateral Organ Growth in Arabidopsis. Plant Cell **27**: 574–590.

Wang, J., Wang, L., Mao, Y., Cai, W., Xue, H., and Chen, X. (2005). Control of Root Cap Formation by MicroRNA-Targeted Auxin Response Factors in Arabidopsis. Plant Cell **17**: 2204–2216.

Wang, L., Yu, X., Wang, H., Lu, Y.-Z., de Ruiter, M., Prins, M., and He, Y.-K. (2011). A novel class of heat-responsive small RNAs derived from the chloroplast genome of Chinese cabbage (Brassica rapa). BMC Genomics **12**: 289–303.

Wang, X., Arai, S., Song, X., Reichart, D., Du, K., Pascual, G., Tempst, P., Rosenfeld, M.G., Glass, C.K., and Kurokawa, R. (2008). Induced ncRNAs allosterically modify RNA-binding proteins in cis to inhibit transcription. Nature **454**: 126–130.

Wapinski, O. and Chang, H.Y. (2011). Long noncoding RNAs and human disease. Trends Cell Biol. **21**: 354–361.

Wei, W., Ba, Z., Gao, M., Wu, Y., Ma, Y., Amiard, S., White, C.I., Danielsen, J.M.R., Yang, Y.G., and Qi, Y. (2012). A role for small RNAs in DNA double-strand break repair. Cell **149**: 101–112.

Weigel, D. et al. (2000). Activation Tagging in Arabidopsis 1. Plant Physiol. **122**: 1003–1013.

Weill, L., Belloc, E., Bava, F.A., and Méndez, R. (2012). Translational control by changes in poly(A) tail length: Recycling mRNAs. Nat. Struct. Mol. Biol. **19**: 577–585.

Westholm, J.O. and Lai, E.C. (2011). Mirtrons: MicroRNA biogenesis via splicing. Biochimie **93**: 1897–1904.

Wu, M.-F., Tian, Q., and Reed, J.W. (2006). Arabidopsis microRNA167 controls patterns of ARF6 and ARF8 expression, and regulates both female and male reproduction. Development **133**: 4211–4218.

Xie, Z., Allen, E., Wilken, A., and Carrington, J.C. (2005). DICER-LIKE 4 functions in trans-acting small interfering RNA biogenesis and vegetative phase change in Arabidopsis thaliana. Proc. Natl. Acad. Sci. **102**: 12984–12989.

Xie, Z., Johansen, L.K., Gustafson, A.M., Kasschau, K.D., Lellis, A.D., Zilberman, D., Jacobsen, S.E., and Carrington, J.C. (2004). Genetic and functional diversification of small RNA pathways

in plants. PLoS Biol. **2**: 642–652.

Xue, T., Liu, Z., Dai, X., and Xiang, F. (2017). Primary root growth in Arabidopsis thaliana is inhibited by the miR159 mediated repression of MYB33, MYB65 and MYB101. Plant Sci. **262**: 182–189.

Yang, L., Liu, Z., Lu, F., Dong, A., and Huang, H. (2006). SERRATE is a novel nuclear regulator in primary microRNA processing in Arabidopsis. Plant J. **47**: 841–850.

Yang, L., Wu, G., and Poethig, R.S. (2012). Mutations in the GW-repeat protein SUO reveal a developmental function for microRNA-mediated translational repression in Arabidopsis. Proc. Natl. Acad. Sci. **109**: 315–320.

Yang, Z., Ebright, Y.W., Yu, B., and Chen, X. (2006). HEN1 recognizes 21-24 nt small RNA duplexes and deposits a methyl group onto the 2′ OH of the 3′ terminal nucleotide. Nucleic Acids Res. **34**: 667–675.

Yap, K.L., Li, S., Muñoz-cabello, A.M., Raguz, S., Zeng, L., Gil, J., Walsh, M.J., and Zhou, M. (2011). Molecular interplay of the non-coding RNA ANRIL and methylated Histone H3 lysine K27 by Polycomb CBX7 in transcriptional silencing of INK4a. Mol. Cell **38**: 662–674.

Ye, X. (2001). A premature-termination mutation in the Mus musculus cyclin-dependent kinase 3 gene. Proc. Natl. Acad. Sci. **98**: 1682–1686.

Yi, D. et al. (2014). The Arabidopsis SIAMESE-RELATED Cyclin-Dependent Kinase Inhibitors SMR5 and SMR7 Regulate the DNA Damage Checkpoint in Response to Reactive Oxygen Species. Plant Cell **26**: 296–309.

Yi, R., Qin, Y., Macara, I.G., and Cullen, B.R. (2003). Exportin-5 mediates the nuclear export of pre-microRNAs and short hairpin RNAs. Genes Dev. **17**: 3011–3016.

Yin, K., Ueda, M., Takagi, H., Kajihara, T., Aki, S.S., Nobusawa, T., Umeda-Hara, C., and Umeda, M. (2014). A dual-color marker system for in vivo Visualization of cell cycle progression in Arabidopsis. Plant J. **80**: 541–552.

Yoshikawa, M. (2013). Biogenesis of trans-acting siRNAs, endogenous secondary siRNAs in plants. Genes Genet. Syst. **88**: 77–84.

Yoshikawa, M., Iki, T., Tsutsui, Y., Miyashita, K., Poethig, R.S., Habu, Y., and Ishikawa, M. (2013). 3’ fragment of miR173-programmed RISC-cleaved RNA is protected from degradation in a complex with RISC and SGS3. Proc. Natl. Acad. Sci. **110**: 4117–4122.

Yu, Y. et al. (2017). ARGONAUTE10 promotes the degradation of miR165/6 through the SDN1 and SDN2 exonucleases in Arabidopsis. PLoS Biol. **15**: 1–26.

Zeng, Y., Sankala, H., Zhang, X., and Graves, P.R. (2008). Phosphorylation of Argonaute 2 at serine-387 facilitates its localization to processing bodies. Biochem. J. **413**: 429–436.

Zhai, J., Arikit, S., Simon, S.A., Kingham, B.F., and Meyers, B.C. (2014). Rapid construction of parallel analysis of RNA end (PARE) libraries for Illumina sequencing. Methods **67**: 84–90.

Zhang, C., Xian, Z., Huang, W., and Li, Z. (2015). Evidence for the biological function of miR403 in tomato development. Sci. Hortic. (Amsterdam). **197**: 619–626.

Zhang, X., Zhao, H., Gao, S., Wang, W.C., Katiyar-Agarwal, S., Huang, H. Da, Raikhel, N., and Jin, H. (2011a). Arabidopsis Argonaute 2 Regulates Innate Immunity via miRNA393*-Mediated Silencing of a Golgi-Localized SNARE Gene, MEMB12. Mol. Cell **42**: 356–366.

Zhang, Z., Zou, J., Wang, G.K., Zhang, J.T., Huang, S., Qin, Y.W., and Jing, Q. (2011b). Uracils at nucleotide position 9-11 are required for the rapid turnover of miR-29 family. Nucleic Acids Res. **39**: 4387–4395.

Zhao, Y., Yu, Y., Zhai, J., Ramachandran, V., Dinh, T.T., Meyers, B.C., Mo, B., and Chen, X. (2012). The arabidopsis nucleotidyl transferase HESO1 uridylates unmethylated small RNAs to trigger their degradation. Curr. Biol. **22**: 689–694.

Zheng, B., Chen, X., and McCormick, S. (2011). The Anaphase-Promoting Complex Is a Dual Integrator That Regulates Both MicroRNA-Mediated Transcriptional Regulation of Cyclin B1 and Degradation of Cyclin B1 during Arabidopsis Male Gametophyte Development. Plant Cell **23**: 1033–1046.

Zhu, H., Hu, F., Wang, R., Zhou, X., Sze, S.H., Liou, L.W., Barefoot, A., Dickman, M., and Zhang, X. (2011a). Arabidopsis Argonaute 10 specifically sequesters miR166/165 to regulate shoot apical meristem development. Cell **145**: 242–256.

Zhu, H., Hu, F., Wang, R., Zhou, X., Sze, S.H., Liou, L.W., Barefoot, A., Dickman, M., and Zhang, X. (2011b). Arabidopsis argonaute10 specifically sequesters miR166/165 to regulate shoot apical meristem development. Cell **145**: 242–256.

Zou, C., Zhang, Z., Wu, S., and Osterman, J.C. (1998). Molecular cloning and characterization of a rabbit eIF2C protein. Gene **211**: 187–194.

Zur, A. and Brandeis, M. (2001). Securin degradation is mediated by fzy and fzr, and is required for complete chromatid separation but not for cytokinesis. EMBO J. **20**: 792–801.

La première partie de l'introduction traitant des différentes voies de régulation du cycle cellulaires chez les eucaryotes est traduite en français dans la section suivante

Introduction

A. Le cycle cellulaire chez les eucaryotes

1. Principes généraux du cycle cellulaire

Le cycle cellulaire est un processus biologique au cours duquel une cellule mère donne naissance à deux cellules filles génétiquement identiques. Au cours de ce processus, les composants cellulaires, y compris le génome, sont d'abord dupliqués, puis répartis dans les deux cellules nouvellement formées. Le cycle cellulaire est fondamental, car il est impliqué dans la reproduction végétative des organismes unicellulaires, mais aussi dans l'organogenèse et la reproduction sexuée chez les eucaryotes supérieurs.

La recherche sur le cycle cellulaire a débuté au cours du 19e siècle. En 1855, l'Allemand Rudolf Virchow fut le premier à affirmer "qu'une cellule provient d'une autre cellule". Par la suite, les chercheurs ont décrit en détail l'aspect cytologique de la division cellulaire (Nurse et al., 1998). Cependant, notre compréhension mécanistique de la régulation du cycle cellulaire n'a explosé que dans les années 80, avec le développement de la biologie moléculaire. Les travaux de Paul Nurse, Leland Hartwell et Tim Hunt sur les gènes du cycle cellulaire chez la levure et l'humain ont été récompensés par un prix Nobel en médecine et physiologie en 2001.

Le cycle cellulaire consiste en quatre phase successives (Figure 1). Le génome est d'abord dupliqué pendant la phase de synthèse de l'ADN (S). Les deux copies du génome sont ensuite séparées pendant la mitose (M). Entre ces deux événements principaux, il y a deux phases de latence appelées gap 1 et 2 (G1 et G2) où les cellules contrôlent le bon déroulement de la phase précédente et préparent l'ensemble des composants nécessaires pour la transition vers la phase suivante. La phase M du cycle cellulaire peut elle-même être subdivisée en quatre étapes : la prophase, la métaphase, l'anaphase et la télophase (Figure 2). Pendant la prophase, l'ADN est condensé en chromosomes fortement enroulés, l'enveloppe nucléaire se désintègre et le fuseau

mitotique commence à se former dans le cytoplasme. En métaphase, les chromosomes atteignent le plan de division (ou plan équatorial) et s'attachent au fuseau mitotique par des régions spécifiques des chromatides, appelées kinétochores. Une fois appariées aux fibres des microtubules du fuseau mitotique, les chromatides sœurs sont séparées et migrent dans des directions opposées pendant l'anaphase. Enfin, la télophase consiste en la réformation de l'enveloppe nucléaire et des organites nucléaires, et en la décondensation de la chromatine. La télophase se produit en même temps que la scission du compartiment cellulaire, ou cytocinèse. Dans les cellules animales, la cytocinèse implique un anneau contractile de filaments d'actine. En revanche, les cellules végétales sont recouvertes d'une paroi cellulaire, leur conférant de la rigidité et, par conséquent, empêche la division d'une manière similaire. En lieu et place, la cytocinèse chez les plantes nécessite un transport actif de composants cellulaires vers la plaque équatoriale. Ceci est réalisé par une structure composée de microtubules, le phragmoplaste, qui est chargé de guider les composants de la paroi cellulaire vers le plan de division par le biais de vésicules Golgiennes (Figure 1).

Le contrôle et la synchronisation des processus qui constituent le cycle cellulaire est essentiel pour tous les organismes. Chez l'animal, la mauvaise régulation de la division cellulaire entraîne une prolifération cellulaire anormale et peut induire le développement de tumeurs. Les plantes se distinguent des animaux par le fait que l'embryogenèse se produit principalement de manière post-embryonnaire. De plus, les plantes sont des organismes sessiles. Par conséquent, ils doivent adapter leur croissance pour faire face à de nombreuses contraintes, telles que la disponibilité des ressources, les conditions environnementales et les attaques de pathogènes. En ce sens, le cycle cellulaire doit être étroitement régulé pendant toute la durée de vie de la plante, et ceci est accompli par un ensemble de gènes essentiels appelés «core cell cycle genes» Le chapitre suivant vise à donner un aperçu des voies de régulation du cycle cellulaire chez les eucaryotes, et en particulier sur les plantes.

2. Régulation du cycle cellulaire

Les preuves de l'existence d'une régulation moléculaire de la prolifération cellulaire ont été découvertes pour la première fois dans oocytes de Xenopes (Masui et Markert, 1971). En effet, le traitement d'oocytes avec un extrait cellulaire d'oocytes traités à la progestérone est suffisant pour stimuler l'entrée en méiose, suggérant l'existence d'un "facteur cytosolique de

maturation/de promotion de la mitose" (MPF). Ce MPF a ensuite été identifié chez *Schizosaccharomyces pombe* et caractérisé comme un hétérodimère contenant la kinase CDC2 (CELL CYCLE CONTROL 2) et une cycline associée (Gautier et al., 1988, 1990), deux acteurs essentiels du cycle cellulaire qui seront décrit plus loin dans ce manuscrit.

a. Les CDK pilotent la progression dans le cycle cellulaire

Les kinases cycline-dépendantes (CDK) sont des kinases à sérine-thréonine qui nécessitent une association avec des sous-unités activatrices appelées cyclines (CYCs) pour leur activité enzymatique (Malumbres, 2014). On trouve des CDK chez tous les eucaryotes, y compris *Saccharomyces cerevisiae* (CDC28, PHO85, KIN28, SRB10, BUR1, CTK1), *Schizosaccharomyces pombe* (CDC2), Human (CDK1-20) et plantes (CDKA-G). Les CDK sont classés en deux groupes : ils participent à la régulation du cycle cellulaire ou à la régulation transcriptionnelle (Malumbres, 2014 ; Joubès et al., 2000). Bien que le niveau d'accumulation des CDK reste globalement constant dans les tissus prolifératifs, leur activité doit être modulée au cours des différentes phases du cycle cellulaire. Cette modulation est apportée par l'interaction avec des cyclines qui, contrairement aux CDK, sont exprimées et dégradées à des moments précis du cycle cellulaire. Ainsi, différents complexes CDK/CYC se forment au cours du cycle cellulaire, et ont une affinité pour une grande variété de substrats. Ceci permet donc l'activation séquentielle de processus moléculaires tels que la transcription des gènes du cycle cellulaire, la réplication de l'ADN, la réparation de l'ADN, la compaction de la chromatine, le réarrangement cytosquelette et le montage du fuseau mitotique (Chi et al, 2008 ; Holt et al, 2010 ; Anders et al, 2011).

b. Diversité et fonctions des complexes eucaryotes CDK/Cyclines

Les CDK eucaryotiques

Parmi les vingt CDK humaines, seuls les CDK1, 2, 3, 4 et 6 favorisent les transitions du cycle cellulaire (Malumbres, 2014). Ces CDK sont classés en deux sous-familles : les groupes CDK1-2-3 et CDK4-6 (figure 3). CDK1 est capable de se lier à tous les cyclines en l'absence d'autres

CDK et est suffisant pour conduire une activité minimale du cycle cellulaire aux premiers stades de l'embryogenèse (Santamaría et al., 2007). De plus, la mutation *cdk1-/-* ou la substitution de CDK1 par CDK2 entraîne une létalité embryonnaire, indiquant que le CDK1 est essentiel à la division cellulaire (Santamaría et al., 2007 ; Satyanarayana et al., 2008). Il est intéressant de noter que les mutations *cdk2, 3, 4* et *6* montrent des interactions génétiques. Les souris *cdk2-/- -, cdk4-/- et cdk6-/-* se développent normalement (Berthet et al., 2003 ; Ye, 2001 ; Tsutsui et al., 1999 ; Malumbres et al., 2004) et présentent seulement des phénotypes dans certains types cellulaires hautement spécialisés. Cependant, les doubles mutants *cdk2-/- ; cdk4-/- et cdk4-/- ; cdk6-/-* sont des mutants embryo-létaux, ce qui suggère une redondance, au moins partielle, des fonctions des CDK (Berthet et al., 2006 ; Malumbres et al., 2004).

Les CDK de plantes sont divisés en huit classes : CDKA à G (figure 3). Le génome d'*Arabidopsis thaliana* code une CDKA unique (CDKA1;1), quatre CDKB (CDKB1;1-2 et CDKB2;1-2), deux CDKC (CDKC;1-2), trois CDKD (CDKD;1-3), trois CDKE (CDKE;1-3), un CDKF (CDKF;1) et deux CDKG (CDKG;1-2) (Gutierrez, 2009 ; Van Leene et al., 2010). Les CDK de type A ont en commun un motif conservé PSTAIRE de liaison aux cyclines que l'on trouve également chez les CDK de levures CDC2/CDC28 et dans les CDK1, 2 et 3 humaines (De Veylder et al., 2003, 2007). Les CDKB sont des CDK spécifiques à la plante qui possèdent des motifs PPTALRE et PS/PTTLRE (pour les CDKB1 et CDKB2, respectivement) (De Veylder et al., 2003, 2007). CDKA est nécessaire pour le cycle cellulaire chez les plantes. En effet, la perte de CDKA affecte le développement du pollen et induit une létalité embryonnaire (Iwakawa et al., 2006 ; Nowack et al., 2006). De plus, CKDA1 ; mais pas CDKB est capable de complémenter les mutants *de S. cerevisiae cdc28-/-* et *S. pombe cdc2-/-*, indiquant que CDKA1 partage des fonctions communes avec ses homologues de levure (Ferreira et al., 1991 ; Porceddua et al., 1999). Contrairement aux CDKA, la perte de la fonction de CDKB1;1 n'affecte pas la progression au cours du cycle cellulaire et les mutants parviennent à se développer normalement. Cependant, le mutant cdkb1;1 montre un nombre de cellules plus important et ces dernieres sont de plus grande taille, indiquant une augmentation du niveau de ploïdie comparativement aux plantes sauvages (Boudolf et al., 2016). Ce mutant est également affecté dans la division des cellules stomatales (Boudolf et al., 2016). De plus, les mutants *cdkb2;1* d'.Arabidopsis présentent une altération de l'organisation du méristème apical (Andersen et al., 2008). Bien que les fonctions des CDK de type B ne soient pas encore claires, ces résultats suggèrent qu'elles sont impliquées dans des processus spécifiques aux développement des plantes. Dans une moindre mesure, les CDKD et les CDKF1 jouent

également un rôle dans le cycle cellulaire en activant d'autres CDK (Shimotohno, 2004 ; Umeda et al., 2005). Cette fonction sera abordée plus loin dans un chapitre dédié.

Les cyclines

Le terme "cycline" désigne l'instabilité de ces protéines. La découverte des premières cyclines a été faite dans des œufs d'oursins, où les chercheurs ont mis en évidence la dégradation de cette protéine pendant la division cellulaire (Evans et al., 1983). Les cyclines se caractérisent par la présence de deux domaines communs : la cyclin box qui est nécessaire à l'activation CDK et qui détermine la spécificité du substrat, et la destruction box (D-box), nécessaire à leur protéolyse (Glotzer et al., 1991 ; Horton et Templeton, 1997). Les cyclines eucaryotiques sont classées en deux groupes : les cyclines mitotiques, qui comprennent les cyclines de type A et B, et les cyclines interphasiques, comprenant les cyclines de type C, D et E. Ces différentes cyclines présentent des profils d'accumulation spécifiques au cours du cycle cellulaire, inhérents à leurs fonctions (Figure 4). Les CYCD s'accumulent dès le début de la phase G1 puis les CYCE pendant la transition G1-S. Les cyclines mitotiques commencent à s'accumuler pendant G2 et atteignent un pic durant la mitose. Cependant, les CYCA sont dégradées en prophase tandis que les CYCB sont dégradées plus tard lors de la sortie de mitose (examiné dans Genschik et al., 2014).

Chez les plantes, les cyclines constituent une grande famille de proteines, composée de plus de 50 membres, réparties en neuf classes. Arabidopsis compte 10 CYCA (CYCA1;1-2, CYCA2;1-4 et CYCA3;1-4), 11 CYCB (CYCB1;1-5, CYCB2;1-5 et CYCB3 ;1) et 10 CYCD (CYCD1;1, CYCD2, CYCD3;1-3, CYCD4;1, CYCD4;2, CYCD5;1, CYCD6;1 et CYCD7;1) (Nieuwland et al., 2007). Comme leurs homologues humains, la fonction de ces cyclines de plantes a été en grande partie caractérisés. D'autres classes de cyclines ont également été identifiées, notamment CYCC, CYCH, CYCL, CYCP, CYCT, CYCT et SDS (SOLO DANCERS) (Nieuwland et al., 2007 ; Van Leene et al., 2011). Cependant, leurs fonctions doivent encore faire l'objet d'une étude plus approfondie pour la plupart d'entre eux.

c. Régulation de l'activité du CDK

Activation des CDK par les cyclines

D'un point de vue structurel, la poche de liaison à l' ATP des CDK est localisée dans un sillon entre les lobes N-terminal et C-terminal. En l'absence de cyclines, un motif « helix-loop » appelée boucle d'activation ou « T-loop » interfère avec ce domaine (De Bondt et al., 1993 ; Morgan, 1997) (Figure 5). Dans cette configuration, la CDK ne peux pas se lier aux substrats et un mauvais positionnement de la molécule d'ATP empêche le transfert du groupe phosphate, conduisant a une CDK inactive. Lors de l'interaction CDK/CYC, la T-loop est transloquée et l'activité CDK est promue. Non seulement les cyclines activent les CDK, mais elles fournissent aussi des motifs supplémentaires nécessaires à la relocalisation des CDK dans le noyau (Brown et al., 1999 ; Pines et Hunter, 1991) ou à la reconnaissance du substrat, conditionnant ainsi la spécificité des CDK, du moins en partie.

Modifications post-traductionnelles des CDK

Bien que la liaison avec les cyclines soit suffisante pour activer les CDK, elles nécessitent toutefois d'être phosphorylées pour être pleinement fonctionnelles. Il a été démontré que la phosphorylation du résidu Thr160 de la CDK2 humaine ou Thr161 de CDC2 de levure, qui se trouve à l'intérieur de la T-loop, améliore l'affinité de certaines paires CDK/CYC (Ducommun et al., 1991 ; Desai et al., 1995 ; Russo et al., 1996) (Figure 5). Les enzymes qui catalysent cette phosphorylation sont appelées "CDK-activating kinases" (CAK). Les CAK ont été identifiés comme étant des dimères liés aux CDK/CYC : MOP1/MCS2 et CDK7/CYC-H, respectivement chez la levure et chez l'homme (Fesquet et al., 1993 ; Fisher et Morgan, 1994 ; Damagnez et al., 1995). Chez Arabidopsis thaliana, quatre CAK ont été identifiés : CDKF;1^{CAK1At}, CDKD;3^{CAK2At}, CDKD;1^{CAK3At} et CDKD;2^{CAK4At} (Shimotohno, 2004 ; Umeda et al., 2005). Bien que les CDKD soient apparentés à la CDK7 humaine, la fonction CDKF, quant à elle, ne dépend pas de la liaison avec CYC-H et est spécifique aux plantes.

Outre le rôle de la phosphorylation dans l'activation des CDK, les CDK peuvent être inhibées par des modifications post-traductionnelles. La phosphorylation des résidus Thr14/Tyr15 de CDK1 humaine par les kinases WEE1 et MYT1 inhibe à la fois la fixation de l'ATP et la liaison du substrat à la kinase, empêchant ainsi l'entrée en mitose (Berry et Gould, 1996 ; Booher et al., 1997) (Figure 5). La kinase WEE1 d'Arabidopsis, ainsi que les kinases humaines WEE1/MYT1 ont été décrites comme contrôlant la transition G2/M et sont chargées d'induire l'arrêt du cycle cellulaire lors de la détection de dommages à l'ADN (De Schutter et al., 2007) (Figure 5). La déphosphorylation de ces résidus est nécessaire pour l'entrée dans la mitose. Ce processus est réalisé par les phosphatases CDC25A, B et C chez l'homme (Strausfeld et al., 1991 ; Morgan, 1997). Il est intéressant de noter que les plantes semblent ne pas avoir de fonction CDC25 et que la façon dont l'inhibition par WEE1 est libérée pendant la mitose est encore matière à débats (Boudolf et al., 2006).

Les Inhibiteurs de CDK/Cyclines (CKI)

Outre la phosphorylation, l'inhibition de l'activité CDK est également médiée par les protéines de liaison au CDK que sont les inhibiteurs CDK (CKI). Chez l'homme, deux familles distinctes de CKI existent : les protéines KIP/CIP (KINASE INHIBITORY PROTEIN / CDK INHIBITORY PROTREIN) et INK4 (INHIBITOR OF CDK4/6) (Besson et al., 2008). Les CKI appartenant à la famille des INK4 ($p16^{INK4a}$, $p15^{INK4b}$, $p18^{INK4c}$, $p19^{INK4d}$) se lient uniquement aux CDK4 et 6 et bloquent l'interaction avec les cyclines de type D (Serrano et al., 1993 ; Hirai et al., 1995) (Figure 6). Les CKI de la famille KIP/CIP ($p21^{CIP1}$, $p27^{KIP1}$, $p57^{KIP2}$) inhibent l'activité des CDK-D, A, E et B en se liant aux complexes CDK/CYC (Besson et al., 2008) (Figure 6). Bien que les modes d'action des CKI soient similaires, leur fonction est spécifique à certains contextes biologiques (Cánepa et al., 2007). Ainsi, les protéines INK4 sont impliquées dans la sénescence cellulaire, l'apoptose et la réparation de l'ADN (Cánepa et al., 2007). p21 est exprimé en réponse aux dommages à l'ADN et induit l'arrêt du cycle cellulaire pendant les phases de gap. p27 est impliqué dans l'arrêt du cycle cellulaire en conditions normales. En plus de p27, p57 est également un gène essentiel pendant l'embryogenèse chez la souris, et est requis pour le bon déroulement de la différentiation cellulaire de l'embryon (Tateishi et al., 2012).

Chez Arabidopsis, 21 CKI sont présents, et sont répartis en deux groupes. La famille KRP/ICK (KIP-RELATED PROTEIN/INHIBITOR OF CDC2 KINASE) est composée de sept membres. Ce sont des orthologues de KIP/CIP humaines (Kumar et Larkin, 2017), et ils présentent un niveau élevé de redondance fonctionnelle avec ces derniers. L'autre famille, la SIM/SMR (SIAMESE/SIAMESE-RELATED) compte 14 membres (SIM et SMR1-13) (Kumar et Larkin, 2017). Ils sont spécifiques aux plantes et ne partagent aucune homologie avec les autres CKI eucaryotiques. Comme chez les animaux, les CKI de plantes jouent des fonctions distinctes sur la croissance et le développement des plantes, principalement en raison des différences dans leurs modes d'expression (Kumar et al., 2015).Par exemples, il a été démontré que les KRP stimulent l'endoreduplication en bloquant la mitose (Verkest et al., 2005), et induisent même l'arrêt du cycle cellulaire et la mort cellulaire lorsqu'ils sont fortement exprimés (Schnittger et al., 2003). Il est intéressant de noter que plusieurs membres de la famille des SIM/SMR sont transcriptionnellement activés en réponse au stress, ce qui conduit à l'hypothèse que les SMR pourraient être impliqués dans l'intégration des signaux environnementaux pour le contrôle du cycle cellulaire (Peres et al, 2007 ; Yi et al, 2014 ; Kumar et Larkin, 2017). Par exemple, les stress oxydatif, ou les traitements à l'hydroxyurée, provoquant la production d'espèces réactives d'oxygène (ROS), induisent la transcription SMR4, SMR5 et SMR7. De plus, les mutants smr5 et smr7 sont plus tolérants aux traitements à l'hydroxyurée (Yi et al., 2014). Plus récemment, il a été démontré que, sous une sécheresse modérée, la transcription SMR1est activée, que la protéine SMR1 s'accumule et que les mutants smr1 sont moins sensibles à l'inhibition de la croissance des jeunes feuilles (Dubois et al., 2018).

d. La dégradation sélective des composants du cycle cellulaire

Pour orchestrer la progression a travers les differentes phases du cycle cellulaire, les cellules ont besoin non seulement de synthétiser des régulateurs spécifiques du cycle cellulaire, mais aussi de les dégrader de manière rapide et sélective à un moment précis. Ce processus nécessite l'activité de l' « ubiquitin proteasome system » (UPS) (Mocciaro et Rape, 2012 ; Genschik et al., 2014) qui est basé sur des enzymes appelées E3 ubiquitine-ligases (E3s). Les ligases E3, pouvant être sois monomérique, sois un complexe, catalyse la fixation covalente et/ou la polymérisation d'un petit peptide de 76 acides aminés appelé ubiquitine sur les résidus lysine du substrat. L'ubiquitination est une modification post-traductionnelle qui, selon la topologie

de la chaîne de l'ubiquitine, intervient dans la réparation de l'ADN, le remodelage de la chromatine, la signalisation, le trafic cellulaire ou la protéolyse ubiquitine-dépendante (Ciechanover et al., 2000 ; Kwon et Ciechanover, 2017). Le mécanisme de transfert de l'ubiquitine à un substrat nécessite trois étapes différentes (Figure 7) (Ciechanover et al., 2000 ; Vierstra, 2009 ; Callis, 2014). L'ubiquitine est d'abord adénylée en position C-terminale par l'enzyme activatrice E1 et transférée sur un résidu cystéine de E1. Il est ensuite transféré dans un résidu cystéine d'une enzyme E2 dite de « conjugaison ». Selon le type de E3, l'E2 couplée à l'ubiquitine peut soit se lier à l'E3 et l'ubiquitine être directement conjuguée au substrat, soit être d'abord transférée à un résidu cystéine sur l'E3, qui sera ensuite chargé de l'ubiquitination du substrat, entraînant sa dégradation par le protéasome 26S. La protéolyse au cours du cycle cellulaire implique quatre classes d'E3 ligases : les SCF (SKP1/Cullin1/F-box), le complexe APC/C (Anaphase promoting complex/cyclosome), les RING monomériques et CRL4-CDT2 (Mocciaro et Rape, 2012 ; Genschik et al, 2014) (Figure 8).

Les complexes SCF

Les complexes SCF sont assemblés autour de la protéine CUL1 (CULLIN 1) (Petroski et Deshaies, 2005). CUL1 ancre le module catalytique, composé de RBX1 (RING-BOX 1) et de E2, et le module de reconnaissance de substrat, comprenant à la fois SKP1 (appelé ASK1-2 chez Arabidopsis, pour ARABIDOPSIS SKP1 HOMOLOGUE 1/2) et une protéine F-box. Les protéines F-box sont des protéines adaptatrices qui assurent la spécificité du substrat (Kipreos et Pagano, 2000 ; Lechner et al, 2006 ; Reitsma et al, 2017). Chez l'animal, le SCF^{SKP2} (S-PHASE KINASE ASSOCIATED PROTEIN 2) joue un rôle dans le contrôle de la transition G1/S et la sortie de la phase S (Figure 9). Il participe notamment à l'ubiquitination des CKI tels que $p21^{CIP1}$ et $p27^{KIP1}$ (Nakayama, 2000 ; Starostina et Kipreos, 2012), favorisant ainsi la ré-entrée dans le cycle cellulaire, mais aussi à l'ubiquitination des composants spécifiques de la phase S, tels que les cyclines E, les facteurs de transcription E2Fs, et CDT1 (Nakayama, 2000 ; Marti et al., 1999 ; Li et al., 2003. La dégradation de ces proteins conduit à la répression transcriptionnelle des gènes en phase S et à l'arrêt de la réplication. Les souris mutantes *skp2* homozygotes sont plus petites mais toujours viables (Nakayama, 2000). Cependant, les cellules prolifèrent à un rythme plus faible. Un niveau plus élevé de polyploïdie et une augmentation de la mort cellulaire sont également observables chez ces mutants, suggérant que, même si SKP2

n'est pas crucial pour la progression du cycle cellulaire, il est impliqué dans le contrôle de la duplication chromosomique. Deux homologues de SKP2, SKP2a et SKP2b, ont été identifiés chez Arabidopsis (del Pozo et al., 2002). Bien qu'il ait été démontré que le SKP2a est impliqué dans la dégradation de E2Fc/DPb, il a été proposé que SKP2b cible les KRP (Ren et al., 2008). La double mutation *skp2a/skp2b* n'altère pas la croissance et le développement de la plante, ce qui suggère l'existence d'autres E3s qui contrôlent l'entrée et le bon déroulement de la phase S. Chez Arabidopsis, une autre protéine F-box, FBL17, a également été identifiée comme un régulateur clef du cycle cellulaire au cours de la gamétogenèse male et, plus récemment, de la prolifération cellulaire et de l'endoreduplication (Kim et al., 2008 ; Gusti et al., 2009 ; Noir et al., 2015). Les mutants *fbl17* présentent un taux de croissance considérablement réduit avec des défauts de séparation des chromosomes. Au niveau moléculaire, le taux de protéine KRP2 est accrue chez les mutants *fbl17*, affectant l'activité de l'ACDK1 (Noir et al., 2015).

L'Anaphase-promoting complex/Cyclosome

L'Anaphase-promoting complex/Cyclosome (APC/C) est une E3 ubiquitine ligase comprenant au moins 12 sous-unités, et de coactivateurs, qui sont CDC20 (CELL CYCLE CONTROL 20) et CDH1 (CDC20 HOMOLOG 1) chez les humains ou CCS52 chez les plantes (Peters, 2006 ; Genschik et al., 2014). Parmi ces protéines, $DOC1^{APC10}$ est également responsable de la liaison au substrat, APC11 se lie à l'enzyme E2 et APC2, qui s'apparente aux Cullines, se lie à $DOC1^{APC10}$ et APC11. CDC20 et CDH1 ainsi que $DOC1^{APC10}$ sont nécessaires pour la spécificité du substrat (Chang et Barford, 2014). Le rôle de l'APC/C est crucial pour la mitose et son activité est fortement régulée au cours du cycle cellulaire (Figure 10). Pendant les phases S et G2, l'APC/C est inactivé par EMI1 (EARLY MITOTIC INHIBITOR 1) pour permettre l'accumulation des cyclines A et B, favorisant ainsi la réplication et la progression de l'ADN par G2. Au début de la mitose, la dégradation de EMI1 est médiée par une autre E3 ligase : $SCF^{\beta\text{-}TrCP}$ (Margottin-Goguet et al., 2003), provoquant ainsi la destruction de la cycline A par l'APC/C^{CDC20}. Mais la caractéristique principale d'APC/C^{CDC20} est la polyubiquitination de la SECURINE en métaphase. Une fois que la SECURINE est dégradée, la SEPARASE est libérée, ce qui a pour conséquence le clivage des anneaux de COHESIN qui maintiennent ensemble les chromatides soeurs (Zur et Brandeis, 2001). Ce mécanisme est également contrôlé négativement par trois protéines du SAC (Spindle Assembly Checkpoint), MAD2 (MITOTIC

ARREST-DEFICIENT 2), BUB3 (BUDDING UNINHIBITED BY BENZYMIDAZOL 3) et BUBR1(BUB1-RELATED) qui forment le MCC (Mitotic Checkpoint Complex) et séquestrent CDC20 afin de vérifier la fixation correcte des chromatides soeurs avant de permettre la séparation de chromatides (London and Biggins, 2014 ; Komaki et Schnittger, 2017). Pendant la télophase, APC/C^{CDH1} intervient dans la dégradation des cyclines B et permet la sortie de la mitose. Pendant la mitose, la kinase AURORA-A phosphoryle la GEMININE et empêche sa reconnaissance par l'APC/C. La GEMININE se lie à CDT1 (CDC10-DEPENDENT TRANSCRIPT 1), empêchant ainsi l'assemblage du complexe de réplication (Tsunematsu et al., 2015). Au cours de la phase G1, AURORA-A est ubiquitinylée par APC^{CDH1} et dégradée, permettant ainsi la dégradation de la forme non phosphorylée de la GEMININE par le protéasome 26S.

Les E3 ligases monomériques de type RING

Chez l'homme, une E3 ligase monomérique de type RING appelé KPC1 (KIP1 ubiquitination-promoting complex 1) favorise la dégradation de p27KIP1 pendant la phase G1 (Figure 9) (Liu et al., 2008 ; Morgan, 1997 ; Kamura et al., 2004). Contrairement à l'activité de SCF^{SKP2}, l'ubiquitination de $p27^{KIP1}$ médiée par KPC1 ne dépend pas de sa phosphorylation par CDK2. De plus, le KCP1 joue également un rôle dans la limitation du développement des tumeurs (Kravtsova-Ivantsiv. NF-κB es et al., 2015) est un régulateur de transcription qui intervient dans plusieurs processus cellulaires dont la prolifération cellulaire. Cependant, le précurseur NF-κB (p105) doit être maturer par le protéasome 26S pour former un dimère p50 actif. Il a été démontré que l'accumulation de KPC1 déclenche la polyubiquitination de p105, et par conséquent, sa maturation (Kravtsova-Ivantsiv et al., 2015).

Un possible orthologue de KPC1 chez les plantes, appelée RKP (RELATED TO KPC1) a été identifiée chez Arabidopsis (Liu et al., 2008). La perte de RKP entraîne l'accumulation de KRP1, mais n'affecte pas la croissance des plantes (Ren et al., 2008). Deux E3 ligases de type RING supplémentaires, RHF1a et RHF2a (RING-H2 GROUPE F1A/2A), qui sont nécessaires pour la gamétogenèse chez Arabidopsis, ont également été identifiées (Liu et al., 2008). En effet, le double mutant *rhf1a/rhf2a* montre un niveau accru de protéine KRP6 qui est en corrélation avec un défaut de division cellulaire chez les gamétophytes mâles et femelles.

Le complexe $CRL4^{CDT2}$ chez les mammifères

La Cullin-RING ligase 4 (CRL4) est structurellement et fonctionnellement similaire au SCF. Les ubiquitine ligases de type CRL4 sont composées de la CULLINE 4 qui se lie à l'E2 et au module de reconnaissance de substrat comprenant une protéine adaptatrice appelée DDB1 (DNA DAMAGE-BINDING PROTEIN 1) et une protéine DCAF (DDB1-CULLIN4 ASSOCIATED FACTOR) (Havens and Walter, 2011 ; Jackson and Xiong, 2009). L'un de ces complexes, $CRL4^{CDT2}$, contient la DCAF CDT2 (CDC10-DEPENDENT TRANSCRIPT 2) et est impliqué dans la réplication et la réparation de l'ADN. La protéine CDT1 est nécessaire au recrutement de l'hélicase MCM2-7 (MINICHROMOSOME MAINTENANCE 2-7) aux origines de réplication (Nishitani et al., 2004). Ce processus se produit pendant la phase G1 et CDT1 est immédiatement détruit en phase S pour éviter toute réinitiation de la replication (Figure 9) (Nishitani et al., 2004). Il a été démontré que la dégradation des proteines CDT1 associées à la chromatine est dépendante d'E3 ligases de type CRL4, et particulièrement du $CRL4^{CDT2}$ (Higa et al., 2006 ; Jin et al., 2006 ; Ralph et al., 2006 ; Sansam et al., 2006). De plus, la dégradation de CDT1 médiée par $CRL4^{CDT2}$ a également été observée en réponse aux dommages à l'ADN (Higa et al., 2006 ; Ralph et al., 2006).

e. Régulation transcriptionnelle des gènes du cycle cellulaire

Au cours du cycle cellulaire, les cellules subissent plusieurs vagues de transcription intensive, en particulier pendant les transitions G1/S et G2/M. Ce processus de régulation transcriptionnelle est déterminé par l'activité des complexes CDK/CYC.

Contrôle de la transition G1/S

Chez les animaux et les plantes, la transition G1/S est principalement régie par la voie RB/E2F. Les protéines E2F (ADENOVIRUS EARLY GENE 2 BINDING FACTOR) sont des facteurs de transcription qui favorisent la transcription des gènes nécessaires à la phase S, notamment les « core cell cycle genes » (CDC6, CDC25, CYCE, ...) et des composants du complexe de

réplication (ORCs, CDT1, MCM3, PCNA, POLα, ...) (Stevens and La Thangue, 2003 ; Gutierrez, 2009). Dans les cellules quiescentes, les E2F sont associées à un inhibiteur transcriptionnel appelé RETIBLASTOMA (RB) (Dick et Rubin, 2013). Lors de stimuli mitogènes, RB est phosphorylé par les complexes CYCD-E/CDK2 conduisant à l'activation de la transcription par les E2Fs. Chez l'homme, la famille E2F comprend six E2F (E2F1-6) et deux autres membres plus éloignés appelés DP (DIMERIZATION PARTNER, DP1 et DP2), tandis que la famille des « pocket proteins » est composée de 3 membres : RB, p107^{RBL1} et p130^{RBL2} (RETINOBLASTOMA LIKE 1-2). Les E2F peuvent être classés en trois sous-groupes, E2F1-3, E2F4-5 et E2F6. Ils possèdent tous un site commun de liaison E2F qui cible la séquence promotrice consensus (TTTSSCGS), et un motif de liaison de à DP. Cependant, le sous-groupe E2F4-5 ne possède ni le site de liaison à CYCA, ni le signal de localisation nucléaire (NLS) présents dans le sous-groupe E2F1-3, mais a plutôt acquis un signal d'exportation nucléaire (NES). E2F6 est encore plus distant, car il ne porte pas le domaine de transactivation et agit donc comme un répresseur transcriptionnel, très probablement en titrant les séquences du promoteur E2F (examiné dans Stevens et La Thangue, 2003). L'inhibition transcriptionnelle par les protéines RB fonctionne par différents mécanismes. La liaison à E2F est suffisante pour cacher le domaine de transactivation et réprimer le recrutement de la machinerie transcriptionnelle. De plus, le RB peut également se lier aux protéines de remodelage de la chromatine, telles que les histone-désacétylases (HDAC) et le complexe Polycomb (Luo et al., 1998 ; Dahiya et al., 2001). Notons que chez les mammifères, la voie RB/E2F est également régulée par le UPS (Sengupta et Henry, 2015).

La voie RB/E2F est également très conservée chez le nématode, la drosophile et les plantes (Shen, 2002 ; Van Den Heuvel et Dyson, 2008 ; Berckmans et De Veylder, 2009). Le génome d'Arabidopsis code trois E2F (E2Fa, b et c), deux DP (DPa et DPb) et une RETINOBLASTOMA-RELATED PROTEIN (RBR1) (Figure 11). Parallèlement, trois autres protéines E2F non canoniques sont également présentes. Contrairement à E2F et DP, E2Fd^{DEL1}, E2Fd^{DEL2} et E2Ff^{DEL3} (DP ET E2F LIKE) n'ont pas besoin de former un dimère E2F/DP pour se fixer à l'ADN. Les E2F végétales ne sont pas seulement régulées par la liaison avec RBR1, mais sont également soumises à des mécanismes de régulation transcriptionnelle et post-traductionnelle (Ramirez-parra et al., 2008). Par exemple, E2Fa, E2Fb, E2Fb, E2Fc et E2Ff^{DEL3} sont fortement enrichis dans les cellules en proliferation et E2fb et c présentent un profil d'expression cycle-dependant, atteignant un pic en phase S (Menges et al., 2005). De plus, les E2F et les DP peuvent être phosphorylés par des complexes CDK/CYC. Bien que le rôle de la

phosphorylation de E2F/DP ne soit pas entièrement compris, les formes phosphorylées de E2Fc et DPb sont ciblées par le SCF^{SKP2A} et degradées par le protéasome 26S (del Pozo et al., 2002).

Contrôle de la transition G2/M

Chez l'homme, l'activation transcriptionnelle des gènes de G2/M nécessite deux facteurs de transcription : B-MYB (B-MYELOBLASTOSE) et FOXM1 (FORKHEAD BOX M1). B-MYB appartient à la famille MYB, qui est composée de 3 membres : A-MYB, B-MYB, C-MYB (ou MYBL2, MYBL1 et MYB, respectivement) (Musa et al., 2017). Alors que A-MYB et C-MYB sont exprimés dans des types cellulaires spécifiques, B-MYB est fortement enrichi dans les cellules en prolifération (Ness, 2003). La nature essentielle de l'activité de transactivation du B-MYB est illustrée par la létalité embryonnaire précoce de la mutation KO de B-MYB chez la souris (Tanaka et al., 1999). Parallèlement, la mutation *foxm1 -/-* montre également un phénotype embryolétal chez la souris, retarde la phase G2 et altère fortement la ségrégation chromosomique et la cytocinèse en culture cellulaire (Kalin et al., 2011 ; Laoukili et al., 2005). B-MYB et FOXM1 interagissent avec des sites de liaison spécifiques présents dans la région promotrice des gènes exprimés G2/M. Parmi les gènes activés par B-MYB/FOXM1, on peut trouver des composants de la machinerie du « core cell cycle » (CYCA/Bs, CDK1/2, CDC25B, PLK1) et des gènes impliqués dans l'assemblage du fuseau mitotique et la cytocinèse (Musa et al., 2017 ; Costa, 2005). Le timing de l'activité de B-MYB et de FOXM1 est cependant différent, ce qui peut s'expliquer en partie par leur activation par les complexes CDK/CYC. B-MYB et FOXM1 sont activés par phosphorylation en G1/S et G2/M par les complexes CDK2/CYCA et CDK1/CYCB, favorisant ainsi le recrutement d'un coactivateur $p300^{CBP}$ (Schubert et al, 2004 ; Major et al., 2004).

Les plantes possèdent également des protéines apparentées aux MYB. Le génome d'Arabidopsis code pour plus d'une centaine de protéines MYB. Parmi eux, MYB3R1,2,3,4,5 sont impliqués dans la régulation des gènes en G2/M en activant ou réprimant leur expression (Haga et al., 2007, 2011). Comme les MYB humains, les MYB3R se lient à un élément cis d'activation spécifique du MYB (MSA) qui est suffisant pour stimuler ou inhiber l'expression génique (Ito, 1998). Conformément à leur fonction dans la régulation des gènes impliqué dans la mitose, la perte de MYB3R1 et de MYB3R1 et de MYB4 induit des anomalies pendant la cytocinèse mais n'entraîne pas de létalité embryonnaire, ce qui suggère que d'autres facteurs

pourraient intervenir dans ce processus (Haga et al., 2007, 2011). Des études sur une suspension de cellules de tabac BY-2 synchronisée ont révélé que la transcription des gènes NtMYBs se produit pendant G2/M (Figure 11) (Ito et al., 2001). En outre, il a été démontré que la phosphorylation par les complexes CDKA/CYCA et B active la fonction de transactivation des NtMYBs (Araki et al., 2004).

Les complexes DREAM et MMB

Des études plus récentes ont mis en évidence l'existence d'un complexe de taille plus importante contrôlant les transitions entre les phases du cycle via l'activation et la répression de la transcription de gènes spécifiques (Fischer et Müller, 2017). Le complexe MUVB (MULTI VULVA-B) est composé de cinq protéines : LIN9, LIN37, LIN52, LIN54 et $p55^{RBBP4}$ (RETINOBLASTOMA-BINDING PROTEIN 4). Il a été proposé que l'ensemble des composants du complexe MUVB sont assemblées autour de la protéine LIN9. LIN52 et LIN54 se lient respectivement à p107/p130 et au motif ADN CHR (cell cycle homology region). p55 interagit avec les histones H3 et H4 par le biais d'un motif WD40 et participe éventuellement à la répression transcriptionnelle en interagissant avec les complexes de remodelage de la chromatine. Le contrôle positif ou négatif de l'expression des gènes dépend de protéines supplémentaires qui s'associent aux MUVB. Par exemple, E2F1-3/DP/p107 ou p130/MUVB, aussi appelé DREAM (DP, RB-like, E2Fs et MUVB), répriment l'expression des gènes G1/S tandis que B-MYB/FOXM1/MUVB ou MUVB-MMB (MYB-MUVB) active l'expression des gènes G2/M.

Chez Arabidopsis, des composants du complexe de type DREAM ont également été identifiés (Magyar et al., 2016). Le complexe MUVB de plante comprend l'orthologue à LIN54 TCX5 (TSO1-LIKE CxC 5) et les orthologues à LIN9 ALY2/3 (ALWAYS EARLY 2 et 3) (Magyar et al, 2016 ; Fischer et Müller, 2017). Les protéines RBR1, CDKA, E2Fs, DPs et MYB3Rs peuvent également faire partie du DREAM. Les fonctions complexes de la plante DREAM sont moins bien documentées que celles de son équivalent chez les animaux. Cependant, des études récentes ont montré qu'il peut activer ou réprimer l'expression des gènes spécifique de G2/M de manière phase-dépendante (Figure 12) (Kobayashi et al., 2015a, 2015b).

Université de Strasbourg

Adrien TROLET

École Doctorale des Sciences de la Vie et de la Santé STRASBOURG

Cell cycle-dependent function and regulation of ARGONAUTE 1 in plants

Chez tous les eucaryotes, la régulation de l'expression génique est primordiale pour le contrôle du cycle cellulaire. Un large éventail de gènes, incluant non seulement des régulateurs essentiels du cycle, mais également d'autre gènes impliqués dans la transduction du signal, la régulation hormonale et le métabolisme est ainsi exprimé durant certaines étapes clefs du cycle cellulaire. Ces changements sont contrôlés à de multiples niveaux, notamment de façon transcriptionnelle et post-traductionnelle. Chez les mammifères, il est aujourd'hui évident que les microARNs contribuent également à cette régulation en ciblant spécifiquement les transcrits d'un grand nombre de gènes régulés au cours du cycle. Cependant, nous n'avons que très peu d'informations à ce jour concernant le rôle des petits ARNs sur le contrôle de la prolifération cellulaire chez les plantes. Mes travaux de thèse ont permis de démontrer que la perte d'AGO1, le principal effecteur du PTGS chez Arabidopsis, affecte la prolifération cellulaire et l'activité du méristème racinaire. Afin de déterminer le répertoire et la fonction des petits ARNs liés la régulation du cycle cellulaire, j'ai également utilisé des suspensions cellulaires de tabac BY-2, qui présentent l'intérêt d'être hautement synchronisables. En collaboration avec P. Baldrich du laboratoire du Professeur Blake C. Meyers (St-Louis, USA), nous avons séquencé les transcrits, les petits ARNs et le dégradome à partir de cellules BY-2 synchronisées en phase S, G2, M et G1. Cette analyse a révélé que peu de microARNs sont différentiellement exprimés au cours du cycle chez les plantes. Cependant, nous avons identifié quelques microARNs qui pourraient réguler l'expression de facteurs de transcription et de gènes de résistances dans les cellules en prolifération. Finalement, nous avons également mis en évidence qu'un ensemble de petits ARNs de 19 nucléotides dérivés d'ARNs de transfert sont différentiellement chargés dans AGO1 au cours du cycle cellulaire. Cependant, leurs fonctions restent à déterminer.

Mots-clefs : AGO1, Cycle cellulaire, PTGS, petits ARNs, microARNs, tRFs, Arabidopsis, cellules BY-2

In all eukaryotes, regulated gene expression is key to orchestrate cell cycle progression. Not only genes encoding important core cell cycle regulators, but also genes of a variety of other factors involved in signal transduction, hormonal regulation and metabolic control are expressed at specific time points of the cell cycle. These changes in gene expression are controlled at multiple levels, including transcriptional and post-translational controls. In mammals, it became evident that microRNAs also contribute to this regulation by targeting the transcripts of numerous cell cycle-regulated genes. However, in plants we still know little about the regulatory roles of small RNAs in the control of cell proliferation. During my thesis, I showed that depletion of Arabidopsis AGO1, the main effector of plant microRNAs, impairs cell proliferation and root meristem activity. To further determine the repertoire and role of sRNAs in cell cycle regulation, I took advantage of the highly synchronizable tobacco BY2 cell suspension. In collaboration with P. Baldrich from Pr. Blake C. Meyers laboratory (St-Louis, USA), we thus sequenced total RNAs and small RNAs, AGO1-associated small RNAs and the RNA degradome of synchronized BY2 cells at S-, G2-, M- and G1-phases of the cell cycle. This analysis revealed that in plants, only a few microRNAs show differential cell cycle expression and microRNA-target pairs were only identified for a small proportion of the more than 23 000 differentially expressed genes during the cell cycle. However, we identified a set of unique miRNA-target pairs at all phases of the cell cycle that may damper the expression of a set of transcription factors and disease resistance genes in proliferating cells. Finally, we also found that AGO1 binds differentially during the cell cycle to a set of 19-mers tRNA-derived fragments. However, their functions and their targets, if any, remain still to be determined.

Keywords: AGO1, cell cycle, PTGS, small RNAs, miRNAs, tRFs, Arabidopsis, BY-2 cells